EXPERIMENTAL STUDIES OF GAS-PHASE ION-MOLECULE REACTIONS

A Thesis
presented for the Degree
of Doctor of Philosophy in Chemistry
in the
University of Canterbury

by
Paul Francis Wilson

University of Canterbury
1994

To My Parents; Thanks for having me.

TABLE OF CONTENTS:

ACKNOWLEDGMENTS:

Thanks are due to many people who have exerted their influence over the completion of this work.

The patient supervision and wisdom of Dr Murray McEwan and also of Dr Colin Freeman has been of great assistance.

Special mention should be made of Dr Vincent Anicich without whom none of this would have been possible.

The advice and experience of Dr Sean Smith, Dr Simon Petrie and Dr John Knight have been greatly appreciated.
Other staff and students whose erudition has been appreciated include; Mark Morrison, Barry Wells, Dr Michael Meot-Ner, Dr Robert Maclagan, Dr Brett Cameron, Dr Steve Grice, Dr Bryce Williamson, Dr Peter Harland, Professor Leon Phillips, David Blunt, Craig Aitken, Cara McConnell and the well known aviator Graham Scott.

The assistance of the technical staff in the Mechanical , Electrical and Glass blowing workshop has been of incalculable worth. Special thanks go to Rob McGregor, Dave McDonald, and Neil McCracken.

Thanks are due to the University of Canterbury for provision of a University of Canterbury Scholarship and to the Chemistry Department for my employment as a Teaching Assistant.

Other influences that deserve mention include; Darel, Neil, Adrian, Dave, Jason, and all the other bad boys (and girls) of Yoshukai. The members of the University Fencing club, especially Nadine, Benoit, Vic and Chris. Special thanks to Simon Feltham for helping me through some serious trouble with crimes and contract.

There are many other persons who have contributed in some way to this work, even if they are unaware of this, so thanks to them.

Extra special thanks are due to C. Northcote Parkinson for inventing a law to describe how this work fitted into the time available.

LIST OF TABLES:

LIST OF FIGURES:

PUBLICATIONS:

The following publications are related to the research presented in this thesis:

Smith S.C., Wilson P.F., Sudkeaw P., Macalgan R.G.A.R., McEwan M.J., Anicich V.G., and Huntress W.T. (1993)
J.Chem. Phys. ***98***, 1944.
Statistical modelling of capture, association, and exit-channel dynamics in the CH_3^+/CH_3CN system.

Wilson P.F., Freeman C.G., and McEwan M.J. (1993)
Int. J. Mass Spectrom. Ion Processes. ***128***, 83
Isomers of $C_3H_6N^+$ and the interstellar synthesis of C_2H_5CN.

Wilson P.F., McEwan M.J., and Meot-Ner (Mautner) M. (1994)
Int. J. Mass Spectrom. Ion Processes. in press
Reactions of $CH_3OCH_2^+$ with Nitrogen bases: A Mechanism for the Formation of Protonated Imines.

Meot-Ner (Mautner) M., McEwan M.J., and Wilson P.F.
To be submitted.
Thermochemical Requirements for Dissociative Processes.

ABSTRACT:

Development on both selected ion flow tube (SIFT) and ion cyclotron resonance (ICR) instruments is described.

Modifications to the SIFT described here include; a new, off-axis ion source, and new hardware and programs to measure the neutral flow and the ion count using a personal computer.

Mechanical, electrical, electronic, and programming modifications to the ICR instrument are described. Several well known ion-molecule reactions are used to calibrate, and monitor the performance of the ICR instrument.

The reactions of t-C_4H_9Cl with a number of protonated bases, BH^+, are reported. The reactions were studied using both the SIFT and the ICR. The branching ratio of the product channels is reported for each reaction. For some bases, the process,

$$BH^+ + t\text{-}C_4H_9Cl \rightarrow t\text{-}C_4H_9^+ + B + HCl$$

appears to be fast, although it is significantly endothermic. The thermochemistry of the system is discussed, and it is suggested that either the tabulated thermochemical values are significantly wrong, or the reaction proceeds via formation of weakly bound complexes which dissociate on focussing in the down stream region of the SIFT.

The chemistry of several srtuctural isomers of protonated ethyl cyanide, $C_3H_6N^+$ is examined. Two reactions thought to be routes to interstellar synthesis of ethyl cyanide are shown to be unlikely to yield that ion upon dissociative recombination. The association of $HCNH^+$ with C_2H_4 is shown to lead to the protonated ethyl isocyanide isomer. The association of CH_3^+ with CH_3CN is reasoned to lead to formation of the $CH_3CNCH_3^+$ structure.

The isomerism observed is rationalised in terms of the potential surface for the system derived from both experimental observation, and several previous *ab initio* studies.

The reactivity of the methoxymethyl cation with several oxygen and nitrogen bases is reported. The exothermic proton transfer channel is not observed, but competing methyl cation and CH^+ transfer dominate.

The reactivity in both the SIFT and the ICR is explained in terms of several factors. An activation barrier to proton transfer proceeds from ring closure to form the neutral product, oxirane. The S_N2 methyl cation transfer process is sterically hindered and results proceeds via a tight transition state, whereas the alkyl transfer process has a greater density of states at the transition state. Where there is a labile hydrogen on the base, the alkyl transfer process dominates because of its' looser transition state.

The association reactions of acrylonitrile are reported in both the ICR and SIFT instruments. The reaction of CH_2CHCN^+ shows competition between proton transfer and association. Proton transfer dominates in the ICR and association dominates in the SIFT. The termolecular rate of formation of the proton bound dimer of acrylonitrile is measured at 1.2×10^{-23} cm^6 s^{-1}.

An RRKM study of the association of CH_3^+ and acetonitrile is reported. The collisional parameters of both helium and acetonitrile bath gases are estimated. The

average downward energy transferred per collision, $<\Delta E_{down}>$, for helium is estimated as 300 cm^{-1}, and for acetonitrile as 950 cm^{-1}. The fall off of the association reaction with pressure is shown in comparison with experimental results.

The ion-molecule reactions of acetylene have been studied, and the results confirm earlier work. The ions $C_6H_5^+$, and $C_6H_4^+$ are shown to exist as a mixture of two or more isomers of differing reactivity. One isomer reacts with unsaturated hydrocarbons at the collision rate while the other is unreactive. $C_6H_5^+$ exists as a mixture of isomers when formed from sequential ion-molecule reactions of acetylene or electron impact or chemical ionisation on halobenzenes. $C_6H_4^+$ exists as a mixture of two isomers when formed from sequential ion-molecule reactions of acetylene.

CHAPTER ONE

INSTRUMENTAL TECHNIQUES FOR THE STUDY OF ION-MOLECULE REACTIONS

1.1. Introduction

This chapter aims to introduce the two instrumental methods used to perform the work described in the following chapters. The backgrounds to both the Selected Ion Flow Tube and Ion Cyclotron Resonance instruments are discussed, and the mechanics of both techniques are described. While both techniques possess inherent advantages and disadvantages, they should not be compared merely as alternative methods for the study of ion-molecule chemistry but as complementary techniques that can be used together to allow an in depth knowledge of a system to be obtained over a wide range of pressures.

1.2. The Selected Ion Flow Tube (SIFT)

The general topic of Selected Ion Flow Tube (SIFT) instrumentation and experiment has been well covered in several thorough review articles including those by Smith and Adams [Smith and Adams (1979)], [Smith and Adams (1988)], [Adams and Smith (1988)] and Graul and Squires [Graul and Squires (1988)]. The development of the SIFT did not constitute a great conceptual leap, it arose as a modification of the flowing afterglow instrument. It soon came to supplant the flowing afterglow as the instrument of choice for investigating thermal ion molecule reactions, at least in the pressure ranges within which flow tube experiments operate. The versatility of the SIFT instrument can be gauged by the large number of papers involving the study of ion molecule chemistry within a SIFT, published by a growing number of groups throughout the world. Before considering the SIFT itself in detail it is helpful to review the development of the instrument from its precursor, the flowing afterglow.

1.2.1. The Flowing Afterglow

The use of flow tube techniques in ion chemistry originated in the research carried out by Eldon Ferguson and the members of his group in Boulder [Ferguson et al

(1964)]. The requirement for rate information about the atmospheric chemistry of ions with truly thermal energy distributions led to the use of fast flowing helium afterglows so that reacting species could be thermalised by collision with the buffer gas.

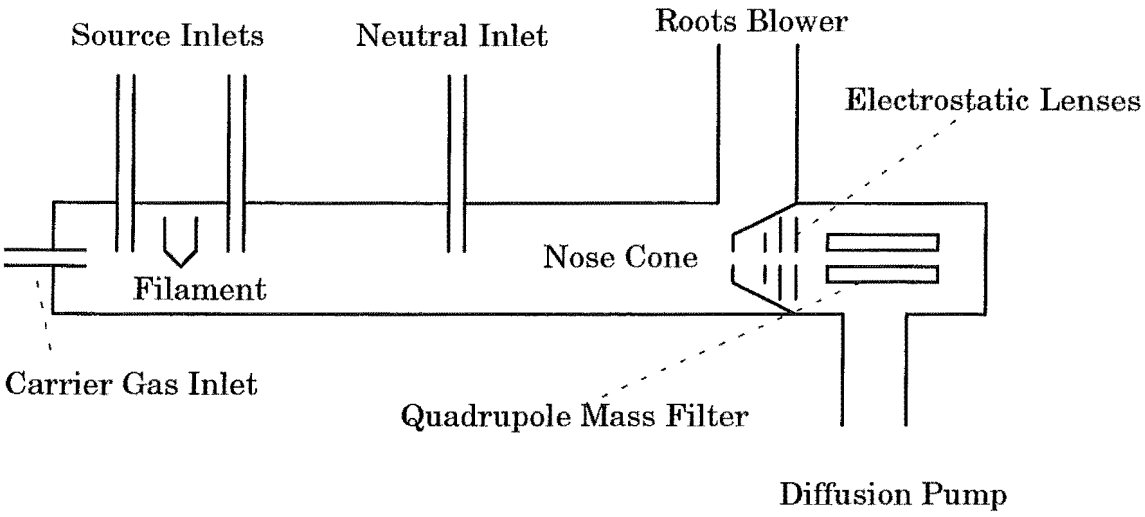

Figure 1-1. Schematic of a flowing afterglow system.

The archetypical flowing afterglow system consists of a flow tube through which a carrier gas is passed. The carrier gas is typically a small species such as He or H_2. The pressure within the flow tube is typically in the range 0.2...0.5 Torr. At the upstream end of the flow tube, ions are formed from a source gas added to the carrier gas stream. Ionisation is usually carried out by electron impact or by microwave discharge, although direct current discharge methods have been used. An afterglow plasma is formed in the ionisation region which contains both positive ions and electrons. As the plasma flows down the tube, the ions become thermalised by collision with the carrier gas.

At a known point in the flow tube a neutral reagent can be added to the flow tube by means of a neutral inlet. The neutral can react with any of the ionic species present during its progress down the tube from the inlet to the detection region. The ion detection system used in a flowing afterglow usually consists of a quadrupole mass filter with a channeltron type continuous dynode particle detector.

The components of the detection system can operate only at pressures of less than 10^{-4} Torr. This means that the chamber containing the detection system must be separated from the flow tube so it can be differentially pumped. Between the flow tube and the detection system is a nose cone surrounding an axially mounted disc with a small orifice through which a small number of ions can be sampled. The bulk of the reaction mixture and carrier gas is pumped out of the flow tube by a high throughput roots pump with a suitable backing pump, while the detection region within the nose cone is pumped by a diffusion pump.

1.2.2. Data Analysis in Flow Tube Experiments

By measuring the ion concentration at a fixed distance Z from the neutral inlet, it is possible to obtain a rate coefficient for the reaction of the ion with the added neutral. Consider the reaction...

$$A^+ + B \rightarrow \text{Products} \tag{1.1}$$

the rate law for the reaction is

$$\frac{d[A^+]}{dt} = -k[A^+][B]. \tag{1.2}$$

The rate law can be expressed in terms of the ion's axial velocity v_i and the axial distance z by the expression

$$\frac{d[A^+]}{dz} = -k\frac{1}{v_i}[A^+][B] \qquad \text{given that} \quad v_i = \frac{dz}{dt}. \tag{1.3}$$

Rearranging and using the assumption that if the flow of B is in large excess then pseudo first order conditions apply

$$\frac{d[A^+]}{[A^+]} = \frac{-k}{v_i}[B]\,dz. \tag{1.4}$$

Integrating both sides between $z = 0$ to Z gives,

$$\int_0^Z \frac{d[A^+]}{[A^+]} = \frac{-k}{v_i}[B]\int_0^Z dz, \tag{1.5}$$

$$\ln\frac{[A^+]_Z}{[A^+]_0} = \frac{-k}{v_i}[B]Z, \tag{1.6}$$

thus

$$k = -\ln\frac{[A^+]_Z}{[A^+]_0}\frac{v_i}{Z}\frac{1}{[B]}. \tag{1.7}$$

Clearly a plot of $\ln[A^+]_Z$ as a function of the neutral flow, [B], allows evaluation of the rate. The above expressions are somewhat simplistic, since the concentration of $[A^+]$ is affected not only by reaction with the neutral, but also by diffusion in both radial and axial directions. A much better description of the variation of $[A^+]$ with axial distance z is

$$v_i(r)\frac{\partial[A^+]}{\partial z} = \frac{D_a}{r}\left(\frac{\partial}{\partial r}\left(r\frac{\partial[A^+]}{\partial r}\right)\right) + D_a\frac{\partial^2[A^+]}{\partial z^2} - k[A^+][B]. \qquad (1.8)$$

In this expression, given by Bolden et al [Bolden et al (1970)], the first term accounts for radial diffusion, the second for axial diffusion and the last term is of course the rate of ion loss by reaction. The quantity D_a is the ambipolar diffusion coefficient. The axial diffusion term is often neglected, and if this is done, [Bolden et al (1970)],[Adams et al (1970)] the expression for the ion concentration reduces to,

$$[A^+]_Z = [A^+]_0 \exp -\left(\frac{\Delta D_a}{r^2} + \Gamma k[B]\right)\frac{Z}{v_i}. \qquad (1.9)$$

In the above expression Δ depends on both the pressure and the so called slip coefficient, r is the tube radius. Γ is the ratio of the bulk carrier gas velocity v_O to the ion velocity v_i. The value of Γ^{-1} has been found [Adams and Smith (1988)] to be around 1.45 at 300K at a pressure of 0.5 Torr. Since most flow tube measurements are made at constant pressure the expression can be restated as,

$$\ln\frac{n_z}{n_o} = -k[B]\Gamma\frac{Z}{v_o}, \qquad (1.10)$$

where the concentration of A^+ is replaced by the number of ions. The concentration of B term can also be replaced, being expressed in terms of the flow rate Q_n of the neutral,

$$\ln\frac{n_z}{n_o} = -\frac{k\,Q_n(Z+\varepsilon)}{\pi r^2 v_o v_i}. \qquad (1.11)$$

In this expression ε is an end correction. The value of this correction is dependant on the characteristics of the particular flow tube set up used.

Variations on the Flowing Afterglow Theme

The flowing afterglow technique was for some time a most popular for the study of positive ion-molecule reactions, and much of the chemistry of the ionosphere was elucidated using this instrument. Several modifications to the basic flow tube design allowed the scope of experimentation to extend beyond the merely thermal room temperature measurement. The variable temperature flowing afterglow instrument was developed by the Boulder group [Dunkin et al (1968)]. Enclosing the flow tube within a copper jacket upon which heating and cooling coils were brazed, extended the range of

temperature over which thermal rate coefficients could be measured to the range 80 to 600K.

A further extension was the flow drift tube. The one piece flow tube was replaced by a series of stainless steel hoops tightly fastened together with rubber O rings between them. Applying a separate voltage to each hoop allowed a constant drift velocity to be attained by the ions within the tube. The ability to vary the centre of mass energy of the reactant ion opened up the study of energy partitioning in ion-molecule reactions. The extension of this instrument, the SIFDT, will be discussed in more detail below.

In more recent years the Selected Ion Flow Tube has become a favourite tool of the positive ion experimentalist, but the flowing afterglow is still yielding important results. The ability to create plasmas containing a mixture of positive ions with either electrons or negative ions, depending on the nature of the bulk gas mixture, allows for a wide range of chemistry to be studied.

Negative ion associative detachment reactions, for example, have been studied using a flowing afterglow [Bierbaum et al (1977)], equipped with a window in the flow tube to allow for observation of IR emissions from the neutral products.

$$O^- + CO \rightarrow CO_2 + e. \qquad (1.12)$$

The product neutral was found to be formed in the highest energetically possible vibrational states.

The dissociative recombination of electrons with positive ions has been studied by the Flowing Afterglow Langmuir Probe (FALP) instrument. The instrument differs from the conventional flowing afterglow in that a moveable Langmuir probe allows the density of electrons to be measured at any given point along the length of the flow tube. In order to measure the recombination coefficient α_e for the reaction

$$O_2^+ + e \rightarrow O + O, \qquad (1.13)$$

for example, an afterglow plasma of He^+ and e is used. In order to remove the metastable He^+ species, argon is added, forming Ar^+. The plasma, containing $He^+$and Ar^+ exhibits negligible recombination, and the density gradient of e along the flow tube, $\frac{\partial n_e}{\partial z}$, is low. Upon addition of O_2 to the flow tube, recombination dominates over diffusion as the primary loss process of e and the expression

$$v_p \frac{\partial n_e}{\partial z} = -\alpha_e n_e n_+ = -\alpha_e n_e^2 \quad \because n_+ = n_e, \qquad (1.14)$$

[Adams and Smith (1988)] can be applied. Although the recombination coefficient is important, the branching ratios of the products of recombination reactions are of great interest at the present time, because although theory can predict the recombination coefficient to within a reasonable margin, (see below), the present state of theory is unable to predict branching ratios with any confidence, even for relatively small systems. With this in mind, a FALP instrument, equipped to examine the neutral products with laser induced fluorescence, resonance enhanced multi-photon ionisation, VUV and visible absorption spectroscopic techniques, has been built at the University of Georgia [Adams (1992)].

1.2.3. The Selected Ion Flow Tube Proper

The major disadvantage of the flowing afterglow was, and still is, that the ion source can produce a number of primary ions, creating a complex mixture of primary and secondary ions making analysis of mechanistic routes and the branching ratios between different reaction processes difficult. It was in order to alleviate these problems the Selected Ion Flow Tube (SIFT) was developed.

The first SIFT was constructed at Birmingham by Adams and Smith [Adams and Smith (1976a)]; the instrument consisted in effect of a flowing afterglow tube with a quadrupole mass filter between the ion source and the reaction region.

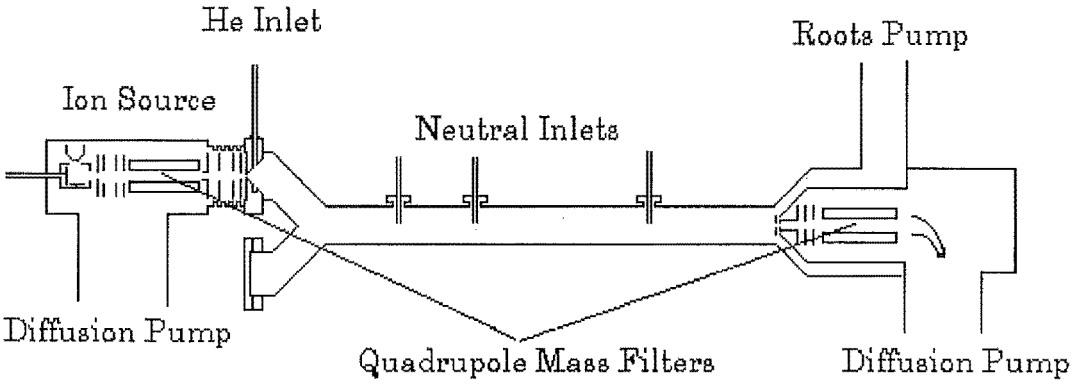

Figure 1-2. Schematic of the Canterbury SIFT.

Although simple in concept, the actual construction of the SIFT raised several difficulties principally related to the requirement that the quadrupole must operate in a region of low pressure, and that the ions passing through the quadrupole must then traverse a sharp pressure gradient to enter the tube.

In order to inject the selected ions from a region at 10^{-4} Torr to a region at up to 1 Torr without subjecting them to forces great enough to cause fragmentation, the designers of the Birmingham SIFT used a small orifice between the ion selection chamber and the flow tube. On the flow tube side of the orifice a ring of small holes

allowed the carrier gas to expand into the tube. This expansion creates a region of hypersonic flow around the orifice, in effect a venturi pump, allowing the ions to enter the flow tube and become entrained within the carrier gas.

The SIFT at Boulder [Howorka et al (1979)] used a concentric ring around the central orifice for admission of the carrier gas. Other designs, including several series of holes, of various sizes, fed by different helium reservoirs [Smith and Adams (1988)] have been suggested, but no single design has proved overwhelmingly popular. One significant point that has emerged from the various experiments with orifice design is that the hypersonic flow region may extend some distance (up to 50 cm) down the flow tube. This flow condition greatly perturbs the flow velocity and leads to serious inaccuracies in rate determination. A simple expedient to prevent this hypersonic flow is to place a bend in the flow tube between the venturi orifice and the reaction region. This has the added advantage that it prevents photons from the ion source travelling down the tube and interfering with an axially mounted particle multiplier.

The exact design of the flow tube is relatively unimportant except that it must be smooth walled. Non magnetic stainless steel is usually used. The exterior of the flow tube may be heated or cooled by the use of resistive heating elements or refrigerant pipes brazed to the surface of a copper jacket tightly enclosing the flow tube.

Reactant gases are admitted to the flow tube through inlets (usually fixed) along the length of the tube. Various designs of inlets have been used, and all posses their individual mixing characteristics. Because the mixing of the neutral with the carrier gas is not instantaneous a correction is made to the reaction distance Z used in the rate determination. This correction factor is calculated using a calibration reaction for which the rate is well known.

Upon reaching the end of the flow tube the great majority of the carrier gas and the reactive species are pumped out of the flow tube, but just as with the flowing afterglow some of the ions are sampled by passing through the orifice in a molybdenum disc on the end of the nose cone. Molybdenum is always used as the material for the orifice disc, since for some (obscure) reason, [Graul and Squires (1988)], this metal seems not only resistant to chemical attack, but also less readily becomes statically charged than other metals. The molybdenum disc is electrically insulated from the nose cone so that the total ion current incident on the disc can be measured. This enables the mass discrimination of the detection system to be measured. The disc itself should be as thin as practical, and the electrostatic lenses of the detection system are usually placed as close as possible to the disc. In the Canterbury SIFT a "top hat" lens element is used to get to within 1 mm of the Mo disc. The field from this lens thus penetrates some distance into the flow tube.

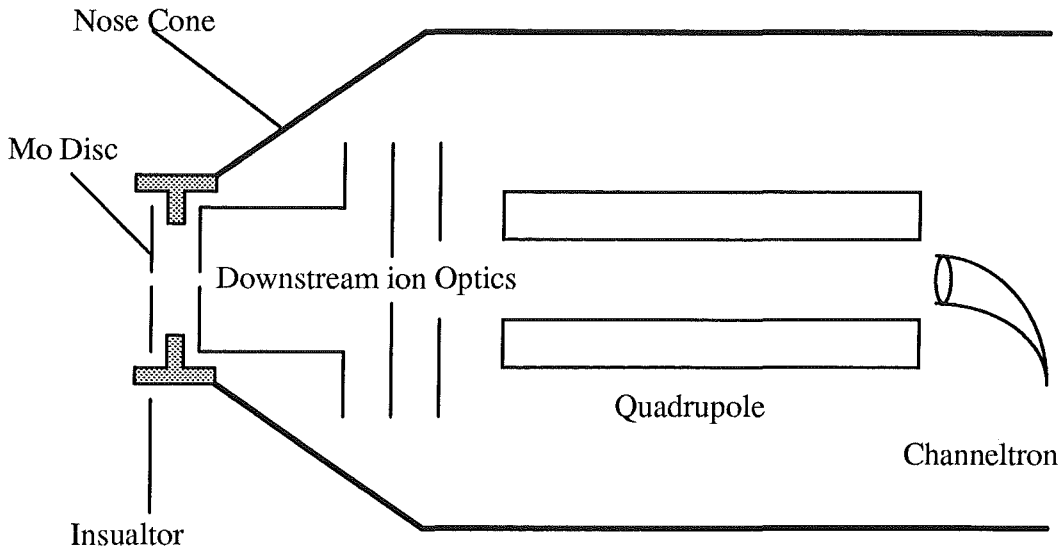

Figure 1-3. Downstream region of the Canterbury SIFT.

Having passed through the molybdenum disc and been focussed into the quadrupole mass filter, the ions of the target mass pass through the mass filter and can be detected by the ion counting system. Usually a channeltron type particle multiplier is used; a detector mounted coaxial with the quadrupole axis gives the best sensitivity, but if the ion source is also coaxial this can lead to interference by photons from the ion source passing through the tube. If the particle multiplier is mounted off axis then a positively charged deflection electrode will need to be used to focus the ions toward the detector.

Data Analysis

The SIFT, being fundamentally a flowing afterglow with a different ion source, relies upon the same principles of data analysis. The only significant difference in data analysis is that the diffusion process in the flowing afterglow is described by an ambipolar diffusion coefficient, D_a, due to presence of both positive ions and electrons, whereas in the SIFT the diffusion of the positive ions is described by D_i, which is the free diffusion coefficient. The equation for the rate coefficient of reaction becomes

$$k = \frac{\pi r^2 v^2}{\Gamma Z(1-\varepsilon)}\left(\frac{d\ln[A^+]}{dQ_n}\right) \qquad Q_n = \pi r^2 v[B], \tag{1.15}$$

where v is the carrier gas velocity, ε is a correction for axial diffusion, and Q_n is the neutral flow.

1.2.4. Error or Uncertainty in Rate Determinations

The error or uncertainty associated with SIFT rate measurements has been assigned various values between 15 and 30 % of the rate coefficient [Smith and Adams (1979)]. There are three major sources of error in a SIFT rate determination; these are;

(*i*) the estimations made in the expressions used to describe the flow dynamics. Adams et al [Adams et al (1975)] estimate these as amounting to an uncertainty of around 7%.
(*ii*) The carrier gas flow velocity, upon which the rate constant depends to the second order. Knight [Knight (1986)] estimates the uncertainty due to this measurement in the Canterbury instrument at around 10%. The use of a new method of measuring the neutral flow (see below) has probably reduced this uncertainty somewhat.

(*iii*) The uncertainty in the slope of $\frac{d \ln[A^+]}{d Q_n}$. This is determined by a least squares fit of the data. The uncertainty in the fitting of the slope varies significantly with the number and accuracy of the data points. This uncertainty is usually less than 10%.

1.2.5. Mass Discrimination

Variation in the sensitivity of the detection system at different masses is a fundamental problem in mass spectrometric systems. The quadrupole mass filter, ubiquitous in SIFT instruments, suffers from this drawback. Depending on the sensitivity setting of the quadrupole, systems can discriminate by an order of magnitude or more over a range of less than 200 mass units.

The mass discrimination of the quadrupole is the single largest cause of error in branching ratio determinations. Because the transmission through the quadrupole depends upon the position and momenta of the ion as it enters the quadrupole, the settings of the downstream ion optics also affect the mass discrimination. The only practical way to allow for mass discrimination is to calibrate the sensitivity of the detection system in any given configuration of quadrupole and lens settings.

The basic procedure for calibrating the mass response is described by Adams and Smith [Adams and Smith (1976b)]. The procedure used in calibration of the Canterbury SIFT is as follows.

The bias voltage on the molybdenum disc is supplied by a separate (battery powered) source which is in series with a Keithley 407 picoammeter. The ion current incident on the disc can be measured, and is typically of the order of 10^{-11} A. The flux of ions through the orifice is assumed to be directly proportional to the incident ion current.

By measuring the number of ions recorded by the particle multiplier the ratio of $\frac{\text{ion current}}{\text{ion count}}$ can be obtained. Plotted over a number of masses this gives a calibration curve valid for the chosen settings of the ion optics and quadrupole resolution used. A convenient means of generating a number of ions of different masses is chemiionisation. Ar^+ can be injected from the source and the mass sensitivity at m/z 40 measured. Neutrals added at the second inlet can be ionised by the Ar^+. If the neutral is added in

excess, ensuring complete removal of Ar^+, then the mass sensitivity for the product ion can be measured. The reactions

$$Ar^+ + SF_6 \rightarrow SF_5^+ + F + Ar, \quad (1.16)$$

and

$$Ar^+ + CF_4 \rightarrow CF_3^+ + F + Ar, \quad (1.17)$$

are often used, providing ions of m/z 127 and 69.

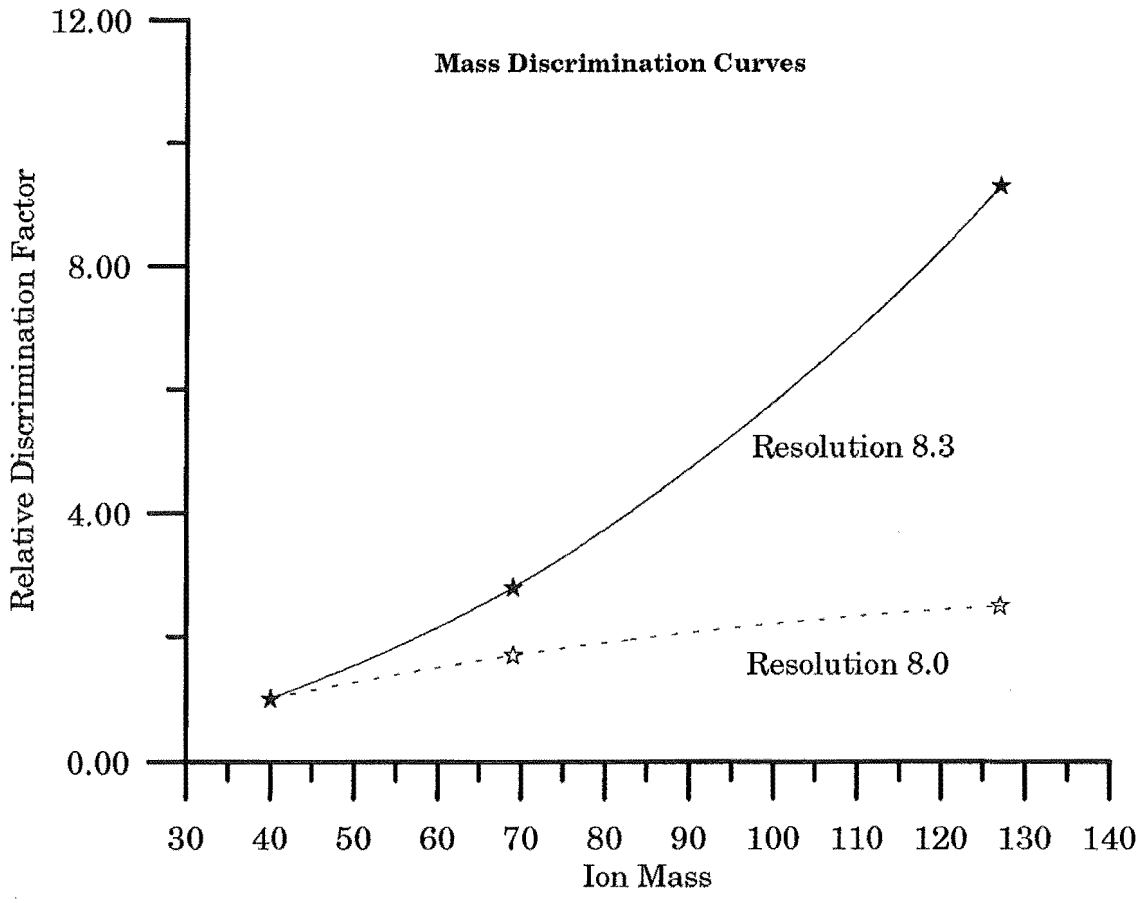

Figure 1-4. Typical mass discrimination curves obtained at different quadrupole resolutions.

A problem encountered with the Canterbury SIFT in measuring calibration curves was the occurrence of significant leakage currents from the nearby electrostatic lenses to the molybdenum disc. These leakage currents were of the same or greater magnitude than the ion current and varied sufficiently that they could not be backed off using the offset current from the picoammeter. It was found that the noise could be eliminated by reducing the voltages on the downstream electrostatic lenses close to ground. Thus the lenses were switched low to measure the ion current on the disc, and returned to their usual potentials to measure the transmitted ion signal.

1.2.6. Measurement of Isomer Ratios in a SIFT

Common to all mass spectrometric techniques is the problem of structure. The mass of an ion does not reveal its structure nor even its formula. The term isomer can be applied in many different ways, but the most common form of isomerism encountered in gas phase ion chemistry is structural isomerism, where the connectivity of the constituent atoms differs between two or more structural isomers with the same molecular formula. This form of isomerism can be exhibited by species with as few as three atoms, for example the CHN^+ system, [Petrie et al (1990)], exhibits the isomers HCN^+ and CNH^+.

The elucidation of isomeric structures from flow tube results is reviewed in detail by McEwan [McEwan (1992)] and aspects of this will be discussed later in this work. This section primarily concerns the phenomenological evidence of isomerism displayed in the SIFT. The presence of two or more isomers of a given mass can be revealed by their different reactivity with a neutral species. This effect is manifest in a noticeable curvature in the plot of $\ln[A^+]$ against neutral flow. In the simplest case, that of two isomers of the same mass but different reactivity, the observed ion signal is given by,

$$I = [A^+]_0 \exp(-kQ_n) \quad + \quad [A'^+]_0 \exp(-k'Q_n). \tag{1.18}$$

The initial concentrations of the two isomers, that is, the concentration when the neutral flow is 0, are $[A^+]_0$ and $[A'^+]_0$, and the rate coefficients of each isomer with the neutral are k and k'. If the intensity can be measured as a function of neutral flow Q_n then the values of the initial concentrations and the rate coefficient for each isomer can be found by numerical means. For example, the Canterbury SIFT laboratory uses a simplex method to find the minimum of the error between the observed and the estimated ion intensity. The program was originally written by H.S Stock and P.W Harland, and adapted for use in the SIFT laboratory by Knight [Knight (1986)].

The observation of curvature in the decay of an ion with addition of neutral reagent is not unequivocal evidence of the presence of two isomers. If a reaction in the flow tube produces a product ion at the same mass as the reactant ion in question, the result will resemble the effect due to the presence of an isomeric form unreactive even at high neutral flows.

Another source of curvature can arise if the resolution of the quadrupole in the detection region is not high enough to separate adjacent mass peaks. The shoulder of an adjacent, unreactive peak may resemble an unreactive fraction at the observed mass.

Of course, if the ions are formed in such a way as to produce significant amounts of vibrationally excited, or even (possibly) electronically excited states, the reactivity of the states may be very different. For example the reaction of O^+ with O_2

$$O^+ + O_2 \rightarrow O_2^+ + O, \qquad (1.19)$$

proceeds at a rate of 2.3×10^{-11} $cm^3 s^{-1}$ for the ground state $O^+(^4S)$ ions, but considerably faster, with a rate of 1.3×10^{-10} $cm^3 s^{-1}$, for the excited state O^+ (^2D,^2P) ions [Glosik et al (1978)].

Other perturbations to the normal linear decay may occur in rare cases where the neutral flow is so large that it influences the thermalisation or stabilisation characteristics of the bulk carrier gas.

Variations on the SIFT Theme

Just as the flowing afterglow instrument was extended to produce the flow drift tube, the SIFT has been developed into the Selected Ion Flow Drift Tube (SIFDT). Just as in the flow drift tube, the reaction region of the flow tube is divided into short sections, each of which is held at a separate potential to drift the ions along the flow tube at drift velocity v_d in an overall field along the tube of E. The drift velocity is related to the field by

$$\mu = \frac{v_d}{E}, \qquad (1.20)$$

where μ is the mobility of the ion in the carrier gas. The centre of mass energy between the ion of mass M_i and a neutral of mass M_n is given by

$$E_{c.m} = \left(\frac{M_n}{M_i + M_n}\right)\left(E_i - \frac{3}{2}k_b T\right) + \frac{3}{2}k_b T, \qquad (1.21)$$

where the kinetic energy of the ion E_i is

$$E_i = \frac{1}{2}(M_i + M_n)\, v_d^2 + \frac{3}{2}k_b T. \qquad (1.22)$$

Among the reactions to be studied using the SIFDT instrument was the reaction between $N^+$and O_2 [Howorka et al (1980)]. The energy dependence of both the rate coefficient and the branching ratio were measured. The authors found that over a significant range the rate constant for the reaction was independent of the centre of mass energy of the ions but that the branching ratio between the three product channels changed with changing centre of mass energy.

The logical extension of the SIFT genre is the Variable Temperature Selected Ion Flow Drift Tube (VT-SIFT). The first VT-SIFDT was built in Birmingham [Smith and Adams (1979)], the construction being necessarily more complex than the SIFDT instrument because of thermal expansion. The drift rings, separated by ceramic insulators are located within the flow tube, together with the required wiring. The VT-SIFDT in Birmingham utilises both electron impact and flowing afterglow ion sources.

1.3. Ion Cyclotron Resonance (ICR)

1.3.1. History of the ICR from the Omegatron to the FTMS

The broad category of "ICR methods" encompasses many different techniques used in a wide variety of areas within physical, organic and inorganic fields of chemistry. In order to understand this multiplicity of techniques it is helpful to trace their development from a historical perspective before concentrating on those areas of greatest relevance to this work.

Today's FTMS instruments have achieved spectacular mass resolution. These instruments are modified forms of the trapping ICR instruments which were and still are used more for kinetic and mechanistic studies than for high resolution measurements. It is interesting and possibly ironic that the trapping ICR instrument is itself a direct descendant of an instrument designed specifically for precise mass measurement. The precursor of the ICR instrument was a device known as an Omegatron [Hipple et al (1949)] [Sommer et al (1951)]. The Omegatron consisted of a cavity surrounded by a number of trapping electrodes. A small positive trapping voltage was applied to these electrodes to prevent the ions moving out of the cavity. The whole was placed between the poles of an electromagnet producing a homogeneous field ***B***. Ions were formed in the centre of the cell by an electron gun fired across the cavity. An rf electric field could be induced in the cavity by plates above and below it. When the field frequency applied is at the cyclotron frequency of an ion, ω_c, that ion will absorb energy,

$$\omega_c = q\frac{B}{m}, \tag{1.23}$$

where q is the ionic charge, m is the ion mass and $\boldsymbol{B}$ is the magnetic field.
As the ion at resonance absorbs energy it moves in a spiral motion with a radius that increases with the ion kinetic energy. The authors derived an expression for the radius of the ions orbit after time t.

$$\text{radius} = V_{rf}\frac{t}{2B}. \tag{1.24}$$

When the radius reached the edge of the cell the ions impacted on the detection electrode and the ensuing ion current was measured by a sensitive electrometer. Thus by measuring the variation of ion current with oscillator frequency the authors obtained a mass spectrum. The instrument was primarily used for mass determination, giving the mass of H_2^+ with a reported resolution of 1 in 35000. The resolution decreased rapidly with mass. N_2^+ could be observed with a reported resolution of 1 in 5000. The authors suggested that the Omegatron could be improved in two important ways. Firstly, instead of measuring the ion current it would be preferable to measure the rf absorption by the

ions within the cell. Secondly, the problem of space charging that plagued the Omegatron could be overcome by generating the ions at some point or region remote from the detection region. The combination of these two improvements led to the ICR instrument.

One of the earliest instruments was reported by Wobschall [Wobschall (1965)]. This was an instrument surrounded by a solenoid magnet. The ions were formed in an ion source at one end of the tube and moved along the long axis of the magnet through an analyser region with an rf field applied from plates above and below the ions path. Although the instrument was primitive in many respects, it was the first reported use of capacitance balanced bridge detection in an ICR system. The two rf plates were the plates of a capacitor; the movement of the ions between the plates created an image current which could be converted into a voltage by the bridge detector. The advantages of this system over the more common marginal oscillator system for direct power absorption measurement are discussed below. The Wobschall ICR used modulation of the magnetic field (at 11 Hz) and a phase sensitive detector to improve the signal to noise ratio. In many respects the signal analysis system used is similar to that used today.

The next improvement made to the instrument was the use of drift electrodes to produce a dc field perpendicular to the magnetic field to drift the ions at a well defined velocity from the source region through the analyser region. The drift plates were usually above and below the cell which was typically placed between the poles of an electromagnet. The sides of the cell were comprised of trapping plates, upon which a positive charge was used to keep the positively charged ions in the centre of the cell. The development of the three section ICR cell led to the manufacture of the first commercial instrument of its type.

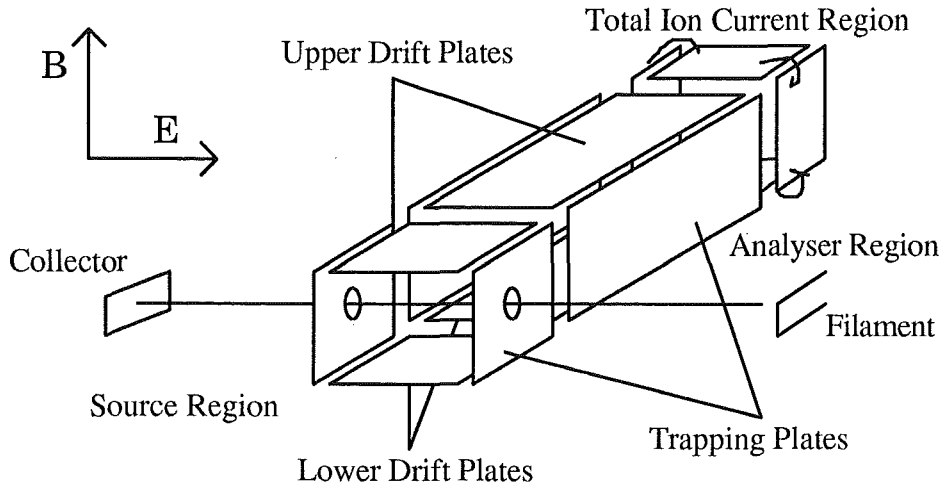

Figure 1-5. Schematic of a three region ICR cell: based on the "Syrotron" design but with the source and analyser trapping plates separate.

The "Syrotron" ICR instrument was manufactured by Varian Associates of Palo Alto California. Much of the developmental work was done by Llewellyn at Varian. The first

report of the use of this instrument was by Beauchamp [Beauchamp et al (1967)]. The cell had separate source, analyser and ion current collection regions. The drift plates in the source and analyser region were separate, but the trapping plates were in one piece across both source and trapping regions. The cell had a square cross section, its dimensions being 2.54 by 2.54 by 12.7 cm. Unlike the Wobschall instrument the authors used a marginal oscillator detection system. The marginal oscillator [Robinson (1959)] had the advantage of being more sensitive than bridge detection but suffered from variable mass sensitivity. Beauchamp et al report the use of double resonance techniques to identify the reactions in the chloroethylene system. In the double resonance experiment the suspected product ion is observed while the parent ion is irradiated by a second rf oscillator. A variation in the product ion signal due to the irradiation shows the parent - daughter ion relationship. This variation can be positive or negative depending on the energetics of the reaction.

After the development of the "Syrotron" instrument the basic design of drift ICR instruments has changed little, although four region cells have been constructed where the analyser region is split into a drift and an analyser region [Clow and Futrell (1971)].

The drift cell ICR was and remains a very versatile instrument for the study of kinetic and equilibrium processes. Like the SIFT technique in which it is necessary to solve the equations for the flow dynamics, the analysis of results in the drift cell requires a solution of the power absorption equations before a rate constant can be calculated. The drift time of the ions in the cell must also be measured, and this may be difficult. To avoid having to measure the drift time a trapped ion cell was developed. In these cells the reaction could be followed as a function of time, greatly simplifying the kinetic analysis of results, and the analysing rf field need only be applied for a short period after the reaction time is over.

The first trapped ion instruments were purpose built. McIver [McIver (1970)] reports replacing the cell of a Varian Associates ICR-9 instrument with a one region rectangular cell enclosed on all sides by plate electrodes. The plates were held at voltages of either + or - 1 V, creating closed equipotentials within the cell within which the ions were trapped. The ions were created by a short (0.1 ms) electron pulse. The pulse was gated by a voltage applied to the grid between the filament and the cell. Both the magnetic and electric fields were on during the whole experiment, but the magnetic field was held off-resonance by ~20 Gauss. After a suitable reaction period the field was brought into resonance and the ion power absorption measured by marginal oscillator. The McIver trapping cell was developed further to allow for double resonance experiments [McIver et al (1971)]. The same cell was used, but the detection period was achieved by changing the voltages on the side trapping plates. This changed the resonance frequency of the ions to ω'.

$$\omega' = \omega_c \left(1 - \frac{2qV_t}{m\omega_c^2 d^2} \right), \tag{1.25}$$

where V_t is the trapping voltage, d is the spacing between the plates, and ω_c is the cyclotron frequency in the absence of the trapping voltage. The authors encountered problems in adapting their system to allow double resonance experiments, so developed a pulse compensator system to apply the double resonance signal 180° out of phase to the marginal oscillator plate, solving their problems of interference.

The authors used the double resonance to study the reactions of CH_4^+. The reaction has two channels, the authors were able to show that as the kinetic energy of CH_4^+ increased, the branching ratio[1] for channel (1.26b) became larger and that for (1.26a) decreased. Channel (1.26b) had not been observed at thermal energies.

$$CH_4^+ + CH_4 \rightarrow CH_5^+ + CH_3 \tag{1.26a}$$

$$\rightarrow CH_3^+ + H_2 + CH_3 \tag{1.26b}$$

While trapping cells of the McIver design provided good ion trapping, especially at high magnetic field strength, some felt that it would be preferable to be able to trap ions in the same instrument that was used for drift experiments. McMahon and Beauchamp [McMahon and Beauchamp (1972)] reported the conversion of a typical three region drift cell for use in trapped ion experiments. The conversion was relatively simple. In order to trap the ions in the source region the authors found it necessary to use an end plate to close the equipotential lines within the instrument to prevent ion leakage. Grids between the filament and the cell and between the collector and the cell were used to prevent the high potentials on those components penetrating into the cell. Trapping was accomplished by holding the drift plates (including the new end plate) at ground and the trapping plates at a positive potential. During the detect phase of the pulse sequence the drift plates were sent to the normal drift voltages, drifting the ions into the detection region.

The development of the trapped ion cell led to improved resolution through the use of lower pressures, but the ICR technique was still primarily used for mechanistic experiments measuring reaction rates or equilibrium constants. Where accurate mass resolution, especially at large masses, was required conventional instruments were used. This situation changed with the advent of Fourier transform methods in instrumentation. At first applied in NMR and IR spectroscopy, Fourier methods were eventually used in ICR by Comisarow and Marshall [Comisarow and Marshall (1974)]. The basis of the

---

[1] The branching ratio is the proportion of the total product ion current that is formed through a given reaction channel.

technique was a trapped ion cell, while the hardware was not much changed the method of signal acquisition and analysis was entirely new [Comisarow (1978)].

In a conventional ICR experiment whether or not double resonance is used, the power absorption, (in the case of a marginal oscillator detector) or the image current, (in the case of a bridge detector) of each ion must be determined sequentially, while the ion is being irradiated. This means that a complete mass spectrum takes some considerable time to complete, and the greater the required resolution the greater the time required.

The Fourier transform method works by exciting all of the ions at the same time, then once all the irradiation has finished, the decay of the image current within the cell is recorded. This decay is known as the time domain transient, and can be converted to a frequency domain signal by Fourier transformation. In order to improve the accuracy of the result the time domain measurement can be repeated and the resulting signal average can be Fourier transformed to give the mass spectrum over the desired range. The first FTICR instrument, as used by Comisarow and Marshall, utilised the conventional McIver trapped ion cell [McIver (1970)]. The ions were excited by a rapid frequency sweep or "chirp" of the rf oscillator. This chirp took typically 1 ms to sweep from 0 to 2 MHz. The time domain signal was obtained by measuring the image current produced by the coherent ion motion in the cell as that motion relaxed. The most striking feature of the FTICR experiment was the increased resolution that was possible using exactly the same cell and magnet as in the trapped ion experiments. The major reason for the increased resolution is that in the conventional ICR experiment the observed ion moves in a spiral path during the combined irradiation / detection period. The same ion in the FTICR experiment is no longer absorbing power and maintains a constant orbit . The spiral path of the ion in the conventional experiment covers more of the cell and the ion is therefore influenced by the inevitable electric and magnetic field inhomogeneities to a much greater extent than the ion in a stable orbit.

The resolution in the FTICR experiment depends on a number of factors. The uncertainty principle indicates that the longer the image current is sampled the greater the resolution, [Comisarow and Marshall (1974)] [Comisarow and Marshall (1976)]. Clearly collisions in the cell causing a decay in the coherent motion of the ions will reduce the resolution, and thus for ultra high resolution the lower the pressure the better [Gross and Wilkins (1982)]. In fact collisional relaxation is only one of a number of relaxation processes that operate to reduce the relaxation time. Broadly speaking these can be divided into two categories, firstly homogeneous relaxation, which involves loss of energy from the excited system, and secondly inhomogeneous relaxation which involves no net loss of energy, but effectively means the ions lose their coherent phase relationship. Examples of homogeneous relaxation are loss of energy by radiation and by electric resistance to the image current in the detection system. Examples of inhomogeneous relaxation are collisions with other bodies and magnetic and electric field

inhomogeneities. An excellent review of these and other relaxation processes has been written by Comisarow [Comisarow (1982)].

Physical processes influence the theoretical limit to the resolution obtainable but the practical limits are influenced more by instrumental factors. Performance is improved by operating at higher magnetic fields, but operation at high fields requires the use of higher rf frequencies and correspondingly higher sampling frequencies. The sampling frequency must be at least twice the highest frequency to be observed. Sampling at a high frequency for as long as possible requires large amounts of fast access memory. Early experiments were greatly hindered by the lack of suitable hardware (PDP 11 computers were the norm, with only 30 K of memory). Over the years the hardware available off the shelf has greatly improved, and so have methods of numerical signal analysis. A simple method of improving resolution at the expense of increasing noise is to multiply the entire time domain signal by an increasing exponential [Marshall (1985)] [Lee and Comisarow (1987)]. This technique has the effect of increasing the contribution from the longer times of the transient.

Another method of analysis is that of heterodyning (or narrow band mode or spectral segment extraction mode)[Comisarow and Marshall (1975)]. This involves mixing the transient with a reference frequency to produce a sum, and a difference signal. The lower frequency, difference component, is separated by a low pass filter and thus the sampling rate required is reduced. The drawback of this technique is that it only works for the narrow band close to the reference frequency. One way around this is to use several reference frequencies at once [Wang and Marshall (1988)].

Instead of using fast Fourier transformation of the time domain signal, Rahbee has developed a method known as the Maximum Entropy Method, MEM [Rahbee (1985)] [Rahbee (1986)]. This method promises improvements in resolution and signal to noise but requires more cpu time than fast Fourier transform.

The resolution in FTICR techniques is phenomenal. As early as 1983 Wanczek and his group report a resolution of 10^8 [Allemann et al (1983)]. The current trend is towards resolution that will enable binding energies to be determined. However the resolution of FTICR experiments is not matched by a corresponding mass accuracy. This lack of mass accuracy is the main reason FTICR, or FTMS as it is more commonly referred to, has not replaced more conventional instruments. The basis of the problem is the difficulty in determining the exact observed cyclotron frequency of a given mass due to defects in the field. This problem was recognised early on by the builders of the Omegatron [Sommer et al (1951)]. The largest contributions to the field defects are made by space charging and by the applied trapping voltages. Some groups have taken an empirical approach and have developed calibration procedures to take account of the effect of space charging on the observed resonance frequency [Francl et al (1983)] using calibrants of known mass observed simultaneously with the unknown mass. The authors also suggest that altering the geometry of the cell can improve the mass accuracy and

report the development of an elongated (along the magnetic field) cell FTICR. The elongated cell [Hunter et al (1983)] minimises the end effects of penetration into the cell by the trapping potentials on the end plates.

1.3.2. Detection Systems

The Omegatron used an electrometer to detect the ion current due to ions at resonance. While later ICR instruments retain the facility to measure ion currents, the detection of resonant ion signals is performed by other methods, marginal oscillator and capacitance bridge detection are the two most common methods employed in conventional ICR experiments. The signal detection used in FTICR experiments differs somewhat from the above methods and will not be discussed in this work. Although a bridge detection system was designed by Wobschall [Wobschall (1965)] it was not initially as popular as the marginal oscillator system. The marginal oscillator works by incorporating the cell by means of the upper and lower analyser plates, in an L C R tuned circuit. The resistance across the ICR contributes to the voltage across the circuit. This resistance is increased by the absorption of power by ions in resonance. This change in resistance in the circuit is measured as a change in voltage [Robinson (1959)]. Marginal oscillator detection is fundamentally more sensitive than bridge detection [Kemper and Bowers (1988)], however the early marginal oscillator systems could operate only at a fixed frequency determined by the tuning of the circuit, requiring the magnetic field to be swept in order to obtain a mass spectrum. Many modifications to the marginal oscillator have been made and several groups have built frequency swept marginal oscillator detection systems [Kemper and Bowers (1982)]. The problem remains however that the gain in a marginal oscillator system varies with frequency, and so such frequency swept oscillators require calibration.

The capacitance bridge detector works on a different principle. The plates of the cell form a capacitor in one side of a L C bridge. A balance capacitor forms the other side of the bridge. The rf signal to be applied to the cell is split, and signals 180° out of phase and half the original amplitude are fed to each arm of the bridge. The resulting rf field across the cell is the sum of the two phase split signals, so has the original amplitude which is ≤ 0.22 V. The bridge is balanced without ions in the cell so that there is no response at the null point over as wide a range of rf frequencies as possible.

The coherent orbital motion of ions during (or in the case of FTICR after) resonance excitation can be described as a rotating electric monopole [Comisarow (1982)].

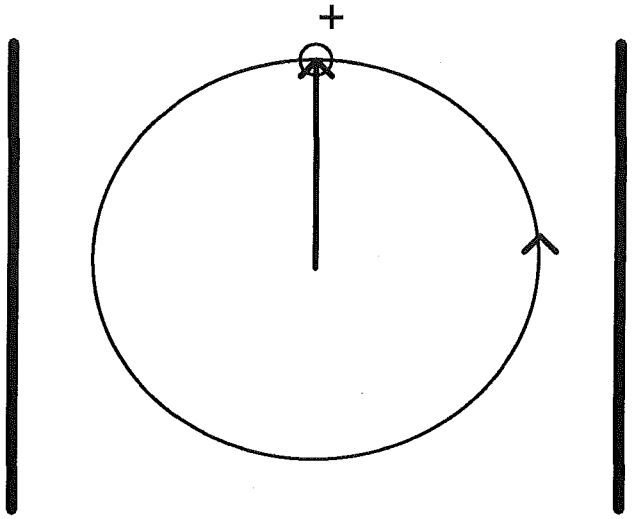

Figure 1-6. Coherent ion motion as a rotating electric monopole: after [Comisarow (1982)].

The field produced by this monopole induces an image current between the plates of the capacitor. This image current produces an imbalance in the bridge and a voltage at the null point. The null point signal is amplified with a broad band preamplifier and fed into a phase sensitive detector which uses a reference signal 90° out of phase with the rf signal applied to the cell.. Thus the signal due to the ion motion is converted into a voltage output from the phase sensitive detector.

The voltage produced at the null point has been found [Wronka] [Kemper and Bowers (1988)] to be independent of the frequency when operating at constant magnetic field. Thus when the bridge detector is used in frequency swept mode there is no requirement to calibrate the mass response of the detector.

Several bridge detector circuits have been reported [Wobschall et al (1963)], [McIver et al (1981)] [Wronka and Ridge (1982)]. The circuits are similar in conception, the Wronka design being the simplest, dispensing with separate amplifiers for each arm of the bridge, and making use of the SYNC signal generated by modern function generators in order to simplify the handling of the reference signal for the phase sensitive detector.

1.3.3. Drift Mode ICR

The ICR instrument described in this work is intended for use in investigating, in conjunction with the SIFT instrument, positive ion-molecule reactions over a wide pressure range. This principally involves the determination of rate constants in both drift and trap modes. The derivation of rate constants in drift mode is complicated, relying on observation of the power absorption or the image current of the ions in the cell to obtain quantitative information. In order to understand the theory of power absorption and its

relation to rate coefficients it is helpful to start with the equations of motion of an ion in the cell.

There are several review articles that summarise the equations of motion and of power absorption in more or less rigorous fashion. One of the most recent is by Kemper and Bowers [Kemper and Bowers MT (1988)]. This work is recommended to the reader as a reasonably complete and readable summary, and only a brief sketch of the fundamentals is attempted here. The conventions and nomenclature used by Kemper and Bowers are used here.

Motion in the Drift Cell

An ion in the presence of constant electric and magnetic fields is subject to the Lorentz force,

$$\mathbf{F} = q(\mathbf{E} + \mathbf{v}\times\mathbf{B}). \tag{1.27}$$

The velocity is usually expressed as being comprised of two components,

$$\mathbf{v} = \mathbf{u} + \mathbf{v}_{drift}, \tag{1.28}$$

$\mathbf{v}_{drift}$ is the drift velocity of the ion perpendicular to both the electric and magnetic fields. In a conventional three region ICR cell it is this motion that moves the ion from the source through the analyser region,

$$\mathbf{v}_{drift} = \frac{\mathbf{E}\times\mathbf{B}}{B^2}. \tag{1.29}$$

Thus the drift velocity is constant in the ideal case of constant electric and magnetic fields. $\mathbf{u}$ is the cyclotron motion of the ion in the magnetic field and is independent of the constant electric field,

$$m\dot{\mathbf{u}} = q\mathbf{u}\times\mathbf{B}. \tag{1.30}$$

This motion occurs with the cyclotron frequency

$$\omega_c = \frac{qB}{m}. \tag{1.31}$$

Clearly the motion depends on the exact nature of the electric field within the cell, including influences due not only to the drift and trapping voltages but also to space charging. Various expressions for the electric field have been developed by different groups, [Bowers et al (1969)] [Beauchamp and Armstrong (1969)] (both concerning the conventional drift cell) [Sharp et al (1972)] (for the trapped ion cell), and these show that the resonance frequency for an ion of mass m will always be modified by the

presence of trapping voltages and space charges. The expression derived by Beauchamp and Armstrong describes the effective frequency ,

$$\omega_{eff}^2 = \omega_c^2 - \omega_t^2, \tag{1.32}$$

where ω_t is known as the trapping frequency. The exact expression for the trapping frequency was shown by Sharp et al to depend on the cell geometry. The effect of collisions on the motion of the ions must also be considered, and Beauchamp [Beauchamp (1967)] has derived a modified Lorentz equation to give

$$\mathbf{F} = q(\mathbf{E} + \mathbf{v} \times \mathbf{B}) - \xi \mathbf{v}, \tag{1.33}$$

where ξ is the reduced collision frequency. The net contribution to ion velocity due to collisions is not large, resulting in a slight movement towards the negative drift plate . The influence of collisions on the absorption of rf power and the coherence of ion motion during the detection period is more significant.

Power Absorption

When an rf field is applied to the ion the expressions above still hold, but must be modified to take account of the alternating field. The quintessential work in this field is by Comisarow [Comisarow (1971)]. Using the modified Lorentz equation above, Comisarow produces an expression for the instantaneous power absorption of an ion in resonance. The general power absorption equation given by Comisarow reduces to,

$$A(t,\xi) = \frac{K}{m} \frac{\left[1 - \exp(-\xi t)\right]}{\xi}, \tag{1.34}$$

where

$$K = \frac{q^2 E_{rf}^2}{4}, \tag{1.35}$$

when the ion is in resonance ie $\omega_{rf} = \omega_{eff}$. In the limiting cases for high pressure, $(\xi >> 1)$ and for low pressure, ($\xi_{\to 0}$) the Comisarow expression reduces to give the expressions that had been derived previously. As can be seen the absorption is a function not only of the field, the collision frequency and ion mass but also of the time the ion is in resonance. What is measured in a drift cell experiment is not the instantaneous power absorption but is, in fact, the integral of this over the time the ion spends absorbing power in the analyser region. This is described by the general line shape equation, also derived by Comisarow. When the ion is in resonance the expression reduces to,

$$\text{Integral} = \frac{K}{m\xi}\left(t - \frac{\left[1-\exp(-\xi t)\right]}{\xi} \right), \qquad (1.36)$$

where t is the time the ion spends absorbing power. In the conventional McMahon Beauchamp cell this corresponds to the time taken to travel the length of the analyser region.

Reactive Ions, Rate Constants from Power Absorption.

The power absorption expressions above were derived for non reactive ions. Where the ions are reactive the ion population will be reduced as time passes, and this must be taken into account. The situation is complicated further if the ion is a secondary or tertiary ion that is formed at a given rate and consumed also at a given rate. The power absorption and line shape equations for primary, secondary, and tertiary ions are also given by Comisarow in his paper.

There are various ways of deriving a rate constant from the observed resonance line shapes, the method used in this work was developed by Anicich utilising an iterated solution of the line shape equations of Comisarow. The method involves measuring the peak heights of the reactant and product ions, and the time taken for the ions to drift through both the source and analyser regions. This drift time is the same for all the ions in the experiment since the frequency swept detector used allows the magnetic field to be kept constant during the experiment. The collision rate for momentum transfer collisions for each ion with the neutral gas (the parametrised ADO rate of Su and Chesnavich [Su and Chesnavich (1982)] is usually used) and the rate of formation of any secondary reactive ion are also required. The cell pressure and the magnetic field are assumed to remain constant during each measurement of the peak heights.

The programs (written by Anicich in FORTRAN) make use of an initial guess of the rate constants and then calculate the expected peak heights for the reactant and product ions. The estimated rates are incremented and the change in the agreement of the estimated with the experimental peak heights is tested. This process is continued iteratively until the solution meets the required accuracy of fit or the maximum number of iterations is exceeded.

Double Resonance Experiments

One of the major problems involved in mechanistic studies is the identification of reaction pathways. In tandem mass spectrometers or selected ion instruments it is simple in principle to show a product-reactant relationship, but in an instrument like the ICR, where there may be several neutral species and several primary ions, the elucidation of such relationships appears to be more difficult.

The ICR double resonance experiment removes the ambiguity and allows accurate determination of reaction pathways. The basis of the technique is the fact that

any ion irradiated at its resonance frequency can be actually removed from the cell, by collision with the cell walls, given sufficiently large power absorption.

As the ion is excited, and its kinetic energy increases so does its cyclotron radius, until the radius exceeds the dimension of the cell and the ion is lost to the wall of the cell. This will occur after time t, where,

$$t = \frac{d^2 B}{V_{rf}}. \tag{1.38}$$

In this expression, see [Kemper and Bowers (1988)], d is the cell dimension, B is the magnetic field and V_{rf} is the magnitude of the double resonance signal experienced by the ion.

Thus, by using a sufficiently strong rf field, each reactant ion can be ejected from the cell by irradiating at that ions resonant frequency. If a product ion is derived from a particular reactant ion, then double resonance ejection of the reactant ion will be manifested as a decrease in the product ion signal. Complete ejection of the reactant ion will of course result in complete loss of the product ion signal for all product ions derived from that reactant ion.

In its simplest form the double resonance experiment consists of monitoring the product ion peak while irradiating a possible precursor ion [Beauchamp et al (1967)]. A somewhat more sophisticated experiment is made possible by the use of a frequency swept detector [Wronka] [Comisarow and Marshall (1974)]. The reactant ion is irradiated at its resonance frequency by a modulated signal. Using the bridge detector (a frequency swept marginal oscillator detector could also be used) the observing oscillator is swept over the entire mass spectrum. The output signal from the phase sensitive detector is fed into a lock in amplifier referenced to the frequency at which the double resonance irradiation is being modulated. The resulting mass spectrum will show only the ions produced from the reactions of the reactant ion.

A common use of double resonance ejection is to remove unwanted ions from the cell to simplify the kinetic analysis or to prevent unwanted side reactions. An interesting variation is afforded by an experiment by Kleingeld and Nibbering [Kleingeld and Nibbering (1982)], where an FTICR study of CH_3OH^+ is reported. In order to elucidate the mechanism it was desirable to use isotope labelling, ie to use $CH_3{}^{18}OH_2{}^+$. Using normal CH_3OH as the bath gas, most of the many ions formed in the source were ejected by double resonance, only $CH_3{}^{18}OH_2{}^+$ was not ejected (natural methanol contains 0.2% of $CH_3{}^{18}OH$). There was sufficient signal of the isotopically labelled ion to carry out the experiment.

An interesting double resonance experiment allows the mean lifetime of a collision complex to be measured. By irradiating at the resonant frequency of the collision complex, the complex can be ejected from the cell. By varying the rf amplitude,

the ejection time can be varied (see Eq 1.38). Complexes that have a lifetime of more than the ejection time will be indicated by a double resonance signal. By plotting the extent of the double resonance ejection against ejection time the distribution of lifetimes of the collision complex is revealed. This technique was pioneered by Anicich for the complex ions $HC_3N.HC_3NH^+$ and $CH_3.CH_3CN^+$, [Anicich et al (1990)][Anicich et al (1994)].

By irradiating an ion at its resonance frequency, the ions kinetic energy is increased. A simple expression, neglecting the influence of collisions for the average ion kinetic energy, can be derived [Kemper and Bowers (1988)] by integrating the power absorption equation in the low pressure limit ($\xi \rightarrow 0$). This gives

$$EK = \frac{q^2 E_{rf}^2 t^2}{8m}. \qquad (1.39)$$

The ability to vary the translational energy of the reactant ion gives the opportunity to examine reactions as a function of ion energy. While this seems like a great boon it must be remembered that accurate characterisation of ion energy is difficult. The expression for ion kinetic energy above requires the amplitude of the rf field experienced by the ion, not that put out by the oscillator. The nature of the connections between the double resonance oscillator and the cell plates will affect the amplitude of the field as experienced by the ion. The influence of collisions will also serve to remove energy from the excited ion. Given that quantitative measurements will be difficult, it is clear that the method is a useful qualitative tool. The method can give information about whether a reaction is exothermic or endothermic, or whether a reaction possesses a channel not observed at normal thermal energies. [McIver (1970)].

1.3.4. Trap Mode ICR

Although, as previously described, the first trapping cells were of the McIver design [McIver (1970)], the discussion below concerns only the considerations involved in carrying out trapped ion experiments using the three region trap drift or McMahon Beauchamp cell [McMahon and Beauchamp (1972)].

In adapting the three region cell for trapping use, McMahon and Beauchamp added an end plate to the ion source in order to close the equipotentials within the source. Apart from this structural change, the TICR also required the development electronics to generate the pulse sequence which controls the filament bias, the plate voltages and the oscillators used. The technical details of the electronics used in the Canterbury ICR are discussed later, but the basic sequence of events in a trapping experiment is described below.

The Pulse Sequence in TICR

In order to accurately define the ion trapping time it is important to form the ions during a short, well defined initiation period. The method usually employed and the one used in this work is to apply a bias to both the filament and the grid. During the initiate pulse the grid bias is more positive than the filament bias, allowing electrons to pass the grid and enter the cell. After the pulse the grid is held negative with respect to the filament. If the experimenter intends to utilise double resonance to excite or remove an ion or ions an irradiate pulse can follow the initiate pulse.

Following the initiate pulse is the trapping period. The drift plates, including the source end plate, are held at ground during this period to prevent ion drift, and the trapping plates are held at a small positive voltage.

After a suitable delay time the detect pulse is applied. During this period the drift plates are held at their normal drift mode potentials and the ions are drifted from the source region into the analyser region. The subject ion is detected with either marginal oscillator or a bridge circuit during the period it takes to drift through.

If it is required, a quench pulse can be applied shortly after the detect pulse. The quench pulse is to purge the cell of any ions present, usually by applying a negative voltage to one or more of the trapping plates. After the quench pulse the sequence starts over again.

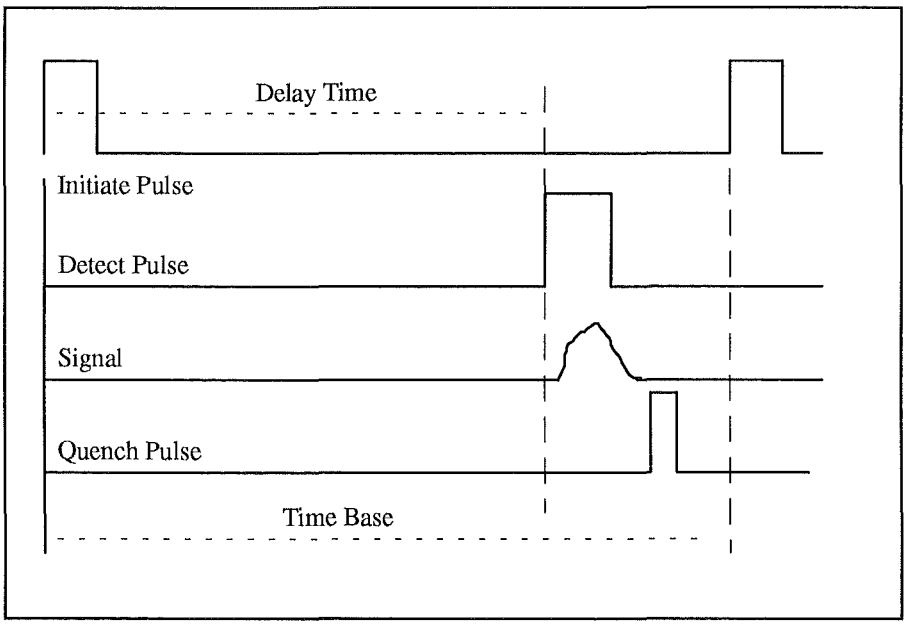

Figure 1-7. A typical pulse sequence for a trap mode experiment.

Data Analysis in the Trap Mode

Data analysis for the kinetic experiments is much simplified in the trap mode. Since the detection is carried out over a short period, around 5 ms, depending on the drift voltages, and the lower pressures under which trapping experiments are carried out, the influence of collisions on the power absorption can be neglected. In fact if a capacitance

balanced bridge detector is used, the area under the signal is directly proportional to the number of resonant ions. [McIver et al (1981)]. A gated integrator is then used to measure this quantity directly. The most important aspect, however, is that the experiment gives a direct measure of the time behaviour of the reactant ion obtained by simply altering the delay time. In order to obtain a rate constant for a bimolecular reaction of an ion with a neutral gas all that is required is to measure a decay curve for the reactant ion before and after adding a known pressure of the neutral.

For the reaction

$$A^+ + B \rightarrow C^+ + D \tag{1.40}$$

the rate law is

$$\frac{d[A^+]}{dt} = -k[A^+][B]. \tag{1.41}$$

Separating the variables gives

$$\frac{d[A^+]}{[A^+]} = -k[B]\,dt \tag{1.42}$$

integrating both sides,

$$\ln \frac{[A^+]}{[A^+]_0} = -k\ [B]\,t. \tag{1.43}$$

In practice a rate coefficient from the trap mode is obtained by measuring the decay of $[A^+]$ with time without [B]. Then a known pressure of [B] is added and the decay measurement repeated. The ratio of the second decay over the first is the quantity $\frac{[A^+]}{[A^+]_0}$, plotting the natural log of this quantity as a function of time a least squares fit of the slope gives $-k[B]$. In the same manner as in the SIFT experiment, curvature in this plot is an indicator of the presence of more than one isomer at the observed mass.

1.4. Other Experimental Techniques

The Flowing Afterglow/SIFT and the ICR/FTMS techniques are probably the two most popular experimental methods for ion molecule kinetic measurements. It must be admitted that the ambit of these two categories is somewhat wide, but each can trace its lineage to a single machine, the original Boulder flowing afterglow, and the Omegatron. There is a wide variety of instruments that were developed separately from either of these two general categories, and that are used for ion molecule chemistry.

One technique that is used particularly for ion thermochemical measurements is that of Pulsed Electron High Pressure Mass Spectrometry (HPMS). A review by one of the leading exponents of this technique, Kebarle, describes the development of the instrument [Kebarle (1988)]. The technique evolved from interest in radiolytic processes at close to atmospheric pressure, using alpha particles or high energy protons for the primary ionisation process. The modern instruments use pulses of high energy electrons to achieve primary ionisation, and analyse the intensity of the ions within the ion source as a function of time.

The most significant feature of this technique is the ability to measure equilibrium processes, as well as the approach to equilibrium. For this reason the instrument lends itself to the study of transfer reactions, ie proton, charge, and ligand transfer phenomena. The major drawback of the technique is the complexity of the reaction mixtures. Unlike SIFT or ICR instruments there is no facility to remove unwanted ions from the reaction mixture. Rate measurements are made by fitting the observed ion intensities with an iterated solution to the coupled rate equations of the system.

Another interesting technique is the Electron Bombardment Flow Tube. The principle behind it is that of analysing the neutral products of ion molecule reactions. This is done by passing large volumes of gas along a tube under bombardment from ionising electrons [Morton (1988)].The ionic products of the reaction are analysed by a quadrupole mass filter coupled with a channeltron particle multiplier in similar fashion to a SIFT, but instead of being pumped out of the tube, the neutral species are trapped in a liquid nitrogen trap. The condensate is later analysed by GC-MS or by NMR.

CHAPTER TWO

SELECTED ION FLOW TUBE EXPERIMENTAL NOTES

2.1. Introduction

The developmental work carried out on the SIFT instrument during the course of this thesis project falls into two distinct categories : mechanical modifications, and, electronic/software modifications. The mechanical modifications were undertaken at the start of the work described in this volume, and the electronic/software changes were made sometime later.

The mechanical, or structural, changes to the instrument centred around the change from an on-axis ion source to an off-axis source. Some modifications were also made as preparation for the installation of drift rings into the flow tube. Although the use of the drift rings was eventually put on hold, the problems encountered in these modifications will be mentioned briefly.

The modifications to the electronic and software aspects of the instrument concerned the neutral flow and ion count measurement systems. The changes were made to allow the instrument to be operated, efficiently, by one person. The measurements of both the neutral flow rate and the ion count could then be made concurrently by computer and recorded onto magnetic disk for later analysis.

2.2. Mechanical and Structural Modifications to the SIFT

2.2.1. The New Ion Source

At the start of this work the Canterbury SIFT possessed an on-axis ion source. The ion detection system used an off-axis particle multiplier. Ions sampled from the flow tube, were mass analysed by the downstream quadrupole mass filter, then deflected by a deflection electrode towards a channeltron type continuous dynode particle multiplier.

A new ion source was produced and installed. The ion optics for the new source were designed by Petrie [Petrie (1991)] using the SIMION program. The new source was housed in a chamber made by aluminium plates screwed and glued with Loc-Tite adhesive. A schematic diagram of the new SIFT configuration is shown in Figure 1-2.

The installation of the ion source allowed for the installation of a new venturi inlet. This was tested by measuring the rate constant for $Ar^+ + O_2$, at different helium flow rates. The rate was the same, or within the experimental error, for each flow. This indicated that the venturi was working correctly.

At the same time as the ion source and venturi inlet were changed, the downstream region of the SIFT was modified. The SIMION program was used to investigate the possibility of improving the downstream ion lenses. The results of the investigation indicated that the system was probably as efficient as any designed using the program would be, given the geometric constraints of the nose cone assembly.

The use of an off-axis ion source greatly reduced the probability of photons from the ion source producing extraneous counts on the particle multiplier. The deflection electrode was removed, and the particle multiplier mounted on axis. Significant background noise was picked up from the RF supply to the downstream quadrupole. In an effort to reduce this noise, the multiplier itself was housed in an aluminium can, and the leads from the multiplier to the shielded connection on the vacuum flange were encased in copper sheet.

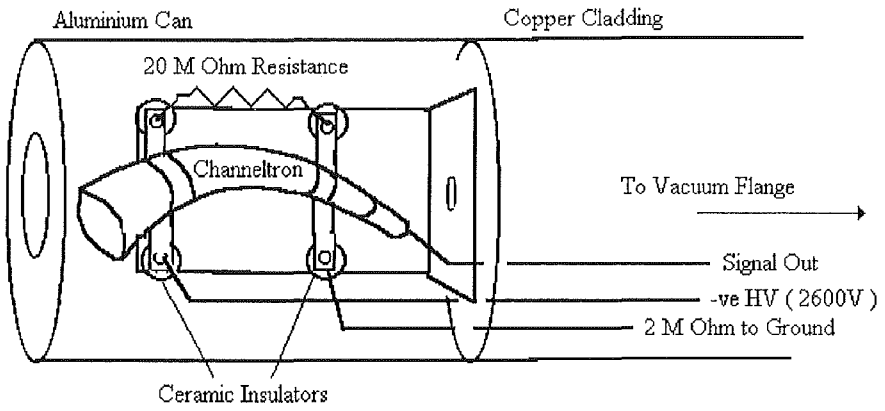

Figure 2-1. Schematic diagram of the on-axis particle multiplier system used in the SIFT.

The insulation of the signal leads reduced the noise due to RF pick up by the bare leads within the vacuum system. The leads external to the vacuum system were also very sensitive to RF noise from the quadrupoles. The exact positioning of the leads, and the preamplifier and discriminator units themselves, could dramatically change the RF noise level.

2.2.2. Preparations for Drift Tube Operation

While the installation of the tube was not carried out during this work, the components are ready to be assembled. Two structural modifications were made to the

SIFT in preparation for the installation. Both modifications were made to allow components to be insulated from the frame of the SIFT.

Perspex insulators were used to isolate the nose cone from the surrounding flanges. "O"-rings were used to provide a vacuum tight seal between the perspex washers and the stainless steel flanges.

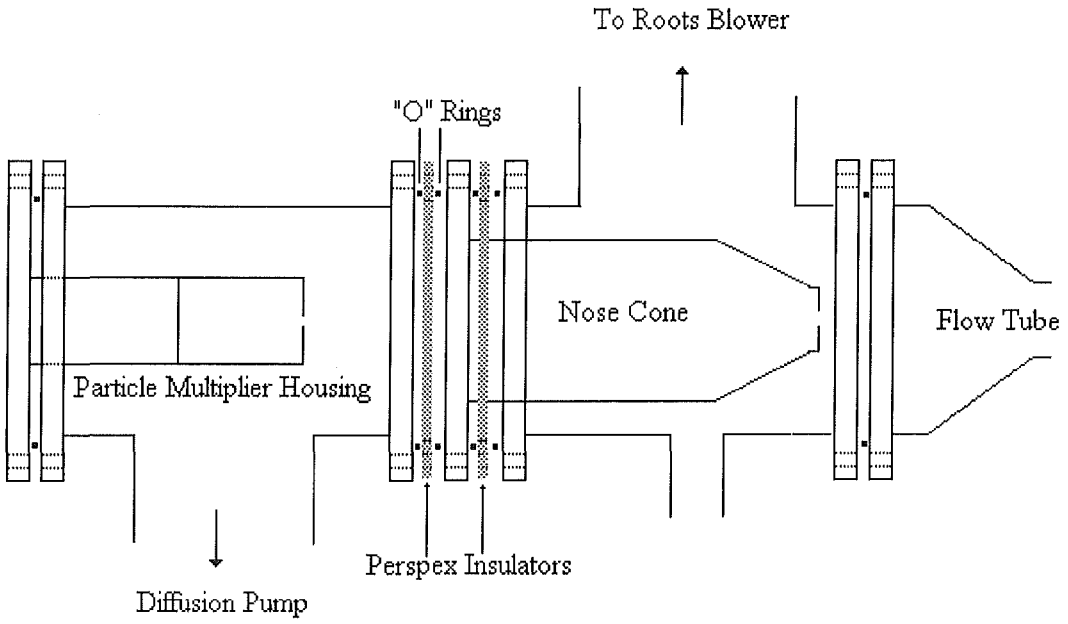

Figure 2-2. Schematic of the SIFT downstream region: showing the use of Perspex insulators to isolate the nose cone from the chassis.

The neutral reactant inlets were also replaced. The old neutral inlets were simply tubes that protruded into the centre of the flow tube. These inlets required a significant end correction to be made when calculating a rate coefficient.

The new inlets were of a ring shaped design, with small holes pointing upstream for admission of the neutral. The metal rings were insulated from the flow tube body a section of pyrex tube. The inlets would have come into contact with the drift rings, hence the need to electrically isolate them from the tube.

After replacing the old inlets with the new insulated models, it was found that the ion signal on the particle multiplier had vanished. Using a probe attached to a picoammeter to measure the ion current, it was found that the ions were not able to get past the new neutral inlets. The problem was due to a positive charge building up on the insulated metal surfaces. Grounding wires soldered from the flange to the ring solved the problem.

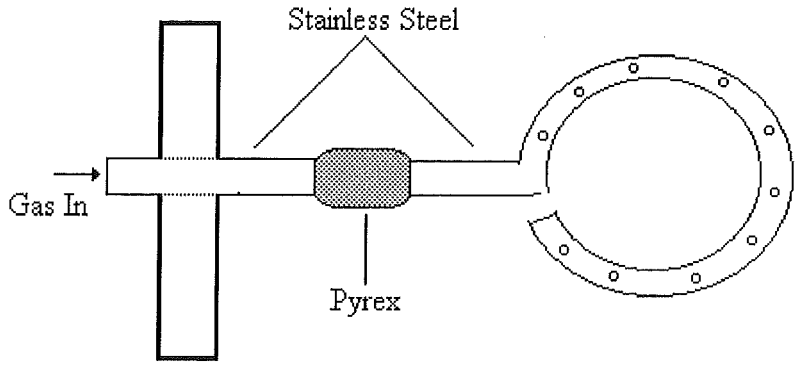

Figure 2-3. Schematic of an insulated neutral inlet before the surface charge problem was solved.

The new inlet design was found to work well, without an appreciable end correction.

2.3. Neutral Flow Rate Measurement

The neutral flow rate is required for the calculation of the rate coefficient, as the coefficient is given by the slope of $\ln[A^+]$ vs Q_n. The neutral flow rate can be found by measuring the rate at which the pressure of the neutral in a calibrated volume changes with time. The Canterbury SIFT has two neutral reagent inlets which can be used to measure the flow of neutral into the tube (and further neutral inlet without such facility, but which is used if a reagent is required for example to form a reactant ion for example by charge or proton transfer from an injected ion). Both reactant neutral inlets are similar in design (for more detail see [Knight (1986)]) as shown below.

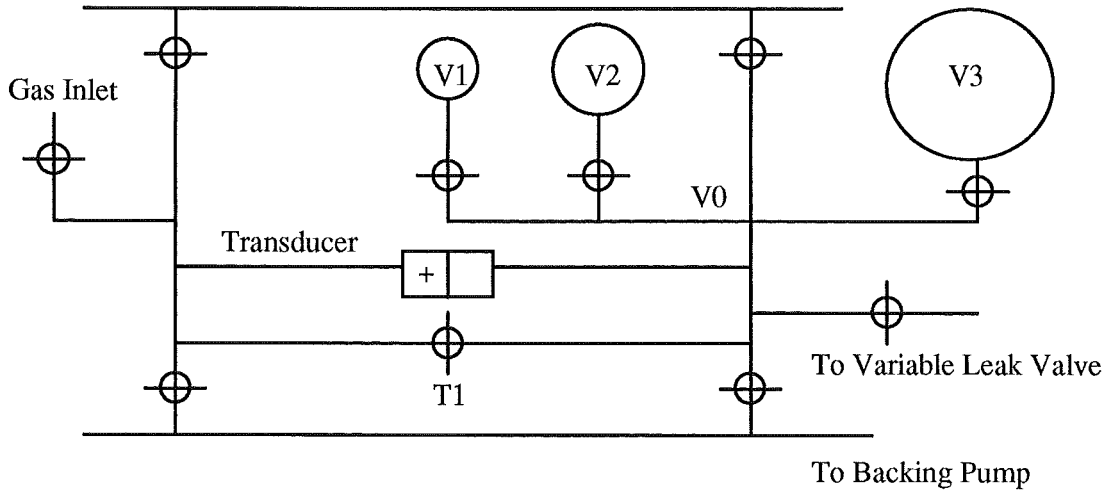

Figure 2-4. Schematic of neutral inlet line: showing the layout used in the SIFT.

As shown in Figure 2-4, the neutral inlet line is designed in two separate regions, connected by a tap T1. The required neutral can be admitted to both sides of the system

from the gas inlet by opening tap T1. The right hand side of the system is connected to the flow tube via a Varian 951-5106 variable leak valve equipped with facility (on the flow tube side of the leak valve) for a He flush to carry the neutral to the flow tube. The right hand side of the line consists of a number of calibrated volumes V0 to V3, so that the volume of that side of the system is known for any combination of calibrated volumes used. A Validyne DP 15.20 differential pressure transducer is placed between the two sides of the system so that with T1 closed the change in pressure in the right hand side due to neutral flow into the tube can be measured. By altering the volume of the right hand side different flow rates can be achieved while still operating the Validyne transducer in its optimal range. Too fast a pressure drop causes the transducer to go off scale, too slow a pressure drop cannot be measured as accurately.

2.3.1. Procedure FLOWREADER

In order to accurately measure the flow rate of neutral it was required to find the rate of change of pressure with time as accurately as possible during the period that the ion count was measured. As described below, the ion count could be measured by dedicated hardware in the background while the computer could measure the neutral flow in the foreground.

The PCL-718 High performance Data Acquisition Card for the SIFT laboratory's 286PC was used. The software to control the measurement was written in Microsoft QuickBASIC 4.5 for two reasons. Firstly to allow the procedures to operate within the SIFT program already used in the SIFT laboratory, secondly to take advantage of the driver routines included with the PCL-718 card. Figure 2-5 shows a flow diagram of the procedure.

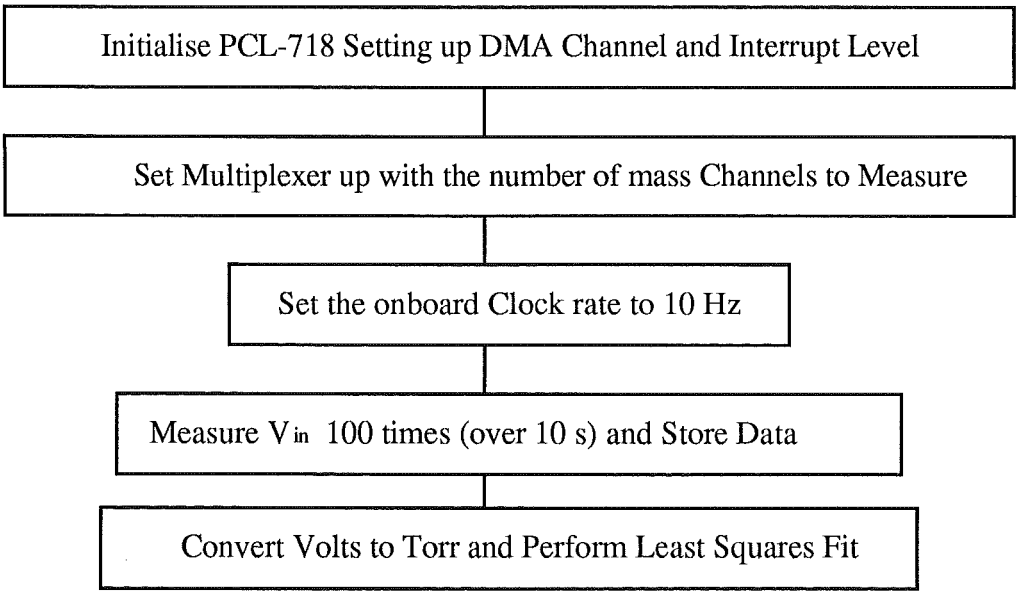

Figure 2-5. Flow diagram of procedure FLOWREADER.

The procedure FLOWREADER was tested by using the HP3314A function generator from the ICR laboratory to generate triangular wave forms of different slopes. The least squares fit over a hundred voltage points proved very accurate. It is likely that the uncertainty in the value of the neutral flow due to measurement error has been eliminated, the remaining uncertainty is that due to assuming that the flow is constant over the period of the measurement.

2.4. Development of a New Ion Counting System

The concentration of ions reaching the end of the flow tube is required for a rate determination. In practice concentration cannot be measured instantaneously using the particle detection system used, so the number of ions reaching the particle detector over a period of time is the actual quantity measured. The flow of neutral and other experimental parameters are assumed to be constant over the period of time taken to count the ions.

The particle detection system used in the Canterbury SIFT is a channeltron type particle multiplier. This was remounted on the axis of the flow tube when the ion source was changed from on-axis to off-axis. The channeltron itself is mounted on ceramic stand off insulators on a moveable plate within an aluminium tin. The mouth of the channeltron is held at a large negative potential (-2600 V) supplied by a Spellman high voltage supply. Signal output from the multiplier is in the form of series of current bursts. These are converted into voltage pulses by a preamplifier and the pulses compared to an adjustable DC level by a discriminator circuit. The discriminator sends TTL pulses corresponding to the ion events to the pulse counting circuitry. A block diagram of the signal handling process is shown in Figure 2-6.

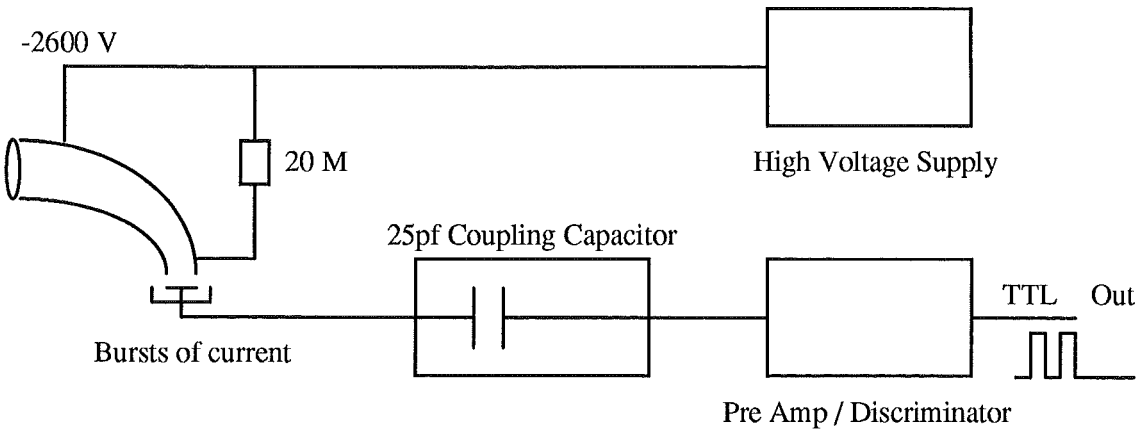

Figure 2-6. Block diagram of the ion detection system used in the SIFT.

The existing pulse counting circuitry was based on a circuit equivalent to an Extranuclear Laboratories Model 275-K2 ratemeter. This unit could be set to count the TTL level

pulses over periods of 1, 10, or 100 s. The output was to an LED display and also as a DC analog signal which could be visualised on a storage oscilloscope. The capacity to visualise the ion concentration on the oscilloscope greatly aids the tuning of the various ion optics and the quadrupoles. However, the ion count had to be manually recorded in a notebook and later entered, together with the flow measured at around the same time into a data file for computer analysis. The system was most inconvenient, prone to error, and required more than one person in order to make a rate measurement.

The purchase of a 286 based computer made it feasible to rewrite the software that was used to run and analyse an experiment. Mark Morrison developed a program, SIFT, using Microsoft QuickBASIC that integrated all the previous software used within the SIFT laboratory [Knight (1986)],[Petrie (1991)] in one interactive package. Unfortunately the software proved unable to record accurately the ion counts recorded by the ratemeter or the neutral flow as measured by the Validyne capacitance manometer.

After some investigation it was found that the ratemeter circuitry was at the heart of the problem and it was decided to develop a new digital ratemeter rather than attempt to adapt the old one.

A New Digital Ratemeter

The new digital ratemeter was designed in collaboration with Neil McCracken of the electronic workshop. The PC controlling the SIFT was equipped with a PCL-718 high performance data acquisition card from PC-LabCard. The card contained three Intel 8254 programmable timer/counters. The two dedicated counters were used for the measurement of the neutral flow by the FLOWREADER procedure. The remaining programmable timer/counter could be set up as a programmable one-shot. Given a suitable clock input the 8254 could be software-triggered, the output going low until a preset number of counts had been received, whereupon the output would be sent high. The 8254 could thus control a simple TTL counter. Since the 8254 was not dedicated within the PCL-718 this did not affect the foreground operation which was measuring the neutral flow.

Thus the principal components required for the new ratemeter circuitry were, a suitable timebase oscillator, a TTL counter, a suitable data multiplexer to allow the PC to read the data from the counter, and the 8254 on board the PCL-718.

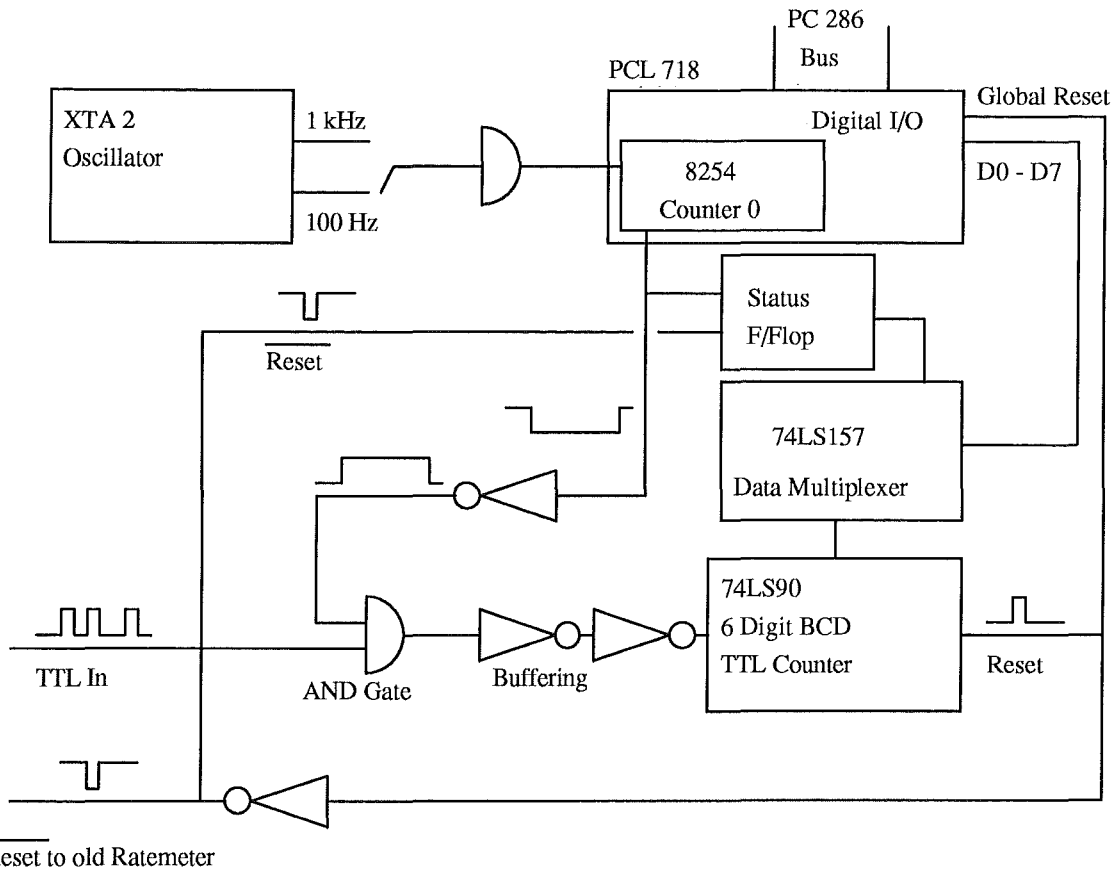

Figure 2-7. Block diagram of the new digital ratemeter system for the SIFT.

Overview of the Operation of the Digital Ratemeter

The digital ratemeter is designed to operate in the background. That is it can be set up by appropriate software controlled OUT statements to the controlling registers and the external circuitry, and triggered by a software OUT statement so that it will carry out the count for the specified time without troubling the CPU. Having completed the count the ratemeter waits until the CPU polls the status indicator. If the indicator shows that the measurement is complete then one of the digital input/output bytes of the PCL718 card can be used to read the count as a sequence of Binary Coded Decimal (BCD) digits from the data multiplexer. Operating in the background allows the CPU to control the dedicated counters and A/D converters on the PCL718 to measure the neutral flow, greatly simplifying the measurement process.

Operation in Detail

To understand the operation of the ratemeter in detail it is helpful to refer to the block diagram of the set up in Figure 2-7.

The principle of operation is that the incoming TTL pulses from the preamplifier and discriminator are coupled to the BCD counter via an AND gate. Only while the other channel input to the gate is high will the pulses be counted. When counter 0 on the PCL718 is set up as a programmable oneshot it will send its output low upon receiving an appropriate trigger and keep it low until it has counted a preset number of counts, whereupon it will go high. The output from the counter is thus inverted before it is used to control the and gate, allowing the TTL pulses to be passed only while it is still counting.

The input pulses to the 8254 Counter 0 are supplied by an external oscillator switchable between 100 Hz and 1 kHz. The 8254 is a 16 bit counter which can be set to count between 2 (2^1) and 65536 (2^{16}) counts. Depending on the setting of the oscillator this allows the ratemeter to count for periods from 2 ms to 655.36 s. The time period used in normal SIFT operation is 10 s.

The high-going pulse at the end of the counting period is also used to control the status flip flop. When the channel goes high the flip flop also goes high, indicating that the measurement is complete. The state of the flip flop can be found by polling the data multiplexer. The status flip flop is set low again by a software controlled OUT statement once the count has been read.

The software can control the external devices by writing to the PCL718 digital output low byte and reading from the PCL718 digital input low byte, which share the address Base + 3.

The operation of the new ratemeter set up, and the interaction of the internal and external devices, can be seen in the following flow diagram (Figure 2-8) of the procedure used to make a complete measurement, of both the neutral flow and the ion count during that period.

EXTERNAL DEVICES SOFTWARE CONTROL

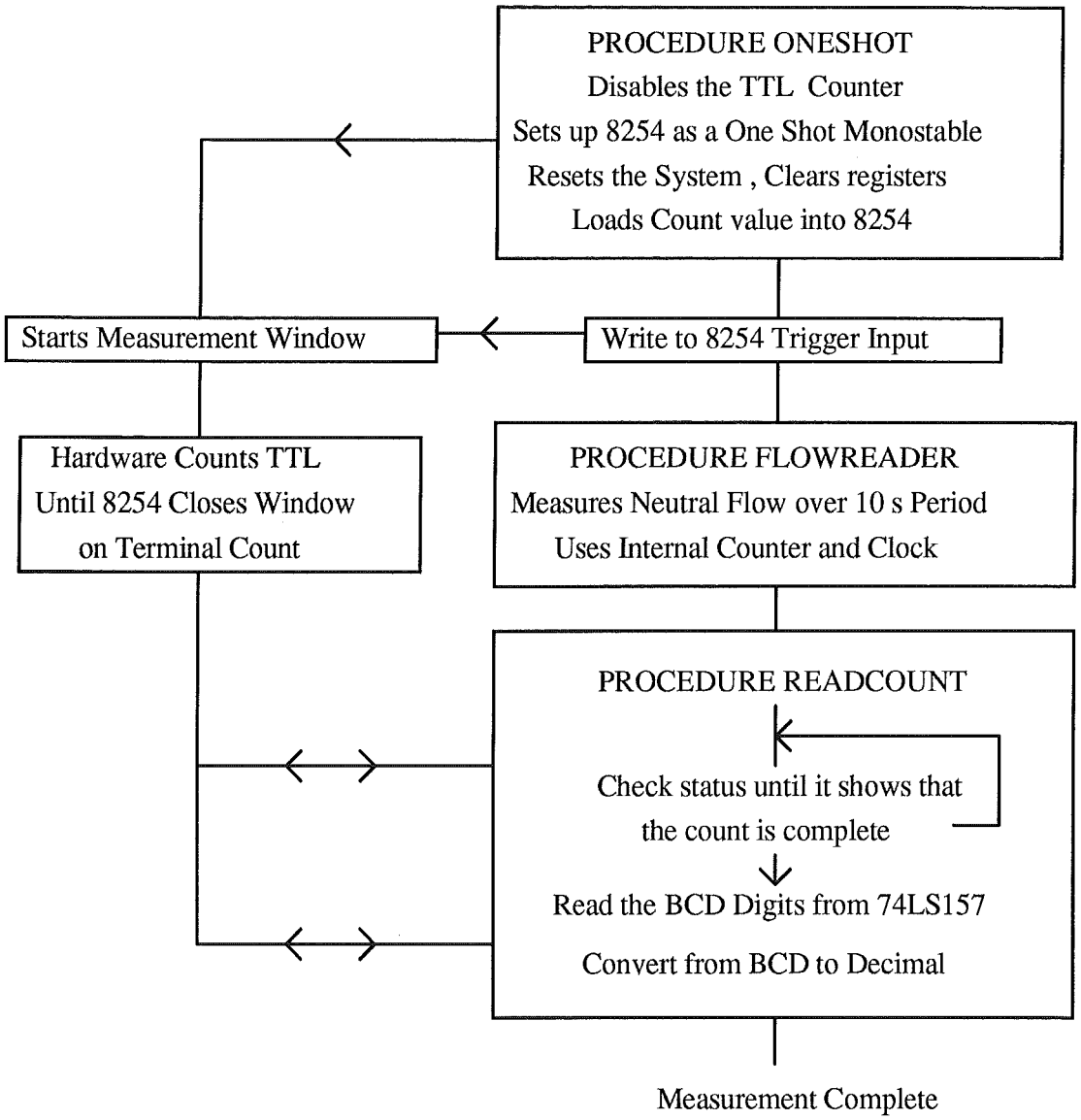

Figure 2-8. Flow diagram of a SIFT measurement.

The new procedures for controlling the neutral flow and ion counting were written in QuickBASIC and incorporated into the SIFT program. The changes required were made without altering the interactive nature of the program as a whole. The modified program was recompiled and is used as SIFT2D, an indication of the number of modifications that were made.

Using SIFT2D : A Calibration Experiment

Several reactions are used for calibration purposes, but two reactions that have been studied in flow tubes are the charge transfer reactions of Ar^+,

$$Ar^+ + O_2 \rightarrow Ar + O_2^+ \qquad (2.1)$$

and

$$Ar^+ + CO_2 \rightarrow Ar + CO_2^+ . \qquad (2.2)$$

In order to check that the SIFT2D program was working correctly, the calibration reaction of Ar^+ with CO_2 was carried out. Three runs were carried out with results of 5.2, 5.2, and 5.3×10^{-10} cm^3 s^{-1}.

The literature values for the bimolecular rate vary from 4.2 to 7.6×10^{-10} cm^3 s^{-1} as tabulated by Ikozoe et al [Ikozoe et al (1987)]. The recent compilation by Anicich [Anicich (1993)] gives only one value for the rate, that the author believes to be the best estimate, this is 4.8×10^{-10} cm^3 s^{-1}. The average value as determined on our SIFT of 5.2×10^{-10} cm^3 s^{-1} is within the uncertainty quoted by Anicich of 15%, but more important is the excellent straight line obtained for the measurement. While the measurement of ion counts by the new system is easier than the manual pen and paper system, it is not inherently any more accurate. The use of the 16 bit A/D converter at 10 Hz, however, makes the measurements of flows much more accurate than was previously possible, especially where the flow is small. Figure 2-9 shows a typical decay plot obtained using the program SIFT2D.

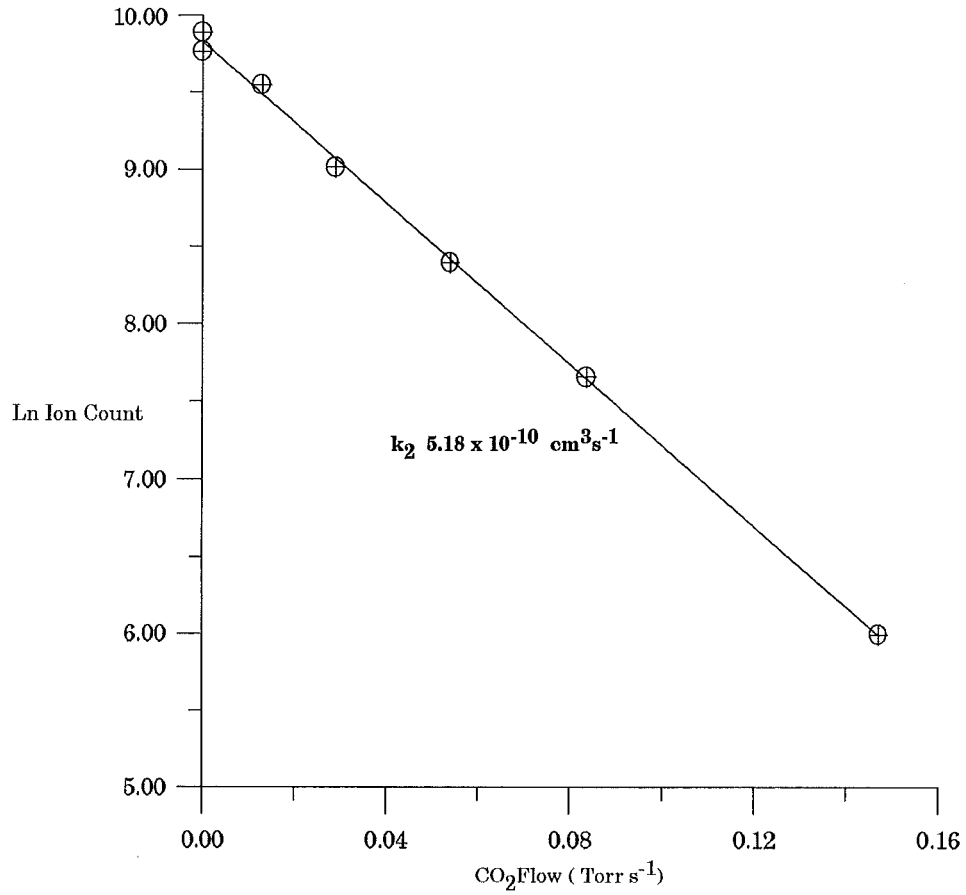

Figure 2-9. Decay of Ar^+ with CO_2 flow measured on the SIFT: using the SIFT2D program to measure the neutral flow and the ion count.

New Developments in Digital Technology

As with many areas of technology the field of digital electronics is continually developing. In fact digital technology that was considered state of the art at the time this work was started are now obsolete. An example of the progress is that the six 74LS90 BCD counters cascaded in the ratemeter circuitry could now be replaced by a single IC, the LS7006 24 bit multimode counter. While this would result in a simplified circuit it would not represent a gain in accuracy or utility.

An area that could present important benefits to the experimenter is analog to digital conversion; the 16 bit 60 kHz board used in both the SIFT and ICR interfacing cost around NZ$1000, at the present time a 14 bit 25 MHz board costs less than NZ$400. Although the current SIFT configuration may not require the ultra fast performance that is becoming available, the plans are under way for the installation of drift rings to create a Selected Ion Flow Drift Tube. With suitable shuttering it could be possible to measure arrival time distributions as a function of drift voltages. This would possibly have significant implications in the study of isomeric ions. If this method is feasible it would require a suitably fast signal analysis. The rapid development of fast A/D technology may allow the experimenter to do away with the use of expensive multi channel analysers or boxcars.

CHAPTER THREE

MODIFICATIONS TO THE ICR INSTRUMENT

3.1. Introduction

The ICR instrument used in this work was loaned to the University of Canterbury by the Jet Propulsion Laboratory. The equipment loaned included the magnet and the cell itself, together with the associated high-vacuum pumps and fittings. Some of the electronic components required to obtain rate measurements were obtained with the instrument.

In the course of this work, various modifications and adaptations were made to the instrument. A considerable number of electronic components were procured through purchase, and several were designed and manufactured within the department. Changes were made to both the cell and to the vacuum system. Software was developed to allow for computer control of ICR measurements.

Development of the instrument was carried out in two phases. The first phase was the installation of the electronics required for the drift and trap mode experiments. This phase included the installation of the capacitance bridge detector, the manufacture of some assorted electronic devices, and changes to the coupling of the cell plates.

The second phase of development centred around adapting the instrument to allow for the determination of rate constants using trap mode experiments. This phase included the development of suitable software and interface hardware. Significant changes were also made to the cell and to the vacuum system.

The actual attainment of *reliable* trap mode results took a considerable amount of trial and error. Two factors were found to be especially crucial. The first was the use of an end plate to close the equipotentials in the ion source. The second factor was the allowance for out gassing of water from the Vespel material used in the construction of the cell itself.

Several problems, and the actions required to remedy them, are also described here. The on-going problem of obtaining quantitative double resonance ejection is also discussed. Rather than discuss the developments in chronological order, the work is reviewed under the headings ; electronic and mechanical modifications, drift mode operation, and trap mode operation.

3.2. Description of the ICR system

3.2.1. The ICR cell

The cell of the ICR instrument, that was kindly lent to the Canterbury laboratory by the Jet Propulsion Laboratory, was a three section drift cell based on the Syrotron design. The Syrotron cell design was produced by Varian associates of Palo Alto, during the late 1960's [Beauchamp et al (1967)]. Several different variants of cell were produced, but most share similar principles of construction.

The cell was comprised of 12 metal plates fixed by screws to two Vespel blocks. (See Figures 3-1 and 3-2.) The cell plates were rhodium flashed, polished copper plate. The upper Vespel block was firmly screwed to two stainless steel supports. All the stainless steel components used were non magnetic, since the cell was of course placed in a strong magnetic field. The supports were in turn affixed to two supporting rods that screwed into the main 6" flange. The main flange supported the weight of the cell and carried all the feedthroughs for the voltages and signals to and from the cell.

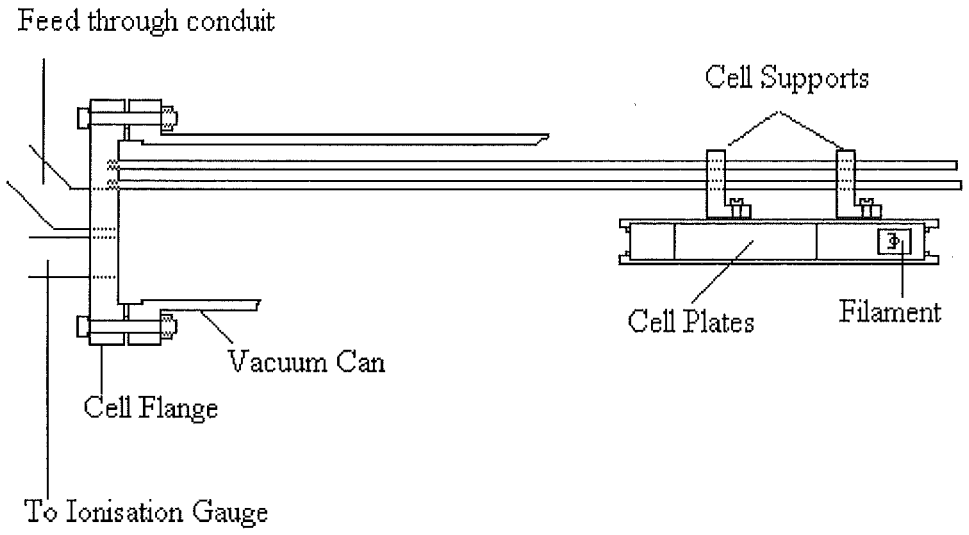

Figure 3-1. Diagram of the ICR cell and mounting of the cell on stainless steel supports fixed to the main flange.

The dimensions of ICR cells vary somewhat, with a square cross section being a common configuration, although rectangular sections are also used. The Canterbury cell has a rectangular section with the internal dimensions of the cell being a height of ½" and a width of 1" (The use of the non SI imperial measure is common amongst machinery

manufactured in the US up to comparatively recent times, so where appropriate inches will be used).

The source region of the cell is 2" long, the resonance or analyser region 3" long and the total ion current region is 1" long. The Cell resembles that of the hybrid drift trap cell used by McMahon and Beauchamp [McMahon and Beauchamp (1972)] except that there are separate trapping plates in the source and analyser regions. The two trapping plates in the analyser region were shorted, and so were the trapping plates in the source region. The trapping plate on one side of the total ion current region was connected to the analyser trapping plate on that side of the cell. The upper and lower plates in the total ion current region were connected to the upper and lower analyser drift plates respectively. The remaining plate in the total ion current region was connected via a feedthrough to a BNC on the cell flange from which the ion current on that plate could be measured.

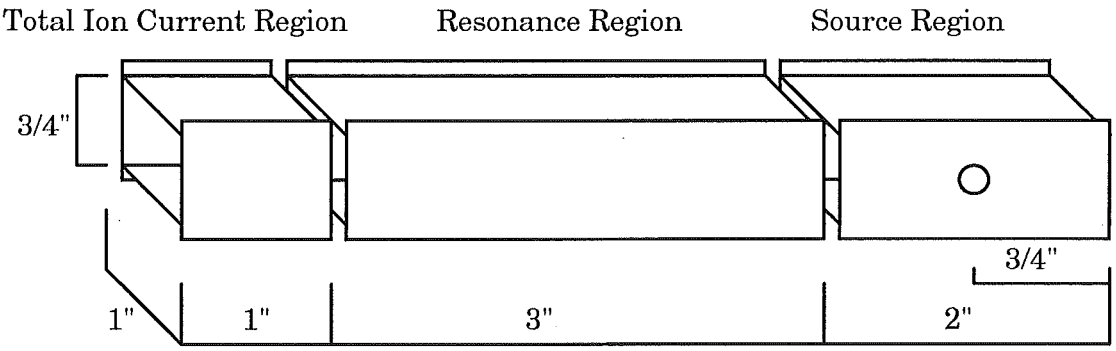

Figure 3-2. Dimensions of the Canterbury ICR cell.

3.2.2. The Vacuum System

The system consisted of a vacuum can enclosing the ICR cell which fitted between the poles of the electromagnet, and an inlet line for the introduction of neutral gases.

The main vacuum can was pumped by a Varian M3 water cooled diffusion pump with a water cooled baffle between the pump and the cell. Backing pumping was provided by a Welch Duo Seal mechanical pump. The pressure in the can could be measured by both ion gauge and capacitive manometer (Baratron™).

The ion gauge was of the Bayerd Alpert type mounted on a flange for ease of replacement. Most of the time the ion gauge controller used was a Perkin Elmer Ultek digital gauge control.

The manometer was a MKS Baratron™ 315 BHS -1 head with a MKS Baratron™ Type 170M-6A electronics unit. The actual details of pressure measurement in the cell will be described below. The backing pressure in the line between the mechanical pump and the diffusion pump was measured with a Granville Phillips

thermocouple gauge. A trap between the mechanical pump and the diffusion pump prevented backfilling of the line with mechanical pump oil in the event of pump failure.

The inlet line was pumped by a Veeco 2" air cooled diffusion pump backed by a Welch Duo Seal mechanical pump. The backing line was arranged to allow two neutral gases to be separately admitted to the vacuum can through two Varian sapphire seal variable leak valves. The pressure of each neutral gas (or the pressure in the backing line) was monitored by two thermocouple gauges controlled by the Ultek gauge controller.

3.2.3. The Magnet System

The magnet system was that used in the Syrotron mass spectrometer produced by Varian. The field was provided by a 9" V3400 water cooled electromagnet. A Varian Fieldial Mark 1 field regulated magnet power supply was used. The field strength was measured by a Hall probe attached to one pole face with double sided Sellotape™. The field could be swept using the Fieldial controller, although the installation of a bridge detection system made rf frequency the easiest component to vary to get a mass spectrum. The magnetic field used for all the quantitative experiments in this work was 13 ± 0.3 kG.

3.2.4. Electronic Components

The power supply of the original Syrotron console was intact, and a pulse sequence and plate voltage control unit built by Dr V Anicich was attached. The filament current was produced by a Hewlett Packard 6281A DC power supply. The filament emission onto the collector was measured by a Keithley Instruments 414A picoammeter. The original marginal oscillator detector was still attached, but when the system was installed a capacitance balanced bridge detector [Wronka and Ridge (1982)] was supplied. In order to process the signals from the instrument an EG&G Princeton Applied Research 5104 Lock in Amplifier was purchased. The rf signal was provided by a Hewlett Packard 2314A function generator purchased specifically for this instrument. The output of the lock in amplifier could be viewed on a Hitachi V-152B 15 MHz oscilloscope and recorded using a Hewlett Packard 7015B X-Y recorder. The total ion current was originally measured by a Carey 401 Electrometer.

3.3. Electronic and Mechanical Modifications to the System

The modifications made to the original system will be dealt with largely in chronological order. The first priority was to ensure that the system would produce a

drift mode signal from which an accurate rate determination could be made. This goal was achieved and the next step was decided to be to achieve trapped ion operation. The final arrangement of the electrical and electronic components of the system is shown, in much simplified form in the block diagram below.

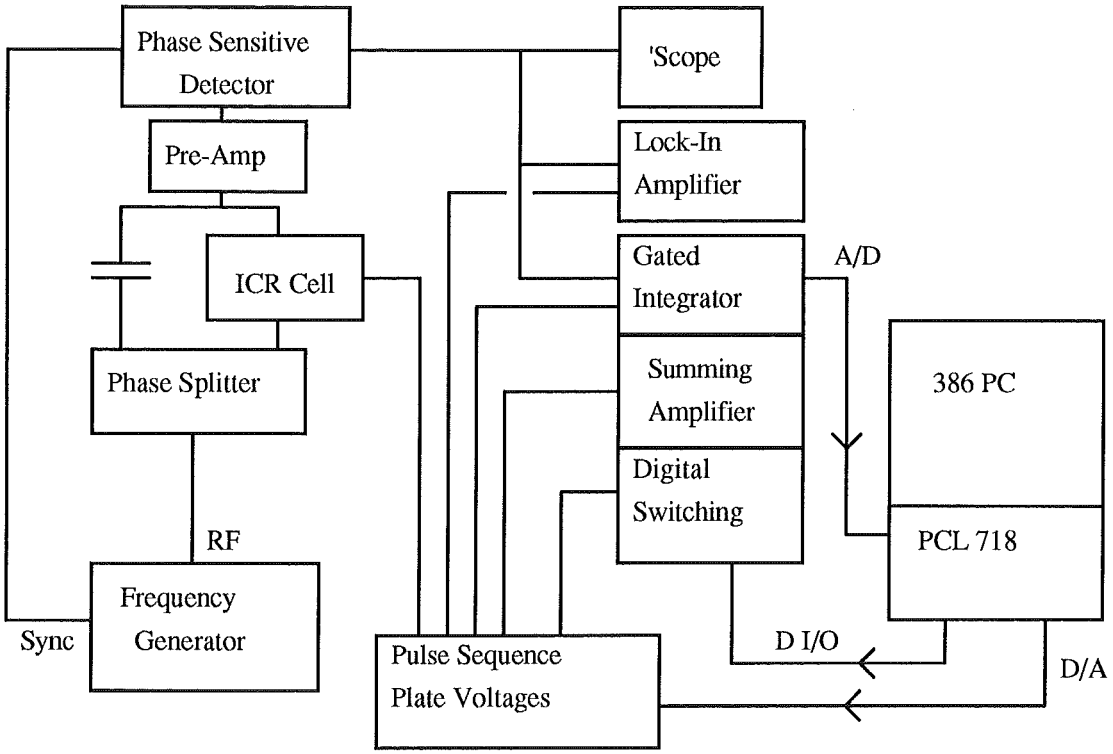

Figure 3-3. Simplified block diagram of the ICR: showing the components and their interconnection.

3.3.1. Installation of a Capacitance Bridge Detection System

The frequency swept bridge detector arrived in three separate units ; an oscillator summer and phase splitter, a bridge preamplifier, and an RF phase sensitive detector. A balance capacitor was also included. The electrical acceptance checks were carried out as per the manual.

The phase sensitive detector showed a significant variation in DC baseline with frequency. While this variation is undesirable it does not produce a frequency dependent effect on the measured signal.

In drift mode, the lock-in amplifier measures only that signal that is modulated at the same frequency as the reference input (in this case 40 Hz, with the filament being modulated at that frequency), the baseline is constant, and in effect is not counted.

In trapping mode, the output of the phase sensitive detector under the detect pulse is integrated, using either a commercial gated integrator card, or more recently a fast analog to digital conversion card with onboard counter (see below). The signal obtained is corrected by subtracting the background signal obtained by integrating the voltage under the detect pulse with the trapping plates held negative.

The next stage of the installation of the bridge detector was balancing the bridge. The driving oscillator, the HP 3314A, was used in scan mode. The frequency was swept over the range expected to be used for experimental observations (around 2 MHz to 100 kHz). The 40 Hz square wave from the pulse sequence unit was used to modulate the rf signal to the phase splitter. The output from the phase sensitive detector was visualised on the oscilloscope.

By adjusting the settings on the balance capacitor until the baseline was as close as possible to flat, then increasing the amplitude of the oscillator output and repeating the process the bridge was brought as close as possible to balance. During this process it was vital to use either a television tuning screwdriver with a plastic shaft, or more practically a sliver of glass fibre circuit board with a bevelled edge, to adjust the variable capacitors that made up the balance capacitor, the capacitance of a metal screwdriver makes careful adjustment impossible.

It was not possible to bring the bridge to balance over the entire recommended frequency range, which was , 1.5 MHz to 3 kHz. However, for most of the systems studied in the ICR the variation of mass between reactant and product was from 12^+ to 100^+. This mass range corresponds to a frequency range of 1.6 MHz to 199 kHz at a magnetic field strength of 1300 Gauss which was the field strength most often used. Over the smaller frequency range it was easier to adjust the bridge so that the response of the phase sensitive detector was relatively flat and the offset close to zero. At 1 V amplitude of the driving oscillator, the detector baseline over the frequency range 199 kHz to 1.6 MHz would typically show a variation of 50 mV from end to end. More important than the variation in baseline was the problem with 50 Hz noise on the signal channel that was experienced. In order to overcome this noise various grounding schemes were tried, more by art than science. Eventually by ensuring that all of the measurement system, ie driving oscillator, oscillator summer, preamplifier and phase sensitive detector were all plugged into and therefore earthed by the same mains socket the worst of the noise was removed. It was noted that the improvement in the level of noise was almost entirely independent of the length (m) of earthing strap used.

3.3.2. Gated Integrator / Digital Switching / Summing Amplifier Unit

In order to allow for computer control of the ICR measurement process, a multi purpose instrument panel was built. The device was constructed from a design by Anicich. The construction was carried out within the department.

The Gated Integrator.

In order to measure a signal in the ion trapping mode it is necessary to measure the transient signal from the phase sensitive detector during the period of the detect pulse. During the detect pulse the ions are drifted from the source region where they have been trapped into the detection region. The signal that the ions produce while travelling

through the analyser region, can be integrated to give a value proportional to the number of ions. To perform this integration a commercial gated integrator, an Evans Model 4130, was purchased. The integrator required a variable gain input amplifier and output to both a computer analog to digital converter and to a chart recorder. The preamplifier had gain settings of 0.1, 0.2, 0.5, 1.0, 2.0, 5.0 × the input signal.

Digital Switching.

In order to allow the trapping mode measurement to be fully computerised a digital switching arrangement, using two solenoid switches was used. One switch would switch the input to the trapping plate voltage supply from +15 V to -15V allowing for the polarity of the plate voltages to be changed for baseline measurements and for quench pulses. The other switch would swap the input to the detect pulse between a manually adjusted potentiometer or a computer generated voltage. This input controlled the delay time.

The ICR pulse sequence unit was modified to allow for computer control via the digital switching. The trapping plate supply was set up to use only the voltage supplied by the digital switching unit. The delay time voltage was also derived only from the digital switching unit.

The solenoids could be controlled by either, operating the micro switches on the front panel of the unit, or sending TTL level signals to the BNC inputs at the rear. A distribution system was set up to allow four bits of the digital output from a PCL-718 card to control the solenoids. The software used to control the PCL-718 card is described below.

RF Summing Amplifier.

The third function of the multi purpose panel was to allow up to four rf signals one of which could be gated by a TTL level pulse to be mixed using a summing amplifier , a Burr Brown 3554 was the summing amplifier chosen and an AH0014 analog switch was used for the gating.

3.3.3. Addition of an End Plate in the Source Region, etc

The cell had been designed for use with a marginal oscillator detector, and the drift plates were capacitively coupled. In order to apply double resonance rf in both the source and analyser regions, and because the rf signal carries the plate bias it was necessary to replace the capacitive coupled connections with direct connections to the drift plates in both the source and analyser regions.

One of the most crucial modifications made to the instrument was the addition of an end plate to the source region. After many attempts to trap ions had failed, it was decided to try using a plate across the open end of the source region. Initially a stainless steel gauze was used. The gauze was spot welded onto a thin stainless steel frame and was electrically connected to ground. The assembly was not rigid, and was difficult to

arrange so that the gauze was flat. Results using the gauze were not promising, and it was removed.

Some time later, after further unsuccessful experiments, the idea of an end plate was revisited. This time a highly polished piece of 2 mm thick stainless steel was used. The plate was screwed into the Vespel block, and was electrically connected to the upper source drift plate.

At the same time that the end plate was put into place, a new plate voltage supply box was added. This box enabled the voltage on each drift plate to be independently varied, during the trap mode delay time. Thus, instead of remaining at ground, the plates could be set to an adjustable voltage.

Using the end plate in conjunction with the independent voltage controls, trapping signals were able to be detected. Later, after the problem of the large water background had been addressed, it was found that the individual voltage controls were not necessary if the trapping conditions were appropriate.

3.3.4. Filament assembly replacement

The filament assembly supplied with the cell comprised a Macor (Dow Corning Machineable Glass Ceramic) block which was screwed into position on one source trapping plate, the block was machined so that a fine screen lay between the filament and the cell. The filament used was 0.007" rhenium wire. The screen between the filament and the cell was used to modulate the transmission of electrons and is referred to as the grid.

Unfortunately, during a periodic servicing, the filament block was broken. Rather than machine a new filament block from Macor it was decided to use a new design of filament assembly. The major design requirements were; that the filament should be as easy as possible to replace, the grid and the filament should be insulated from each other and the cell so that a separate bias could be applied to each, and, that the whole assembly should be non magnetic.

It was decided to try the use of rhenium strip instead of wire for the actual filament, since the strip could last effectively indefinitely, obviating the need to replace the filament. At the time it was not clear whether or not the DC power supply, rated up to 6 A, could supply sufficient power to obtain emission from the strip.

An ion source from an obsolete instrument was obtained, and after a minimum of machining it was arranged to suit the design requirements. The filament strip was spot welded to two Rhodium spars insulated from the block by ruby washers. The block itself formed the grid and was insulated from the trapping plate and the supporting screws by Vespel stand offs.

Testing the filament showed that excellent emission could be achieved at only a slightly higher current than was used for the wire filament. A problem was that the

assembly was close to the wall of the can, and the grid was shorted to ground. This was solved by machining a block of Vespel that served as a spacer.

The use of the spacer had the added advantage of correctly locating the cell within the vacuum can. A consistent problem in the past had been locating the cell within the can with the floor of the cell normal to the pole pieces of the magnet. The cell had tended to move as the supporting rods could bend and twist while the cell was inserted into the can. The use of the Macor spacer solved this problem.

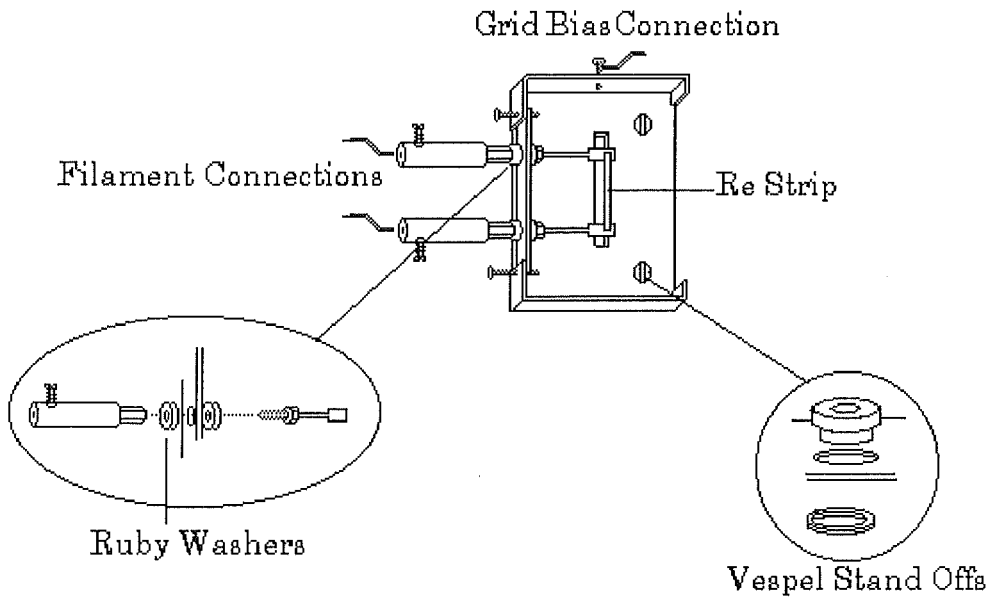

Figure 3-4. Diagram of the new filament assembly: after being adapted for use on the ICR.

3.3.5. Magnet cooling coil replacement

During operation of the instrument a catastrophic failure occurred in the water cooling jacket of the right hand electromagnet coil. The thin copper wall of the cooling jacket had over a period of time become eroded from the inside. Whether this erosion was by chemical action or by the action of particulate matter in the high pressure water supply was not clear, but the result was that the cooling jacket failed in a number of places. Attempting to patch the holes by using solder was not successful and a replacement coil was available at the time. A field repair was effected by soft soldering a length of 1 cm O.D copper tubing in a coil to the face of the copper cooling jacket. To the ends of the copper tubing plastic hose pipe was crimped which was fitted to the original cooling system. This expedient served well, and although the right hand coil ran hotter than the left hand coil no noticeable effect was noticed on the experimental performance of the system.

3.3.6. Water Background Problems

The inability to trap Ar^+ for reasonable periods was initially diagnosed as arising from factors to do with the cell plates or the voltages upon those plates. When the source end plate had been fitted, and separate adjustable voltage supplies for all the drift plates had been installed, and the cell was carefully aligned with the electron beam perpendicular to the magnetic field, the problem remained. Looking at the trap mode signal it was clear that the Ar^+ ion was being removed from the cell, but it was not by physical processes, it was by chemical means. Sweeping the analysing frequency revealed that there were significant trapped ion populations at 18^+ and at 19^+. The 18^+ signal decayed with time as did the signal at 40^+, however the signal at 19^+ increased before decaying away at longer times.

The reaction of $Ar^+$with water has been comprehensively studied and occurs rapidly with a rate coefficient of 1.6×10^{-9} cm^3 s^{-1} [Anicich (1993)];

$$Ar^+ + H_2O \rightarrow H_2O^+ + Ar \qquad 0.80 \qquad (3.1a)$$

$$\rightarrow ArH^+ + OH\,. \qquad 0.20 \qquad (3.1b)$$

The reaction of H_2O^+ with water is also well studied and produces 19^+ with a rate coefficient of $1.85 \times 10^{-9} cm^3$ s^{-1} [Huntress and Pinizzotto (1973)];

$$H_2O^+ + H_2O \rightarrow H_3O^+ + OH \qquad (3.2)$$

The reactions above clearly explained the failure to trap Ar^+ for a reasonable period. The question arose of how did the water get into the cell. The pressure was not remarkably high, being less than 7×10^{-7} Torr, and although the water signal was present there was no sign of N_2^+ or O_2^+. The signs were that there was some material in the cell from which water was desorbing over a period of time.

In order to determine which of the contents of the vacuum can were causing the problem a simple experiment was carried out. Parts of the cell assembly were removed, the system pumped down for a period of hours, the pressure was then measured and the process repeated, this time with a different part of the cell assembly. The results are shown below.

Table 3-1.. Determining the source of the water background pressure.

Contents of the Vacuum Can	Pressure (Torr)
The Entire Cell Assembly	5×10^{-7}
Nothing	1×10^{-7}
Insulation Material	1×10^{-7}
Cell Alone	4×10^{-7}
Metal Parts of Cell	1.5×10^{-7}
Vespel Block	6×10^{-7}

While the experiment was only a rough series of measurements, it showed clearly that the problem was the Vespel block upon which the cell plates were fixed. This block was an integral part of the cell and would be difficult to replace. There were two choices, firstly to replace the Vespel with another suitable insulator, secondly to find a way of minimising the water background.

Addressing the first choice, the out gassing properties of several common insulators were examined using a Spectramass Dataquad mass spectrometer. The quadrupole was fitted to the ICR vacuum can using the flange which normally carried the feed throughs to the cell. The residual gas mass spectrum was observed on the built in display. Although the unit was equipped only with ion current rather than particle multiplier detection it worked well enough for a qualitative assessment. The materials examined were Vespel, Macor [machinable ceramic from Dow Corning], Teflon, and a variety of Teflon filled with mica for structural strength. The residual gas analysis showed that the Teflon varieties released more N_2 and O_2 than H_2O, but still almost as much H_2O as the Vespel. The Macor used showed no tendency to out gas.

Clearly the best choice for a new insulating material would be Macor, however the machining required to construct a suitable component from Macor was considered to be prohibitive in terms both of time and expense. This left only the second option, to minimise the existing water background.

The only way to remove the water from the cell was to bake the cell for a number of days. It was found that, after a week of constant bake out, the water level in the cell was down to an acceptable level. Running the filament at a low emission and keeping the ionisation gauge filament on were important to prevent condensation on these components during the bake out period. The water background means the system must be permanently pumped out, since from atmospheric pressure it is at least a week before any trap mode measurements can be made.

3.4. Drift Mode Operation

3.4.1. Drift Time Measurement

In order to obtain a rate constant in a drift mode experiment it is necessary to accurately know the time taken by the ions to drift through the cell. The separate drift plates in the source and analyser region mean that the drift field is not homogeneous along the length of the cell. Thus, in practice, what is required is the time taken for the ions to drift through the source, and also the time taken by the ions to drift through the analyser or resonance region. Although the drift velocity can be calculated given the electric and magnetic fields it is much easier and more accurate to determine the drift times empirically.

The method used to determine the ion transit times is based on that developed by McMahon and Beauchamp [McMahon and Beauchamp (1971)]. In this experiment a pulse sequence is used. The filament is pulsed while the instrument is in drift mode. Immediately following the ion formation pulse the ions move through the source region towards the analyser region. After an adjustable delay time a quench pulse is applied to the analyser region, reversing the polarity of the analyser trapping plates. For this purpose the capacitive filtering of the trapping plates is removed. The quench pulse removes all the ions in the analyser region when it is applied. The ion current reaching the ion current plates is measured using an electrometer, while the initiate pulse and the quench pulse are visualised on an oscilloscope. At short delay times, there will be a measurable ion current, because the ion slug is still travelling through the source when the quench pulse is applied to the analyser region. At delay time t_{source} the ion current drops to zero, this is the time taken for the ions to reach the analyser region. In fact the t_{source} is taken as the point at which the ion current has dropped to half its original value. This represents the average drift time through the source region.

As the delay time is increased to the time taken for the ions to drift through both source and analyser region t_{total} the current increases again, the time taken for the current to reach half its total value is taken as t_{total}. From these two values the drift times through both the source and analyser regions are known, since

$$t_{analyser} = t_{total} - t_{source}. \tag{3.3}$$

Clearly, a rapid response from the electrometer is important for this operation. Unfortunately the Carey 401 electrometer used was almost useless in anything other than charge mode, which could not be used for a drift time measurement since it involves measuring the time taken for a charge to build upon the detection electrode. The answer was to use a Keithley Instruments 602 Solid State Electrometer which was originally purchased for use with a flow drift tube. Using this instrument measuring drift times was

simple. Typical drift times obtained using normal drift voltages were t_{source} = 0.2 ms and $t_{analyser}$ = 1.9 ms.

3.4.2. Pressure Measurement.

The most likely source of error in an ICR experiment is in the measurement of pressure. The pressure measurement during the experiment was made in all cases with a Bayerd Alpert type ionisation gauge. Such ion gauges have a linear response of ion current to pressure, with zero current at zero pressure. The gauge response curve, expressed as the slope of the current vs pressure, varies with the ionisation cross section of the neutral species by electrons of the energy emitted by the filament of the gauge tube.

The pressure response of the gauge tube for each reactant gas used was calibrated against the Baratron™. The Ultek digital gauge controller was chosen because of its linear voltage output with pressure, rather than the logarithmic output often given by ionisation gauge controllers. The output of the gauge controller was used as the Y input on the Hewlett Packard X-Y recorder and the Baratron™ voltage output was used as the X output. Adjusting the variable leak valve to admit the neutral varied the pressure in the cell and the X-Y recorder gave a copy of the calibration curve. It is important that the calibration is performed with the magnet on at the field used for the experimental observations, since the ion current on the gauge collector is affected by the magnetic field to a significant extent.

Initially the Baratron™ signal was too unstable for this calibration technique, but the problem was solved by insulation. The Baratron™ head used did not have an internal heating coil and was found to be sensitive to the slightest breeze or vibration, either of which would induce a large zero drift.

The Baratron™ head was fixed firmly in place and was insulated by a cardboard box filled with polystyrene chips and covered with aluminium foil. This arrangement completely solved the noise problem, and, minimised the zero drift of the Baratron™. The zero drift in the Baratron™ still occurred, but not over the time scale of the calibration experiment.

The calibration experiment was usually carried out over the pressure range 0 to 15×10^{-5} Torr. At pressures above this level, ie up to 10^{-3} Torr, there was a discernible curvature in the gauge tube response. Most rate measurements were carried out in the range 0 to 10^{-4} Torr. Calibration experiments were carried out before each experimental run and preferably after each one as well, since the calibration changed from day to day, presumably due to surface reactions on the filament. The filament emission was kept as low as possible in order to extend the life of the gauge tube.

Table 3-2. Ionisation cross sections vs gauge calibration factors for some neutrals.

Neutral	Ionisation Cross Section (10^{-16} cm^2) at 75 eV [a]	Calibration Factor [b] (Typical Value)
He	0.38	0.10
Ne	0.62	0.36
CO	2.99	1.16
CH_4	4.30	1.70
C_2H_2	4.98	2.00

[a] [From "Mass Spectrometry " by Keiser]

[b] $\frac{P(gauge)}{P(baratron)}$

There is a further factor to be taken into account when dealing with the pressure measurement by the ionisation gauge. This is referred to as the system factor, f_{sys}.

$$f_{sys} = \frac{P_{cell}}{P_{gauge}} . \tag{3.4}$$

The system factor is determined by the distance from the gauge to the cell, the size of the tubing used, and other factors that go to the conductivity of the system. Pumping speed also has a significant effect on the system factor. The usual way of determining the system factor is to carry out a calibration reaction and see by what factor the (calibrated for the neutral) ion gauge reading must be adjusted by. Bruce and Eyler [Bruce and Eyler (1992)] report using the reaction of CH_4^+ with methane, yielding CH_5^+ and CH_3, as a calibration reaction. In their case a system factor of around 2.0 was observed. They used an ionisation gauge placed 1.5 m from the cell, in the ICR described in the present work the gauge was only 50 cm from the cell. The results of a calibration experiment using the above reaction are described in detail below, but it was found that the system factor in the Canterbury ICR was as close to 1.0 as could be determined given the other uncertainties in the experiment.

3.4.3. Pumping speed reduction

The report of Bruce and Eyler described above includes reference to the use of a gate valve between their oil diffusion pump and the ICR cell. The gate valve was routinely used only ¼ open. This arrangement reduced pressure fluctuations. The same problems were encountered using the Canterbury ICR, especially when high pressures, of 10^{-4} Torr or more were used. A suitable gate valve was procured, and placed between the pump and the cell. The valve however possessed a small leak, which although unable

to be traced to a particular location was evidenced by a significant increase in the background pressure.

A simple solution was used to the problem of reducing the pumping speed. An aluminium plate was cut to just over the internal diameter of the flange between the pump and the cell. A small hole drilled in the centre of this plate served as an orifice to limit the pumping speed. The plate was held in place by resting on the flange of the diffusion pump, the surface of the opposite flange face being cut away slightly to admit the plate. The diameter of the hole was chosen as around 5 mm. The device worked well and no adjustments were deemed necessary.

The combination between the insulation of the Baratron™ and the reduction of the pumping speed greatly improved the ease and accuracy of the ionisation gauge calibration.

3.4.4. The reaction $CH_3CN^+ + CH_3CN$

The first system studied quantitatively using the instrument was the reactivity of CH_3CN^+ with neutral acetonitrile. This system was known to give rapid formation of the protonated nitrile. [Gupta et al (1967)] [Vogt and Beauchamp (1975)] [Franklin et al (1966)],

$$CH_3CN^+ + CH_3CN \rightarrow CH_3CNH^+ + CH_2CN\,. \qquad (3.5)$$

Acetonitrile was used after being purified by freeze-pump-thaw cycles. The ionisation gauge was calibrated using the neutral in the cell. The calibration factor was found to be 1.8. After calibrating the ionisation gauge, the drift times through both the source and analyser regions were measured using the method described above. The drift time through the source was 0.75 ms and that through the analyser was 2.5 ms.

Rate Constant Measurement

Having carried out the relevant calibrations, the rate measurement proper was made. The output of the phase sensitive detector was connected to the scope and input into the lock in amplifier. The lock in amplifier was locked to the 40 Hz square wave used to modulate the filament bias. The output of the lock in amplifier was used as the Y input to the X-Y recorder. The X input to the recorder was the X axis drive from the HP3314A function generator.

Using the function generator in linear frequency sweep mode, the recorder would give a hard copy of the lock in amplifier output, as a function of frequency. By adjusting the width of the sweep and the sweep time together with the gain of the recorder and the sensitivity of the lock in amplifier the conditions could be modified to give optimum ease of measurement.

In the case of the present reaction where the product was one mass unit larger than the reactant ion, both reactant and product ion peaks were observed in the same frequency sweep. Where the products and reactants are at significantly different masses, separate sweeps of the region around each ion peak are used.

Typically a region of the mass spectrum five mass units wide centred on the observed peak would be swept. This technique saves time and allows for greater resolution of the important regions of the mass spectrum. It is greatly facilitated by the use of the programmable function generator, allowing up to six sweeps to be programmed at one time.

The peak heights of reactant and product ions were obtained by measuring the peak heights on the recorder output with a ruler. This stage of the process may well be amenable to computerisation, but the manual method works well and is probably quicker than a computerised method would be.

The units of peak height are arbitrary, what is important is the relative peak heights of the reactant ion and all the product ions. Where one ion signal is much smaller than the other the sensitivity of the lock in amplifier can be increased as long as it is remembered to divide the resulting signal by the appropriate scale factor.

The software used to analyse this primary to secondary ion reaction was ICRC2.FOR written by Dr V Anicich at JPL. The program is for reactions yielding secondary ions studied using a bridge detector. As described on p. 23 the program uses the Comisarow line shape equations to derive the rate constants by an iterated series of approximations.

The original programs were written to be compiled by Ryan McFarlane Fortran on a PC-XT. The programs did not initially compile successfully using Microsoft Fortran requiring several changes to format statements. Using free format READ (5, *) statements throughout solved the problem. The program was eventually also compiled on the VAX system after a few small changes to file handling.

Results

The mass spectrum of the system revealed that in addition to 41^+ ions at 40^+ and 43^+ were produced. These ions did not appear to react significantly, and their intensities were small compared to 41^+. The peak heights observed at each pressure together with the derived rate constant at that pressure are tabulated below in Table 3-3

Table 3-3. Peak heights[a] and rate constants for the reaction $41^+ \rightarrow 42^+$.

Pressure [c]	43^+	42^+	41^+	40^+	k_2[b]
1.11	8	35	123	61	4.23
3.28	4	59	121	65	2.22
6.77	3	114	93	60	2.11
12.78	1	52	18	14	1.97
21.67	0	63	11	13	1.54

[a] Arbitrary Units
[b] Units of $cm^3\ s^{-1} \times 10^{-9}$
[c] Units of (Torr $\times 10^{-6}$)

The rate coefficients show a slight negative pressure dependence, that may or may not be pronounced at low pressure, depending on whether or not the lowest pressure point is valid. The slight negative dependence at higher pressures could well be due to the product ion CH_3CNH^+ reacting further;

$$CH_3CNH^+ + CH_3CN \rightarrow CH_3CNH.\ CH_3CN^+. \qquad (3.6)$$

This reaction was observed to occur as pressure increased, but rate measurements were not made. The anomalously high rate coefficient at a pressure of 1.11×10^{-6} Torr is not likely to be due to secondary reaction, since the reaction has a termolecular rate coefficient of around 7×10^{-23} $cm^6\ s^{-1}$ [Fisher and McMahon (1990)] and will not be significant at low pressures. One possible explanation for the anomalous rate is the presence of a large amount of water present as a background impurity.

3.4.5. The Rate Coefficient of the Reaction $CH_4^+ + CH_4$

The reaction of CH_4^+ in neutral CH_4 has been studied by many groups and the results are well characterised.[Bruce and Eyler (1991)] [Ryan and Harland (1974)] [Smith and Futrell (1972/73)]. The reaction, at 298K without translationally or vibrationally excited ions proceeds through one channel only.

$$CH_4^+ + CH_4 \rightarrow CH_5^+ + CH_3 \qquad (3.7)$$

The accepted value for the bimolecular rate constant is 1.14×10^{-9} $cm^3\ s^{-1} \pm 15\%$ [Anicich (1993)]. At higher energies, for example in double resonance experiments a further channel has been observed leading to formation of CH_3^+ [McIver and Dunbar (1971)]. This channel was not observed in the present experiments. The reaction was used in an attempt to check the calibration of the pressure measurement system.

Experimental

The experimental set up used for the rate measurements was the same as for the reaction of CH_3CN^+ described above. Because the reactant and product ion differed in mass by only one mass unit both reactant and product ion could be observed in the same frequency sweep without any loss of resolution.

The measurements were made over a period of three days. Before and after each series of peak height measurements the ionisation gauge was calibrated using methane. The results of the calibration experiment varied from day to day, so the measurements made each day used the calibration result obtained that day. The amount of background varied from day to day, but a typical value was 3.1×10^{-6} Torr. Unfortunately it was impossible to calibrate the Baratron™ with this background gas, but if it is assumed that it was mostly water, then given the total ionisation cross section for water (2.96×10^{-26} cm^2) then on the basis of Table 3-2 above it is likely to have a calibration factor close to that of CO which was ≈ 1. Thus the background pressure in real terms was around 3×10^{-6} Torr. In order to take some account of this background it was subtracted from the observed ion gauge pressure.

$$P_{corr} = \frac{(P_{gauge} - P_{background})}{f_{calibration}} \tag{3.8}$$

The calibration factor for CH_4 was variable, but the average was 1.7 ± 0.5.

The drift times were measured by the method described above, and typical results were 0.25 ms for the source drift and 1.60 ms for the analyser drift time. The program ICR2C was used as described above. The rates used for the collisions of both ions with the neutral gas were calculated by the parametrised ADO method.[Su and Chesnavich (1982)]

$$k_{coll}\, CH_4^+ = 1.32 \times 10^{-9}\ cm^3\ s^{-1}$$
$$k_{coll}\, CH_5^+ = 1.31 \times 10^{-9}\ cm^3\ s^{-1}.$$

Results

The results obtained in the three runs are tabulated below.

Table 3-4. Peak heights[a] and rate constants for $16^+ \rightarrow 17^+$

Pressure[c]	16^+	17^+	k_2[b]
0.38	92	12	1.42
0.67	91	29	1.76
1.01	94	47	1.67
1.3	86	55	1.56
1.7	70	65	1.56
1.8	35	34	1.51
2.5	43	63	1.42
2.5	39	62	1.50
3.2	43	99	1.44
3.4	36	82	1.36
4.2	29	92	1.32
4.3	19	66	1.36
4.6	27	109	1.36
5.5	18	115	1.42
1.1	58	27	1.32
1.8	77	68	1.29
3.0	29	58	1.31
5.1	27	130	1.23
9.3	5.3	130	1.39
0.38	35	5	1.38
1.0	43	20	1.42
2.3	44	53	1.21
4.6	24	87	1.16
8.1	9	102	1.16
11.7	3	129	1.43

[a] Arbitrary Units
[b] Units $cm^3\ s^{-1} \times 10^{-9}$
[c] Units of Torr $\times 10^{-5}$

In the first experimental run, the rate coefficients, k_2, determined at pressures of less than 2×10^{-5} Torr show an unexpected negative pressure dependence. The rate coefficients determined at higher pressures show no such trend. Over the next three days two further experimental runs were carried out. These were performed over a wider range of pressures.

The variation of the rate coefficient with pressure for each experimental run is shown in Figure 3-5.

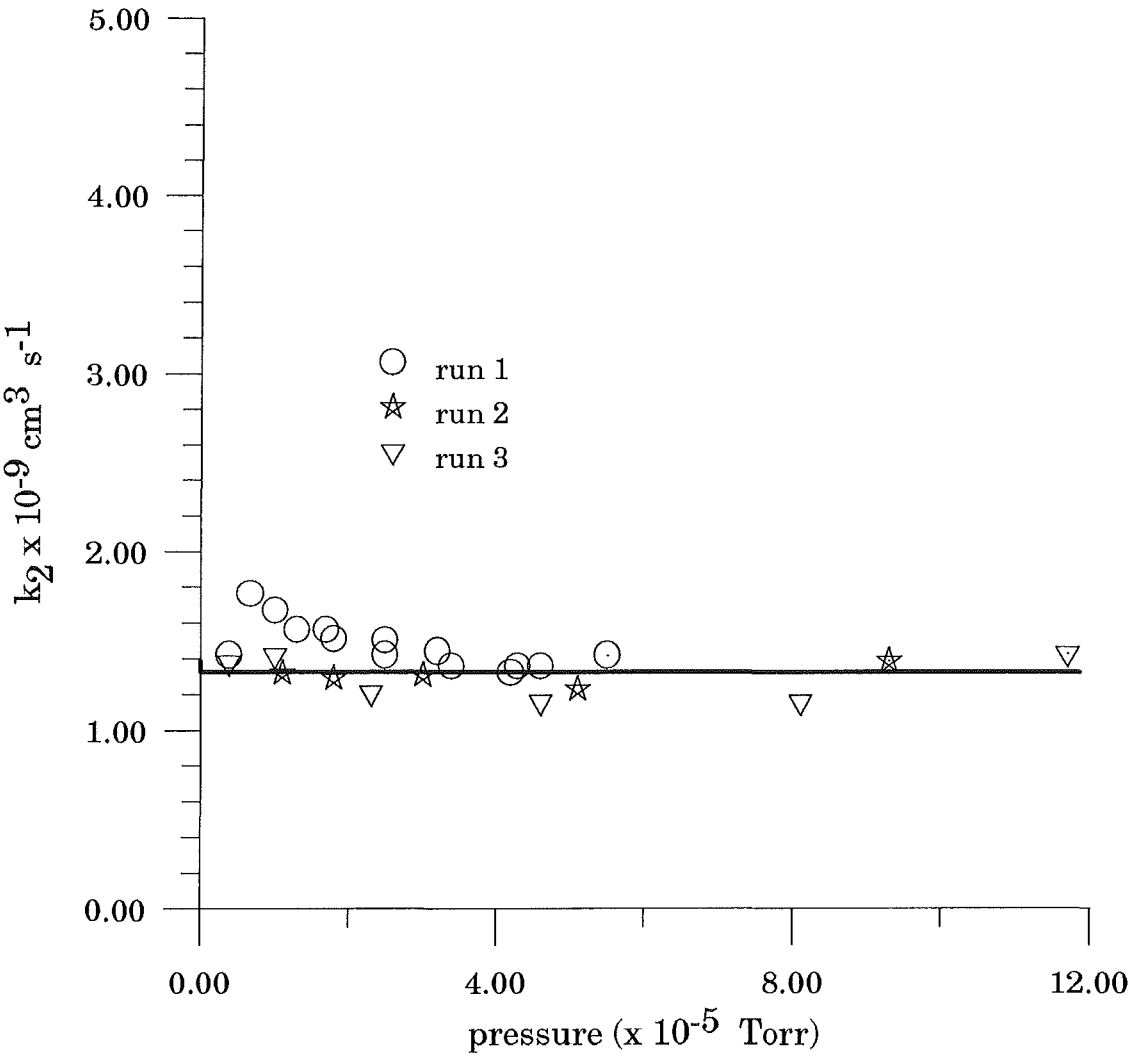

Figure 3-5. ***k2*, for the reaction $CH_4^+ + CH_4 \rightarrow CH_5^+ + CH_3$: measured in drift mode .**

The results of both the later runs do not show the same pressure dependence as the first, and it is possibly because the background pressure had decreased by that time. The presence of H_2O in the cell would have created an artificially high measured rate constant, because of the removal of CH_4^+. The reaction of CH_4^+ with H_2O has been studied before in an ICR instrument and is known to be fast

$$CH_4^+ + H_2O \rightarrow H_3O^+ + CH_3 , \qquad (3.9)$$

Huntress et al [Huntress et al (1980)] report the rate to be 2.5×10^{-9} cm^3 s^{-1}. If the background pressure is in fact largely due to water vapour then there will be a perturbation in the observed peak heights due to this reaction. The effect will be most noticeable at lower pressures, where the partial pressure of H_2O is a significant fraction of the partial pressure of CH_4. If the above reasoning is accepted and the pressure variation of the first experiment is ignored for $P < 2 \times 10^{-5}$ Torr the rate coefficient for the reaction is independent of pressure and the result is a value of k_2 of 1.3×10^{-9} cm^3 s^{-1}. This value is somewhat higher than the rate accepted above of 1.14×10^{-9} cm^3 s^{-1}, but is

within the margin of error which is usually assumed to be around 20% for ICR measurements.

The main reason for carrying out this reaction was to estimate the system factor for the instrument after the addition of the baffle above the diffusion pump. The result shows that the system factor was close to unity, and the uncertainty in the calibration of the ionisation gauge would have a larger effect on the determination of rate constants. For this reason the system factor was treated as being unity for the experiments described in this work.

3.5. Trap Mode Operation

3.5.1. Programming for the PCL 718 Data Acquisition Card

It is well to start by considering just what information is required to make a trap mode rate measurement. The rate law expression for the reaction of A^+ with B can be written as

$$\frac{d[A^+]}{dt} = -k[A^+][B], \tag{3.10}$$

integrating this expression yields

$$k = -\ln\frac{[A^+]}{[A^+]_0}\frac{1}{[B]}\frac{1}{t}. \tag{3.11}$$

Thus to obtain a rate constant, all that is required is to measure $[A^+]$ as a function of time, then add a known pressure of B, and again measure the time decay of $[A^+]$. The ratio of the two decays is $\frac{[A^+]}{[A^+]_0}$. Plotting the natural log of this quantity, $\ln\frac{[A^+]}{[A^+]_0}$ against time, the rate coefficient is simply the slope divided by (using the appropriate units) [B].

Thus for a rate coefficient to be measured the important quantities are; pressure, which can be measured simply by manually reading the ionisation gauge, and the ion signal as a function of time. The only practical way of measuring the time dependence of the ion concentration is by using a short initiate pulse and varying the delay before ion detection. Thus any software used to measure the rate must be able to vary the detect

pulse delay time. Another requirement of the software is that it take into account any background on the signal channel not due to resonant ions, such background may be eliminated by measuring the signal curve with the trapping plates held negative, removing all the ions from the cell. Thus the ability to control the polarity of the plate voltages is important.

3.5.2. Using the Gated Integrator in Trap Mode

During the course of the work encompassed by this thesis several programs were written to control the ICR. The first program written to measure rate constants in the trap mode was RateconA. The trap mode signal was analysed by the Evans Model 4130 gated integrator board, and the dc voltage output from the integrator was measured by the PCL-718 data acquisition card.

Two of the 16Bit A/D channels were used, one to measure the signal from the Gated Integrator, the other to monitor the detect pulse.

One analog output channel was used to supply a DC voltage that controlled the detect pulse delay time using the modified pulse sequence board.

The 16 Bit digital output was used to provide four TTL outputs which could control the digital switching between manual or remote control for the delay time and between positive and negative plate polarity.

The software was written entirely in QuickBASIC 4.5 since the PCL-718 was supplied with a library of QuickBASIC 4.5 driver routines for software control of the on-board functions. As indicated by the name, Ratecon.A was based on RATECON.FOR which was written by Dr Vince Anicich for the ICR instrument in his laboratory. Although the language and interfacing are entirely different, the overall sequence of the program is the same as that used by Anicich. The overall sequence of events in the trap mode measurement is shown in Figure 3-6.

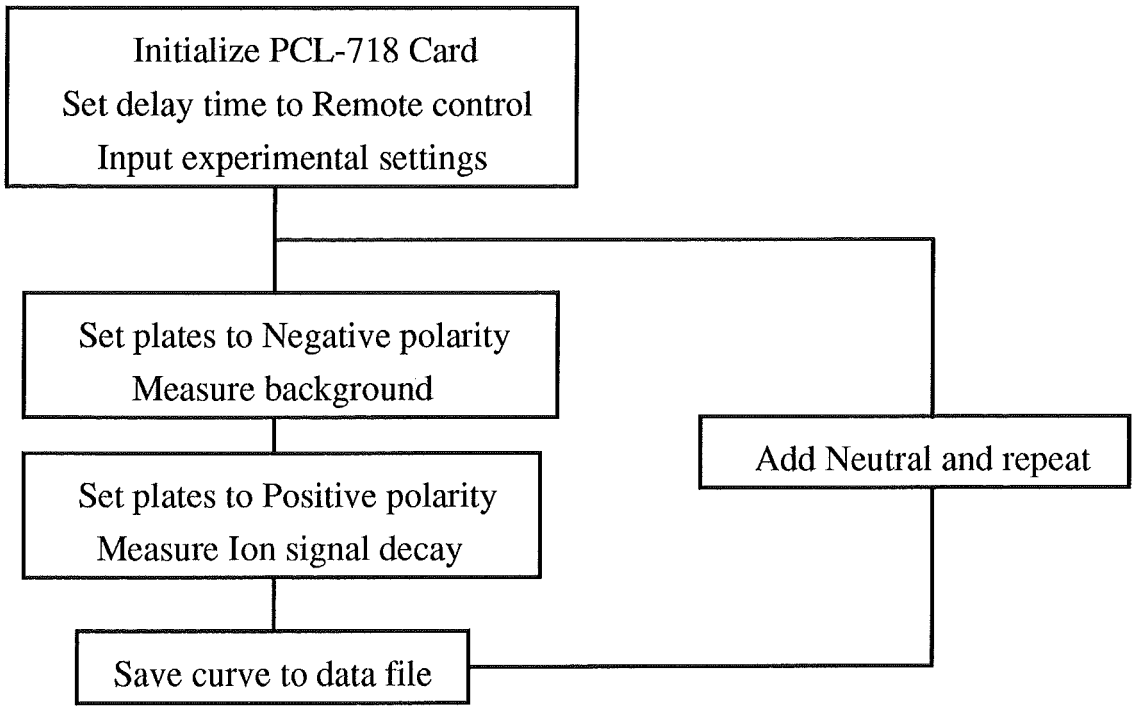

Figure 3-6. The overall process used to make a trap mode measurement in the ICR.

The actual measurement of each curve is described in Figure 3-7. Typically 10 points would be measured with anywhere up to 100 samples per point. The gain in accuracy in having many samples per point reduces random noise effects, but if an experiment runs for too long fluctuations in pressure, magnetic field and filament emission can occur. Thus the optimum number of samples per point is not necessarily the maximum available.

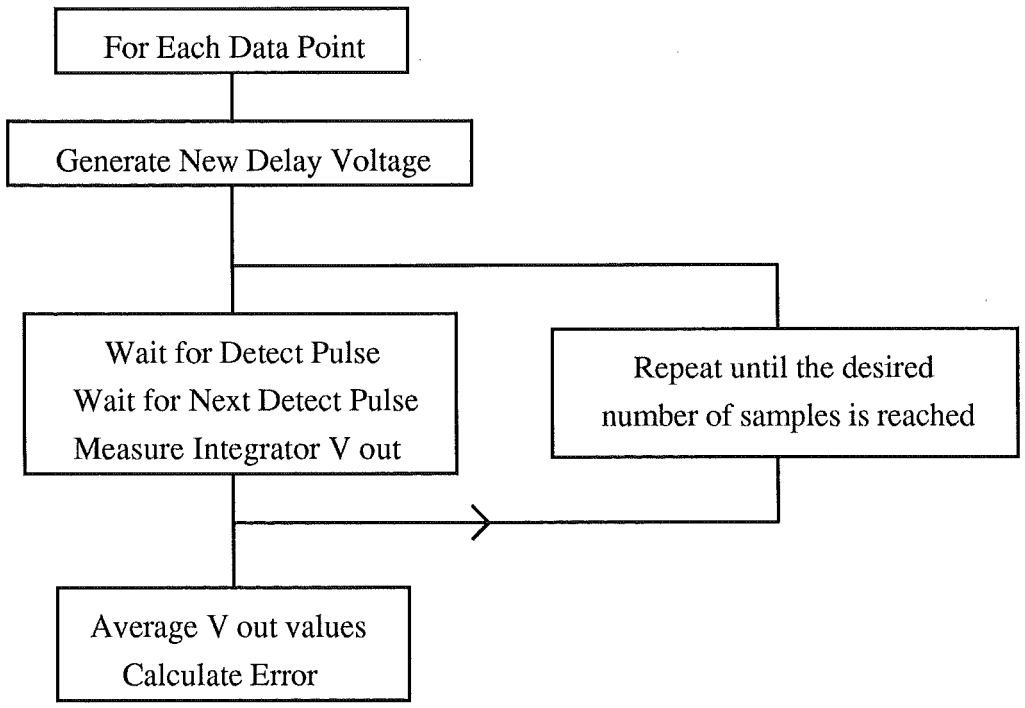

Figure 3-7. Flow diagram of the measurement sequence in the program RateconA.

The program RateconA measures the experimental decays and saves them together with the relevant parameters and any comments into data files on the selected drive. The data files can be read and the rate constant calculated by the program RateconX. This program reads the data files and calculates the ratio of the decays. The natural logarithm of this ratio is plotted against time and the rate coefficient calculated by least squares (the least squares routine is adapted from the Fortran code of Anicich).

The program allows the user to edit (remove) data points and re-plot the data, and of course to print out a hard copy of the result.

3.5.3. $Ar^+ + CO$, A Trap Mode Measurement

The first trap mode measurement made using the Canterbury ICR was the measurement of the rate coefficient for charge transfer from Ar^+ to CO,

$$Ar^+ + CO \rightarrow Ar + CO^+. \qquad (3.12)$$

This reaction has been studied by many different groups using a wide variety of methods. The reported rate coefficients vary from 3.3 to 9×10^{-11} cm^3 s^{-1} [Ikezoe et al (1987)] with the average being around 4.6×10^{-11} cm^3 s^{-1}. The only ICR measurement reported is by Marx et al [Marx et al (1983)], the measured coefficient being 5×10^{-11} cm^3 s^{-1}.

The Ion gauge was calibrated with both gases. The ion decays were measured over a 100 ms time base. At first many of the experiments failed because of space charging or the addition of too much neutral. Another significant problem was the drifting of the magnetic field over the duration of the experiment resulting loss of resonance. After considerable trial and error the experiment yielded reasonable results, ie reproducible straight lines for the log of the ratio of ion signals. The results were somewhat high, with the average being 8.6×10^{-11} cm^3 s^{-1}. A typical experimental result is shown in Figure 3-8.

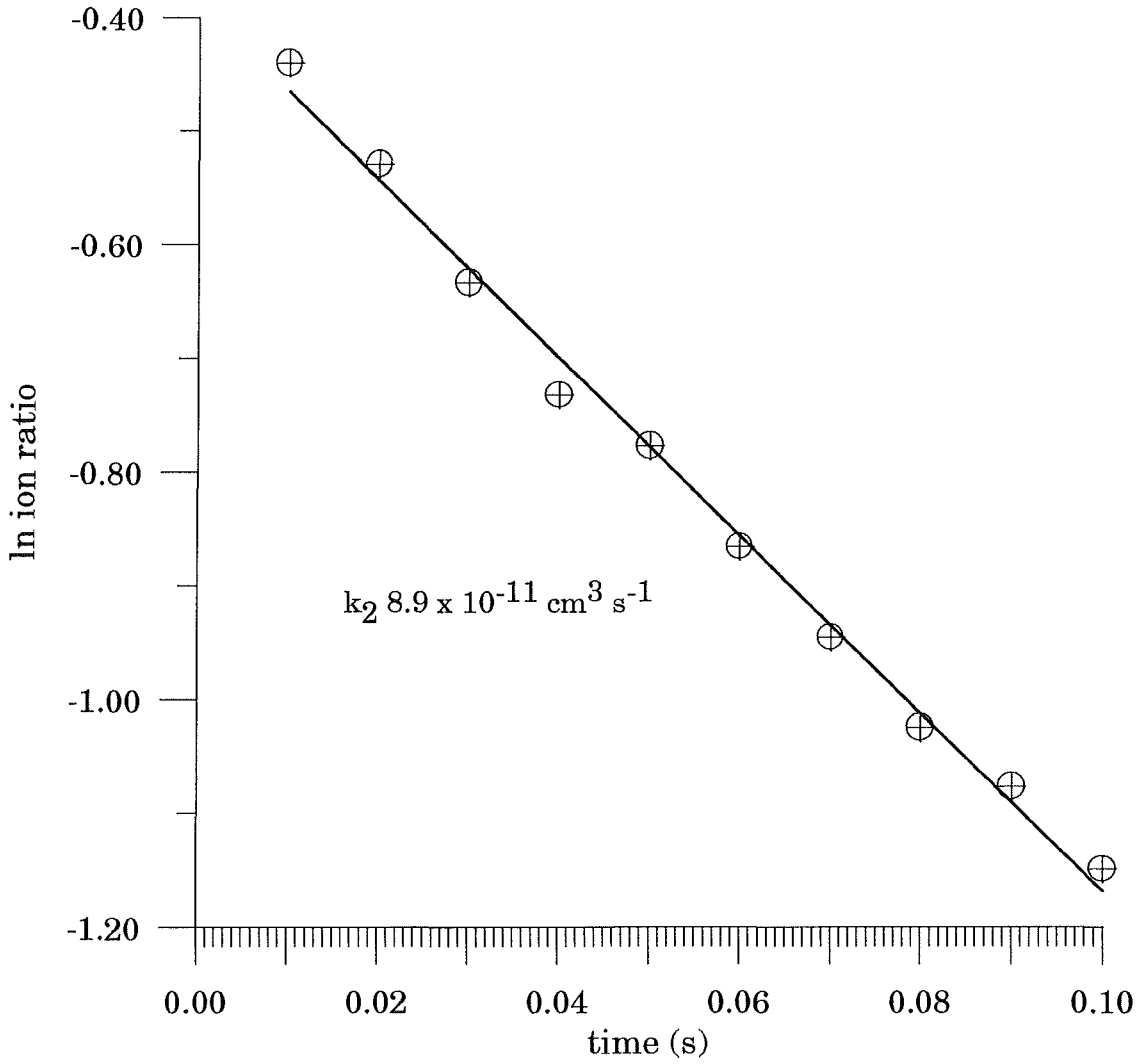

Figure 3-8. Trap mode rate measurement of Ar^+ + CO.

The reason for the high rate constant is not obvious. The measured rate constants were all between 7 and 11 $\times$ 10^{-11} cm^3 s^{-1}. The most likely cause of error was in the calibration of the ionisation gauge. This experiment was carried out before the Baratron™ was completely insulated and the baffle was fitted to the diffusion pump. Subsequent trapping mode experiments have shown good agreement with both SIFT, and drift mode ICR results. The trap mode measurements on the reactions of the C_2H_2 system, described below agree with the results obtained by other Trap mode ICR experiments.

3.5.4. Using the Computer as a Gated Integrator / Storage Scope

While the gated integrator works well where the signal is clean, one problem that has plagued the operation of the Canterbury ICR is coupling of the detect pulse onto the signal in the trap mode. Depending on the voltages on the drift plates the detect pulse can cause significant noise on the signal channel. The noise is manifest as spikes at both ends of the detect period. These spikes impinge upon the detection period and so are measured by the gated integrator. When the signal is small this causes significant

problems. Increasing the time constant of the detection system reduces the problem slightly, but it is not a solution.

In order to investigate a better or at least more versatile system of analysing the results of trapped ion experiments it was decided to make better use of the capabilities of the PCL-718 card. The result of this work is the program SCOPE, which in effect allows the computer to act as a digital storage scope with signal averaging facility, in effect similar to a Multi Channel Analyser.

The maximum sampling rate is not high, only 50 kHz, but this allows 50 points to be sampled per ms which gives a good indication of the shape of the signal transient, which in general is at a peak at least 2 ms wide.

The sampling window, which starts at the detect pulse can be set to between 1 and 6 ms. (At the present time an adjustable delay after the trigger is not a feature, although this could be incorporated.)

The display can be changed from 1 V to 0.000001 V per division although the limited (16 Bit) range of the analog to digital converter limits the number of discrete values to 65536 over the range of the instrument, which is nominally 0 to 10 V. This gives a scale with an average voltage between points of 1.5×10^{-4} V. The range of the instrument can be reduced to 0 to 1V with a corresponding ten fold increase in definition, but this requires changes to on-board DIP switches and to the source code.

The position of the signal can be changed by adding or subtracting a constant, analogous to a DC offset.

When used as a storage scope emulator the program can display either a single measurement or can display an averaged result of up to 10 iterations. Each data point (50 every ms) can be thought of as a separate channel, the values for each channel are averaged over the number of iterations and the resulting signal displayed. The integral of the signal is determined by summing the averaged values of each channel over the entire window used. The integral is displayed with the signal.

When the program is used to measure a curve for use in a rate determination the process used is similar to that in RateconA. The operator sets up the timebase, the window, any offset required, and the number of iterations per point. Having thus set up the parameters for each individual point, the operator sets the number of points to be measured and starts the measurement. The plate polarities are set to negative and a background measurement is made. The integral of each point is recorded. Then the plates are set positive and the experimental curve is measured. The background integral is subtracted for each point and the results are displayed graphically. The data can then be saved to a suitable location for further processing.

The data from SCOPE can be analysed by a modified version of the RateconX program. This program allows entry of data from the keyboard or from data file. It performs similar operations to RateconX, allowing for editing and display of the data,

and calculation of the rate constant by least squares fit. The main differences lie in the editing and graphics which are somewhat improved, but not yet fully developed.

3.6. Double Resonance Techniques

Double resonance excitation can be applied to the analyser region of the cell along with the signal of the observing oscillator. This is done using the oscillator summer built into the phase splitter unit.

The addition of double resonance into the source region was facilitated by the design and manufacture of a similar phase splitter for the source region. The double resonance signal is split and the opposing phases fed to opposite source drift plates. It is important to ensure that the source and the drift region double resonance signals are in phase. Thus the top plate in each region should receive the same phase.

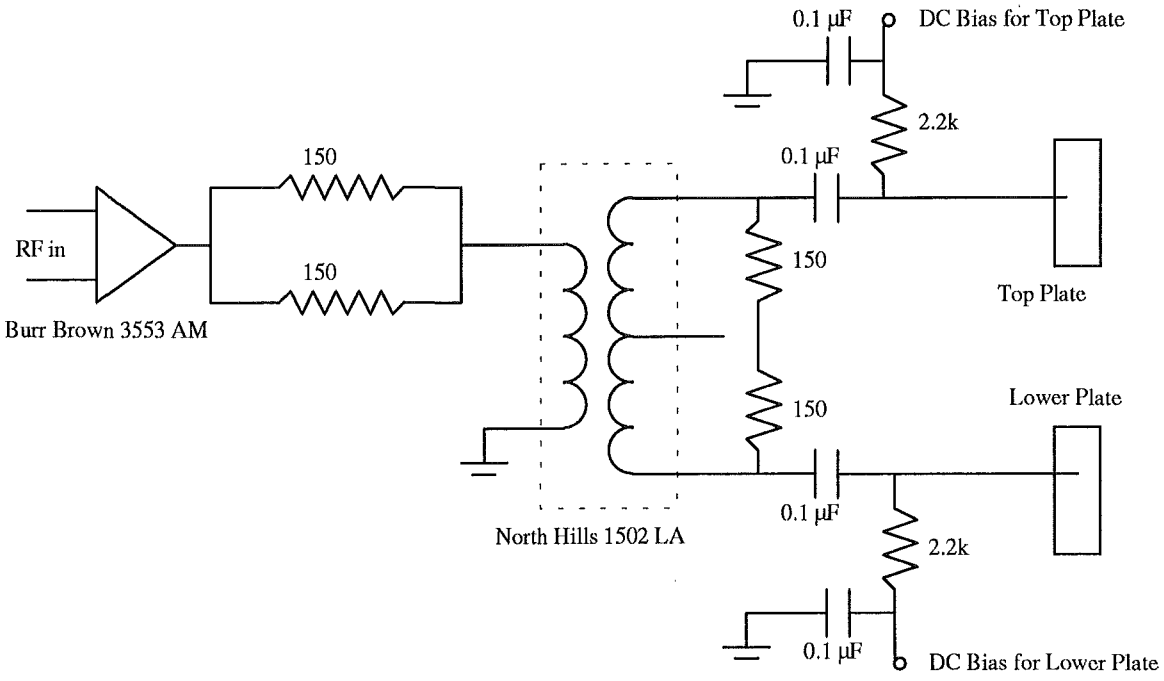

Figure 3-9. The arrangement to apply double resonance RF to the source region.

The use of double resonance as a quantitative tool to determine the branching ratio of a reaction requires the facility to sweep the double resonance oscillator while holding the observing oscillator at a given frequency. The Topward 8112 frequency generator that was purchased for double resonance experiments lacked a sweep facility. The HP 3314A function generator could be used as the double resonance oscillator, but the Topward lacked the signal stability to be used as the observing oscillator. A compromise was reached in that the PRD 7828 Frequency Synthesiser was to be adapted for use as the observing oscillator. This instrument has good stability, but lacks a sync output capable of driving the phase sensitive detector. A suitable modification to the PRD device is

currently being tested by the electronic work shop. It is hoped that this will allow quantitative double resonance experiments to be carried out in the near future.

3.7. Conclusion

The development of the Canterbury ICR has involved the modification of electric, electronic, and mechanical systems. The instrument is now capable of operating in both the drift and the trap mode.

Rate coefficients derived from the instrument in both drift and trap mode agree with the literature values for previously studied reactions.

CHAPTER FOUR

A SIFT STUDY OF THE REACTIONS OF t-C_4H_9Cl

4.1. Introduction

One of the assumptions made by researchers in the field of ion-molecule chemistry over the years has been that the rate of an ion molecule reaction is dependant on the sign of the enthalpy change associated with that reaction. Established wisdom has it that an exothermic reaction may or may not be fast, but an endothermic process cannot proceed at anything more than a small fraction of the collision rate.

Many measurements of thermochemical quantities have been made based on this assumption, [Haney and Franklin (1969)] [Deakyne et al (1987)], especially measurements of proton affinities [Lias et al (1988)] and other properties where a thermochemical ladder may be constructed. As a rule of thumb, if a proton transfer reaction is exothermic it will proceed at the collision rate, but there are significant exceptions to this rule. If the proton transfer involves a rearrangement there may be an activation barrier to the reaction, as is discussed in this work concerning the reactions of $CH_3OCH_2^+$. A more controversial exception may apply if the enthalpy change of the process is small. It has been suggested that where the enthalpy change is small the reaction rate may be influenced by the change of entropy involved.

The use of the free energy change ΔG rather than the enthalpy change ΔH as a criterion of whether or not a reaction will be fast has been suggested by Meot-Ner [Meot-Ner (1991)]. The existence of fast endothermic processes has been questioned by several groups. In order to examine this phenomenon a series of measurements were made on the reactions of t-C_4H_9Cl with different protonated bases. The channel

$$BH^+ + \text{t-}C_4H_9Cl \rightarrow \text{t-}C_4H_9^+ + B + HCl \qquad (4.1)$$

should show a significant entropy increase due to the increase in the number of translational and rotational modes in the products compared to the reactants. Henchman [Henchman (1987)] suggests that such reactions yield typical entropy increases of 80 J K^{-1}

mol^{-1}. The other channel that was observed was formation of the adduct B.t-$C_4H_9Cl^+$ and HCl. By selecting bases with differing proton affinities the enthalpy change of the reaction could be varied, and the variation of branching ratio for t-$C_4H_9^+$ formation in comparison to the other available channel could be measured as a function of ΔH.

The measurements made on the SIFT were complementary to measurements made in both a Pulsed Electron High Pressure Mass Spectrometer and an ICR. As will be discussed below the results are of some interest, but many questions are raised regarding the interpretation of these results.

4.2. Experimental

The reactions below were carried out using the Canterbury SIFT and in one case the Canterbury ICR. The majority of the reagents were used as supplied as AR or Spectroscopic grade, after being purified by freeze-pump-thaw-cycles. Where the reagent was a liquid at room temperature the liquid phase was cooled by an ice-water bath to prevent condensation upon expansion through the needle valve or sapphire seal variable leak valves used in the reagent handling lines.

Cyanoacetylene, HC_3N, was used after being prepared previously by the ammoniolysis of methyl propiolate as described by Moreu and Bongrand [Moreu and Bongrand (1920)].

Hydrogen cyanide, HCN, was produced by the action of orthophosphoric acid on potassium cyanide.

The reactions were carried out at room temperature, typically 25 ± 5° C. The pressure used in the SIFT flow tube was 0.300 ± 0.005 Torr of helium carrier gas. The program SIFT2D was used to collect the data and calculate the rate constants, and the program RATIO2 was used to calculate the branching ratios.

4.3. Results

4.3.1. Reaction of t-C_4H_9Cl with HCO^+

Paraformaldehyde was heated in a hot water bath and the resulting monomer was used in the ion source at a pressure of around 8×10^{-5} Torr. Upon reaction with t-

C_4H_9Cl the only observed product was the t-butyl ion at 57^+. The rate of loss of HCO^+ was measured at 2.3×10^{-9} cm^3 s^{-1}.

4.3.2. Reaction of t-C_4H_9Cl with $HCNH^+$

Hydrogen cyanide was used in the ion source at a high pressure, yielding the protonated ion which was injected into the flow tube without significant interference by HCN^+. The only ionic product of the reaction was the ion at 57^+, and the rate of loss of $HCNH^+$ was 2.5×10^{-9} cm^3 s^{-1}.

4.3.3. Reaction of t-C_4H_9Cl with HC_3NH^+

Cyanoacetylene was used in the ion source to inject HC_3NH^+ into the flow tube. The major product of the reaction ($\approx$ 90 %) was t-$C_4H_9^+$, with some cluster ion detected. The rate of loss of HC_3NH^+ was 2.2×10^{-9} cm^3 s^{-1}.

4.3.4. Reaction of t-C_4H_9Cl with $CH_3OH_2^+$

Initially methanol was used in the ion source, but the conditions required to inject $CH_3OH_2^+$ led to the fragment ion, CH_3^+, forming in the flow tube. In order to reduce the amount of CH_3^+ present a mixture of methanol in H_2 was used in the ion source, and this gave a much improved ratio of $CH_3OH_2^+$ to CH_3^+. Upon addition of t-C_4H_9Cl the rate of loss of $CH_3OH_2^+$ was found to be 2.5×10^{-9} cm^3 s^{-1}, but product ions were found at both mass 57^+ and mass 89^+. The ion at 57^+ can be assumed to be t-$C_4H_9^+$ and that at 89^+ to be the cluster t-C_4H_9. CH_3OH^+. The production of t-$C_4H_9^+$ was the dominant channel.

4.3.5. Reaction of t-C_4H_9Cl with CH_3CHOH^+

Acetaldehyde was used in the ion source and the protonated species was injected. Complicating the experiment were break up products at 18^+ and 29^+, but these were minimised by careful tuning of the injection conditions. The major product of the reaction was 57^+ with a minor channel giving the association product at 101^+. The major break up product was 29^+ and when this was injected on its own it reacted to give only 57^+. Thus before calculating the branching ratio the 29^+ background was subtracted from the 57^+ signal (after appropriate scaling to take account of mass discrimination). After this

process the branching ratio was found to be about 9:1 in favour of t-$C_4H_9^+$. The rate of loss of CH_3CHOH^+ was 2.2×10^{-9} cm^3 s^{-1}.

4.3.6. Reaction of t-C_4H_9Cl with $C_2H_5OH_2^+$

Initially paraformaldehyde was used in the ion source to generate HCO^+ which was injected into the flow tube to react with ethanol added from the first neutral inlet. The ensuing proton transfer reaction yielded the desired reactant ion $C_2H_5OH_2^+$.

When t-C_4H_9Cl was added at the second neutral inlet the rate of loss of $C_2H_5OH_2^+$ was measured at 2.1×10^{-9} cm^3 s^{-1}. The only product ions were t-$C_4H_9^+$ and the cluster ion at 103^+. There were however too many ions present in the flow tube to obtain an accurate branching ratio. In order to get a clean ion signal C_2H_5OH was used in the ion source. Because of the low vapour pressure of ethanol the liquid in the bulb connected to the inlet line was cooled by an ice water bath to prevent condensation in the variable leak valve.

The low pressure of ethanol in the inlet line made controlling the pressure in the ion source difficult, but a signal of $C_2H_5OH_2^+$ sufficient for a product analysis was obtained. The branching ratio was found to be ≈ 60:40 in favour of formation of t-$C_4H_9^+$ over the adduct t-C_4H_9. $C_2H_5OH^+$.

4.3.7. Reaction of t-C_4H_9Cl with CH_3CNH^+

When acetonitrile was used in the ion source to produce CH_3CNH^+ the signal was unstable and rate determination was impossible. In order to achieve a more stable ion signal formaldehyde was used in the ion source to produce HCO^+ by electron impact. The HCO^+ was injected and reacted with acetonitrile at the first neutral inlet to produce CH_3CNH^+ by proton transfer. The drawback in this procedure was the formation of the proton bound dimer of acetonitrile, which occurs rapidly in the collisionally dominated SIFT regime. By adding just enough CH_3CN to remove all but a small fraction of the HCO^+ the signal of CH_3CNH^+ was optimised.

The signal was stable, and strong enough for the experiment. The rate of loss of CH_3CNH^+ was 1.5×10^{-9} cm^3 s^{-1}. Both the channel leading to formation of t-$C_4H_9^+$ and the collisionally stabilised cluster were observed. The branching ratio was found to be ≈ 50:50 for the formation of t-$C_4H_9^+$, see Figure 4-1.

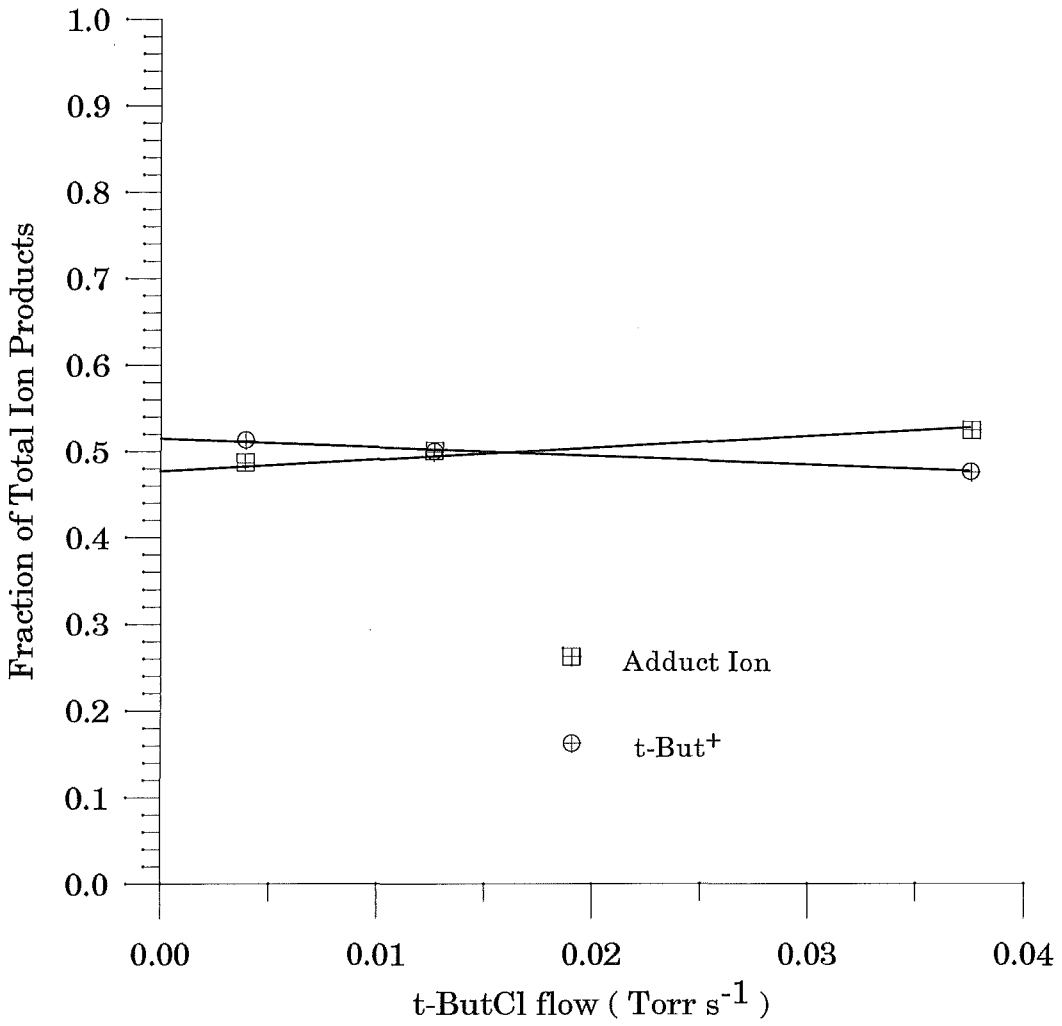

Figure 4-1. Branching ratio of products of t-C_4H_9Cl + CH_3CNH^+:as determined in the SIFT.

This experiment was repeated using the trap mode on the Canterbury ICR. The intention was to utilise double resonance techniques to confirm the branching ratio determined in the SIFT experiment. Unfortunately the double resonance oscillator was unable to be used quantitatively, (see Chapter 3). The rate constant for loss of CH_3CNH^+ with added t-C_4H_9Cl was determined at trapping pressure (the pressure of CH_3CN was 3×10^{-7} Torr), to be 1.5×10^{-9} cm^3 s^{-1}, in good agreement with the SIFT result.

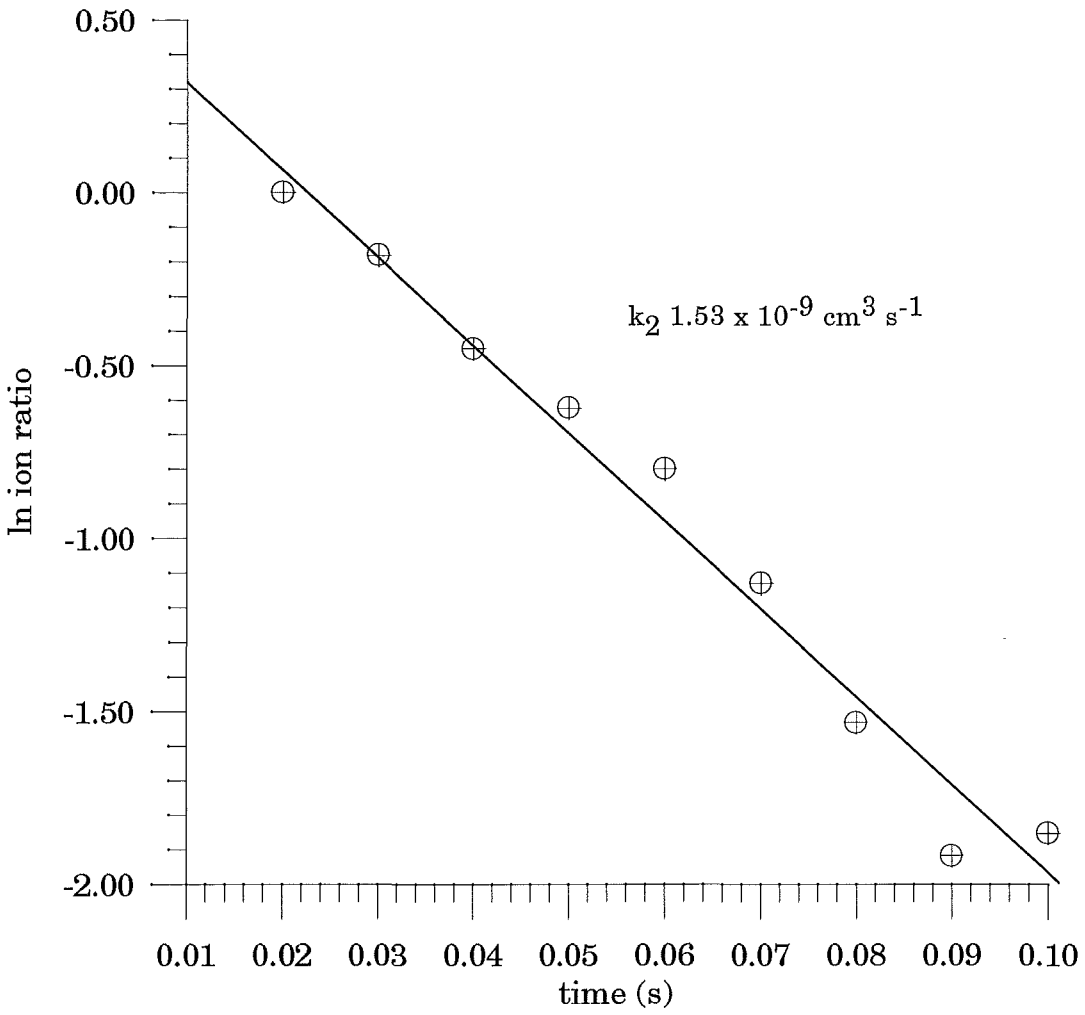

Figure 4-2. trap mode bimolecular rate coefficient for the reaction CH_3CNH^+ + t-C_4H_9Cl.

4.3.8. Reaction of t-C_4H_9Cl with CH_2CHCNH^+

In order to inject the protonated species CH_2CHCNH^+ a pressure of 9×10^{-5} Torr of acrylonitrile was used in the ion source of the SIFT. Although this gave a good signal of CH_2CHCNH^+ it led to the appearance of $HCNH^+$ in the flow tube due to break up of the injected ion. Attempts to use $HCNH^+$ from the ion source to protonate acrylonitrile added from the first neutral inlet failed due to the rapid formation of the proton bound dimer of acrylonitrile which reduced the CH_2CHCNH^+ signal too greatly. Using the direct injection of CH_2CHCNH^+ from the ion source, allowance had to be made for the reactivity of the $HCNH^+$ in the flow tube. In calculating the branching ratio it was assumed that the $HCNH^+$ would react with the neutral to give exclusively the product t-$C_4H_9^+$ at 2.5×10^{-9} cm^3 s^{-1} (see above). Thus after correcting the ion signals for mass

discrimination the 57^+ signal was reduced by the amount of the background $HCNH^+$ signal. Using this method a branching ratio of 25:75 for the channel giving t-$C_4H_9^+$ compared to the formation of the cluster at 110^+ was obtained.

4.3.9. Reaction of t-C_4H_9Cl with CH_3SCNH^+

CH_3SCN was used in the ion source to generate the protonated species CH_3SCNH^+. There was a small signal at 28^+ which was assumed to be $HCNH^+$ produced as a fragment of the injected ion. The reactivity of this fragment ion was taken account of as described above for the reaction of protonated acrylonitrile. The branching ratio was obtained and the ratio of t-$C_4H_9^+$ formation to cluster formation was found to be ≈ 25:75, see Figure 4-3. The overall rate of loss of CH_3SCNH^+ was 1.1×10^{-9} cm^3 s^{-1}.

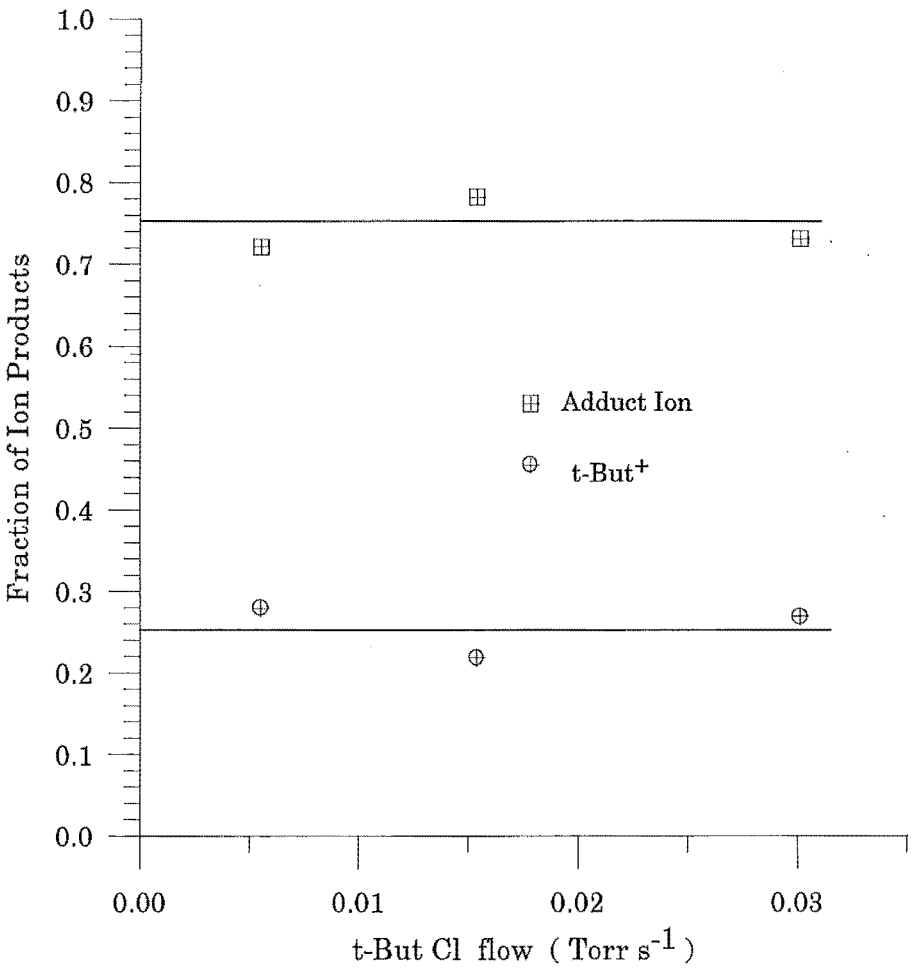

Figure 4-3. Branching ratio of products of the reaction CH_3SCNH^+ + t-C_4H_9Cl: as determined in the SIFT.

4.3.10. Reaction of t-C_4H_9Cl with $(CH_3)_2OH^+$

The protonated species $(CH_3)_2OH^+$ was produced by injecting $HCNH^+$ from the ion source and allowing proton transfer to dimethyl ether flowing from the first neutral inlet. The ion signal was reduced by the rapid formation of the proton bound dimer of dimethyl ether, but was sufficient for the purposes of the experiment.

The small impurity due to residual $HCNH^+$ was subtracted from the 57^+ signal in the usual fashion. The overall reaction rate was 1.3×10^{-9} cm^3 s^{-1} and branching ratio was roughly 50:50 for the channels leading to cluster ion formation and to t-$C_4H_9^+$.

4.3.11. Reaction of t-C_4H_9Cl with Protonated Methyl Oxirane

Again $HCNH^+$ was produced in the ion source and used as a proton donor. Methyl oxirane or propylene oxide, as it is also known, was added at the first neutral inlet. Upon reaction with t-C_4H_9Cl a number of products were observed. The two major products were 115^+ and 58^+. The ion at 115^+ is the cluster ion of t-$C_4H_9^+$ with the methyl oxirane, while the ion at 58^+ could conceivably be either $C_4H_{10}^+$ or $C_3H_6O^+$.

A small signal at 57^+ was observed, but this could have been due to the reaction of residual $HCNH^+$ rather than the protonated methyl oxirane. The overall rate of reaction was 1.2×10^{-9} cm^3 s^{-1}.

4.3.12. Reaction of t-C_4H_9Cl with $(CH_3)_2COH^+$

The proton donor $HCNH^+$ was used to protonate acetone added from the first neutral inlet. The protonated species $(CH_3)_2COH^+$ was in turn reacted with t-C_4H_9Cl at the second neutral inlet. The overall rate of reaction was 2.5×10^{-10} cm^3 s^{-1}. The major product observed was the cluster ion at 115^+ and no t-$C_4H_9^+$ ion was observed.

Table 4-1. Reactions of t-C_4H_9Cl with selected ions.

Reactant Ion	Products	ΔH°[a]	Branching Ratio[b]	k_2[c]
HCO^+	t-$C_4H_9^+$ + CO + HCl	-152.8	1.0	2.3
$HCNH^+$	t-$C_4H_9^+$ + HCN + HCl	-27.3	1.0	2.5
HC_3NH^+	t-$C_4H_9^+$ + HC_3N + HCl	+9.2	> 0.9	2.2
	t-C_4H_9. HC_3N^+ + HCl		< 0.1	
$CH_3OH_2^+$	t-$C_4H_9^+$ + CH_3OH + HCl	+12.5	> 0.9	2.4
	t-C_4H_9. CH_3OH^+ + HCl		< 0.1	
CH_3CHOH^+	t-$C_4H_9^+$ + CH_3CHO + HCl	+35.9	> 0.9	2.2
	t-C_4H_9. CH_3CHO^+ + HCl		< 0.1	
$C_2H_5OH_2^+$	t-$C_4H_9^+$ + C_2H_5OH + HCl	+42.2	0.60	2.1
	t-C_4H_9. $C_2H_5OH^+$ + HCl		0.40	
CH_3CNH^+	t-$C_4H_9^+$ + CH_8CN + HCl	+42.6	0.50	1.5
	t-C_4H_9. CH_3CN^+ + HCl		0.50	
CH_2CHCNH^+	t-$C_4H_9^+$ + CH_2CHCN + HCl	+46.7	0.25	1.5
	t-C_4H_9. CH_2CHCN^+ + HCl		0.75	
CH_3SCNH^+	t-$C_4H_9^+$ + CH_3SCN + HCl	+55.2	0.25	1.4
	t-C_4H_9. CH_3SCN^+ + HCl		0.75	
$(CH_3)_2OH^+$	t-$C_4H_9^+$ + $(CH_3)_2O$ + HCl	+55.5	0.50	1.3
	t-C_4H_9. $(CH_3)_2O^+$ + HCl		0.50	
$C_3H_6OH^+$[d]	t-$C_4H_9^+$ + C_3H_6O + HCl	+69.4	< 0.1	1.2
	t-C_4H_9. $C_3H_6O^+$ + HCl		> 0.9	
$(CH_3)_2COH^+$	t-$C_4H_9^+$ + $(CH_3)_2CO$ + HCl	+76.5	< 0.1	0.25
	t-C_4H_9. $(CH_3)_2CO^+$ + HCl		> 0.9	

[a] kJ mol^{-1} from [Lias et al (1988)]
[b] Branching ratios are no more accurate than ≈ 10%
[c] Units $cm^3\ s^{-1} \times 10^{-9}$
[d] Protonated methyl oxirane, other minor product channels are not considered.

4.4. Discussion

The measurements of rate coefficients and branching ratios described above, and listed in Table 4-1 raise several interesting questions. At first sight the results imply that bimolecular reactions that are up to 40 kJ mol^{-1} endothermic are occurring at a significant fraction of the collision rate. If this is true then several assumptions that have been used by ion-molecule chemists for many years may be threatened. If it is not true then how can the observations be reconciled within the framework of existing theory ?

Historically the enthalpy change associated with an ion-molecule reaction rather than the free energy change has been considered as an indicator of whether or not the reaction can proceed at near the collision rate. It has generally been assumed that if a reaction occurs at a significant fraction of the collision rate then the reaction must be significantly exothermic. The issue of whether or not thermoneutral or even slightly endothermic reactions can be fast has been raised by several authors, and the postulate of "entropy driven reactions" has arisen. The concept of reaction kinetics being "driven" or dictated by entropy, which is fundamentally a thermodynamic term is somewhat contentious, but can this effect be explained within the ambit of more conventional kinetic models, and if so can this shed light on the present series of reactions ?

4.4.1. Fast Endothermic Reactions ?

The fundamental question to be addressed is whether an endothermic reaction can be fast. Several reports indicate that this is the case, at least for small endothermicities. Meot-Ner has, in conjunction with several authors over the years, studied bimolecular exchange reactions using High Pressure Mass Spectrometry and ICR techniques. The use of temperature variation allows determination of both ΔH and ΔS using the Van't Hoff relation [Meot-Ner and Sieck (1991b)]. Both proton and charge transfer reactions have been studied [Sieck and Meot-Ner (1982)] [Meot-Ner (1987)], [Meot-Ner (1991a)]. These authors report reactions endothermic by up to 30 kJ mol^{-1} as proceeding at close to the collision rate, although most of the fast endothermic processes reported are less than 12 kJ mol^{-1} endothermic. A report by Lias [Lias (1987)] points out that some of the earlier charge transfer results may have been wrongly attributed as endothermic when in fact they were exothermic.

Meot-Ner proposes the existence of a class of intrinsically fast reactions, where the reaction efficiency is determined by the equilibrium constant for the reaction. These

intrinsically fast reactions are characterised by a single well potential with no activation barriers and with product-like transition states.

The suggestion that the magnitude of a rate constant can be inferred from thermodynamic parameters is not unusual, the basis of the activated complex or transition state theory of kinetics is that a rate constant can be expressed as a product of a frequency term and a thermodynamic term [Eyring (1935)]. There are several different derivations of the transition state result but the result is the same,

$$k = \left(\frac{k_b T}{h}\right) K^* , \tag{4.2}$$

in this expression k_b is the Boltzmann constant, h is Plancks constant, T is the temperature and k the rate coefficient for the reaction. In the transition state expression the equilibrium constant K^* represents the equilibrium constant for the process going from reactants to the activated complex. It is central to activated complex theory that the activated complex is in a "virtual" equilibrium with the reactants. It is important to note that the equilibrium constant is determined as the ratio of partition functions of complex and reactants multiplied by the energy term and that the activated complex has one less vibrational degree of freedom than the reactants, that mode being taken to be the reaction coordinate.

If the equilibrium constant, instead of being expressed as a ratio of partition functions, is written in terms of the thermodynamic parameters of the transition state we have

$$k = \frac{k_B T}{h} \exp\left(\frac{\Delta S^*}{R}\right) \exp\left(\frac{-\Delta H^*}{RT}\right). \tag{4.3}$$

In this expression ΔS^* and ΔH^* are respectively the entropy and enthalpy of activation. That is the change in entropy or in enthalpy in going from reactants to the transition state. R is the gas constant in the appropriate units. The use of the thermodynamic state functions of the activated complex is unusual, but just as valid as the use of partition functions. The use of additive or group properties to estimate the enthalpy and the entropy of the activated complex is discussed by Benson [Benson (1976)]. Thus the use of thermodynamic parameters to estimate the rate of a reaction is certainly established practice and in fact activated complex theory forms the basis of the most common statistical rate theories used widely today.

The thermodynamic parameters of the transition state are clearly indicators of the energy and structure of the system. The use of statistical thermodynamics to produce an entropy and an enthalpy for the transition state requires the properties of the individual molecule of the activated complex to be known, in terms of energies and structure. Can thermodynamic properties determined experimentally from the bulk properties of the reactants and products be used to determine or to estimate the reaction rate ?

The assumption central to the discussion of the intrinsically fast reactions is that the transition state is close to the products. It is this suggestion that allows the transition state expression

$$k = \frac{k_B T}{h} \exp\left(\frac{\Delta S^*}{R}\right) \exp\left(\frac{-\Delta H^*}{RT}\right), \tag{4.4}$$

to be written in terms of the entropy and the enthalpy change of the reaction.

$$k = \frac{k_B T}{h} \exp\left(\frac{\Delta S^\circ}{R}\right) \exp\left(\frac{-\Delta H^\circ}{RT}\right). \tag{4.5}$$

The concept that the parameters of the transition state can be approximated by the parameters of the products clearly requires the absence of any activation energy or tightening of the collision complex. A simplified diagram is shown below.

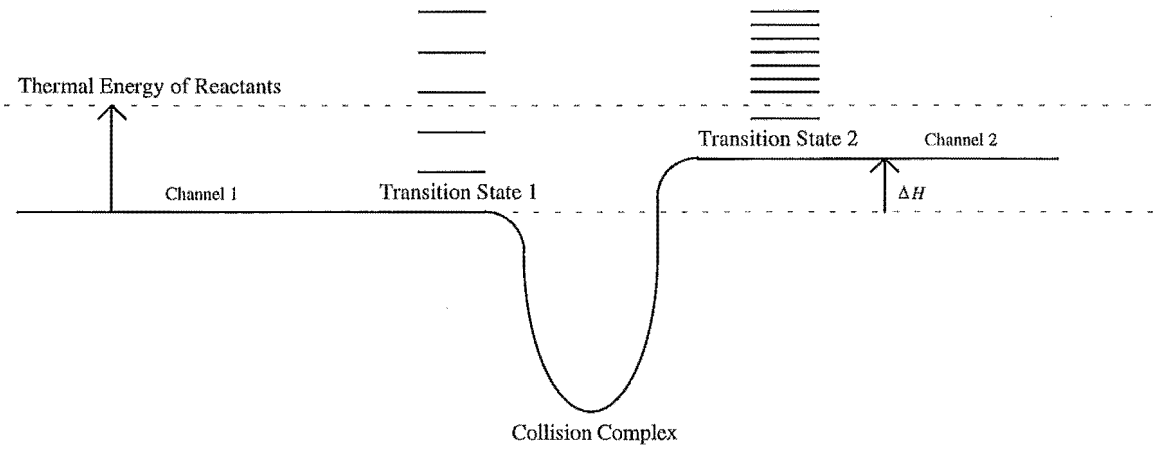

Figure 4-4. A potential surface of an ion-molecule reaction with product like transition states.

This treatment is clearly not rigorous since even if the enthalpy of the transition state is similar to that of the products, the entropy must be different since not only is the reaction coordinate excluded from the transition state, but it is inconceivable that the transition state should have the same translational and rotational freedom as the separated products, there must be some tightening of these modes.

It is plausible that for the proton and charge transfer reactions that constitute the majority of the reactions for which thermodynamically driven kinetics is postulated, a loose transition state may exist.

In this context the description "loose" refers to a transition state which retains many of the rotational modes, both internal and external of the reactants. The expression "tight" refers to a transition state in which the interaction between the particles is sufficiently strong that the rotations become vibrations.

In the majority of ion-molecule reactions, including proton transfer reactions with hindered bases [Meot-Ner and Smith (1991)] and any reaction involving substantial rearrangement, a more or less tight (or locked rotor) transition state will apply. In this case the overall thermodynamics of the process will have no bearing on the magnitude of the rate which is determined by the potential surface in the transition state region.

The question of how to account for a rapid endothermic reaction using conventional kinetic theory can be considered qualitatively. The first step is to look at the system in terms of energy rather than enthalpy, since the usual method of estimating rate coefficients is to average the microscopic rate coefficients $k(E)$ over the populations of the different energy levels. Where there is an energy of activation $E°$, $k(E)$ will be zero for all values of E less than $E°$. The energy E is the energy contained in the various translational, rotational, and vibrational modes of the reactants. A common assumption amongst kinetic theories is that the energy E can be rapidly randomised within the modes of the complex, but the theories differ as to the extent to which some of this energy is locked into inactive modes and is unable to contribute to the crossing of the barrier. For a more complete discussion on this point see the chapter below dealing with association reactions.

An estimate of the amount of thermal energy available for barrier crossing can be made by summing the contributions from the various degrees of freedom that are occupied at room temperature. Effectively in most cases these will be translational and rotational, each active mode contributing ½ RT or 1.25 kJ mol^{-1} at 300 K. In the case of bimolecular reactions the energy in these modes, given that there are two separate reactants (assuming both to be non linear) is of the order of 15 kJ mol^{-1} at 300 K. Where the reactants are large they may contain internal rotations, such as the methyl rotations in t-C_4H_9Cl, and

where there are heavy atoms there may be low vibrational frequencies that contribute at 300 K. Clearly the reactants will in many cases posses sufficient energy to surmount an activation barrier.

Conventional unimolecular theory views the bimolecular exchange reaction

$$AH^+ + B \rightarrow A + BH^+ \tag{4.6}$$

as the dissociation of the collision complex species A..H..B$^+$ into two competing channels. The unimolecular rate of dissociation via a given channel being a function of energy described by the expression

$$k(E) = \frac{W^{ts}\left(E - E^0\right)}{\rho(E)\, h} \tag{4.7}$$

where W^{ts} is the sum of available states of the activated complex between the energy E and the activation energy E^o at the energy given and ρ is the density of states of the dissociating species at that energy.

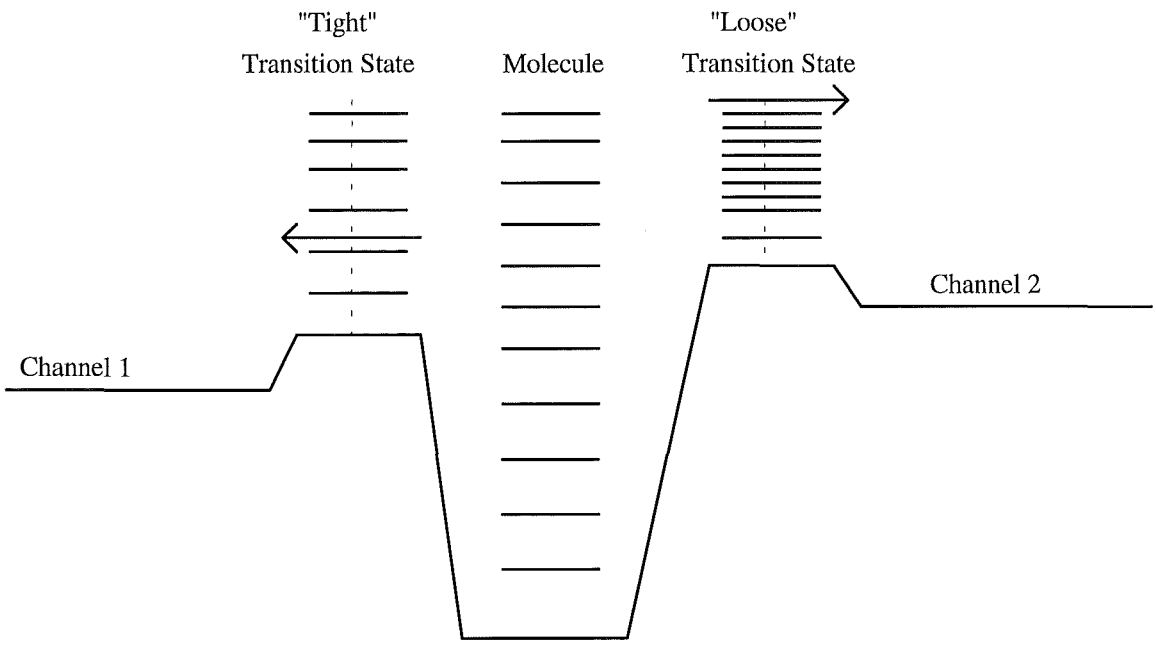

Figure 4-5. Simple surface for an ion-molecule reaction having both a "loose" and a "tight " transition state .

Clearly the greater the difference between E and E° the greater the sum of the states will be (ie the lower the barrier to a given channel the higher the rate will be). This is in essence an enthalpic effect, and is often described as such.

Clearly also the greater the density of available states in the activated complex the greater the rate. Since low lying states make the largest contributions to the density of states a "loose" transition state with a number of rotational modes will generally have a greater density of states than a "tight" transition state. This effect is often described as an entropic effect.

It is a generalisation to say that the "entropic" effect will dominate at higher energies and the "enthalpic" at lower energies, as indicated in Figure 4-5. Whether or not a channel with a significantly higher barrier can dominate by means of a very loose transition state cannot be determined except by carrying out the appropriate calculations. At the present time these calculations have not been reported for the systems of interest, since prerequisites for meaningful calculations are accurate structures and energies.

The only reliable statement that can be reached with regard to the question of whether or not an endothermic process can be fast is that no conclusion can be reached.

The fact that a reaction is endothermic does not conclusively mean that it will be slow. On the other hand the ΔG of a reaction gives no information as to the kinetics without knowledge of the transition state region.

One worthwhile work could be to model using a statistical rate model such as RRKM or Phase Space theory the dissociation of a model system into two channels at different energies to see the effect of altering barrier height and the tightness of the transition state.

Having discussed the evidence concerning the class of reactions described as intrinsically fast, attention must focus on the present system, involving the apparent formation of three product moieties from two reactants with, in some cases, a significant endothermicity of reaction. The nature of this process, as discussed below, is likely to involve more than one step, so it falls outside the realm of the processes discussed briefly above, however the general principles discussed above will still apply.

4.4.2. Thermochemistry of $BH^+ + t\text{-}C_4H_9Cl$

Before considering in which way the thermodynamics of the system influence or illuminate the kinetics of the above reaction, it is important to discuss what is known or can sensibly be estimated about the thermodynamics of the system. While the enthalpies of formation and the entropies of many neutral species are tabulated with some accuracy

the same information is not available for many of the ionic species. This leads to the somewhat unfortunate circumstance that many of the quantities that are central to the thermochemistry of the above system are not known and must be estimated.

Enthalpies of Formation

For the reactions described in this chapter accurate information is available for ΔH_f° of the neutral species, but values for the protonated species and the t-$C_4H_9^+$ ion are not known accurately. The ΔH_f° values for the protonated compounds have been determined in the main by measurements of the proton affinity of the corresponding neutral [Lias et al (1988)]. The thermochemical data compilation of Lias et al is one of the largest, and has become a standard reference over the years. In recent years however, there have been several reports that the proton affinity scale of Lias et al is significantly inaccurate especially at the higher end of the scale.

Meot-Ner and Sieck [Meot-Ner and Sieck (1991a)] reported a series of variable temperature measurements from which Van't Hoff plots for proton transfer equilibria were obtained. From these measurements, which accurately determine the enthalpy of reaction by allowing the entropy to be eliminated, the authors suggested that several of the higher proton affinities such as those of NH_3, CH_3CH_2 and others should be increased. This was followed by a paper by Szulejko and McMahon [Szulejko and McMahon (1993)] which suggested that the value of ΔH_f°(t-$C_4H_9^+$), an important standard value in the proton affinity ladder, could be as much as 17 kJ mol^{-1} larger than previously thought. A recent paper by Smith and Radom [Smith and Radom (1993)] compared a number of proton affinities calculated by ab-initio means to G2 level with the different experimental scales, and suggested that the results of Szulejko and McMahon are in good agreement with their theoretical results.

The value of ΔH_f°(t-$C_4H_9^+$), which is of fundamental importance to the thermochemistry considered in this chapter, as well as to the various proton affinity scales is not well known. The value used by Lias et al is 694 kJ mol^{-1}, that derived by Smith and Radom by G2 calculations is 714 kJ mol^{-1}, and a recent experimental result by Keister et al [Keister et al (1993)], utilising photoelectron photoion coincidence methods is even higher, at 734 kJ mol^{-1}.

In order to appreciate the effect of the recent reports on the thermochemistry of the reaction described above the ΔH_f values for the relevant species are tabulated below.

The neutral enthalpies of formation are from [Lias et al (1988)], the enthalpies of formation of the protonated species have been determined using the proton affinity values of [Szulejko and McMahon (1993)] or from the calculations of [Smith and Radom (1993)]. For comparison with the enthalpy of reaction data derived from Lias et al, which

is used in Table 4-1. the enthalpies of reaction calculated using the revised $\Delta H_f(BH^+)$ values and the larger value of $\Delta H_f^\circ(t\text{-}C_4H_9^+)$ reported by Smith and Radom are shown in Table 4-2.

Table 4-2. Comparison of thermochemical values from [Lias et al (1988)]with recent measurements.

Base (B)	$\Delta H_f^\circ(B)$[a]	$\Delta H_f^\circ(BH^+)$[b]	$\Delta H_f^\circ(BH^+)$[c]	ΔH° reaction[d]	ΔH° reaction[e]
CO	-110.5	826	826	-152.8	-133
HCN	135	946	953	-27.3	-15
HC_3N	352	1126		9.2	
CH_3OH	-202	569	569	12.5	34
CH_3CHO	-166	582	595	35.9	44
C_2H_5OH	-235	506		42.2	
CH_3CN	75.3	816	826	42.6	53
CH_2CHCN	184	921	929	46.7	57
CH_3SCN	159	887		55.2	
$(CH_3)_2O$	-184	544	553	55.5	67
Methyl Oxirane	-94.6	619		69.4	
$(CH_3)_2CO$	-217	490	503	76.5	84

[a, b, d] From [Lias et al (1988)] units kJ mol^{-1}

[c] From [Szulejko and McMahon (1993)] or [Smith and Radom (1993)] units kJ mol^{-1}

[e] Calculated using $\Delta H_f(t\text{-}C_4H_9^+)$ 714 kJ mol^{-1} [Smith and Radom (1993)]

Entropy Values

The suggestion that ΔG rather than ΔH should be used as a criterion in the study of ion-molecule processes has a significant drawback quite apart from whether or not it is theoretically correct. This drawback is that experimentally measured entropy values are simply not available for most species. The equilibrium measurements made at different temperatures using Pulsed Electron High pressure Mass Spectrometers for proton transfer and other such reactions allow for experimental determination of ΔS, but the measurement of ΔS values by flow tube experiment requires the use of either a VT-SIFT or a SIFDT.

The measurements described in this chapter were forward rate measurements only, so the entropy change in the reactions can only be estimated. While tables of entropies of gas phase molecular species exist these are limited to small species of up to 2 carbon atoms, and the entropies of ions are rarely recorded. In order to estimate the entropy change in the process

$$BH^+ + t\text{-}C_4H_9Cl \rightarrow t\text{-}C_4H_9^+ + B + HCl \qquad (4.1)$$

several assumptions have been made. The primary assumption is that the entropy of the protonated base will be similar to that of the neutral base itself. Since this amount is on both sides of the reaction it cancels. The second assumption is that the entropy of t-$C_4H_9^+$ can be replaced by the entropy of the t-$C_4H_9^{\cdot}$ radical, which is known. The entropy of HCl is well known, but that of t-C_4H_9Cl is not.

Calculating the entropy of t-C_4H_9Cl can be done utilising the methods developed by Benson [Benson (1976)]. The molecule can be thought of as comprised of a number of groups, each of which has a calculated contribution to such molecular properties as entropy and heat capacity. The contributions from the groups are added, and then the total is corrected by subtracting $R \ln \sigma$ which is the correction for the total symmetry of the system, both internal (the three methyl rotors) and external.

Table 4-3. Calculation of Standard Entropy of t-C_4H_9Cl.

Group	Contribution (J K^{-1} mol^{-1})
3 [C-(C)$(H)_3$]	3×127.3
[C-(Cl)$(C)_3$]	1×22.6
Symmetry Correction	$-R \ln 27$
Total S 300K	≈ 377 J K^{-1} mol^{-1}

The other entropy values are tabulated by Benson $S°_{300}$ (HCl) is 188 J K^{-1} mol^{-1} and $S°_{300}$ (t-$C_4H_9^{\cdot}$) is 301 J K^{-1} mol^{-1} . Thus the overall $\Delta S°$ is 113 J K^{-1} mol^{-1} for the reaction.

The major source of error in the above quantity probably arises from the assumption that $S°$ (BH^+) = $S°$ (B). This error can reasonably be assumed to be greatest for the smallest neutral species. Comparing the tabulated values for the entropies of CO and the radical HCO (the value for HCO^+ is not tabulated) the entropy of the radical is 27 J $K^{-1}mol^{-1}$ higher than that of CO. This corresponds to an error of 23 % in the estimation of the entropy change in the reaction. For larger neutrals the error can be expected to be much lower.

Overall Thermodynamics of $BH^+ + t\text{-}C_4H_9Cl \rightarrow t\text{-}C_4H_9^+ + B + HCl$

Irrespective of any kinetic analysis, for a process to proceed spontaneously it must have a negative free energy change. If ΔG for a process is positive then that process will not be spontaneous, and if both ΔG and ΔH are positive then that process should not be observed in a SIFT system.

Given that the entropy change $\Delta S°$ is around 110 J K^{-1} mol^{-1} the factor $T\Delta S$ at the temperature of the SIFT experiment ($\approx$ 300K) is 33 kJ mol^{-1}. This value is, as described above very much an estimate but it can be compared with the calculated endothermicities of the respective reactions in Table 4-1. Clearly the reactions of $C_3H_6OH^+$ and of $(CH_3)_2COH^+$ cannot have a negative $\Delta G°$ unless the estimate of $\Delta S°$ is very wrong. The reactions of several of the other ions are also much more than 33 kJ mol^{-1} endothermic. The comparison leads to the conclusion that either the calculated entropy change is grossly too small, or the enthalpies of reaction are incorrect, or that the proposed mechanism is not in fact operating.

Before reaching a conclusion on what mechanism is operating in this series of reactions, consider several possible pathways.

4.4.3. Possible Mechanisms

The available evidence, with which to postulate a mechanism for the reactions can be quickly summarised.

Firstly the ionic products of the reactions are t-$C_4H_9^+$ and the cluster ion B.t-$C_4H_9^+$ where B is the base used. Unfortunately the observation of the ionic products does not define the nature of the neutral products. It is possible that where the observed ion product is t-$C_4H_9^+$ the neutrals exist as a complex B.HCl. The possibility also exists that a weakly bound cluster ion may be formed, which may be dissociated by the voltages on the downstream ion optics.

Secondly there are results of isotope labelled experiments carried out by Meot-Ner using Pulsed Electron High Pressure Mass Spectrometry. In these experiments the reactions of protonated C_2H_5OH, C_2H_5CN and CH_3CN were studied using t-C_4D_9Cl. The results indicate that the ionic product formed in the first instance (the PHPMS instrument allows a number of secondary and tertiary reactions to occur) is t-$C_4D_8H^+$.

Given the above experimental results what can be said about the mechanism of the reaction ? There are three basic mechanisms that can be postulated.

Initial proton transfer followed by loss of HCl.

In this mechanism the first step could be thought of as a simple proton transfer between BH^+ and t-C_4H_9Cl. The resultant complex could then lose HCl,

$$BH^+ + \text{t-}C_4H_9Cl \rightarrow B + [\text{t-}C_4H_9Cl.H]^+ \rightarrow B + \text{t-}C_4H_9^+ + HCl\ . \qquad (4.8)$$

The main argument against this mechanism is that the proton affinity of t-C_4H_9Cl, while not reported, is likely to be considerably lower than that of the majority of the bases used in the study. The proton affinity of CH_3Cl is 682 kJ mol^{-1}, in order to estimate the effect of increasing substitution the compounds CH_3OH, C_2H_5OH and t-C_4H_9OH can be considered. Their proton affinities are, in kJ mol^{-1}, 761, 788 (+ 27) and 810 (+ 49). Comparison with the corresponding series of chlorides gives PA(CH_3Cl) 682, PA(C_2H_5Cl) 707 (+ 25) and the estimated PA(t-C_4H_9Cl) ≈ 732 (+ 50). This value for the proton affinity is lower than that of all the bases used in this experiment except CO and HCN.

Formation of a Tight Complex followed by Simultaneous Loss

In this mechanism a tight complex incorporating both reactant species that rearranges to allow for the simultaneous rupture of two bonds to leave the three product bodies is postulated,

$$BH^+ + t\text{-}C_4H_9Cl \rightarrow [B.\ HCl.\ t\text{-}C_4H_9]^+ \rightarrow B + HCl + t\text{-}C_4H_9^+. \qquad (4.9)$$

The most compelling argument against this mechanism is that the simultaneous rupture of two bonds is statistically unlikely to be a rapid process.

Formation of a Complex Followed by Sequential Loss

This is a general description which envisages the formation of a more or less tight complex, which dissociates twice to produce the postulated three body product channel. The complex may dissociate once to give loss of HCl, the resulting [t-C_4H_9· B]$^+$ complex can either dissociate to give t-$C_4H_9^+$ or be collisionally stabilised,

$$BH^+ + t\text{-}C_4H_9Cl \rightarrow [BH.\ t\text{-}C_4H_9Cl]^+ \rightarrow [B.\ t\text{-}C_4H_9]^+ + HCl \rightarrow B + t\text{-}C_4H_9^+ + HCl \qquad (4.10)\ .$$

Among the points in favour of this general mechanism is that it, unlike the two mechanisms above, allows for both the observed product channels, that is formation of t-$C_4H_9^+$ and the stabilisation of the cluster [B. t-$C_4H_9^+$]. The first complex formed must be sufficiently long lived that the observed isotopic scrambling can occur before the loss of HCl. The formation of [B. t-C_4H_9]$^+$ + HCl is exothermic, and if there is insufficient energy left after the loss of HCl the cluster cannot dissociate.

Other Possibilities

It must be remembered that the SIFT can only observe the ionic products of the chemistry within the flow tube. The observation of t-$C_4H_9^+$ as an ionic product leads to the assumption that the neutral products are HCl and the appropriate base. While this seems a

reasonable assumption it is just an assumption. It is possible that the neutral products could exist as a weakly bound cluster. This was proposed by Fisher and Armentrout [Fisher and Armentrout (1990)] as an explanation for the facility with which the apparently endothermic process

$$HCN^+ + CF_4 \rightarrow CF_3^+ + HF + HCN \qquad (4.11)$$

proceeds. The bimolecular rate measured by Petrie et al [Petrie et al (1990)] was 1.15×10^{-9} cm^3 s^{-1}. Fisher and Armentrout suggest that the neutral products could well be present as a Van der Waals complex with a binding energy of up to 14 kJ mol^{-1}. The authors also point out that the reaction could also produce such species as CF_3. HF^+ or $CF_3.CN^+$. If these clusters were bound by less than 0.4 eV (36 kJ mol^{-1}) it is suggested that a flow tube experiment might be unable to detect them due to fragmentation in the ion detection region.

The analogous formation of cluster products in the reactions described in this chapter cannot be discounted. The voltages used on the downstream ion optics of the SIFT are not expected to produce significant fragmentation of cluster ions, and the observation of ≈ 100 % cluster ion formation for the reactions of both protonated methyl oxirane and protonated acetone suggests that such fragmentation was not a major problem. The formation of neutral clusters seems unlikely if a two step mechanism operates, with loss of HCl giving $[t\text{-}C_4H_9.B]^+$ which can dissociate further or be stabilised, since of course the HCl has left. The formation of a neutral cluster could however be a competing mechanistic channel.

4.5. Conclusion

The $t\text{-}C_4H_9Cl + BH^+$ system studied in the SIFT and the ICR exhibits an apparent endothermic product channel to yield the $t\text{-}C_4H_9^+$ ion together with HCl and B. The branching ratio of this channel seems to be up to 50% of a total reaction rate that is close to the collision rate even though the channel may be up to 50 kJ mol^{-1} endothermic.

The entropy change ΔS associated with the reaction has been estimated to produce a $T\Delta S$ factor of around 33 kJ mol^{-1} at 300K. This cannot be used to definitively rule out the proposed mechanism because of the uncertainties involved in the estimation.

Given that a barrier can be overcome by thermal energy within the reactants a qualitative estimation of that energy for the reactants t-C_4H_9Cl + BH yields 26 kJ mol^{-1}. Since there are a total of 6 translational degrees of freedom and 9 rotations (including the three internal methyl rotors), and there are three vibrational modes (C-C-Cl bends) at 400cm^{-1} that may be occupied at 300K. This amount of thermal energy is significant, and if this energy is thought to be all within the active modes it is reasonable to expect some of the collision complex to overcome the endothermicity. It seems on a purely qualitative basis however that the energy of the system is insufficient to allow fast passage through the endothermic channel, since even though the transition state may be very loose, the number of states available will necessarily be low so close to the top of the barrier.

The conclusion that suggests itself is that unless the thermochemical information is significantly wrong, some fraction of the products may be formed as weakly bound clusters which dissociate on sampling.

CHAPTER FIVE

ISOMERS OF $C_3H_6N^+$

5.1. Introduction

The neutral species C_2H_5CN, ethyl cyanide, has been detected in interstellar clouds by observation of its microwave emission spectrum. The concentration of C_2H_5CN has been measured in two interstellar cloud regions, OMC-1, Orion, and Sgr B2 [Johnson et al (1977)]. The observation of the compound in the interstellar environment begs the questions, how did it get there, and what are the mechanisms for production of this species? Two different association reactions have been proposed as possible synthetic routes to C_2H_5CN.

Reaction of CH_3^+ with CH_3CN

The association of CH_3^+ with CH_3CN followed by dissociative recombination with an electron to yield C_2H_5CN + H has been postulated as a synthetic route by Smith and Adams [Smith and Adams.(1989)].

CH_3^+ ions are thought to play a central role in the synthetic chemistry of interstellar clouds [Smith (1988)]. The formation of CH_3^+ is effected from the reaction of the primary ion H_2^+ with the ubiquitous H_2 to give H_3^+ which can react with a C atom to give CH_3^+.

The neutral CH_3CN is thought [Smith (1988)] to arise through the radiative emission stabilised association

$$CH_3^+ + HCN \rightarrow CH_3CNH^+ + h\nu, \qquad (5.1)$$

followed by dissociative recombination,

$$CH_3CNH^+ + e \rightarrow CH_3CN + H. \qquad (5.2)$$

The association CH_3^+ + HCN is reported to yield two isomers of $C_2H_4N^+$, the nitrile and the iso-nitrile, with the lower energy isomer, the nitrile, predominating [Knight et al (1986)]. While the branching ratio of products from dissociative recombination reactions is difficult to predict, the rule of thumb that less rather than more rearrangement will take place favours the CH_3CN structure as the eventual neutral product.

The reaction between CH_3^+ and HCN has been studied in the laboratory by both SIFT and ICR techniques [McEwan et al (1980)] [Kemper et al (1985)]. At first it was thought that the association would proceed via a fast radiative channel at low pressures, but subsequent work revealed that this channel was in fact slow under laboratory conditions, $k_2 < 5 \times 10^{-12}$ cm^3 s^{-1} at 300K, but it is thought that it will still be a significant process in the tenuous and very cold interstellar cloud environment.

Regardless of synthetic considerations, the fact is that CH_3CN has been observed at significant concentrations in the same interstellar regions as has C_2H_5CN [Solomon et al (1971)].

The reaction of CH_3^+ and CH_3CN has also been studied, and the rate measured by both ICR and SIFT techniques [McEwan et al (1989)],[Knight et al (1986)]. The association channel dominates at SIFT pressures, proceeding at close to the collision rate, but at lower pressures the two exothermic bimolecular channels are significant;

$$CH_3^+ + CH_3CN \rightarrow C_3H_6N^+ + h\nu \quad (5.3a)$$
$$\rightarrow HCNH^+ + C_2H_4 \quad (5.3b)$$
$$\rightarrow C_2H_5^+ + HCN\,. \quad (5.3c)$$

The three body association rate coefficient in the parent gas is 1.9×10^{-22} cm^6 s^{-1}, and in helium it is 1.0×10^{-23} cm^6 s^{-1}.

The above system has been extensively studied using *ab initio* methods [Smith S.C et al (1993)], [Deakyne and Meot-Ner (1990)] as a preliminary to modelling the association process. The *ab initio* results suggest that the association product of the above reaction is not in fact $C_2H_5CNH^+$, but actually has the structure $CH_3CNCH_3^+$.

Thus the association reaction of CH_3^+ with acetonitrile was certainly a synthetic route to $C_3H_6N^+$, but whether or not the product had the protonated ethyl cyanide structure was a matter of some conjecture.

The reaction of $HCNH^+$ with C_2H_4

Association between $HCNH^+$ and C_2H_4 followed by dissociative recombination was also put forward as a synthetic pathway to ethyl cyanide [Herbst et al (1989)], on the basis that CID studies showed that protonated ethyl cyanide decomposed to $HCNH^+$ and C_2H_4. The association reaction

$$HCNH^+ + C_2H_4 + M \rightarrow C_3H_6N^+ + M, \quad (5.4)$$

was measured by Herbst et al over a range of temperatures using a VT-SIFT, giving a termolecular rate coefficient of 7×10^{-27} cm^6 s^{-1} in He carrier gas at 300K. The authors attempted to model the system, but found that they were unable to match the observed termolecular rate coefficient using the assumption that $C_2H_5CNH^+$ was the association product.

Clearly then, the observation that ethyl cyanide was a significant interstellar species implied that a pathway exists to synthesise this compound. The assumption was made that the C_2H_5CN neutral arises from dissociative recombination of the $C_2H_5CNH^+$ ion. Two pathways were proposed, so the problem became one of finding the isomeric composition of the products of each pathway and then identifying, if possible the isomers in terms of their structure.

5.1.1. The Use of Proton Affinities to Distinguish Isomers

The use of the SIFT to examine the isomeric structures of various small ions is discussed in the recent review article by McEwan [McEwan (1992)]. The principle behind the elucidation of isomer structure is to characterise the reactivity of each isomer, then to identify that isomer. The smaller the ion is, generally the fewer possible isomers there are and, at least theoretically, the easier the task.

A class of reactions that is of great use in studies of isomerism in the gas phase is proton transfer. Large compilations have been made listing the experimentally determined or theoretically calculated proton affinities of many species. If the isomers in question are listed then the identification is simple. If the isomers have not been studied then a proton affinity measurement is a convenient tag for that isomer, allowing possible structures to be eliminated, and providing a known property of the species that can be calculated by *ab initio* methods to test a predicted structure.

Proton Affinity Defined

The proton affinity of a neutral species X can be defined in terms of the enthalpy change required to protonate that species. For the reaction

$$X + H^+ \rightarrow XH^+ \tag{5.5}$$

the proton affinity of the compound X is defined as the negative enthalpy of reaction,

$$PA(X) = - \Delta H^0 . \tag{5.6}$$

Thus

$$PA(X) = \Delta H_f^0 (X) + \Delta H_f^0 (H^+) - \Delta H_f^0 (XH^+). \tag{5.7}$$

The quantities required for an exact experimental determination of PA(X) are not easily measured, so over the years a number of indirect methods for derivation of proton affinity have been used.

Proton Affinity Measurements

The most common method for measuring a proton affinity is the equilibrium method. This technique was developed in the early seventies by Bowers et al [Bowers et al (1971)]. The method relies upon setting up an equilibrium between two competing

proton transfer reactions. Two bases, X, and, B, with comparable proton affinities are used.

$$XH^+ + B \rightleftharpoons BH^+ + X\,. \tag{5.8}$$

The equilibrium constant for the system is

$$K = \frac{[BH^+][X]}{[XH^+][B]}. \tag{5.9}$$

The authors found K by measuring the ratio $\frac{[BH^+]}{[XH^+]}$ at a given ratio of $\frac{[B]}{[X]}$ using both drift and trapped ion ICR methods. The authors initially treated $\Delta H°$ as being the same as $\Delta G°$ obtained from the equilibrium constant, ie entropy was neglected. This simple treatment yields

$$\Delta G \approx \Delta H° = \text{PA(X)-PA(B)}. \tag{5.10}$$

At around the same time equilibrium measurements were made using FA measurements [Roche et al (1971)] [Bohme et al (1973)]. In these measurements the equilibrium constants were measured by two means. The first entailed the addition of both neutrals to the flow tube to obtain equilibrium conditions, then measuring the ratios of ionic abundances. The second method involved measuring the forward and reverse reaction rates and using the expression

$$\Delta H^0 \approx \Delta G^0 = -RT \ln\left(k_f / k_r\right), \tag{5.11}$$

where k_f is the forward rate coefficient and k_r is the rate coefficient for the reverse reaction. Again the entropy term was disregarded, and the experimenters reported that the values obtained for the proton affinities were the same for both methods.

The method of measuring the forward and reverse rate coefficients is well suited to the SIFT instrument, since it is possible to prevent extraneous ions and competing reactions from complicating the results. An example of a recent SIFT experiment is afforded by that of Petrie et al [Petrie et al (1989)].

The equilibrium method can give accurate results only if two conditions are met, firstly that the proton affinity scale be anchored to one or more primary standards, which will be discussed below, and secondly that entropy effects are accounted for.

Accounting for the entropy factor has been done approximately by various methods. One is to assume that the vibrational modes of the species do not change appreciably so that the only contribution to the entropy term will be rotational,

$$\Delta S_{rot} = R \ln \frac{q_{BH^+} q_X}{q_{XH^+} q_B}. \tag{5.12}$$

Since the proton will not greatly alter the moment of inertia of the moieties a further simplification is often used, replacing the rotational partition functions q_i by the symmetry numbers of each species,

$$\Delta S_{rot} \approx R \ln \frac{\sigma_{BH^+} \sigma_X}{\sigma_{XH^+} \sigma_B}. \tag{5.13}$$

Other, more elaborate treatments have been made, but the only really accurate method is to measure the equilibrium constant as a function of pressure, so that the $T\Delta S$ factor can be measured. This has been done by two recent high pressure mass spectrometer studies [Meot-ner and Sieck (1991)] and [Szulejko and McMahon (1993)].

Absolute Proton Affinities

However accurate the measurement of the equilibrium constant and the connected entropy component, the experiment can only return the difference in proton affinity between the two bases. Using a series of such equilibrium measurements a thermochemical ladder can be constructed, but in order to obtain absolute values for the ladder it must be anchored with a number of 'primary standards' for which the proton affinity is well known.

In order to know the absolute proton affinity of a base B the following enthalpy changes must be known accurately, ΔH_f^0 (B),ΔH_f^0 (H^+) and ΔH_f^0 (BH^+). It is the measurement of the final quantity that is difficult. The two usual methods for calculating ΔH_f^0 (BH^+) are appearance energy and measuring the ionisation potential of BH. The method of appearance energies can be accurate but is not suitable for use on all systems because alternative fragmentation channels may exist or the fragmentation may posses an activation barrier. The use of *ab initio* calculations of the proton affinities of small species may now be sufficiently accurate that *ab initio* values can be used instead of experimental results. For example, as a primary standard for their absolute gas phase proton affinity scale, Szulejko and McMahon used the proton affinity of CO. They chose a value of 593.9 kJ mol^{-1} as a mean value between the value of 594.3 ± 2.9 kJ mol^{-1} obtained by dissociative photoionisation of formyl compounds [Treager (1986)] to yield ΔH_f^0 (HCO^+) combined with a value of ΔH_f^0 (HCO) obtained by photoelectron

spectroscopy, and the value of 589.2 ± 2.1 kJ mol^{-1} calculated from *ab initio* results [Del Bene and Frisch (1989)].

Proton Affinity Bracketing

In circumstances where it may not be practical to accurately measure the proton affinity of a species it may serve the experimental purpose just as well to be able to bracket the proton affinity of the species between two limiting values.

The assumption that proton transfer will only occur if the process is exothermic was applied by Haney and Franklin [Haney and Franklin (1969)]. This assumption is demonstrably untrue in that the successful equilibrium method relies on measuring the rate of both exo and endothermic proton transfer processes. It is more accurate to assume that fast proton transfer will only occur if the process is exothermic. Deakyne et al measured the proton affinities of C_4H_2, HC_3N, and C_2N_2 by bracketing techniques, and made the assumptions that the direction of the enthalpy change could be indicated by the ratio of the observed rate coefficient to the collision rate.[Deakyne et al (1987)]

$$\begin{aligned} &\text{for } \frac{k}{k_{coll}} > 0.6 && \Delta G < 0 \\ &\text{for } 0.2 < \frac{k}{k_{coll}} < 0.6 && \Delta G = 0. \\ &\text{for } \frac{k}{k_{coll}} < 0.2 && \Delta G > 0 \end{aligned} \tag{5.14}$$

Limitations to Proton Affinity Measurements

The measurement of proton affinities can be complicated by several factors. Competition from other reaction channels can be a major problem [Deakyne et al (1987)], as is the general difficulty of ensuring that the true temperature of the reactant ion used is known. While these problems can be overcome with careful techniques, there remain other, less tractable, difficulties.

The existence of entropy effects that can enhance or diminish the rate of a proton transfer reaction to a significant extent has been suggested by several groups, but other groups insist such effects need not be invoked. These views are discussed in the chapter on the reactions of t-C_4H_9Cl. Another effect that, although uncommon in ion-molecule chemistry, can greatly affect the rate of a reaction is activation energy. The proton transfer from $CH_3OCH_2^+$ to NH_3 and a number of other bases, for example, discussed elsewhere in this work, is significantly exothermic but occurs at a negligible rate at room temperature due to an activation barrier.

Given the above discussion it is clear that the existence of tables of proton affinity values including those of most of the important $C_3H_6N^+$ isomers, the isomers of $C_3H_6N^+$

formed in ion-molecule reactions can be identified by bracketing their proton affinities in relation to the proton affinity tables.

5.1.2. Derivation of Thermochemical Data

Table 5-1 lists the thermochemical data used throughout the present chapter. Much of the data comes from compiled experimental results [Lias et al (1988)]. Where experimental results were not available the ΔH_f° and PA values were based on the energy reported for $CH_3CNCH_3^+$ by *ab initio* results in the comprehensive paper by Smith et al [Smith S (1993)]. The theoretical study by Bouchoux et al [Bouchoux et al (1989)] reported the energies of the isomers $CH_2CHCHNH_2^+$ and $CH_2CHNHCH_2^+$ (among others) relative to their calculated energy for $CH_3CNCH_3^+$. These energies were treated by assuming that $CH_3CNCH_3^+$ had the same energy as calculated from the results of Smith et al.

The isomers of $C_3H_6N^+$ listed in Table 5-1 are those for which experimental data has been obtained and also two isomers reported as observed by Bouchoux at el in their recent compendious study of the possible isomeric structures of $C_3H_6N^+$ cations. While other structural isomers may exist, they are unlikely to be stable or if so to be formed in any of the reaction schemes considered in this study.

Table 5-1. Thermodynamic quantities used in the study of $C_3H_6N^+$ isomerism.

Species	ΔH_f° [a d]	Proton Affinity of neutral [a d]	Ref
$C_4H_8O_2$	-315	811	e
$(CH_3)_2CO$	-217.2	823	e
NH_3	-46	854	e
CH_3NH_2	-23	896	e
$C_2H_5NH_2$	-47	908	e
CH_3CN	75		e
CH_3^+	1093		e
$C_2H_5CNH^+$	774	806	e
$C_2H_5NCH^+$	820	852	e
$HCCCH_2NH_3^+$	870	882	e
$CH_3CNCH_3^+$	(780)		e, f
$CH_2CHCHNH_2^+$	(788)	(856)	f, g
$CH_2CHNHCH_2^+$	(841)	(898)	f, g
azabicyclo[1.1.0]butane.H^+	(958)	(887)	f,g

a Units kJ mol^{-1}

b Calculated from well depth of $CH_3CNCH_3^+$ relative to CH_3CN and CH_3^+

d Brackets indicate use of *ab initio* result

e [Lias et al (1988)],f [Smith S et al (1993)], g [Bouchoux et al (1989)]

5.1.3. Uncertainty in Proton Affinity Scales

It is important to note that the data obtained from the NIST data base [Lias et al (1988)] is subject to revision by more recent measurements, in particular the recent work of Meot-ner and Sieck and Szulejko and McMahon. These authors report new values for some of the proton affinities listed in Table 5-1. Unfortunately the two works do not agree, as can be seen from Table 5-2.

Although there is considerable discrepancy between the three compilations, they occur mainly in the proton affinities of bases with proton affinities greater than that of NH_3. The relative position on the proton affinity scale is the important factor in this bracketing study, and the only two bases whose position may change depending on which scale is used are NH_3 and C_2H_5NC whose proton affinities are close together anyway, so that their relative positions should be the same if the same scale is used throughout. Since the NIST data base is the most complete scale this scale is used throughout.

Table 5-2. Comparison of proton affinity values from recent reports.

Species	PA kJ mol^{-1} [a]	PA kJ mol^{-1} [b]	PA kJ mol^{-1} [c]
$C_2H_5NH_2$	935	908	
CH_3NH_2	919	896	901
NH_3	872	854	851
$(CH_3)_2CO$	830	823	810
C_2H_5CN	806	806	

[a] Meot-ner and Sieck (1991)
[b] Lias et al (1988)
[c] Szuleko and McMahon (1993)

5.2. Experimental

All the experiments described in this chapter were carried out on the SIFT. The results were analysed using the SIFT2D program. All measurements were made at room temperature of 295 ± 5 K, using a pressure of 0.30 ± 0.01 Torr of He carrier gas. The methods used to produce the different reactant ions are described in the results section below. Most of the neutral reagents were obtained from commercial sources and purified by repeated freeze-pump-thaw cycles. Ethyl isocyanide had been prepared using the method of Casanova et al [Casanova et al (1963)]. HCN was produced by the reaction of KCN with phosphoric acid. All reagents were used in pure form, although those with low vapour pressures required the use of an ice-water bath to lower the

temperature of the liquid phase to prevent condensation on expansion through the needle valve or variable leak valves.

5.3. Results

5.3.1. $C_3H_6N^+$ from protonated ethyl cyanide

Ethyl cyanide (propionitrile) was used in the ion source. Electron impact and the ensuing self proton transfer reaction produced a strong signal at 56^+ with minimal fragmentation or interference from 55^+.

Reaction with 1.4 Dioxane

Upon addition of 1.4 dioxane ($C_4H_8O_2$) from the downstream neutral inlet the 56^+ signal reacted rapidly with an overall rate of 1.1×10^{-9} cm^3 s^{-1}. The ionic products were 89^+ and 144^+, due to proton transfer and cluster channels respectively. Although the branching ratio was 80:20 in favour of cluster formation the proton transfer channel was clearly fast and therefore apparently exothermic.

Reaction with $(CH_3)_2CO$

The 56^+ signal reacted with $(CH_3)_2CO$ rapidly with a rate of 2.8×10^{-9} cm^3 s^{-1}. The only product channel observed was proton transfer to form $(CH_3)_2COH^+$.

These results indicate that clearly the PA (C_2H_5CN) is less than 823 kJ mol^{-1} and probably less than or equal to 811 kJ mol^{-1}. This agrees with the reported PA (C_2H_5CN) of 806 kJ mol^{-1}.

5.3.2. $C_3H_6N^+$ from protonated ethyl isocyanide

Paraformaldehyde was used in the inlet line to the ion source. The solid polymer was heated in a hot water bath to produce CH_2O which was admitted into the ion source. Electron impact on CH_2O produced HCO^+ which was injected into the flow tube. Ethyl isocyanide (C_2H_5NC) was added at the first neutral inlet until all the HCO^+ signal had just disappeared. The product of this initial reaction was at mass 56^+ and was thought to be protonated ethyl isocyanide.

Reaction with 1.4 Dioxane

Upon addition of 1.4 dioxane at the second neutral inlet only cluster formation was observed, at a rate of 3.5×10^{-10} cm^3 s^{-1}.

Reaction with $(CH_3)_2CO$

On addition of $(CH_3)_2CO$ from the second neutral inlet, the 56^+ signal underwent reaction at 7.9×10^{-10} cm^3 s^{-1}. The only product channel observed was formation of the collisionally stabilised cluster ion $(CH_3)_2CO.C_2H_5NCH^+$. No proton transfer was observed.

Reaction with NH_3

Addition of NH_3 from the second neutral inlet led to a reaction which occurred at a rate of 8.5×10^{-10} cm^3 s^{-1}. Both cluster formation and proton transfer to form NH_4^+ were observed. Proton transfer was the dominant process with a branching ratio of 0.85.

The lack of proton transfer from $C_2H_5NCH^+$ to either 1.4 dioxane or $(CH_3)_2CO$ shows that PA (C_2H_5NC) > 823 kJ mol^{-1}. The facile proton transfer to NH_3 shows that 853 kJ mol^{-1} ≥ PA (C_2H_5NC) ≥ 823 kJ mol^{-1}. This agrees with the reported value of PA (C_2H_5NC) of 852 kJ mol^{-1}.

5.3.3. $C_3H_6N^+$ from $HCNH^+ + C_2H_4$

Hydrogen cyanide (HCN) was used in the ion source. The pressure and ion focussing voltages were adjusted to optimise the $28^+/27^+$ratio. C_2H_4 was added at the first neutral inlet to produce 56^+.

Reaction with NH_3

NH_3 was added from the second neutral inlet. The 56^+ ion signal reacted with a rate coefficient of 1.1×10^{-9} cm^3 s^{-1}. Both proton transfer and cluster formation were observed, proton transfer dominated with a branching ratio of ≥ 0.95.

Reaction with $(CH_3)_2CO$

Upon addition of $(CH_3)_2CO$ from the second neutral inlet the rate of loss of the selected ion was 7.2×10^{-10} cm^3 s^{-1}. The major channel was cluster formation. A small amount of $(CH_3)_2COH^+$ was observed, but this was found to be an artefact from the small amount of unreacted $HCNH^+$ in the flow tube.

Reaction with 1.4 Dioxane

In order to confirm the result with $(CH_3)_2CO$, 1.4 dioxane was used as a reactant neutral. The 56^+ ion reacted at the rate 3.7×10^{-10} cm^3 s^{-1}. The only product attributable to the 56^+ ion was the cluster at 144 $^+$, $C_4H_8O_2.C_3H_6N^+$. These results seem to bracket the proton affinity in the range; 856 kJ mol^{-1} ≥ PA (C_3H_5N) ≥ 823 kJ mol^{-1}

This implies that $C_3H_6N^+$ formed in the ion molecule association of $HCNH^+$ and C_2H_4 has the protonated ethyl isocyanide ($C_2H_5CNH^+$) structure.

5.3.4. $C_3H_6N^+$ from $CH_3^+ + CH_3CN$

CH_3^+ was generated from electron impact on CH_3Br in the ion source. CH_3CN was added at the first neutral inlet until almost all of the CH_3^+ had been reacted.

Reaction with NH_3

Upon addition of NH_3 from the second neutral inlet no reaction was observed.

Reaction with CH_3NH_2

Upon addition of CH_3NH_2 from the second neutral inlet no reaction was observed.

Reaction with $C_2H_5NH_2$

On addition of $C_2H_5NH_2$ from the second neutral inlet the $C_3H_6N^+$ signal reacted slowly, with a rate of 0.028×10^{-9} cm^3 s^{-1}. The only observable product was the cluster ion $C_2H_5NH_2 \cdot C_3H_6N^+$.

The lack of proton transfer with any of the bases NH_3, CH_3NH_2, and $C_2H_5NH_2$ indicates that the $C_3H_6N^+$ ion formed from $CH_3^+ + CH_3CN$ has very different reactivity from the isomers $C_2H_5CNH^+$ and $C_2H_5NCH^+$ and unless there is a distinct mechanistic barrier to proton transfer, the proton affinity of the conjugate base of this isomer is greater than that for any of the isomers listed in table 5-1. This excludes both the isomers, $HCCCH_2NH_3^+$, and the bicyclo compound, as possible structures for the $C_3H_6N^+$ ion. It also excludes the two possible isomers reported by Bouchoux et al.

Table 5-3. Reactions of $C_3H_6N^+$ isomers with selected neutrals.

Reactant Ion	Neutral	Products	Branching Ratio	k_2 [a]	k_{coll} [b]
$C_2H_5CNH^+$	$C_4H_8O_2$ [c]	$C_4H_8O_2H^+ + C_2H_5CN$	0.20	1.1	1.1
		$C_2H_5CNH^+ . C_4H_8O_2$	0.80		
$C_2H_5CNH^+$	$(CH_3)_2CO$	$(CH_3)_2COH^+ + C_2H_5CN$	1.0	2.8	2.8
$C_2H_5NCH^+$	$C_4H_8O_2$	$C_2H_5NCH^+ . C_4H_8O_2$	1.0	0.35	1.1
$C_2H_5NCH^+$	$(CH_3)_2CO$	$C_2H_5NCH^+ . (CH_3)_2CO$	1.0	0.79	2.8
$C_2H_5NCH^+$	NH_3	$NH_4^+ + C_2H_5NC$	0.85	0.85	2.2
		$C_2H_5NCH^+ . NH_3$	0.15		
$C_3H_6N^+$ [d]	$C_4H_8O_2$	$C_3H_6N^+ . C_4H_8O_2$	1.0	0.37	1.1
$C_3H_6N^+$	$(CH_3)_2CO$	$C_3H_6N^+ . (CH_3)_2CO$	1.0	0.72	2.8
$C_3H_6N^+$	NH_3	$NH_4^+ + C_3H_5N$	0.95	1.1	2.2
		$C_3H_6N^+ . NH_3$	0.05		
$C_3H_6N^+$ [e]	NH_3	No Reaction			2.2
$C_3H_6N^+$	CH_3NH_2	No Reaction			1.8
$C_3H_6N^+$	$C_2H_5NH_2$	$C_3H_6N^+ . C_2H_5NH_2$	1.0	0.028	1.7

[a] Units of cm^3 s^{-1}; [b] Calculated by method of [Su and Chesnavich (1982)] units of cm^3 s^{-1}.
[c] $C_4H_8O_2$ is 1.4 Dioxane; [d] Ion formed by reaction of $HCNH^+ + C_2H_4$
[e] Ion formed by reaction of $CH_3^+ + CH_3CN$

5.4. Discussion

5.4.1. Isomeric Distribution

Each source of $C_3H_6N^+$ that was used produced only one isomer. More accurately it must be stated that each source of $C_3H_6N^+$ produced an overwhelming majority of a single isomer so that no curvature was noticeable in the decay of the $C_3H_6N^+$ signal with added neutral, for any combination of ion preparation method and neutral reagent. The decays of two of the $C_3H_6N^+$ species used in this experiment are shown as functions of neutral flow in Figure 5-1.

5.4.2. Isomeric Structures

The two reactions that were postulated as leading to the $C_2H_5CNH^+$ structure were in fact found to yield other isomers.

$CH_3^+ + CH_3CN$

The product of this reaction could not be positively identified, however it was clear that the proton affinity of the conjugate base was higher than that for any of the $C_3H_6N^+$ isomers for which the thermochemical information was available.

The *ab initio* results suggest that the structure is $CH_3CNCH_3^+$. There are other possible structures for which the proton affinities of the corresponding neutrals are not known, including some of the immonium ion structures reported by Bouchoux et al [Bouchoux et al (1989)]. The immonium ions, that were observed in that work, were however the product of dissociation of cyclic or unsaturated amines, and mechanisms to produce these products from a collision complex of CH_3^+ and CH_3CN are not clear.

Support for the $CH_3CNCH_3^+$ structure is given by CID experiments carried out by Bouchoux et al which indicate that this structure may be formed by methylation of both ethyl cyanide and ethyl isocyanide.

$HCNH^+ + C_2H_4$

The product of the association between $HCNH^+$ and ethylene can be reasonably confidently assigned the structure of ethyl isocyanide. Although at least one other ion, $CH_2CHCHNH_2^+$, is calculated to have a conjugate base with similar proton affinity to that of the conjugate base of $C_2H_5NCH^+$, the fact that the rates of reaction of the mystery isomer correspond to those of ethyl isocyanide, and a mechanism that leads to the formation of the amine is not apparent, supports the assumption that the product of the association is $C_2H_5NCH^+$.

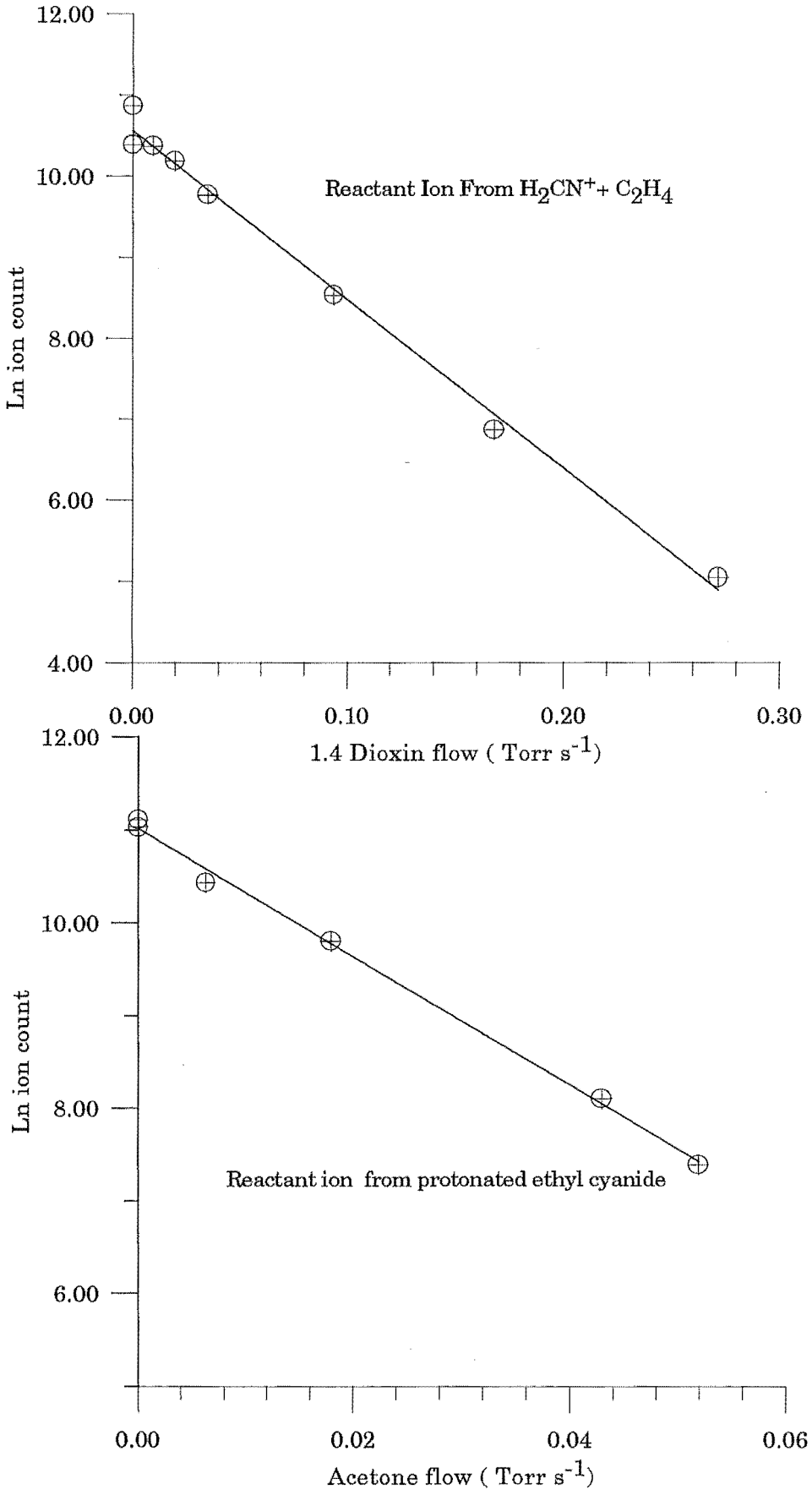

Figure 5-1. Plots of $C_3H_6N^+$ ion count against neutral flow measured by the SIFT, the $C_3H_6N^+$ is derived from various sources, note only one isomer in each plot.

5.4.3. *The Potential Surface*

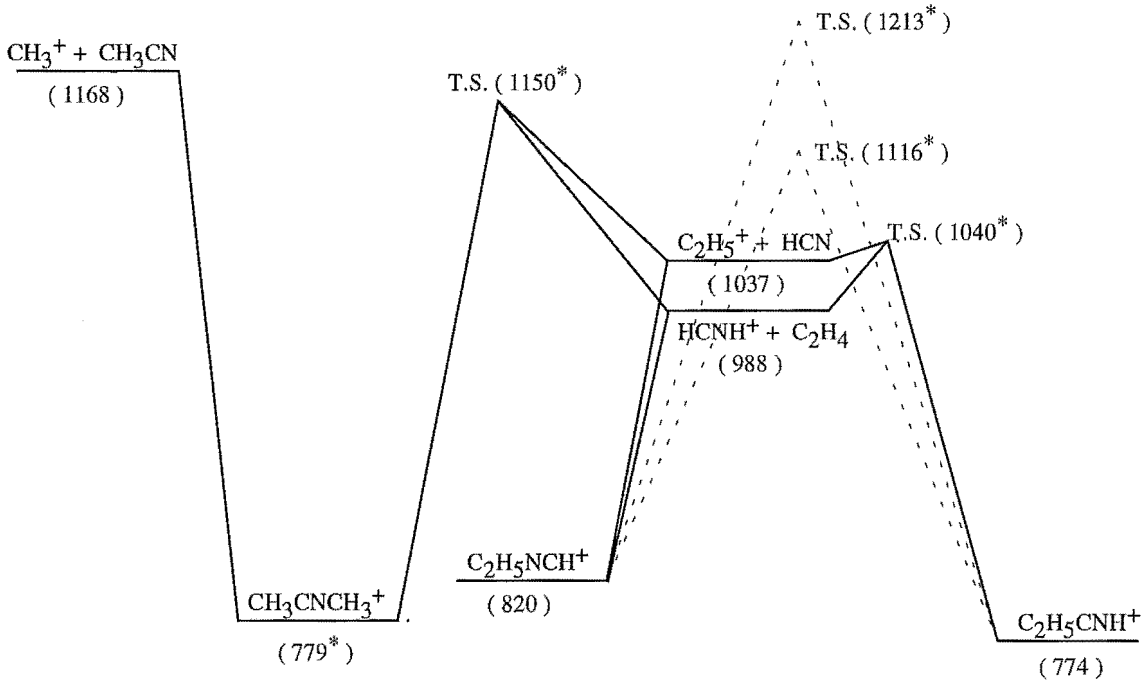

Figure 5-2. Potential surface for $C_3H_6N^+$ system: derived from both measured and calculated data. Transition states are denoted by (T.S.). Ab initio energies are denoted by an asterisk.

Some relevant parts of the potential energy surface for $C_3H_6N^+$ are shown above. The energies shown[1] are obtained from the literature[2] [Lias et al (1988)], and the two theoretical studies [Smith S et al (1993)] [Bouchox et al (1992)]. The surface is quite complex, and only the most important features have been included in the Figure. Low lying transition states and some intermediate states have been omitted. The surface can be considered from the 'point of view' of the reactants and the experimental results viewed in perspective with the *ab initio* results.

$HCNH^+ + C_2H_4$

The results of Bouchoux et al indicate that there is a barrier of 40 kJ mol^{-1} between the species $HCNH^+$ and C_2H_4 and the $C_2H_5CNH^+$ ion, whereas they predict no such barrier in the channel to formation of $C_2H_5NCH^+$ (the transition state between reactants and products is calculated to have an energy of 43 kJ mol^{-1} less than the reactants). The experimental results support these predictions, showing that the product of $HCNH^+$ and C_2H_4 is indeed the isonitrile.

The results of Smith et al show that there is a large barrier between the reactants and the linear $CH_3CNCH_3^+$ species ; this is confirmed by the experiment. The first step in the reaction is likely to be electrophillic attack followed by an intramolecular hydrogen shift to yield $C_2H_5NCH^+$.

---

[1] *Ab initio* energies are denoted by an asterisk

[2] Energies are in units of kJ mol^{-1}

$CH_3^+ + CH_3CN$

The reactants possess an energy larger than the calculated transition state between them and the $C_2H_5CNH^+$ ion, and experiments using both SIFT and ICR techniques [McEwan et al (1989)] [Knight et al (1986)] have confirmed that this barrier can be overcome to yield the products $HCNH^+ + C_2H_4$ and also $C_2H_5^+ + HCN$. At the higher pressures of the SIFT experiment the dominant process is collision stabilised association, and this work strongly suggests that the isomer formed is in fact $CH_3CNCH_3^+$.

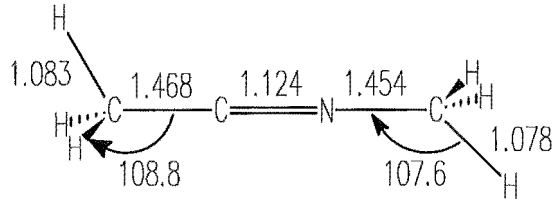

Figure 5-3. $CH_3CNCH_3^+$ from *ab initio* calculations see [Smith S.C et al (1993)]

At the lower pressures of the ICR experiment the collision complex is not stabilised as rapidly, and in effect has time to 'see' more of the potential surface. The dominant processes are exit out of the reactant channel and dissociation to give the products described above. Although the collision complex has sufficient energy to overcome the barrier to form $C_2H_5CNH^+$ the lifetime of the complex, with respect to dissociation, is too short for it to reach that part of the surface.

$C_2H_5^+ + HCN$

The reaction between $C_2H_5^+$ and HCN might seem to be the most likely to lead to formation of ethyl cyanide. The transition state between these reactants and the $C_2H_5CNH^+$ species is calculated by Bouchoux et al to be around 3 kJ mol^{-1} higher in energy than the reactants, which given the uncertainty of *ab initio* measurements can probably be thought of as not a significant barrier.

The reaction of these species has been studied in a SIFT experiment [Mackay et al (1980)] and the only channel was rapid proton transfer,

$$C_2H_5^+ + HCN \rightarrow HCNH^+ + C_2H_4 \qquad (5.15)$$

The bimolecular rate coefficient for the reaction was measured at 2.7×10^{-9} cm^3 s^{-1} which is close to the collision rate of 3.6×10^{-9} cm^3 s^{-1} . Although the ethyl cyanide ion is a much more stable species than the products of this reaction the dynamics of the system favour proton transfer, which is a reminder not to read too much into potential energy calculations in the absence of experimental guidance.

Interconversion of $C_3H_6N^+$ Isomers

The barriers to interconversion between the isomers of $C_3H_6N^+$ are large, the barrier between the isomers $C_2H_5NCH^+$ and $C_2H_5CNH^+$ is calculated by Bouchoux et al to be

at least 250 kJ mol^{-1}, depending on which of three proposed mechanisms is chosen. The possibility of isomerisation of the reactant ions is therefore remote.

5.4.4. Electron -Ion Recombination

The formation of a given isomer of $C_3H_6N^+$ is only the first step in the process thought to result in a stable neutral. The dissociative recombination of that product ion with an electron is the process that is thought to lead to the neutrals observed in interstellar clouds.

Ion electron recombination can be expressed as

$$XY^+ + e \rightarrow X + Y. \qquad (5.16)$$

The process results in the ionisation potential of A^+ being distributed amongst the neutral fragments. The process is clearly therefore energetic and the number of energetically available products is usually large. In order to predict which products will arise from the recombination of an ion with an electron the nature of the process must be considered. Theoretical studies [Bates (1950)], [Bardsley (1968)] have suggested two mechanisms may apply.

The Direct Mechanism

In this mechanism, proposed by Bates, the capture of the electron leads to an antibonding state XY', the moieties repel each other and potential energy is converted to kinetic energy as the separation increases. Eventually the potential is below the ionisation threshold and auto-ionisation can no longer occur.

$$XY^+ + e \rightarrow XY' \rightarrow X + Y \qquad (5.17)$$

The Indirect Mechanism

This mechanism was proposed by Bardsley and others. In this process the electron is first captured by surrendering its kinetic energy to either rotational or vibrational motion of the molecule. The electron then occupies a hydrogen-like orbital with a high quantum number so that the system can be described as a vibrationally excited Rydberg state XY*. This state is not repulsive but can lead to autoionisation or a radiationless transition to a repulsive state XY' which can result in dissociation.

$$XY^+ + e \rightarrow XY^* \rightarrow XY' \rightarrow X + Y \qquad (5.18)$$

The two mechanisms can be distinguished by the temperature dependence of the rate coefficient for recombination α_e. The direct process predicts a minimal dependence on ion temperature, whereas the indirect process is predicted to depend upon

temperature to the power T^{-1}. The fact that both mechanisms are observed can be seen in the observation by Smith and Adams [Smith and Adams (1989)] that the α_e values so far studied fall into two categories, those with large α_e values but no temperature dependence and those with small α_e values but with a temperature dependence between $T^{-0.5}$ and $T^{-1.0}$. It is not clear which process dominates under any set of conditions since at the present time there is just not enough experimental information [Adams (1992)]

Prediction of Product Branching Ratios

The absolute value of the electron ion recombination coefficient is of course important for modelling of the rate processes in the interstellar environment but of just as great importance is the branching ratio between the possible products. Even for very simple ions such as O_2^+ there are many possible electronic states available after electron capture. If both the initial and final vibrational wave functions are known then there are methods available to calculate predicted values of α_e, but these are not practical even for moderately sized systems [Mitchell (1990)], although calculations have been made for triatomics to attempt to elucidate whether favourable curve crossings exist.

A statistical approach was adopted by Herbst [Herbst (1978)], in which the existence of a multiplicity of suitable curve crossings for large species was assumed, so that phase space theory can be applied. The branching ratio of a channel is increased both by its exothermicity and the density of states in the products. This model tends to predict large branching ratios for channels which involve the loss of H atoms. This can be qualitatively explained by the large relative velocity of the fragments and hence the rapid passage along the reaction coordinate.

The statistical model of Herbst was criticised by Bates [Bates (1989)] in that the assumption that every channel will have a suitable curve crossing was physically unrealistic. The statistical approach was modified by Galloway and Herbst [Galloway and Herbst (1991)] to disregard channels that seem to require extensive rearrangement, but has not yet incorporated any factor to take account of the density of favourable crossings as suggested by Bates.

Bates approached the problem from a different angle, suggesting that the ion be considered as a valence bonded structure with the charge localised as a missing electron in one valence bond. Upon capture of the free electron the 'odd' electron is also promoted to an antibonding orbital, breaking the bond. This method predicts that the bonds involving atoms that can be thought of as carrying a significant portion of the positive charge are most likely to be broken. It also predicts that channels that will dominate will be those involving minimal rearrangement, ie. that two bond processes will not be significant, meaning that, for example, the channels that involve loss of two H atoms cannot occur as a one step process. The most significant prediction of Bates approach is that multiple bonds may be able to be broken.

Unfortunately the present lack of experimental results means that the theories remain a bare qualitative guide, and are far from the predictive stage.

Dissociative Channels of $C_3H_6N^+ + e$

Clearly it is impossible to confidently predict the products that will be formed from the ion electron recombination of the two species that this work indicates are likely to be formed in the interstellar cloud regions, that is $C_2H_5NCH^+$ and $CH_3CNCH_3^+$. Table 5-3 lists several possible product channels for each ion. Channels that involve three products have been neglected in accordance with the reasoning of Bates. It is also clear from inspection that many of the remaining channels involve substantial rearrangement of the ion.

Table 5-4. Some possible product channels for dissociative recombination of $C_3H_6N^+$ Ions.

Ion	Products[a]	ΔH^o kJ mol^{-1} [b]
$C_2H_5NCH^+$	$C_2H_5CN + H$	-551
	$C_2H_5NC + H$	-461
	$C_2H_5 + HCN$	-568
	$CH_3 + CH_3CN$	-500
$CH_3CNCH_3^+$	$C_2H_5CN + H$	-510
	$C_2H_5NC + H$	-420
	$C_2H_5 + HCN$	-527
	$CH_3 + CH_3CN$	-558

[a] The products are assumed to be in their ground state
[b] Using values from [Lias et al (1988)]

The *ab initio* study of Bouchoux et al predicts that the positive charge will be substantially held by the N atom in both structures. If the most likely channels are deemed to be those that involve, cleavage of a bond involving the N atom and or loss of a proton, and as little rearrangement as possible, then for the recombination of $C_2H_5NCH^+$ the favoured channels might well be those giving rise to $C_2H_5NC + H$ and $C_2H_5 + HCN$. For the recombination of $CH_3CNCH_3^+$ the favoured channel might well be $CH_3 + CH_3CN$. Neither ion seems likely as a route to C_2H_5CN upon dissociative recombination.

5.5. Conclusion

The association reactions

$$CH_3^+ + CH_3CN \rightarrow C_3H_6N^+ \qquad (5.1)$$

and

$$HCNH^+ + C_2H_4 \rightarrow C_3H_6N^+ \qquad (5.19)$$

are unlikely to lead, upon dissociative recombination of the product ion, to formation of the neutral species C_2H_5CN since the recombination process would require considerable rearrangement of the product ion structure. The interstellar synthesis of this neutral therefore proceeds by some other route. The reaction of $C_2H_5^+$ with HCN is known to result in fast proton transfer rather than association so can also be regarded as an unlikely route to the synthesis of C_2H_5CN.

CHAPTER SIX

SIFT STUDIES OF THE METHOXYMETHYL CATION

6.1. Introduction

The reactivity of the methoxymethyl cation, $CH_3OCH_2^+$, is of interest for two main reasons; firstly for its possible importance in interstellar chemical processes, and secondly because of the general interest in the mechanism of its reactions with both oxygen and nitrogen bases.

The ion $CH_3OCH_2^+$ can be formed in several ion molecule reactions, perhaps the most important being the reaction of protonated methanol with formaldehyde [Karpas and Meot-Ner (1989)],

$$CH_3OH^+ + H_2CO \rightarrow CH_3OCH_2^+ + H_2O\ . \qquad (6.1)$$

The species CH_3OH^+ and H_2CO have both been reported in dense interstellar clouds [Blake et al (1987)],[Smith (1992)]. Other notable reactions leading to the formation of $CH_3OCH_2^+$ are (6.2) [Kim et al] and (6.3) [Okada et al (1987)],

$$CH_3^+ + (CH_3)_2O \rightarrow CH_3OCH_2^+ + CH_4\ , \qquad (6.2)$$

$$CH_3O^+ + (CH_3)_2O \rightarrow CH_3OCH_2^+ + CH_3OH\ . \qquad (6.3)$$

Both reactions (6.2) and (6.3) are fast, occurring with rate coefficients close to the collision rate. Clearly the reactivity of the methoxy methyl cation may well be of importance in the interstellar environment. The reactions of this species with several neutrals reported in dense interstellar clouds along with other neutrals are reported in this chapter.

The possibility of transfer reactions from $CH_3OCH_2^+$ has been reported by several groups [Okada et al (1987)],[Kinter and Bursey (1986)], [Matsumotu et al (1975)]. These groups have studied the reaction of the methoxymethyl cation with ammonia. The reaction can exhibit CH^+ transfer, methyl cation, (CH_3^+), transfer, and proton transfer channels. The reactivity of $CH_3OCH_2^+$ with ammonia and other bases provides an example of all three competing channels. The factors that control the

relative efficiency of each reaction channel provide interesting examples of the effect of activation and steric barriers in ion-molecule chemistry.

6.2. Experimental

The SIFT studies of $CH_3OCH_2^+$ were carried out at room temperature, 295 ±5K. A pressure of 0.300 ± 0.005 Torr of helium carrier gas was used in the flow tube. For the most part the $CH_3OCH_2^+$ ions were formed by electron impact ionisation of dimethoxymethane, $(CH_3O)_2CH_2$, in the ion source. A pressure of around 9×10^{-5} Torr of dimethoxymethane was found to yield the best results.

The $CH_3OCH_2^+$ ions thus formed were injected into the flow tube through the venturi orifice. Unfortunately this method of preparation produced fragmentation of some of the injected ions. The $CH_3OCH_2^+$ signal was accompanied by HCO^+ and CH_3^+ fragment ions. By adjusting the voltages on the ion optics of the injection system the fragmentation could be minimised but not prevented, as reducing the voltages to lower the levels of HCO^+ and CH_3^+ reduced the $CH_3OCH_2^+$ signal.

An alternative method of producing $CH_3OCH_2^+$ was used, but only briefly, as this required the use of dimethyl ether. Supplies of dimethyl ether, $(CH_3)_2O$, were exhausted during the experiment. The method involves injecting CH_3^+, formed from electron impact on CH_3Br in the ion source, while adding a flow of $(CH_3)_2O$ from the first neutral inlet. The flow of $(CH_3)_2O$ must be large enough to just remove the CH_3^+ signal. The resulting $CH_3OCH_2^+$ is rapidly thermalised by collision with the carrier gas and can be reacted with a neutral added from the second neutral inlet.

This latter method is to be recommended over the direct injection technique since the highly reactive HCO^+ and CH_3^+ ions are not produced. The HCO^+ ion in particular readily undergoes proton transfer to most bases. The proton transfer from this impurity to the added base complicated the analysis of products. Where proton transfer from $CH_3OCH_2^+$ was exothermic it was impossible to determine whether the observed proton transfer was occurring from $CH_3OCH_2^+$ or from HCO^+. It was possible to estimate the contribution to proton transfer from HCO^+, but the large amount of fragment ion present, coupled with the uncertainty in the mass discrimination of the detection system, made quantitative measurements of a branching ratio impossible.

In conjunction with the reactions in the SIFT several experiments were carried out by McEwan [McEwan (1993)] using the ICR instrument of Anicich et al. For several of the more important reactions, results of these ICR experiments by McEwan will be cited.

6.3. Results

The reactions of the methoxymethyl cation with selected bases are listed in Table 6-1. The products of each reaction and the observed bimolecular rate constant at 0.3 Torr are given . The bimolecular rate can be compared to the collision rate, k_{coll}, calculated by the parametrised method of Su and Chesnavich [Su and Chesnavich (1982)].

Table 6-1. Reactions of $CH_3OCH_2^+$ with selected neutral species .

Reactant Neutral	Products [a]	k_2 [b]	k_{coll} [b,c]
HCN	no reaction	< 0.1	3.35
HCOOH	products	> 0.29	1.71
CH_3OH	CH_3OCH_2. CH_3OH^+	0.013	2.13
C_2H_5OH	$C_2H_5OCH_2^+ + CH_3OH$	0.24	2.05
CH_3CN	$CH_3CNCH_3^+ + CH_2O$ CH_3OCH_2. CH_3CN^+	0.35	3.94
NH_3	$CH_2NH_2^+ + CH_3OH$ $CH_3NH_3^+ + CH_2O$	0.59	2.23
CH_3NH_2	$CH_3NHCH_2^+ + CH_3OH$	1.5	1.82
$C_2H_5NH_2$	$C_2H_5NHCH_2^+ + CH_3OH$	1.5	1.78
$(CH_3)_2NH$	$(CH_3)_2NCH_2^+ + CH_3OH$	0.36	1.66
$(CH_3)_3N$	CH_3OCH_2. $(CH_3)_3N^+$	1.4	1.42

a In some cases proton transfer could also be a channel
b Units 10^{-9} cm^3 s^{-1}
c Calculated by classical trajectory based method of [Su and Chesnavich (1982)]

6.3.1. Reaction of $CH_3OCH_2^+$ with HCN

The reactant ion $CH_3OCH_2^+$, produced by electron impact on dimethoxymethane showed no measurable reaction with HCN added from the second neutral inlet.

6.3.2. Reaction of $CH_3OCH_2^+$ with HCOOH

$CH_3OCH_2^+$ was produced by electron impact on dimethoxymethane and injected into the flow tube, along with the fragmentation products HCO^+ and CH_3^+. The rate of reaction of the $CH_3OCH_2^+$ signal was > 2.9×10^{-10} cm^3 s^{-1}. The rate could not be more accurately measured because of the tendency of HCOOH to dimerise, making the partial pressure of HCOOH in the neutral flow somewhat less than the measured value. The reactions of the fragment ions complicated the analysis of the system. The reactions of both CH_3^+ and HCO^+ have been studied previously [Freeman et al (1978)],

$$CH_3^+ + HCOOH \rightarrow CH_5^+ + CO_2 \qquad (6.4)$$

$$HCO^+ + HCOOH \rightarrow CH(OH)_2^+ + CO. \quad (6.5)$$

Both (6.4) and (6.5) are reported to occur at close to the collision rate. The product $CH(OH)_2^+$ was observed in the present study but CH_5^+ was not observed. This was possibly due to the rapid secondary reaction of CH_5^+ with the neutral HCOOH, which is reported by Freeman et al to yield $CH(OH)_2^+$ at a rate of 3×10^{-9} $cm^3 s^{-1}$. It could also be that the products of reaction (6.4) have been wrongly assigned. The work of Freeman et al was carried out using a Flowing Afterglow apparatus, which lacked facility to select a chosen reactant ion. This instrument is prone to difficulty in analysing the complex kinetics due to the many primary and secondary ions present. Whatever the reason for the failure to observe CH_5^+ in the present study, it was clear that the system was too complex to interpret accurately the reactions of the $CH_3OCH_2^+$ ion.

6.3.3. Reaction of $CH_3OCH_2^+$ with CH_3OH

$CH_3OCH_2^+$ was again formed by electron impact on dimethoxymethane in the ion source. The resulting ion was injected into the flow tube producing the fragmentation ions HCO^+ and CH_3^+. The rate of loss of $CH_3OCH_2^+$ was very slow; 1.3×10^{-11} $cm^3 s^{-1}$. The only product that could be assigned to reaction of $CH_3OCH_2^+$ was the cluster with CH_3OH. Karpas and Meot-Ner [Karpas and Meot-Ner (1989)] report a methyl transfer reaction observed in a low pressure ICR experiment,

$$CH_3OCH_2^+ + CH_3OH \rightarrow (CH_3)_2OH^+ + H_2CO\,. \quad (6.6)$$

The authors suggest, on the basis of double resonance behaviour, that reaction (6.6) has an activation barrier. Reaction (6.6) was not a significant channel in the SIFT where the reactant ion can be assumed to be thermalised. A possible channel that cannot be either confirmed or denied is CH^+ transfer, analogous to the reaction of $CH_3OCH_2^+$ with C_2H_5OH which is reported below,

$$CH_3OCH_2^+ + CH_3OH \rightarrow CH_3OCH_2^+ + CH_3OH\,. \quad (6.7)$$

Without isotopic labelling reaction (6.7) cannot be shown to occur since the reactant and product ions are the same. Although the reaction is thermoneutral the presence of an 'invisible' channel could explain the low rate of cluster formation.

6.3.4. *Reaction of $CH_3OCH_2^+$ with C_2H_5OH*

Injection of the reactant ion was accompanied by the fragmentation products HCO^+ and CH_3^+. The reactions of both of these ions with C_2H_5OH have been reported previously. [Smith and Futrell (1978)] [Mackay et al (1978)],

$CH_3^+ + C_2H_5OH$	$\rightarrow C_2H_5^+ + CH_3OH$	0. 50	(6.8a)
	$\rightarrow C_2H_6^+ + CH_3O$	0. 03	(6.8b)
	$\rightarrow C_2H_8^+ + HCO$	0. 23	(6.8c)
	$\rightarrow C_2H_5O^+ + CH_4$,	0. 20	(6.8d)
$HCO^+ + C_2H_5OH$	$\rightarrow H_3O^+ + C_2H_4 + CO$	0. 45	(6.9a)
	$\rightarrow C_2H_5OH_2^+ + CO$.	0. 55	(6.9b)

A large signal was observed at 59^+ which could not be accounted for as a product of either (6.8) or (6.9). This was clearly a product of reaction of $CH_3OCH_2^+$ but proton transfer could not be ruled out as a competing channel. The overall rate of loss of $CH_3OCH_2^+$ was 2.4×10^{-10} cm^3 s^{-1}. The reaction to produce 59^+ involves CH^+ transfer from the reactant ion,

$$CH_3OCH_2^+ + C_2H_5OH \rightarrow C_2H_5OCH_2^+ + CH_3OH\,. \qquad (6.10)$$

A small signal was observed corresponding to the cluster at 91^+ of $CH_3OCH_2^+$ with C_2H_5OH. While an accurate branching ratio was not measured the cluster channel was clearly the minor channel.

6.3.5. *Reaction of $CH_3OCH_2^+$ with CH_3CN*

Initially $CH_3OCH_2^+$ was produced by electron impact on dimethoxymethane. This method of ion production gave rise to problems with HCO^+ and CH_3^+ as described for the reactions above. The overall rate of loss of $CH_3OCH_2^+$ was 3.5×10^{-10} cm^3 s^{-1}. The significant product ions were 56^+, 83^+, and 86^+. The 83^+ ion product was the proton bound dimer of acetonitrile produced rapidly from secondary reaction of protonated acetonitrile,

$$CH_3CNH^+ + CH_3CN \rightarrow CH_3CNH.CH_3CN^+\,. \qquad (6.11)$$

The protonation of neutral acetonitrile is reported by Mackay et al [Mackay et al (1976)] as the only channel for the reaction with HCO^+,

$$HCO^+ + CH_3CN \rightarrow CH_3CNH^+ + CO\,. \qquad (6.12)$$

The reaction (6.13) is fast with a rate coefficient of 4.1×10^{-9} $cm^3\ s^{-1}$. The reaction of CH_3^+ with CH_3CN has also been reported [Knight et al (1986)], [McEwan 89], the reaction has three major channels.

$$CH_3^+ + CH_3CN \rightarrow C_2H_5^+ + HCN \qquad (6.13a)$$
$$\rightarrow HCNH^+ + C_2H_4 \qquad (6.13b)$$
$$\rightarrow C_3H_6N^+ \qquad (6.13c)$$

In the SIFT pressure regime the association channel dominates, with ~ 90% of the reactant going to produce $C_3H_6N^+$. Thus in the present experiment the observed product ions could have arisen from either the selected ion, $CH_3OCH_2^+$, or the fragment ions.

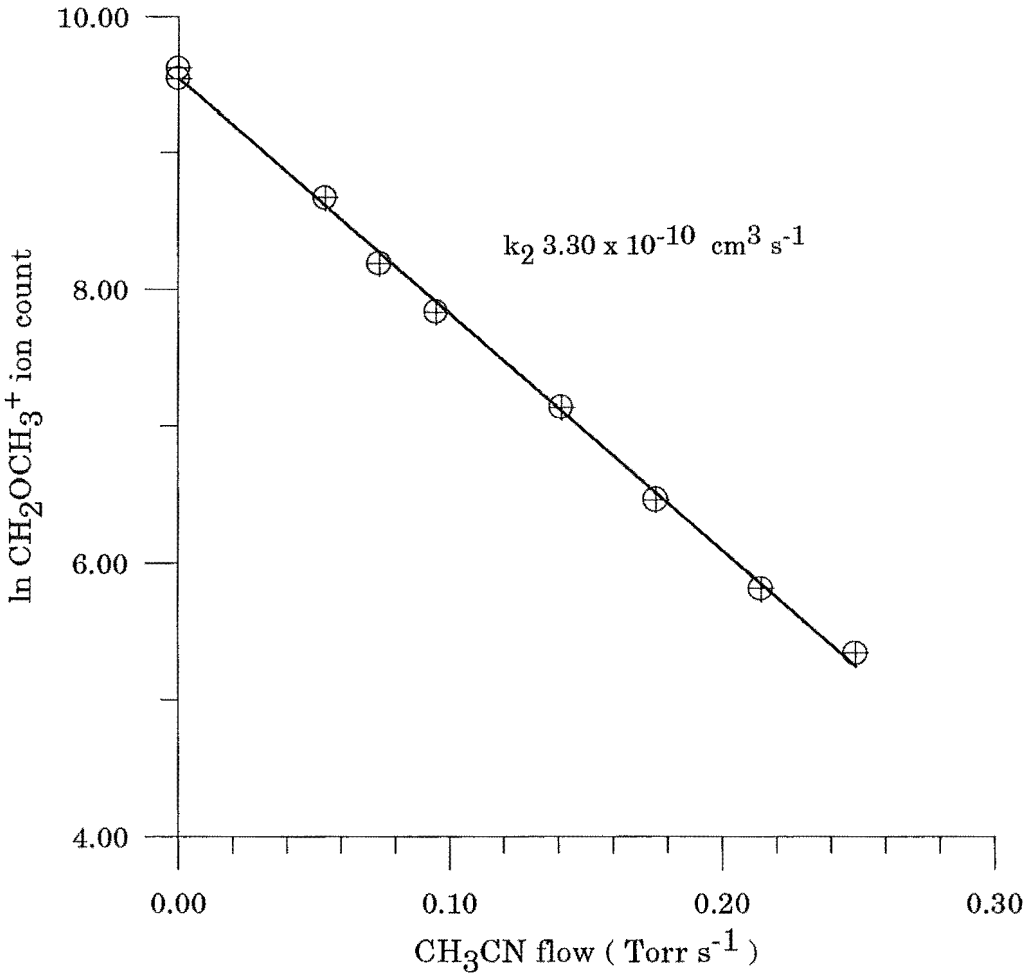

Figure 6-1. Plot of $CH_3OCH_2^+$ ion count against CH_3CN flow measured in the SIFT, at 300 K and 0.3 Torr.

In order to solve this dilemma it was decided to produce $CH_3OCH_2^+$ by injecting CH_3^+ produced from methyl bromide in the ion source and adding $(CH_3)_2O$ from the first

neutral inlet. .This method gave a workable signal of $CH_3OCH_2^+$ with no HCO^+ and minimal CH_3^+. The products of the reaction were found to be a mixture of $C_3H_6N^+$ and the cluster $CH_3OCH_2{\cdot}CH_3CN^+$. The structure of the $C_3H_6N^+$ ion formed by the transfer of CH_3^+ from $CH_3OCH_2^+$ is likely to be the same as formed from methyl ion attack, reaction (6.13). This ion has been found to have the structure $CH_3CNCH_3^+$. This reaction is discussed in great detail in chapter 5 of this work.

6.3.6. Reaction of $CH_3OCH_2^+$ with NH_3

The reactant ion, $CH_3OCH_2^+$, was produced by electron impact on dimethoxymethane in the ion source. The fragment ions HCO^+ and CH_3^+ were both present. The overall rate of reaction was found to be 5.9×10^{-10} cm^3 s^{-1}. Products were observed at 18^+, 30^+, and 32^+. The reactions of CH_3^+ and HCO^+ have been reported by Huntress et al [Huntress et al (1980)] and Adams et al [Adams et al (1978)] respectively,

$$CH_3^+ + NH_3 \rightarrow NH_4^+ + CH_2 \qquad 0.15 \qquad (6.14a)$$

$$\rightarrow CH_2NH_2^+ + H_2\,, \qquad 0.85 \qquad (6.14b)$$

$$HCO^+ + NH_3 \rightarrow NH_4^+ + CO\,. \qquad (6.15)$$

Both reactions are reported as going at nearly the collision rate. The sizes of the ion signals in the present experiment showed that almost all of the 18^+ was due to proton transfer from HCO^+, so the two product channels available for $CH_3OCH_2^+$ are $CH_2NH_2^+$ and $CH_3NH_3^+$. The $CH_3NH_3^+$ signal was ~ 10% of the size of the $CH_2NH_2^+$ signal, but due to reaction (6.14) it was not possible to get an accurate branching ratio. So the observed reactivity of the methoxy methyl cation with ammonia was ,

$$CH_3OCH_2^+ + NH_3 \rightarrow CH_2NH_2^+ + CH_3OH \qquad (6.16a)$$

$$\rightarrow CH_3NH_3^+ + H_2CO. \qquad (6.16b)$$

In an attempt to elucidate, or confirm this result, McEwan carried out an experiment using the ICR instrument at JPL. The results of that experiment [McEwan (1993)]agree well with the SIFT result; the rate in the ICR was 4.3×10^{-10} cm^3 s^{-1} and the only reported product was $CH_2NH_2^+$. The lack of the $CH_3NH_3^+$ product in the ICR experiment is explained in terms of the lifetime of the collision complex in the discussion below. This reaction has been studied by other groups over recent years and their results are also discussed below.

6.3.7. *Reaction of $CH_3OCH_2^+$ with CH_3NH_2*

$CH_3OCH_2^+$ was injected in the manner described above, using dimethoxymethane. The injection of the ion produced CH_3^+ and HCO^+ fragment ions. The overall rate of reaction of the $CH_3OCH_2^+$ ion was 1.5×10^{-9} cm^3 s^{-1}. The ionic products observed were 31^+, 32^+, 44^+, and 63^+. The reaction of CH_3^+ with CH_3NH_2 has been reported previously [Adams and Smith (1978)] also [Kim et al].

$$CH_3^+ + CH_3NH_2 \rightarrow CH_2NH_2^+ + CH_4 \quad 0.45 \quad (6.17a)$$
$$\rightarrow CH_3NH_2^+ + CH_3 \quad 0.55 \quad (6.17b)$$

The reaction of HCO^+ is not reported, but the highly exothermic proton transfer channel is the most likely. This would lead to $CH_3NH_3^+$. The ion at 63^+ is the proton bound dimer produced by further reaction of $CH_3NH_3^+$ with the neutral. The major product channel for $CH_3OCH_2^+$ was formation of $CH_3NHCH_2^+$. This was confirmed by further work by McEwan [McEwan (1993)]. This shows the reaction of $CH_3OCH_2^+$ in the ICR has a rate of 9.4×10^{-10} cm^3 s^{-1}, and the only observed product is $CH_3NHCH_2^+$. Figure 6-2 shows a typical SIFT result.

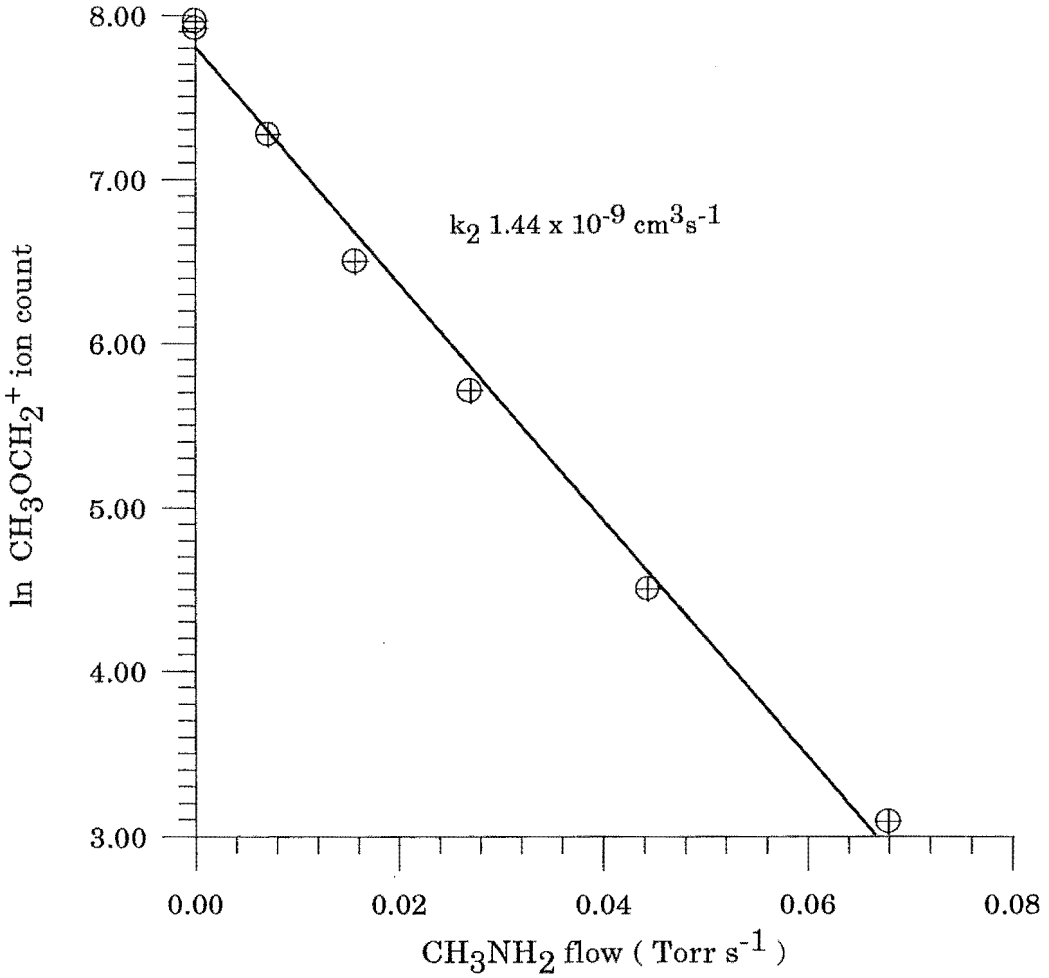

Figure 6-2. Reaction of $CH_3OCH_2^+$ with CH_3NH_2 measured in the SIFT, at 300 K and 0.3 Torr.

6.3.8. *Reaction of $CH_3OCH_2^+$ with $C_2H_5NH_2$*

Injection of $CH_3OCH_2^+$ was accompanied by CH_3^+ and HCO^+. Upon addition of $C_2H_5NH_2$ from the second neutral inlet the rate of reaction was 1.5×10^{-9} cm^3 s^{-1}. Three product ions were observed, these were 46^+, 58^+ and 91^+. The ion at 46^+ was the protonated species $C_2H_5NH_3^+$ which reacted further to produce the proton bound dimer $C_2H_5NH_2.C_2H_5NH_3^+$. Proton transfer from both CH_3^+ and HCO^+ is exothermic by 84 kJ mol^{-1} and by 316 kJ mol^{-1} respectively. The product ion 58^+ was formed from $CH_3OCH_2^+$ and was assigned the structure $C_2H_5NHCH_2^+$. While this was clearly the major channel, proton transfer could not be ruled out as minor channel. The absence of a proton transfer channel was confirmed [McEwan (1993)] by ICR experiments. The only product was $C_2H_5NHCH_2^+$ which was formed at a rate of 1.4×10^{-9} cm^3 s^{-1}.

6.3.9. *Reaction of $CH_3OCH_2^+$ with $(CH_3)_2NH$*

The rate of reaction of $CH_3OCH_2^+$ with $(CH_3)_2NH$ was 3.6×10^{-10} cm^3 s^{-1}. Due to the fragment ion CH_3^+ and HCO^+ a mixture of products was observed, these were 46^+, 58^+ and 91^+. It is most likely that the 46^+ was the protonated species $(CH_3)_2NH_2^+$ and that 91^+ was the proton bound dimer formed by further reaction of the protonated species with the amine. The reaction of HCO^+ to give $(CH_3)_2NH_2^+$ is highly exothermic,

$$HCO^+ + (CH_3)_2NH \rightarrow (CH_3)_2NH_2^+ + CO\,. \qquad (6.\ 18)$$

The reaction of CH_3^+ with the neutral amine was also found to proceed wholly via proton transfer, see reaction (6.19) below. The product 46^+ was produced from $CH_3OCH_2^+$, and was assigned the structure $(CH_3)_2NCH_2^+$.

6.3.10. *Reaction of $CH_3OCH_2^+$ with $(CH_3)_3N$*

The rate of reaction of $CH_3OCH_2^+$ was fast; 1.4×10^{-9} cm^3 s^{-1}. The fragment ions CH_3^+ and HCO^+ complicated the analysis of products, but it was clear that the only product ion from $CH_3OCH_2^+$ was the cluster ion $CH_3OCH_2.(CH_3)_3N^+$ at mass 104^+. It is important mechanistically that although transfer of a CH^+ moiety would have been exothermic, this was not observed.

6.3.11. *Reaction of CH_3^+ with $(CH_3)_2NH$*

The reaction of CH_3^+ with $(CH_3)_2NH$ was of interest because it was of importance in elucidating the reaction between $CH_3OCH_2^+$ and $(CH_3)_2NH$, and was not

reported. CH_3^+ was produced by electron impact on CH_3Br. The injection of CH_3^+ into the flow tube was accompanied by some C^+, but this was minimised by careful tuning and did not affect the results. Upon addition of $(CH_3)_2NH$ from the second neutral inlet the methyl ion reacted with a rate of 2.1×10^{-9} cm^3 s^{-1}. The only product observed was 46^+ which was the protonated species $(CH_3)_2NH_2^+$,

$$CH_3^+ + (CH_3)_2NH \rightarrow (CH_3)_2NH_2^+ + CH_2 \,. \qquad (6.19)$$

It is interesting that proton transfer was the dominant process in this reaction, since the reaction of CH_3^+ with CH_3NH_2 [Adams and Smith (1978)], [Kim et al] proceeds through charge transfer and hydrogen atom abstraction only (see reaction (6.17) above).

6.3.12. Reaction of CH_3^+ with $(CH_3)_2O$

The reaction of CH_3^+ with $(CH_3)_2O$ has been reported, [Kim et al] as a route to production of $CH_3OCH_2^+$,

$$CH_3^+ + (CH_3)_2O \rightarrow CH_3OCH_2^+ + CH_4 \,. \qquad (6.20)$$

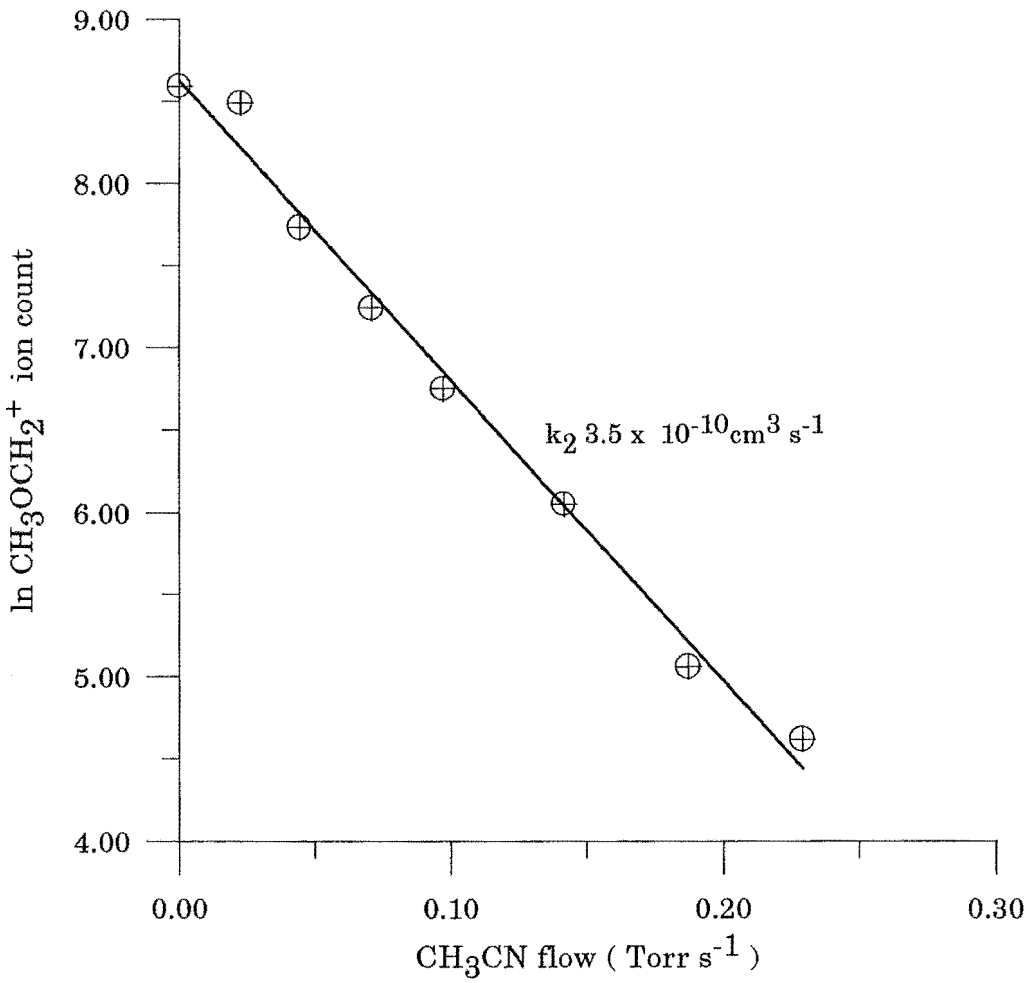

Figure 6-3. Reaction of $CH_3OCH_2^+$ (from CH_3^+ + CH_3CN) with CH_3CN, measured in the SIFT at 0.3 Torr and 300 K.

The reaction is reported to be fast, at 3.0×10^{-9} cm^3 s^{-1}. Upon injecting CH_3^+ formed from electron impact on CH_3Br, a fast reaction of the order of the collision rate was observed with $(CH_3)_2O$. The product was indeed 45^+. In order to confirm the identity of the product, CH_3CN was added from the second neutral port. The rate of reaction was measured as 3.5×10^{-10} cm^3 s^{-1}, with the products being mostly 56^+, with a small amount of 86^+ (see Figure 6-3). This reactivity was similar to that of the $CH_3OCH_2^+$ ion obtained by electron impact on dimethoxymethane. The lack of curvature in the decay shows that only one isomer of $CH_3OCH_2^+$ was formed.

6.4. Discussion

6.4.1. The Isomers of $C_2H_5O^+$

It is important to note that $CH_3OCH_2^+$ (ΔH_f° 657 kJ mol^{-1}) is not the most stable isomer of $C_2H_5O^+$. Protonated acetaldehyde, CH_3CHOH^+, is more stable (ΔH_f° 582 kJ mol^{-1}), as is the ion $CH_2CHOH_2^+$ (ΔH_f° 619. 2 kJ mol^{-1}). Another isomer that has been observed is protonated oxirane (ΔH_f° 690. 4 kJ mol^{-1}).

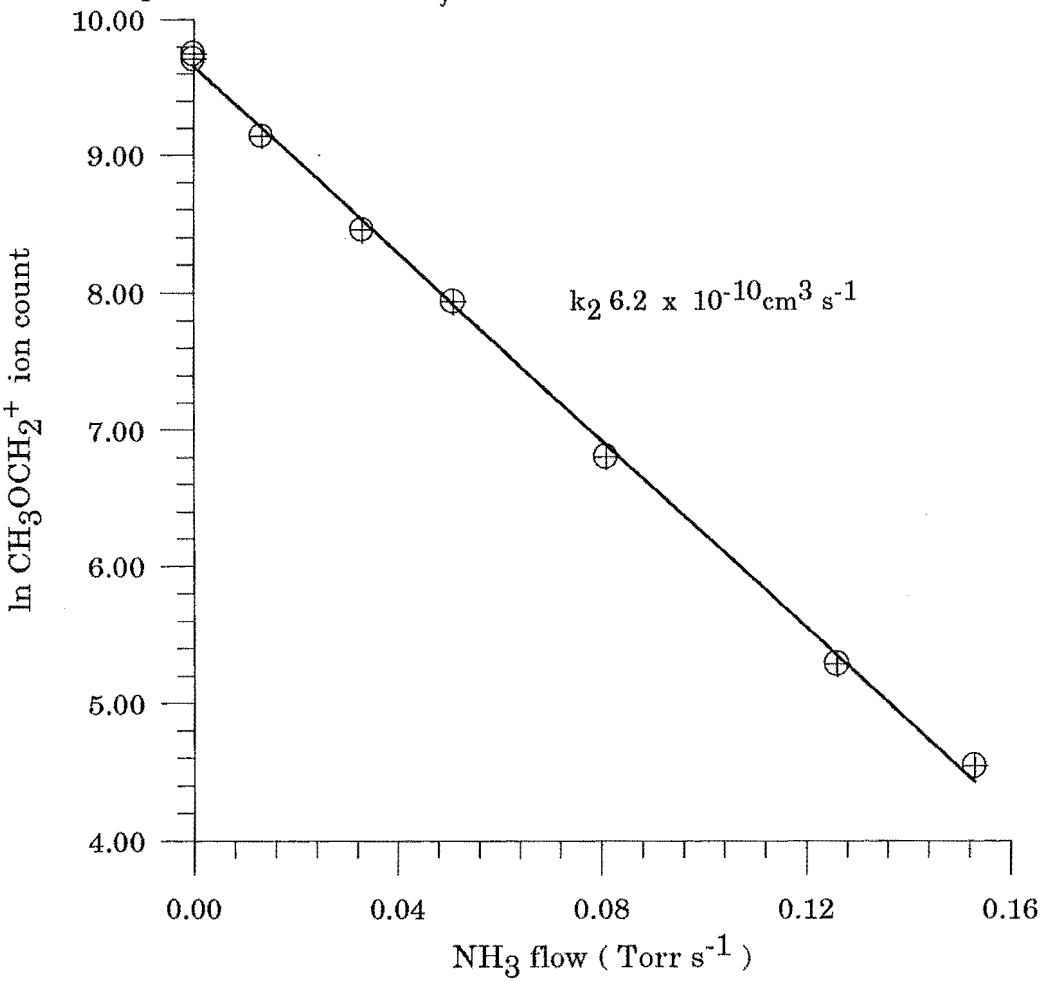

Figure 6-4. Reaction of $CH_3OCH_2^+$ with NH_3 measured in the SIFT, note the lack of curvature indicating that the ion population is single isomer.

It is clear from the straight line relationship between the log of the ion intensity and the neutral flow (eg see Figure 6-4) for all the rate measurements listed in Table 6-1 that the $C_2H_5O^+$ signal corresponds to an ion population comprising a single isomer.

From a qualitative view it seems likely that electron impact ionisation of $(CH_3O)_2CH_2$ should lead to formation of $CH_3OCH_2^+$ rather than CH_3CHOH^+ which would require more extensive rearrangement. In order to confirm this McEwan carried out ICR studies of two reactions of protonated acetaldehyde [McEwan (1993)], which, combined with the present SIFT studies, serve to identify the two isomers.

Reaction with NH_3

The reactions of both isomers with NH_3 have been studied by several groups, [Matsumato et al (1975)] [Kinter and Bursey (1986)] [Okada et al (1987)]. What is clear is that proton transfer from $CH_3OCH_2^+$ can occur but does so slowly, since there is a potential barrier along the reaction coordinate. This is seen in the positive variation in proton transfer rate with increasing ion centre-of-mass energy in the triple quadrupole study of Kinter and Bursey. In the present SIFT study proton transfer was clearly not a major channel and in the ICR study [McEwan (1993)] the channel was not reported. The major channel at room temperature seems to be the production of $CH_2NH_2^+$ and the overall rate of reaction a relatively sedate 4.3×10^{-10} cm^3 s^{-1} measured in the ICR, to 5.9×10^{-10} cm^3 s^{-1} measured in the SIFT. The reaction of CH_3CHOH^+ has been reported by Kinter and Bursey and by McEwan. The former study does not report a rate, but notes that proton transfer by CH_3CHOH^+ falls off with increasing ion centre-of-mass energy. This indicates that the process is exothermic without a potential barrier, and proceeds via formation of a relatively loose collision complex [Bowers et al (1972)] . The ICR study [McEwan (1993)] shows that proton transfer is the dominant channel and proceeds rapidly with a rate of 1.8×10^{-9} cm^3 s^{-1}. This is entirely consistent with the thermochemistry of the process.

$$CH_3CHOH^+ + NH_3 \rightarrow NH_4^+ + CH_3CHO \qquad (6.21)$$

using the thermochemical values of [Lias et al (1988)] this process is exothermic by 70 kJ mol^{-1}.

Reaction with CH_3CN

The reaction of $CH_3OCH_2^+$ formed both from electron impact on dimethoxymethane and by ion molecule reaction of CH_3^+ with $(CH_3)_2O$ occurs with a rate coefficient of 3.5×10^{-10} cm^3 s^{-1} to give a mixture of $CH_3CNCH_3^+$ and the adduct ion. [McEwan (1993)] has carried out the corresponding reaction with protonated acetaldehyde CH_3CHOH^+ using ICR techniques. This reaction proceeds considerably faster, with a rate coefficient of 3.2×10^{-9} cm^3 s^{-1}. The main reaction channel is observed to be proton transfer from CH_3CHOH^+,

$$CH_3CHOH^+ + CH_3CN \rightarrow CH_3CNH^+ + CH_3CHO\,, \qquad (6.22)$$

using the data from [Lias et al (1988)] the reaction is exothermic by an amount of 6.1 kJ mol^{-1}. From the results of the two sets of reactions, it seems clear that the isomer formed by electron impact on dimethoxy methane is not protonated acetaldehyde. On purely structural grounds the other two reported isomers can be ruled out as requiring too much rearrangement to be formed in the conditions of the SIFT ion source. The result that the reaction of CH_3^+ with $(CH_3)_2O$ produces a single isomer with the same reactivity as that produced from electron impact on dimethoxymethane is further evidence for this conclusion.

6.4.2. Reactivity of $CH_3OCH_2^+$

It has been established that the reactions described above correspond to those of the $CH_3OCH_2^+$ ion. The ion clearly exhibits three possible channels in reaction with the oxygen or nitrogen bases; association, methyl cation transfer, and CH^+ transfer.

Table 6-2. Thermochemistry of the reactions of $CH_3OCH_2^+$[a].

Neutral	ΔH^o proton transfer[b]	ΔH^o methyl ion transfer	ΔH^o CH^+ transfer
HCN	100.9	-43.1	219
CH_3OH	61.1	-20	
C_2H_5OH	31.4	-37	-29.8
CH_3CN	31.0	-55[c]	
NH_3	-31.8	-168.8	-67.8
CH_3NH_2	-75.7	-152.7	-141.1
$C_2H_5NH_2$	-89.1	-166.1	-158.6
$(CH_3)_2NH$	-101.2	-182.5	-179.2
$(CH_3)_3N$	-121	-201.9	

[a] Thermochemical data from [Lias et al (1988)], units of kJ mol^{-1}.
[b] The neutral product of proton transfer is assumed to be oxirane, ((c)-CH_2OCH_2).
[c] Value of ΔH_f^o $CH_3CNCH_3^+$ from [Smith S. C et al; (1993)].

The proton transfer process while exothermic in almost every case (see Table 6-2) is apparently not a major channel. This behaviour is interesting, given that an exothermic proton transfer process will generally dominate other processes. Also of note is the apparent facility with which the CH^+ transfer process takes place. In most cases the two processes have similar endothermicities. The transfer of the CH^+ moiety seems intuitively less likely than the transfer of a methyl cation since more rearrangement is required. In order to explain the reactivity of the $CH_3OCH_2^+$ it is necessary to examine the mechanisms of the proton transfer and CH^+ and CH_3^+ transfer processes in detail.

Alkyl Transfer Reactions in General

Alkyl transfer reactions have been reported in a wide variety of ion-molecule systems [Karpas and Meot-Ner (1989)] [Okada et al (1987)] [Sen Sharma and Kebarle (1982)] [Meot-Ner and Karpas (1986)] [Deakyne and Meot-Ner (1990)] [Kleingeld and Nibbering (1982)]. The reactions involve the transfer of a methyl cation CH_3^+ or larger alkyl group. Kleingeld and Nibbering have shown by means of clever isotope labelling experiments that the formation of protonated ethers by alkyl transfer from protonated alcohols occurs through an S_N2 mechanism,

$$CH_3OH_2^+ + CH_3OH \rightarrow (CH_3)_2OH^+ + H_2O\,. \qquad (6.23)$$

Sen Sharma and Kebarle report methyl transfer from chloronium ions to a variety of organic bases,

$$(CH_3)_2Cl^+ + B \rightarrow CH_3B^+ + CH_3Cl\,. \qquad (6.24)$$

The reaction rate varies in accordance with the increasing basicity of B. For the least basic species used, benzene, there was a potential barrier to methyl transfer. The barrier dropped as basicity increased, and for the bases NH_3 and $(CH_3)_3N$, methyl ion transfer occurred at the capture rate.

Meot-Ner and Karpas report alkylation reactions in a number of systems involving nitriles, ethers and alcohols. The reaction of protonated alcohols with nitriles yields isocyanides through an apparent S_N2 process,

$$ROH_2^+ + R'CN \rightarrow R'CNR^+ + H_2O\,. \qquad (6.25)$$

The mechanism for the alkylation of alcohols by protonated nitriles, must, however, involve somewhat greater rearrangement,

$$CH_3CNH^+ + CH_3OH \rightarrow CH_3CNCH_3^+ + H_2O\,. \qquad (6.26)$$

Further examples of alkyl transfer reactions are given by the same authors [Karpas and Meot-Ner (1989)] and the rates of methyl transfer reactions between alcohols are suggested to depend upon the R^+ --- OH_2 bond dissociation energy. This relationship is also reported for the alkyl transfer from alcohols to formaldehyde. This supports the suggestion of an S_N2 type mechanism, but confirmation will require further experiments with isotope labelling. Methyl transfer in many systems has been reviewed [Deakyne and Meot-Ner (1990)] and a methyl cation affinity (MCA) scale, analogous to the proton affinity scale has been produced. The methyl cation affinity of a base is defined as the negative of the enthalpy change of the process,

$$CH_3^+ + B \rightarrow BCH_3^+ \qquad (6.27)$$

The MCAs of a number of species are related to that of dimethyl ether. The authors draw several parallels between the trends observed in their MCA scale to trends observed in proton affinity scales. For example the substitution of a methyl group rather than a hydrogen tends to increase the methyl cation affinity of a base. This is also observed in proton affinity scales, a result of the ability of the larger group to stabilise positive charge better than a hydrogen. The methyl cation affinity scale, like any thermochemical "ladder" gives information about the nature of the equilibrium distribution of products rather than the mechanism of reaction.

Proton Transfer Reactions in General

Proton transfer process are among the most well studied processes in the field of ion-molecule chemistry. A more complete description and discussion of some aspects of proton transfer is given in chapter 4.

Most proton transfer processes involve little rearrangement, since the structures of the protonated species differ little from the neutral structure. For this reason there are rarely activation barriers to proton transfer processes. Meot-Ner and Smith [Meot-Ner and Smith (1991)] discuss the phenomenon of "entropy barriers" in proton transfer reactions. In the reactions of large species such as sterically hindered pyridines and amines the authors report that the tight, locked rotor, transition states limit the rate. The negative temperature dependence is explained by the suggestion that as the temperature increases the formation of the tight intermediate becomes increasingly unlikely. As will be seen below this steric hindrance argument can also be applied to S_N2 processes.

Proton Transfer from $CH_3OCH_2^+$

Since exothermic proton transfer reactions are usually quick, why is the proton transfer from $CH_3OCH_2^+$ not a major channel ? The answer lies in the structure of the neutral. In order to lose a proton the $CH_3OCH_2^+$ species must undergo a significant rearrangement. There are several known structural isomers of the neutral C_2H_4O. Included are CH_3CHO, CH_2CHOH, CH_3COH and oxirane. In order to form any of these products extensive rearrangement is needed. The most likely neutral product is oxirane.

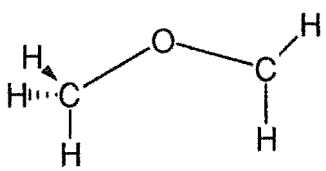

$CH_3OCH_2^+$

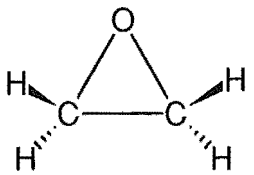

oxirane, C_2H_4O

Oxirane is the only neutral product which can be formed without breaking a C-O bond. In forming oxirane, a ring closure must be performed. The closure of the three membered ring will result in a "tight" transition state with a considerably negative entropy of activation . The transition state will also be likely to have a significant activation barrier. The ab-initio study of Okada et al [Okada et al (1987)] shows that for the reaction of $CH_3OCH_2^+$ with NH_3 the proton transfer channel has an estimated activation barrier of 165 kJ mol^{-1} . The large energy of activation is mainly connected with the ring closure.

Since the activation energy is connected with the ring closure of the neutral product rather than the transfer of the proton per se, it is reasonable to assume that the proton transfer channel will have a similar activation barrier irrespective of the structure of the base species.

Methyl Cation Transfer from $CH_3OCH_2^+$

Given that the methyl cation transfer is at least as exothermic as CH^+ transfer and appears to involve less rearrangement, it might be expected to be the dominant process. The transfer of CH_3^+ is, however, observed in only two reactions; with CH_3CN, and also with NH_3. In order to understand this observation the mechanism of CH_3^+ transfer in this system must be examined. The most plausible mechanism for methyl ion transfer is an S_N2 process similar to that postulated by Kleingeld and Nibbering and Meot-Ner and Karpas.

An S_N2 mechanism was examined by Okada et al [Okada et al (1987)] when the authors examined the reaction of $CH_3OCH_2^+$ with NH_3. The reaction was assumed to proceed through a traditional pentavalent carbon transition state. A similar transition state can be envisaged for the reaction with CH_3CN.

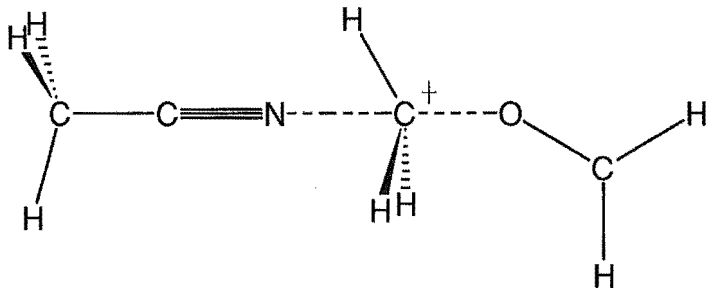

Possible transition state for S_N2 methyl ion transfer from $CH_3OCH_2^+$ to CH_3CN.

The attack by a nucleophile on the methyl carbon leads to the S_N2 process. As discussed by Okada et al the transition state can only be achieved if the reactants adopt an appropriate configuration. This steric constraint means that the transition state is a tight, locked rotor, complex. Meot-Ner and Smith [Meot-Ner and Smith (1991)] have shown, as discussed above, that the existence of such a tight, hindered transition state should lead to a strong negative temperature dependence of the rate. This prediction is

confirmed by the triple quadrupole study of the reaction $CH_3OCH_2^+ + NH_3$ [Kinter and Bursey (1986)]. The methyl transfer channel in the reaction above showed a strong negative dependence on ion kinetic energy. As the kinetic energy of the reactants increases, the lifetime of the collision complex [Bowers et al (1973)] decreases, and the complex may dissociate through other channels before the critical configuration is reached. One of these other channels through which the complex may dissociate is the CH^+ transfer channel.

CH^+ Transfer from $CH_3OCH_2^+$

In some of the reactions described above the transfer of a CH^+ group from the $CH_3OCH_2^+$ ion is a major channel. The general processes are described below,

$$CH_3OCH_2^+ + R_2NH \rightarrow R_2NCH_2^+ + CH_3OH \qquad (6.28)$$

$$CH_3OCH_2^+ + C_2H_5OH \rightarrow C_2H_5OCH_2^+ + CH_3OH\,. \qquad (6.29)$$

The above mechanism was not observed for the neutral CH_3OH, since the products are the same as the reactants. This reaction would have been thermoneutral, and the lack of any moderately fast, observable reaction suggests this CH^+ transfer may have taken place. The mechanism was not observed where the neutral was HCN, since in that case the reaction would have been very endothermic.

Methyl cation transfer would in all cases have been slightly more exothermic than CH^+ transfer, and presumably would have involved less bond rearrangement. The methyl cation transfer, however, was only observed in the reaction with CH_3CN, and to a minor extent as a channel in reaction with NH_3. Where the base had a labile hydrogen CH^+ transfer predominated. Where there was no labile hydrogen the dominant processes were formation of the collisionally stabilised adduct ion or methyl cation transfer.

The experimental evidence suggests that after formation of the collision complex, the first step in the mechanism of CH^+ transfer is hydride transfer from the base to the $CH_3OCH_2^+$ ion. This supports the mechanism suggested, by Okada et al, for the reaction with NH_3. In this mechanism the first step is formation of the collision complex. The second step is hydrogen transfer from the base to the oxygen atom of $CH_3OCH_2^+$ concurrent with the transfer of CH_2^+ to the base.

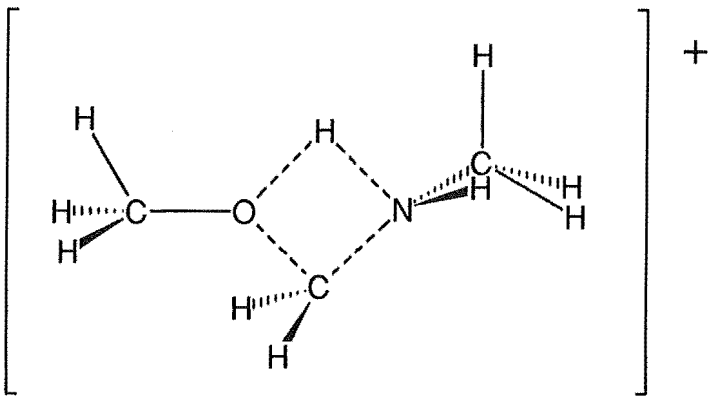

Possible transition state (based on the work of Okada et al) for the CH^+ transfer from $CH_3OCH_2^+$ to CH_3NH_2.

One feature of the transition state is that the hydrogen transfer to the oxygen is much less sterically hindered than the S_N2 attack at the methyl carbon site of the $CH_3OCH_2^+$ ion. Even though the energy of activation of the methyl cation transfer process was calculated by Okada et al to be lower (by 24 kJ mol^{-1} in the reaction with NH_3) than that for CH^+ transfer, the less hindered nature of the transition state for CH^+ transfer means that it is the dominant dissociation channel for the collision complex.

The reactivity of the $CH_3OCH_2^+$ ion can be satisfactorily explained in terms of the interplay of the three mechanisms for dissociation of the collision complex. Where there is a labile hydrogen the CH^+ transfer is favoured. Where there is not, the methyl cation transfer channel can occur. At high temperatures or energies, the activation barrier to proton transfer can be overcome. In the SIFT experiment a further factor is the collisional stabilisation of the collision complex with the resulting observation of the adduct ion.

In the case of the reaction with CH_3CN the slow methyl ion transfer channel allows some dissociation, but in the case of reaction with $(CH_3)_3N$, the steric hindrance is so great that the only dissociative channel is back to reactants, and the only product observed is the adduct.

A word of caution regarding the result of the reaction of $CH_3OCH_2^+$ with C_2H_5OH must be sounded. A study by Pau et al [Pau et al (1987)] used ICR methods to observe the reactions of $CH_3OCH_2^+$ with a number of alcohols and amines, including C_2H_5OH. The reactions reported with the amines and with substituted alcohols were CH^+ transfer. Isotopic labelling using ^{18}O in the $CH_3OCH_2^+$ supports the mechanism of hydrogen transfer to the ether oxygen atom followed by loss of CH_3OH or in this case $CH_3{}^{18}OH$. These authors however report that C_2H_5OH did not react with the ion. It is not reported whether clustering occurred or not. This result was supported by a recent ICR experiment [McEwan (1993)], where no product at 59^+ was seen. While the SIFT result was unable to give an accurate product distribution, the 59^+ product was certainly observed. In the ICR the collision complex is not collisionally stabilised as in the SIFT. This stabilisation of the collision complex is probably the reason that the methyl cation

transfer from $CH_3OCH_2^+$ to ammonia is observed in the SIFT, where the collision complex is stabilised somewhat by collision, and not in the lower pressure ICR experiment.

As far as the reaction with ethanol is concerned; it is plausible that the lifetime of the collision complex in the ICR is not sufficient to allow sufficient rearrangement for the CH^+ transfer intermediate to be formed. If this is the case dissociation back to reactants would be favoured over the other channels. This explanation is open to doubt since it does not explain why the channel was available with other, substituted alcohols. It may be that the energy barrier for CH^+ transfer to the substituted alcohols was lower than that for ethanol.

6.4.3. Relevance to possible formation of Interstellar Compounds

As described earlier, several reactions; (6.1), (6.2), and, (6.3) have been reported [Karpas and Meot-Ner (1989)] [Kim et al] [Smith (1992)] to possibly lead to the formation of $CH_3OCH_2^+$ in interstellar clouds. The importance of $CH_3OCH_2^+$ as a reactive species may be greatest in interstellar environments where water is present. Millar et al [Millar et al (1991)] present a reaction scheme to explain the abundance of oxygen containing compounds in the Orion Compact Ridge region [Blake et al (1987)].

The scheme is initiated by the radiative association of CH_3^+ with H_2O to produce protonated methanol,

$$CH_3^+ + H_2O \rightarrow CH_3OH_2^+ + h\nu\,. \qquad (6.30)$$

This can lead to methanol upon dissociative recombination and eventually the protonated methanol can react with the neutral,

$$CH_3OH_2^+ + CH_3OH \rightarrow (CH_3)_2OH^+ + H_2O\,. \qquad (6.\,23)$$

The protonated dimethyl ether is postulated to undergo dissociative recombination to lead to formation of the neutral $(CH_3)_2O$.

The $(CH_3)_2O$ produced through this and other processes can undergo reactions (6.2) and (6.3) with the common species CH_3^+ and CH_3O^+ to produce $CH_3OCH_2^+$. The likelihood is therefore that $CH_3OCH_2^+$ could be a significant species in the chemistry of water rich dense interstellar clouds, especially in view of its rapid reaction with the abundant species NH_3 to form $CH_2NH_2^+$ which, upon dissociative recombination could lead to the neutral CH_2NH.

6.5. Conclusion

The reactions of the ion $CH_3OCH_2^+$ with various oxygen and nitrogen nucleophiles have been studied in the SIFT. The existence of an activation barrier to proton transfer means that proton transfer is not a major reaction channel at room temperature. The reactivity of the ion can be adequately explained in terms of competing methyl cation transfer, CH^+ transfer, and collisional stabilisation of the collision complex. The results for the reaction of $CH_3OCH_2^+$ agree with ICR and triple-quadrupole experiments carried out previously. The reaction of $CH_3OCH_2^+$ with C_2H_5OH however seems to exhibit different product channels in the SIFT to those seen in the ICR.

CHAPTER SEVEN

EXPERIMENTAL STUDIES AND THEORETICAL MODELS OF ION-MOLECULE ASSOCIATION REACTIONS

7.1. Introduction

7.1.1. Expressions for the Observable Rate Constants

The rate constants observed in an ICR or in a flow tube experiment correspond to the rate of change of an ion population with time, averaged over the population of that ion. This does not necessarily correspond to a single, fundamental process, but could incorporate several coupled rate processes. The relationship of the observed rate constant to these fundamental rate processes is described below for the general case of an association process.

The process proceeds through the preliminary step

$$A^+ + B \xrightarrow{k_f} AB^{+*}, \tag{7.1}$$

where AB^{+*} is the collision complex. The collision complex is formed with all the energy of the reagents, and unless it is stabilised it can dissociate back to form the starting reagents or other fragments. For simplicity, only the dissociation back to reagents is shown, if there are other channels then k_d, the unimolecular dissociation rate for the collision complex is the sum of all the possible dissociation rates

$$AB^{+*} \xrightarrow{k_d} A^+ + B. \tag{7.2}$$

Before AB^{+*} dissociates it can be stabilised to give the association product AB^+. This can occur in two ways, radiative stabilisation (7.3) or collisional stabilisation (7.4),

$$AB^{+*} \xrightarrow{k_r} AB^+ + h\nu, \tag{7.3}$$

$$AB^{+*} + M \xrightarrow{k_c} AB^+ + M. \tag{7.4}$$

From these fundamental rate processes expressions for the observed bimolecular and termolecular association rates can be derived. The bimolecular association rate constant k_2 is defined by ,

$$A^+ + B \xrightarrow{k_2} AB^+. \tag{7.5}$$

The first step is to assume a steady state population of the collision complex AB^{+*},

$$\frac{d[AB^{+*}]}{dt} = 0 = k_f[A^+][B] - k_d[AB^{+*}] - k_c[AB^{+*}][M] - k_r[AB^{+*}], \tag{7.6}$$

this yields

$$k_f[A^+][B] = (k_d + k_c[M] + k_r)[AB^{+*}], \tag{7.7}$$

thus

$$[AB^{+*}] = \frac{k_f[A^+][B]}{(k_d + k_c[M] + k_r)}. \tag{7.8}$$

Now by the definition of k_2 in (7.5)

$$\frac{d[AB^+]}{dt} = k_2[A^+][B], \tag{7.9}$$

And by (7.3) and (7.4)

$$\frac{d[AB^+]}{dt} = k_r[AB^{+*}] + k_c[M][AB^{+*}]. \tag{7.10}$$

Combining these expressions and substituting for $[AB^{+*}]$

$$k_2[A^+][B] = \frac{(k_r + k_c[M])k_f[A^+][B]}{(k_d + k_r + k_c[M])}, \tag{7.11}$$

this gives the expression for the bimolecular rate constant

$$k_2 = k_f \frac{(k_r + k_c[M])}{(k_d + k_r + k_c[M])}. \tag{7.12}$$

The termolecular rate constant is defined by

$$A^+ + B + M \xrightarrow{k_3} AB^+ + M, \tag{7.13}$$

thus

$$\frac{d[AB^+]}{dt} = k_3[A^+][B][M], \tag{7.14}$$

this gives

$$k_3 = \frac{k_2}{[M]}. \tag{7.15}$$

Dividing the expression for the bimolecular rate constant by [C] yields

$$k_3 = \frac{k_f k_r}{(k_d + k_c[M] + k_r)[M]} + \frac{k_f k_c}{(k_d + k_c[M] + k_r)}. \tag{7.16}$$

Some authors use different conventions in stating these expressions. Commonly the collisional stabilisation rate is expressed as the product of the capture collision rate of the collision complex, k_{coll}, and a constant β representing the efficiency of the collisions in stabilising the complex

$$k_c = \beta k_{coll}. \tag{7.17}$$

The unimolecular dissociation rate (which can be the sum of all the dissociation rates) is often expressed as the inverse of the average lifetime of AB^{+*} with respect to unimolecular dissociation

$$k_d = \frac{1}{\tau}. \tag{7.18}$$

Having expressed the observable rate coefficients k_2 and k_3 in terms of the elementary rate coefficients k_f, k_r, k_c and k_d it is possible to consider the physical processes these rate constants describe. This can be done by examining the models used to describe each process individually. It must however be noted that it is impossible for any model to give a result for k_c, k_r, or k_d in isolation.

The Master Equation Defined

The individual rate coefficients are of course averages of the microscopic rate coefficients over some population distribution. That is the canonical rate constant can be related to the microcanonical coefficients by the expression,

$$k_i = \sum_{E,J} f(E,J) k_i(E,J), \tag{7.20}$$

where $f(E,J)$ is the population in state (E,J) and $k_i(E,J)$ is the microscopic rate coefficient for channel i from initial state (E,J). Often the angular momentum is neglected and the microscopic rate constant is considered as a function of energy only

$$k_i = \sum_E f(E) k_i(E). \tag{7.20}$$

While this approximation is often valid it can lead to error where the transition state has a markedly different moment of inertia from that of the reactant, which is often the case in ion molecule systems.

The theory of association reactions is most often treated from the point of view of unimolecular reaction theory, since all the important rate equations can be expressed in terms of the population of the collision complex. Clearly the population $f(E)$ depends on several coupled rate equations. Consider a simple example of a system where only collisional energy transfer (with the bath gas M) and unimolecular dissociation back to reactants can occur. Collision with the bath gas can either remove energy or increase the internal energy of the complex.

If $k_c(i,j)$ is the microscopic rate of collisional energy transfer from state i to state j and $k_c(j,i)$ s the analogous rate of transfer from state j to state i, and $k_{d\,i}$ is the microscopic dissociation rate from state i, then an expression for the rate of change of the population of state i with time can be developed

$$\frac{\partial f_i}{\partial t} = [\mathrm{M}] \sum_j \left(f_j k_c(j,i) - f_i k_c(i,j) \right) - f_i k_{di}. \tag{7.21}$$

This is a simple example of the master equation for the system, and shows the dependence of f_i on not only $k_{d\,i}$ but also on all other populations and rate constants in the system. In most real systems the number of states is large and the summation can be replaced by an integral

$$\frac{\partial f(E,t)}{\partial t} = [\mathrm{M}] \int \left(f(E',t)\, k_c(E',E) - f(E,t)\, k_c(E,E') \right) dE' - f(E,t)\, k_d(E). \tag{7.22}$$

The master equation is of fundamental importance in the study of unimolecular reactions. The topic is discussed in detail by Gilbert and Smith [Gilbert and Smith (1990)] and is also covered by Pritchard [Pritchard (1984)]. Solving the master equation one can derive k_{uni} for a channel and this unimolecular rate coefficient can be related to the observed rate by the equations above. Where k_{uni} is that for the channel back to reagents it is possible to obtain k_2 for the association process directly from the solution of the master

equation. This is shown by Troe [Troe (1979)] and by Gilbert and McEwan [Gilbert and McEwan (1985)]. The unimolecular process leading back to reactants can be related to the bimolecular rate from reactants to the bound molecule, which rate is known in unimolecular parlance as the recombination rate, k_{rec}. In the case of an ion molecule association, k_2 is the same as k_{rec}. The relationship between the rates is shown to be...

$$\frac{k_{rec}}{k_{uni}} = K = \frac{Q_{AB}}{Q_A Q_B} \exp\left(\frac{\Delta H^\circ}{k_B T} \right). \tag{7.23}$$

By separating the internal from the translational partition functions Gilbert and Smith [Gilbert and Smith (1990)] show that...

$$\frac{k_{rec}}{k_{uni}} = 5.33 \times 10^{21} \frac{Q_{AB}^{int}}{Q_A^{int} Q_B^{int}} \left[\frac{M_A + M_B}{M_A M_B} \frac{1}{T} \right]^{\frac{3}{2}} \exp\left(\frac{\Delta H^\circ}{k_B T} \right). \tag{7.24}$$

Thus if the master equation is solved, ie the separate $k_i(E)$ for all channels i, and the collisional energy transfer function is known, a comparison can be made between k_2 observed by experiment and k_{rec} calculated by theory.

Another comparison that can be made is that of the unimolecular lifetime of the collision complex. The unimolecular lifetime can be defined as

$$\tau = \frac{1}{\sum_i k_{uni}^i}. \tag{7.25}$$

A recent development by Anicich et al [Anicich et al (1991)] [Anicich et al (1994)] allows for the experimental determination of unimolecular lifetimes by ICR double resonance techniques. This allows comparison of τ and also τ_i for each individual channel. Moreover the technique allows for an absolute determination of β ; the collision efficiency for stabilisation of the buffer gas.

7.1.2. Capture Collision Rates: a Classical Approach

The rate at which an ion and a molecule form a collision complex is known as the capture rate constant. Because of the nature of the potential between an ion and a molecule, there are long range attractive forces, especially in the case of a molecule with a permanent dipole. Counterbalancing these forces is an angular momentum barrier to capture, the so called centrifugal barrier. Various methods have been used to obtain simple, easily used expressions for $k_{capture}$ and some of these are summarised below.

Ion Induced Dipole Interactions.

The simplest case of an ion molecule interaction is that between a point charge, and a molecule that can be considered as a polarisable point lacking both structure and a permanent dipole moment. Although there is no significant long range repulsion, in order for the capture event to occur the system must overcome the so called centrifugal barrier. This is shown below [Bowers and Su (1975)].

The total energy of the system is initially the kinetic (translational) energy of the components at large separation

$$E_{total} = \frac{1}{2}\mu v^2, \tag{7.26}$$

where μ is the reduced mass and v is the relative velocity. The ion induced dipole potential becomes important as the particles approach

$$V(r) = -\frac{\alpha q^2}{2r^4}, \tag{7.27}$$

where α is the polarizability of the neutral, and q is the ionic charge. The energy of the system as r decreases comprises translational energy, rotational energy and potential energy due to the ion induced dipole interaction. The rotational energy can be expressed as a function of the separation for a given impact parameter b

$$E_{\text{rotational}} = \frac{\mu^2 v^2 b^2}{2\mu r^2} = \frac{1}{2}\mu v^2 \frac{b^2}{r^2} = E_{\text{total}} \frac{b^2}{r^2}. \tag{7.28}$$

The rotational energy can be thought of as a repulsive component to the central potential, yielding an effective potential as a function of separation

$$E_{\text{effective}}(r) = -\frac{q^2 \alpha}{2r^4} + E_{\text{total}} \frac{b^2}{r^2}. \tag{7.29}$$

The potential reaches a maximum at the centrifugal barrier. Two different approaches have been used to derive a capture rate from this effective potential. Eyring et al [Eyring et al (1936)] treated the centrifugal barrier as an activated complex, the line of centres separation r as the reaction coordinate, and solved for the velocity of the system crossing the barrier using activated complex theory [Eyring (1935)]. Later Gioumousis and Stevenson [Gioumousis and Stevenson (1955)] used classical dynamics. Both solutions give the same expression for a thermal distribution of energies, but the later work could be applied to non thermal ion populations in mass spectrometer ion sources. The thermal expression for the capture rate, usually referred to as the Langevin capture rate is

$$k_{langevin} = 2\pi\, q\sqrt{\frac{\alpha}{\mu}}\,. \tag{7.30}$$

Ion Permanent Dipole Interactions

The interaction energy between a structureless ion of point charge, q, and a dipole with dipole moment, μ_d, and polarizability, α, is a function not only of separation r, but also of the orientation of the dipole. The dipole can be considered as a vector with the angle between it and the line of centres angle θ. The expression for the potential as a function of r and θ is,

$$V(r,\theta) = -\frac{\alpha\, q^2}{r^4} - \frac{\mu_d\, q}{r^2}\cos\theta\,. \tag{7.31}$$

The interaction due to the dipole is a longer range potential than that of the induced dipole, but has an angular dependence which means the expression cannot be solved as a central potential. If θ can be held constant then the problem reduces to one of a central potential. An approximation can be made if it assumed that the dipole will "lock" into the most stable configuration, $\theta = 0$ [Moran and Hamill (1963)],

$$V(r)_{locked} = -\frac{\alpha\, q^2}{r^4} - \frac{\mu_d\, q}{r^2}\,. \tag{7.32}$$

The problem, thus reduced to a central potential, can be solved using the same approach(es) as for the ion induced dipole problem. The locked dipole approximation, however, dramatically overestimates the capture rate, and represents an upper limit.

Other theorists have attempted to reduce the problem to a central potential by finding some average angle $\theta(r)$ which describes the overall properties of the system. The complicating factor is that the angular momentum of the system must be conserved, and this involves both the orbital angular momentum of the collision partners, and the angular momentum of the dipole rigid rotor. Su and Bowers [Su and Bowers (1973)] developed an average dipole orientation or ADO theory. The use of variational transition state theory was the next step in theoretical developments. The variational method varies the properties of the transition state (in this case the separation r) until the rate is a minimum. In the microcanonical variational treatment of Chesnavich et al [Chesnavich et al (1980)] $k(E)$ was varied, and the values of $k(E)$ integrated over a Boltzman distribution. A similar variational approach was taken by Celii et al [Celii et al (1980)].

The methods above were derived analytically, and to a greater or lesser extent tend to overestimate the observed capture rates. While such methods shed light on the physical processes involved in the collision process, where capture rates are needed

pursuant to another end (such as rate constant determination) an accurate value is of more assistance than a rigorously derived one. The capture rates used throughout this work are those calculated from the parametrised version of Su and Chesnavich. [Su and Chesnavich (1982)]. The authors carried out classical trajectory calculations to obtain an empirical expression for the ratio of the dipole capture rate to the Langevin capture rate. The authors found that the ratio depended upon a reduced parameter χ

$$\frac{k_{dipole}}{k_{langevin}} = \begin{cases} 0.4767\chi + 0.6200 & \chi \geq 2 \\ \dfrac{(\chi + 0.5090)^2}{10.526} + 0.9754 & \chi \leq 2 \end{cases} \qquad (7.33)$$

$$where... \qquad \chi = \frac{\mu_d}{\sqrt{(2\,\alpha\, k_B T)}}$$

This parametrised expression, in which k_B is the Boltzmann constant gives a good general agreement with experimental results. The experiments usually used to test the capture rate expressions are exothermic proton transfer reactions. The reactions are assumed to occur at the collision rate, which is a reasonably valid assumption as long as the reaction is sufficiently exothermic.

Problems with the above expressions for rate constants arise due to the assumption of point charges and symmetrical top dipoles in the derivations. Where the species are large these assumptions may lose validity, and it is possible that the physical cross section of a species could exceed it's cross section as determined above.

7.1.3. Unimolecular Dissociation Rates

The process of unimolecular dissociation is simply the fission of a molecule into two or more fragments, although it is assumed that only one bond can break at a time. For species with a given internal energy E and angular momentum, J, the microscopic rate of dissociation is $k(E,J)$

$$AB^+(E,J) \xrightarrow{k_{(E,J)}} A^+ + B. \qquad (7.34)$$

Many different theories have been developed in order to calculate $k(E)$ and $k(E,J)$, but only one will be mentioned in this work, and that is RRKM theory. Several texts exist that cover this theory in detail, [Robinson and Holbrook (1972)], [Forst (1973)] and [Gilbert and Smith (1990)].

The principle behind RRKM theory is that the internal energy of a molecule is distributed between the active modes in a random fashion, and that all distributions of a

given energy are equally probable. If sufficient energy becomes located in a given mode, the bond can be broken. At some point a critical configuration, the transition state, is reached. This can be thought of as a point of no return, if the system reaches this configuration it will proceed to products. Thus, embodied in RRKM theory are two basic assumptions, the ergodicity assumption, that energy is rapidly randomised, and the transition state assumption that a surface exists in phase space between reactant and product regions which can be crossed only in one direction for a trajectory arising in the reactant region.

The rate coefficient can be qualitatively thought of as the flux of trajectories passing through the transition state surface, divided by the total ensemble of states. The flux of trajectories passing through the transition state surface has been shown to be $W^{ts}(E-E^{\circ})\,h^{n-1}$, where $W^{ts}(E-E^{\circ})$ is the sum of states of the transition state between energy 0 and E-E°, if E° is the critical energy. The population of the ensemble is given by $h^{n}\,\rho(E)$ where $\rho(E)$ is the density of states of the molecule at energy E. The expression for $k(E)$ then is...

$$k(E)=\frac{W^{ts}(E-E^{\circ})}{\rho(E)\,h}. \tag{7.35}$$

Since all the trajectories that go through the transition state are treated as going to products, it is clear that the expression gives an upper bound to the rate of reaction. The transition state can thus be chosen by a variational method as the separation of minimum flux for a given energy, this is called microcanonical variational transition state theory [Gilbert and Smith 1990]. This method is of crucial importance in modelling ion molecule association, where there is no activation barrier to separation, and the position of the transition state is affected by both the potential and the tightness of the transition state. Although the potential well is deeper at small separations the ion molecule interaction is stronger, and the low lying translational modes start to take on vibrational character, reducing the density of states.

Clearly also angular momentum becomes important where there is no chemical barrier, and the centrifugal barrier dominates the potential [Troe (1977)] [Dove and Raynor (1979)]. Conservation of angular momentum is achieved by expressing the rate coefficients and the master equation in terms of the active internal energy ε.Where $\varepsilon+R=E$ where R is the rotational energy and E is the total energy. The two dimensional master equation can then be solved [Smith and Gilbert (1990)].

7.1.4. Collisional Stabilisation

Collisional stabilisation is the removal of energy from the complex AB^{+*} to produce the stable AB^{+} by one collision or several consecutive collisions.

Experimental Studies

The experimental study of collisional stabilisation in ion molecule chemistry has traditionally focussed on comparing the relative stabilisation efficiencies of various buffer gases. The stabilisation efficiency β is defined by

$$AB^{+*} + M \xrightarrow{k_{coll}\,\beta} AB^{+} + M \qquad (7.36)$$

where k_{coll} is the collision rate. By measuring the termolecular association rate for a variety of buffer gases, it is possible to obtain a series of relative β values. [Cates and Bowers (1980)] [Anicich and Bowers (1974)] [Miasek and Harrison (1975)] [Kemper et al (1985)] [McEwan et al (1987)] [Anicich et al (1990)]. The relative β are obtained by comparing the termolecular rates after dividing by the collision rates

$$\beta_{rel} = \left(\frac{k_3^x}{k_{coll}^x}\right) \Big/ \left(\frac{k_3^y}{k_{coll}^y}\right). \qquad (7.37)$$

Tables of β_{rel} for various species have been compiled and various explanations or rationales presented for the trends in β_{rel}. The relative efficiencies are usually quoted as a fraction of the efficiency of the parent gas, which is assigned the arbitrary value of 1.0. In Table 7-1 below the β_{rel} values from several experimental studies have been compared. Since the parent gases vary in each case the values have been calculated relative to helium, which was common to all the studies. Several studies have investigated the efficiency of larger species, these are not included because they cannot be compared with the results from other studies.

The Table reveals that although there are general trends, the nature of the ion has a great effect on the collisional stabilisation efficiency of a given neutral. Attempts to predict β_{rel} values for a wide variety of systems have not been successful. In loosely bound systems the nature of the collision may be significantly different to that in strongly bound systems, also some systems are more strongly affected by rotational energy transfer than others.

Table 7-1. Relative stabilisation efficiencies of small molecules

Species	Relative Stabilisation Efficiencies (β_{rel})						
He	1.0[a]	1.0[b]	1.0[c]	1.0[d]	1.0[e]	1.0[f]	1.0[g]
Ne	1.2	1.1	1.1	1.9	3.4	2.8	2.1
Ar	1.0	1.2	1.5	—	2.5	1.4	2.3
Kr	1.1	1.0	—	—	—	—	—
N_2	1.5	1.7	1.7	4.8	2.3	1.8	—

[a] Ion was proton bound dimer of $(CH_3)_3N$ [Cates and Bowers (1980)]
[b] Ion was $C_5H_4^+$ [Maisek and Harrison (1975)]
[c] Ion was proton bound dimer of $(CH_3)_2O$ [McEwan et al (1987)]
[d] Ion was proton bound dimer of CH_3CN [McEwan et al (1987)]
[e] Ion was $C_6H_4^+$ [Anicich et al (1990)]
[f] Ion was $C_6H_5^+$ [Anicich et al (1990)]
[g] Ion was CH_3. HCN^+ [Kemper et al (1985)]

Experiments using laser excitation of aromatic molecules, followed by UV absorption spectroscopy [Hippler et al (1983)] [Damm et al (1991)], or by IR fluorescence measurement [Yerram et al (1990)] [Toselli et al (1991)] of the relaxation of the species have yielded information on the average energy transferred per collision $\langle\Delta E\rangle$ between the vibrationally excited molecule and the bath gas. Several conclusions have been drawn from these studies [Weston and Flynn (1992)].

1. There is an approximately linear dependence of the amount of energy lost per collision, that is $\langle\Delta E\rangle$, with the energy of the excited molecule.

2. $\langle\Delta E\rangle$ is strongly dependant on the size of the buffer gas in terms of number of atoms, also the higher the boiling point of the buffer gas the greater $\langle\Delta E\rangle$.

While these experiments have been confined to aromatic neutrals such as azulene, benzene, and toluene, rather than excited ions, the general rules probably apply to the ionic systems as well, and the quantitative $\langle\Delta E\rangle$ information can be used as a guide by modellers.

Theoretical Approaches

In order to solve the master equation for a unimolecular process, it is necessary to take account of collisional energy transfer. In the master equation treatment of Gilbert and Smith [Gilbert and Smith (1990)] collisional energy transfer is described by a function $R(E,E')$ which is the rate of collisional energy transfer for the molecule from energy E to energy E'. Various expressions have been derived for $R(E,E')$, but all use $\langle\Delta E\rangle$ or on the root mean square value $\langle\Delta E^2\rangle^{1/2}$. The expressions fall into two basic groups.

1. Weak collision expressions. In these expressions the function $R(E,E')$ is dependant on E. The collisions are sufficiently short lived that $R(E,E')$ decreases as $|E-E'|$ increases.

2. Strong collision expressions. In these expressions the function R(E,E') is dependant on E', the collisions are so long lived and the coupling so strong that it is the distribution of the final energy and not of the initial energy that is important.

Although strong collision treatments are computationally easier they are not physically realistic, as has been shown by experiment. A weak collision model, known as the exponential down model used by Gilbert and Smith and Hippler et al [Hippler et al (1986)] is more realistic, predicting the linear relationship

$$\langle \Delta E_{down} \rangle = A + B E_{initial}. \tag{7.38}$$

$<\Delta E_{down}>$ is the average energy transferred per downward collision and can be related directly to $<\Delta E>$.

In any treatment where angular momentum is conserved, the transfer of rotational energy in collisions must also be considered, especially where, as in ion molecule association, the angular momentum of the reactant is very different from that of the transition state. The transfer of rotational energy can be described by using the same exponential down model with a suitable value for $<\Delta R>$.

The dearth of experimental knowledge about energy transfer, and in particular about $<\Delta E>$ and $<\Delta R>$ for ion-neutral collisions means that these quantities are usually taken as variables, to be altered to give agreement between rates predicted by models and the observed association rates. Provided the other parameters of the model are realistic this gives qualitative information about the nature of the collisional process.

7.1.5. Radiative Stabilisation

Bates and Herbst [Bates and Herbst (1988)] differentiate between the two kinds of radiative association processes. The first class of process concerns the addition of neutral H_2 to an ion in the absence of competing channels, ie

$$C^+ + H_2 \rightarrow CH_2^+ + h\nu. \tag{7.39}$$

The rate coefficient is small, about 10^{-15} cm^3 s^{-1}, but the large concentration of H_2 in the interstellar medium makes this class of reaction an important process. The other class of association reaction is that between polyatomic species that can lead to large association products. It is this more general class of processes that is described below

Experimental Observations

Direct observation of radiative stabilisation (ie the emission of the IR photon) has not been reported, due largely to the problem that to observe radiative stabilisation the pressure must be very low, (in the region of 10^{-7} Torr), so that the intensity of the IR emission would be too low to measure. The evidence for the process is commonly

observed in the shape of a non zero intercept when the bimolecular association rate, k_2 is extrapolated to zero pressure. This has been reported in numerous systems by a number of different groups. [Sen et al (1991)] [Bass et al (1981)] [Fisher and McMahon (1990)] [Anicich et al (1990)] [McEwan et al (1989)] [Kofel and McMahon (1988)] [Dunbar (1990)] [Orlando et al (1990)].

At low pressure in such cases, the bimolecular rate coefficient k_2 is found to be independent of pressure and to have a non zero intercept. This pressure independent rate is often reported as k_{rad} [Sen et al (1990)] with units $cm^3\ s^{-1}$. This is not the unimolecular rate constant k_r but is the low pressure limit of k_2,

$$k_{rad} = k_f \frac{k_r}{(k_d + k_r)}. \tag{7.40}$$

While some authors report k_{rad}, others such as Fisher and McMahon, [Fisher and McMahon (1990)] use the collision rate for k_f and use the strong collision approximation for k_c in order to obtain values for k_d and k_r from the slope and intercept of k_2. These rates are true unimolecular rates, but the physically unrealistic strong collision assumption casts doubt on the exact values derived.

Table 7-2. Observed radiative association rates.

Reaction Complex	Ref	k_r (s^{-1})	k_{rad} ($cm^3\ s^{-1}$)
$((CH_3)_2CO)_2H^+$	a		9.2×10^{-12}
$((CH_3)_2CO)_2H^+$	b	65	9.2×10^{-12}
$(CH_3CN)_2H^+$	b	41	0.8×10^{-12}
$((CH_3)_2O)_2H^+$	b	48	2.0×10^{-12}
$((C_2H_5)_2O)_2H^+$	b	18	25×10^{-12}
$CH_3CNCH_3^+$	c		9.0×10^{-11}
$(CH_3)_3Si.(CH_3)_2CO^+$	d		1.8×10^{-10}
$HC_3N.HC_3N^+$	e		6.5×10^{-11}
$HC_3N.HC_5N^+$	e		5.0×10^{-10}

[a] [Dunbar (1990)]
[b] [Fisher and McMahon (1990)]
[c] [McEwan et al (1989)]
[d] [Orlando et al (1990)]
[e] [Sen et al (1991)]

From Table 7-2 some trends are observed, the larger the collision complex, and the greater the binding energy, the larger the radiative stabilisation rate, whether it is expressed as k_r or as k_{rad}.

Theoretical Approaches

There are three principal mechanisms by which radiative stabilisation is thought to occur. In the first mechanism the process occurs without an electronic transition. The collision

complex is formed in an excited vibrational state, of the ground electronic state of the molecule, and radiative emission corresponds to a vibrational transition to a lower vibrational level of the same electronic state.

The emitted photon will be in the infrared region of the spectrum. Herbst [Herbst (1985)] has developed an expression for the rate of such a vibrational transition,

$$k_r = \sum_n P(E_{vib}) \sum_m A_{n\to m}, \tag{7.41}$$

where P_n (E_{vib}) is the probability of the complex being in vibrational state n, and the factor $A_{n\to m}$ is the Einstein A coefficient for spontaneous emission from state n to state m. Herbst also points out that if the harmonic oscillator assumption is made that the expression can be approximated by

$$k_r = \left(\frac{E}{s}\right) \sum_{i=1}^{s} \frac{A_{1\to 0}^{(i)}}{h\,\nu_i}, \tag{7.42}$$

where s is the number of vibrational modes, $A_{1\to 0}^{(i)}$ is the spontaneous emission coefficient for the fundamental transition of mode i. E is the total vibrational energy. The advantage of this expression is that $A_{1\to 0}^{(i)}$ can in principle be determined by spectroscopy, although measurements on ionic systems have rarely been reported.

The second mechanism is where the complex is formed in an excited electronic state, and the emission of a photon corresponds to an electronic transition to a vibrational level of the ground state. This process can lead to the emission of a photon at greater ν than that of the above mechanism. Bates and Herbst [Bates and Herbst (1988)] have expressed the spontaneous emission coefficient as,

$$A_{n\to m} = C\, h^3 \nu_{n\to m}^3 \left| \langle m | n \rangle \right|, \tag{7.43}$$

where C contains the transition dipole moment, h is Planck's constant, ν is the frequency of the transition. Where the two electronic states are similar in structure it is clear that the vibrational overlap integral will be small unless $m=n$

Where the structures of the electronic states are different there will be little chance of a stabilising transition from the excited to the ground state, but the third mechanism may apply, that is, a transition from a high vibrational level of the ground state, to a low lying vibrational state of the excited electronic state which may occur as long as there is sufficient overlap.

The question remains, of what is the rate of radiative stabilisation for a given species. Because of the plurality of mechanisms and the paucity of experimental

measurements reliable and accurate rate data cannot be predicted as a matter of course, however qualitative or approximate rates can be obtained.

An interesting approach to the estimation of radiative stabilisation rates is that taken by Dunbar [Dunbar (1990)]. The author addresses the problem in terms of estimating the ratio of radiative stabilisation to unimolecular dissociation back to reactants. The simplifying assumption used by Dunbar is that the association species can be described by a limited set of frequencies. In other words all active modes are treated as vibrations, and each molecule is limited to six vibrational frequencies ν_i. Each frequency has a fractional degeneracy n_i, so that in a molecule with N active modes the number of modes with frequency ν_i is Nn_i. This assumption allows for a very simple RRKM treatment to calculate the dissociation rate, and since the IR absorption properties are known for the standard frequencies the radiative emission rate is easily calculated. On the basis of this model Dunbar suggests that radiative association will be a significant process only for those species with a binding energy greater than 0.5 eV (48 kJ mol^{-1}). The rate of radiative association is also predicted to increase as the total number of degrees of freedom increase.

7.2. Association of Acrylonitrile

7.2.1. Introduction

Acrylonitrile, or vinyl acetylene as it is also known, has the molecular formula CH_2CHCN. Interest in the ion-molecule chemistry of acrylonitrile revolves around its importance as a compound in the interstellar cloud environment and around its role in the chemistry of planetary atmospheres.

The neutral species has been detected by microwave spectroscopy in both the Sgr B2 [Gardner and Winnewisser (1975)] and TMC-1 [Matthews and Sears (1983)] interstellar clouds. In fact, acrylonitrile was the first olefin to be reported in the interstellar regions. The observation by Voyager 1 that molecular nitrogen was the main constituent of the atmosphere of Titan led researchers to the conclusion that acrylonitrile and other complex nitriles could be present in that atmosphere.

Capone et al [Capone et al (1981)] suggested that a mechanism leading to the formation of acrylonitrile might well be

$$HCNH^+ + C_2H_2 + M \rightarrow CH_2CHCNH^+ + M \qquad (7.44)$$

as reported by McEwan, [McEwan (1980)] followed by dissociative ion-electron recombination. The same reactants being stabilised in a radiative process was suggested by Herbst [Herbst (1985)].

In recent years the suggestion has arisen [Herbst and Leung (1990)] that the reaction of a radical precursor, CN·, might be an important route to formation of acrylonitrile,

$$CN\cdot\cdot + C_2H_4 \rightarrow CH_2CHCN + H\cdot. \qquad (7.45)$$

However the species itself is produced, the ion-molecule chemistry of acrylonitrile has been extensively studied by Petrie and McEwan [Petrie et al (1991)] [Petrie et al (1992)]. The chemistry reported by Petrie et al was studied using a SIFT at pressures of ≈ 0.3 Torr. The reaction of CH_2CHCN^+ with neutral acrylonitrile was found to result only in rapid formation of the collisionally stabilised dimer,

$$CH_2CHCN^+ + CH_2CHCN + M \rightarrow CH_2CHCN.\ CH_2CHCN^+ + M. \qquad (7.46)$$

The bimolecular rate for dimerisation at 0.3 Torr was 2.0×10^{-9} cm^3 s^{-1}. The possibility that proton transfer, which is a common process amongst ionic nitriles and amines, might compete with association at lower pressures suggested the use of the ICR instrument to investigate the association reaction at low pressures.

The investigation of the low pressure chemistry of acrylonitrile showed that the reaction of CH_2CHCN^+ with neutral acrylonitrile proceeded through a different channel in the ICR, and that even at SIFT pressures this channel was operating in competition with collisionally stabilised association.

7.2.2. ICR Results

The system was studied using acrylonitrile as the neutral in the ICR cell. The primary ion CH_2CHCN^+ was formed in the ion source by electron impact, and was found to react rapidly to produce the protonated species CH_2CHCNH^+. This species underwent a secondary reaction to yield the proton bound dimer. The electron impact ionisation also revealed some ions at masses 59^+ and 60^+. After trying in vain to assign these ions as products of some ion molecule reaction, a fresh sample of acrylonitrile was procured. After freeze pump thaw purification the sample was used in the cell. The ions at 59^+ and 60^+ were no longer present.

The assignment of the tertiary ion as the proton bound dimer at 107^+ rather than the dimer at 106^+, can be made much more easily on the ICR system than on the SIFT instrument because of the far greater mass resolution of the ICR frequency swept detector, in comparison with the quadrupole used in the SIFT

The largest source of error in the measurements made in both the drift and the trap mode lies in the absolute pressure determination. While, as has been described

above the system factor of the instrument is close to unity, the calibration of the ionisation gauge introduces a significant uncertainty.

7.2.3. The Reaction $CH_2CHCN^+ + CH_2CHCN$

The only product of the primary ion $CH_2CHCN^+$was the protonated CH_2CHCNH^+,

$$CH_2CHCN^+ + CH_2CHCN \rightarrow CH_2CHCNH^+ + C_3H_2N. \qquad (7.47)$$

The reaction was studied in both drift and trap mode. The results are tabulated below.

Drift Mode Results

The drift mode experiment was carried out using pressures of the neutral between 0.5×10^{-5} to 1.91×10^{-5} Torr. The source drift time was 0.35 ms and the analyser drift time was 1.8 ms. The following [Su and Chesnavich (1982)] rates for momentum transfer collisions with the neutral gas were used.

$$k_{coll}\ CH_2CHCN^+ = 3.64 \times 10^{-9}\ cm^3\ s^{-1}$$
$$k_{coll}\ CH_2CHCNH^+ = 3.62 \times 10^{-9}\ cm^3\ s^{-1}$$

The program ICRC2 was used to derive rate constants from the peak heights.

Table 7-3. Peak heights[a] and rate constants for $53^+ \rightarrow 54^+$.

Pressure[c]	53^+	54^+	k_2[b]
0.50	25	15	3.25
0.74	65	60	2.99
1.0	52	63	2.66
1.21	37	62	2.70
1.47	32	69	2.58
1.71	31	77	2.40
1.91	24	72	2.38

[a] Arbitrary Units
[b] Units $cm^3\ s^{-1} \times 10^{-9}$
[c] Units of Torr $\times 10^{-5}$

As can be seen there is an apparent increase in the bimolecular rate at low pressures, this is possibly due the partial pressure of water in the cell, a gradual decrease in rate constant with increasing pressure may be due to the secondary ion reacting further with the neutral.

Trap Mode Results

Trap mode experiments were carried out to confirm the drift mode results, these were the first experiments (except for the initial calibration reactions with Ar^+) attempted

using the trap mode. The nature of the trap mode experiment makes it more sensitive than the drift experiment to the conditions used, primarily electron current and pressure.

The trap mode experiments were carried out using a timebase of 0.1 s. The first experiments were unsuccessful because of space charging due either to excessive pressure or excessive filament current. The space charging caused loss of the ions from the cell during the measurement of the decay of the high pressure curve. The rates from the successful experiments are shown in Figure 7-1 combined with the drift mode results.

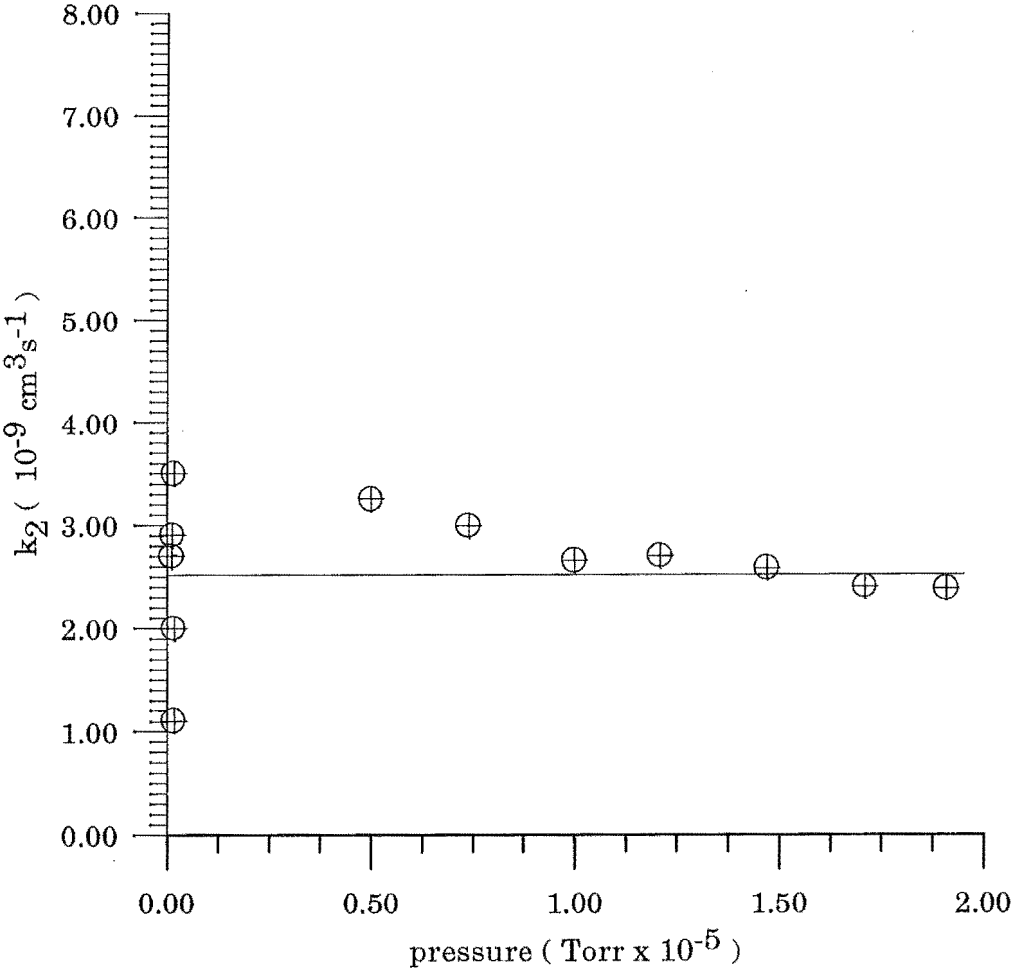

Figure 7-1. k_2 for CH_2CHCN^+ + CH_2CHCN proton transfer measured in the ICR, as a function of pressure.

Conclusion

The spread of results in both experimental modes was wide, but the agreement between the experiments at different ends of a wide range of pressures allows a determination of the rate of reaction. The average result over both the drift and trap experiments is 2.5×10^{-9} cm^3 s^{-1}. The broad agreement in rate over the pressure range used, from 8×10^{-7} to 2×10^{-5} shows the behaviour expected of a purely bimolecular reaction.

7.2.4. *The Reaction $CH_2CHCNH^+ + CH_2CHCN$*

The only apparent product of the reaction was the proton bound dimer at 107^+,

$$CH_2CHCNH^+ + CH_2CHCN \rightarrow CH_2CHCN.\ CH_2CHCNH^+. \qquad (7.48)$$

Drift Mode Results

The drift mode experiment was carried out using pressures of the neutral between 0.5×10^{-4} to 2.9×10^{-4} Torr. Five different experimental runs were carried out over a period of three days, with good agreement. The source drift time was 0.35 ms and the analyser drift time was 1.65 ms. The following ADO [Su and Chesnavich (1982)] rates for momentum transfer collisions with the neutral gas were used.

$$k_{coll}\, CH_2CHCN^+ = 3.64 \times 10^{-9}\ cm^3\ s^{-1}$$

$$k_{coll}\, CH_2CHCNH^+ = 3.62 \times 10^{-9}\ cm^3\ s^{-1}$$

$$k_{coll}\, CH_2CHCN.CH_2CHCNH^+ = 3.14 \times 10^{-9}\ cm^3\ s^{-1}$$

The program ICRSP was used to derive rate constants from the peak heights, with the primary $\rightarrow$ secondary rate coefficient input as 2.5×10^{-9} $cm^3\ s^{-1}$.The reason that the ICRSP program was used rather than the program ICRC3 was that at the pressures used to obtain an adequate signal of the tertiary ion the primary ion signal was not observable, it having reacted away to give the secondary ion.

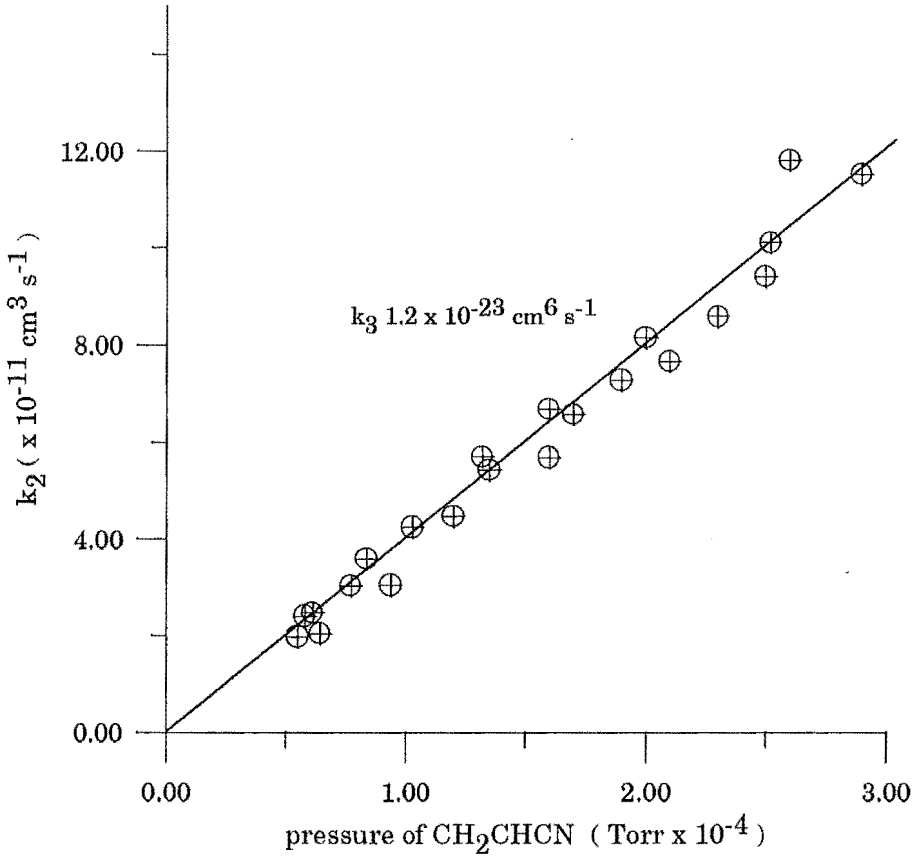

Figure 7-2. Ternary association of CH_2CHCNH^+in CH_2CHCN, measured in the ICR.

The bimolecular rate constant shows the expected linear dependence on pressure, with an apparent zero intercept. The termolecular rate constant for association can be derived using $k_3 = \frac{k_2}{[M]}$. The appropriate conversion factor to give k_3 in $cm^6\ s^{-1}$ is

$$k_3 = \frac{k_2}{P(Torr) \times 3.24 \times 10^{16}} \tag{7.49}$$

From the slope of the apparent bimolecular rate coefficient with pressure the observed termolecular rate k_3 was 1.2×10^{-23} $cm^6\ s^{-1}$.

Helium Stabilised Association

McEwan, using the ICR instrument at JPL, carried out several experiments in conjunction with this work. The result obtained by McEwan for association in the presence of the parent gas [McEwan (1993)] was identical to that reported in this work, k_3 1.25×10^{-23} $cm^6\ s^{-1}$, with no evidence of a radiative process at low pressures. McEwan also examined the association reaction in helium bath gas and found that the termolecular rate in helium was between 1.4 and 1.7×10^{-24} $cm^6\ s^{-1}$. If the stabilisation by helium is expressed in terms of β_{rel} as defined above, that is, assuming that the parent gas has unit stabilisation efficiency, the relative stabilisation efficiency of He is 0.40.

SIFT results

The reaction of CH_2CHCN^+ with neutral acrylonitrile is reported by Petrie at al [Petrie et al (1992)] to yield the dimer $CH_2CHCN \cdot CH_2CHCN^+$. The proton transfer channel is not reported, and the bimolecular rate coefficient at 0.3 Torr is reported as 2.0×10^{-9} $cm^3\ s^{-1}$. In the same reference the authors report that at 0.3 Torr, the protonated species, CH_2CHCNH^+, reacts with neutral acrylonitrile to form the protonated dimer only, with a bimolecular rate coefficient of 1.3×10^{-9} $cm^3\ s^{-1}$.

The SIFT results reported by Petrie et al are interesting in that the bimolecular rate for reaction of CH_2CHCN^+ in the SIFT is less than that observed in the ICR, and of course the reported product is association rather than proton transfer.

In order to confirm the results of Petrie et al the reaction of CH_2CHCN^+ with acrylonitrile was reexamined using the SIFT instrument. Unfortunately it was impossible to inject only CH_2CHCN^+ without also injecting CH_2CHCNH^+ into the flow tube. It was possible to measure the rate of loss of the reactant ion, but not to determine the branching ratio between association and proton transfer, as the protonated species not only reacts with the neutral to form the proton bound dimer, but may be formed by proton transfer at the same time. It was however possible to confirm that proton transfer did occur. As the neutral was added to the flow tube the signal due to the protonated

species increased, and at larger flows the proton bound dimer signal was several times larger than the original CH_2CHCNH^+ signal that was injected into the flow tube.

The presence of a proton transfer channel was also suggested by the observation that using Ar^+ to ionise CH_2CHCN added at the first neutral inlet also produced a significant amount of the protonated species. Reducing the neutral flow reduced the 54^+ signal faster than the 53^+ signal, another qualitative indication that CH_2CHCNH^+ was a secondary ion. The overall rate of loss of CH_2CHCN^+ was similar to the rate reported by Petrie et al, the bimolecular rate constant was 1.5×10^{-9} cm^3 s^{-1}.

The rate of formation of the proton bound dimer was difficult to measure since it was impossible to inject 54^+ without also injecting 53^+. Using HCO^+, formed from dimethoxymethane in the ion source, to protonate acrylonitrile added at the first neutral inlet was tried, but resulted in a small signal at 53^+ accompanying the 54^+. In fact the decay of 54^+ as a function of the flow rate of the neutral species did not show the curvature that might be expected if a large amount of proton transfer was occurring on addition of the neutral. The measured rate for loss of the protonated species was 1.3×10^{-9} cm^3 s^{-1}, in agreement with the result by Petrie et al.

Table 7-4. Reactions of CH_2CHCN with ions in the SIFT[a].

Ion	Products	k_2[b]	k_{coll}[c]
CH_2CHCN^+	$CH_2CHCN.CH_2CHCN^+$ $CH_2CHCNH^+ + C_3H_2N$	1.5	3.6
CH_2CHCNH^+	$CH_2CHCN.CH_2CHCNH^+$	1.3	3.6

[a] 295 K at 0.302 Torr
[b] Units of cm^3 s^{-1}
[c] Units of cm^3 s^{-1} calculated by method of Su and Chesnavich (1982)

7.2.5. Discussion

The use of only drift mode methods to study the pressure dependence of the association rate gave good information on the collisional process of stabilisation. The lack of good low pressure information however, obscures the detail of the possible radiative process. Since direct observation of radiative association is not possible in the ICR instrument it is usually inferred from the observation of a non zero intercept in the slope of k_2 as a function of pressure. Such a non zero intercept was not observed in this experiment.

McEwan et al [McEwan et al (1987)] studied the analogous formation of the proton bound dimers of acetonitrile and dimethyl ether also using only drift mode. They reported no evidence of radiative association. The experiments were repeated by Fisher and McMahon [Fisher and McMahon (1990)] using low pressure FTICR measurements.

These authors report radiative channels for both reactions. The authors were able to measure the association rate down to very low pressures by using a trapped cell FTICR instrument with a superconducting magnet. Pressures as low as 5×10^{-9} mbar (3.8×10^{-9} Torr) were used, with trapping times of up to 500 s. The maximum pressures used were 3×10^{-6} mbar, so the authors were observing only the very start of the termolecular regime. The accuracy of the experiment is sufficient to show the very small intercept due to bimolecular processes at low pressure.

The drift mode experiments carried out in this work, and by other authors cover more of the termolecular pressure range and lack the detail to reveal the bimolecular process. Thus although the radiative process was not observed in this work, it is quite reasonable to suspect that it will occur with a rate similar in magnitude to that observed [Fisher and McMahon (1990)] for the association of other small proton bound dimers, those of acetone, acetonitrile, and dimethyl ether, the reported rates of radiative stabilisation observed for these reactions being $\leq$ 65.2 s^{-1}, 40.7 s^{-1}, and 48.3 s^{-1}, respectively.

The rate of collisional stabilisation in the parent gas as indicated by the termolecular rate constant of 1.2×10^{-23} cm^6 s^{-1} is small compared to the rates reported for the ternary association rates of some larger proton bound dimers.

Table 7-5. Ternary association rates for selected proton bound dimers .

Parent Species	k_3 in Parent Gas [f]	$k_3$in He[f]	Ref
NH_3	6.4		a
CH_3NH_2	180		a
$(CH_3)_2NH$	1070		a
$(CH_3)_3N$	1200		a
$C_2H_5NH_2$	1700		a
n-$C_3H_8NH_2$	7500		a
$(C_2H_5)_2NH$	2800		a
i-$C_4H_9NH_2$	19800		a
$(CH_3)_2CO$	26.7		b
$(CH_3)_2CO$	18		c
$(C_2H_5)_2O$	165.2		b
CH_3CN	7.0		b
CH_3CN	0.2	0.0072	d
$(CH_3)_2O$	6.1		b
$(CH_3)_2O$	1.0	0.079	d
CH_2CHCN	1.2	0.15	e

[a] [Nielson et al (1978)]
[b] [Fisher and McMahon (1990)]
[c] [Kofel and McMahon (1988)]
[d] [McEwan et al (1987)]
[e] This Work and result by McEwan see above
[f] Units of 10^{-23} cm^6 s^{-1}

A notable feature of the Table is the discrepancy between the ternary association rates measured by Fisher and McMahon and those by McEwan et al for the formation of the proton bound dimers of CH_3CN and of $(CH_3)_2O$. The rates as measured by Fisher and McMahon are much higher.

One possible explanation for the discrepancy is that the two groups used different methods to calibrate their ionisation gauges. The method used by McEwan et al was the common method of calibrating the gauge against a Baratron capacitive manometer for each gas used. This method is described in detail in Chapter three above. The method used by Fisher and McMahon was chemical calibration. Within each system they studied there were several precursor or side reactions. For example, when the dimerisation of CH_3CN was being studied, the authors measured the rates of the following reactions;

$$CH_3CN^+ + CH_3CN \rightarrow CH_3CNH^+ + CH_2CN\,, \qquad (7.50)$$

$$CH_2CN^+ + CH_3CN \rightarrow CH_3CNH^+ + CHCN. \qquad (7.51)$$

The authors report that these reactions were assumed to occur at the collision rate as determined by ion/polar molecule trajectory calculations of Su and Chesnavich [Su and Chesnavich (1982)]. The literature values for both reactions, however, reveal that the rates are closer to half of the collision rate.

Table 7-6. Reactions of neutral CH_3CN .

Reaction	k_2 ($\times 10^{-9}$ cm^3 s^{-1})	k_2/k_{coll}[d]	ref
$CH_3CN^+ + CH_3CN$	2.01	0.49	a
$CH_3CN^+ + CH_3CN$	2.2	0.54	b
$CH_3CN^+ + CH_3CN$	> 2.1	> 0.51	This Work
$CH_3CN^+ + CH_3CN$	2.09	0.50	c
$CH_2CN^+ + CH_3CN$	0.97	0.24	c
$CH_2CN^+ + CH_3CN$	1.78	0.43	a

[a] [Franklin et al (1966)]
[b] [Harrison and Shannen (1965)]
[c] [Vogt and Beauchamp (1975)]
[d] [Su and Chesnavich (1982)]

Greater discrepancies between the collision rate and the observed reaction rate apply to the case of the reactions of acetone. The literature values for the reactions

$$CH_3CO^+ + (CH_3)_2CO \rightarrow (CH_3)_2CH^+ + CH_2CO, \qquad (7.52)$$

and

$$(CH_3)_2CO^+ + (CH_3)_2CO \rightarrow (CH_3)_2COH^+ + CH_3COCH_2, \qquad (7.53)$$

are almost an order of magnitude below the collision rate. The literature values for the rate coefficents are listed in Table 7-7.

Table7-7. Reactions of neutral $(CH_3)_2CO$.

Reaction	k_2 ($\times 10^{-9}$ cm^3 s^{-1})	k_2/k_{coll}[c]	ref
$CH_3CO^+ + (CH_3)_2CO$	0.2	0.07	a
$CH_3CO^+ + (CH_3)_2CO$	0.43	0.14	b
$(CH_3)_2CO^+ + (CH_3)_2CO$	0.38	0.14	b

[a] [Van der Hart and Van Sprang (1977)]
[b] [MacNeil and Futrell (1972)]
[c] [Su and Chesnavich (1982)]

The possibility is that the pressure calibration was not correct thus casting a certain amount of doubt on the exact rate values quoted for the k_3 values above. It is certainly clear, however that the termolecular rate is a strong function of molecular size. It must be borne in mind that this is not only due to the unimolecular behaviour of the association species, but also to the collisional deactivation of the collision complex by the parent gas. The larger the parent gas, the greater the stabilisation effect, and the greater the termolecular rate. Unfortunately, most authors do not measure the rate in a variety of bath gases, so that the influence of structure of the association complex cannot be directly observed.

Another point of note is that the overall bimolecular rate of reaction for the proton transfer step was lower in the SIFT than in the ICR, and that channel occurred in competition with a dimerisation channel that was insignificant at ICR pressures. A true comparison between rate measurements in the SIFT and in the ICR is difficult because the reactant ions in the two systems may have considerably different energy distributions. As will be discussed in the section below, the formation of ions in the low pressure ICR instrument by electron impact, and the subsequent influence of electric fields upon those ions may produce ions with considerably more energy than a room temperature distribution. On the other hand the rapid thermalisation of ionic species in the SIFT due to collision with the bath gas means the temperature of the reactant ion can be more realistically represented as 'room temperature '.

7.3. An RRKM Study of the $CH_3^+ + CH_3CN$ System

7.3.1. Introduction

The work described in this section was carried out over a long period of time in collaboration with several people. The ab initio results eventually used were calculated by Pravit Sudkeaw [Sudkeaw (1991)] and Robert Maclagan. The RRKM modelling package used was developed by Gilbert and Smith [Gilbert and Smith (1990)].

The reaction between CH_3^+ and CH_3CN is of interest because of the presence of three channels, two giving exothermic products, and the third being the association channel,

$$CH_3^+ + CH_3CN \rightarrow H_2CN^+ + C_2H_4 \quad (7.54a)$$
$$\rightarrow C_2H_5^+ + HCN \quad (7.54b)$$
$$\rightarrow CH_3CN.CH_3^+. \quad (7.54c)$$

The exothermic product channels dominate at the low pressure conditions in the ICR experiment, [McEwan et al (1989)], yet the association reaction dominates in the SIFT pressure regime, [Knight et al (1986)] where the reaction proceeds at almost the collision rate. It was this variation in product distribution over the different pressure regimes that made this system seem an excellent choice upon which to use modelling techniques.

The preliminary studies used spectroscopic data for some parameters, such as the reactants and exothermic product ions structures and vibrational frequencies, combined with *ab initio* results and some guesswork for the structure and modes of the complex and transition state species. Some time later a full *ab initio* study was performed and the results were used in the model. This yielded the results described in detail below. At a later date, using the same parameters, Dr Sean Smith used a new RRKM treatment incorporating allowance for uncoupled modes and the results of that analysis were published [Smith S.C et al (1993)]. The principle differences between the modelling described below and those results obtained using the uncoupled mode treatment will be discussed.

The Existing Experimental Information

The SIFT study of Knight et al [Knight et al (1986)] and one by McEwan[1] examined the system in the pressure range 0.2..0.4 Torr. At this pressure the reaction gave 88% association with a minor, 12% channel, giving $H_2CN^+ + C_2H_4$. The rate of reaction was 5.5×10^{-9} cm^3 s^{-1} which is effectively the collision rate.

---

[1] .....

At the lower pressure of the ICR instrument (below 10^{-4} Torr) the exothermic product channels dominated. McEwan et al reported [McEwan et al (1989)] that the channel giving $H_2CN^+ + C_2H_4$ had a branching ratio of 58%, the channel giving $C_2H_5^+ +$ HCN had a branching ratio of 37%, and the remaining 5% of reactants formed the adduct. Because of the complicating factor of sequential reactions the rate coefficients of the various reactions were determined by computer modelling of the system. The reported termolecular association rate being 1.9×10^{-22} cm^6 s^{-1} in acetonitrile bath gas, and 1.0×10^{-23} cm^6 s^{-1} when the stabilising species was helium. At very low pressures the association channel exhibited bimolecular kinetics. By making various approximations for the elementary rate constants, McEwan et al estimated the unimolecular lifetime τ to be $14 \leq \tau \leq 46$ μs and the unimolecular radiative stabilisation rate to be $4.9 \times 10^2 \leq k_r \leq 1.2 \times 10^3$ s^{-1}. The reported lifetimes represent lower limits since they are in effect values of β .τ where β is the collision efficiency.

7.3.2. Ab Initio Values

The structural and vibrational parameters required for the modelling were initially based on a combination of spectroscopic and *ab initio* information. The structure of the loose transition state was assumed to be that of CH_3^+----CH_3CN, with the individual moieties having the structures and vibrational modes observed spectroscopically. The association product, or rather the 'molecule' in unimolecular parlance was described by the parameters obtained by *ab initio* methods. The tight transition state in the channel to the exothermic products was not known, and so various estimates of its' parameters, based on "chemical intuition" were made. It became clear that with the sum of states at the transition state surface, the energy at the transition state surface, the collisional deactivation parameters and the temperature all not clearly defined the model could reveal only a limited amount of information.

It was decided to use only self consistent *ab initio* results for all parameters. This would entail calculations to be performed over a large region of the potential energy surface. These calculations were carried out by Pravit Sudkeaw. Referring to two previous studies of the potential surface [Bouchoux et al (1989)] [Deakyne and Meot-Ner (1990)] it was finally decided that the reaction probably proceeded through a pathway proposed by Wincel at al [Wincel et al (1980)]. The potential energy surface and the *ab initio* structures used are shown in Figure 7-3.

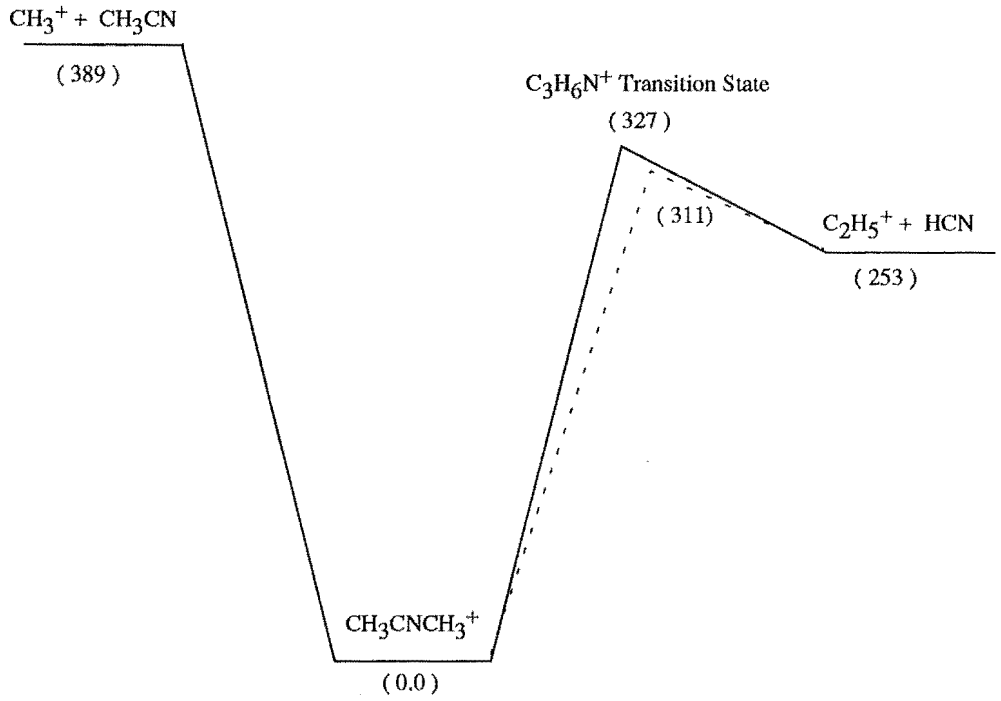

Figure 7-3. Potential energy surface for $CH_3^+ + CH_3CN$ association, calculated by *ab initio* methods and used in the RRKM modelling. The dotted line represents the transition state (chemical barrier) energy selected by fitting the branching ratio at 450 K. (energies in kJ mol^{-1}).

While the literature and the ab-initio results seemed to support the $CH_3CNCH_3^+$ structure for the association product of CH_3^+ and CH_3CN, there was at the time no direct experimental evidence to suggest that that structure would be favoured. The experiments on the isomeric forms of $C_3H_6N^+$ described earlier in this work provided support for this assumption. Although the results did not confirm the structure unambiguously, they eliminated the most likely alternative structures. There do however remain several outside possibilities for alternative structures, although plausible reaction mechanisms to produce these structures seem unlikely. A complete table of possible isomers is given in the work of Bouchoux et al [Bouchoux et al (1989)].

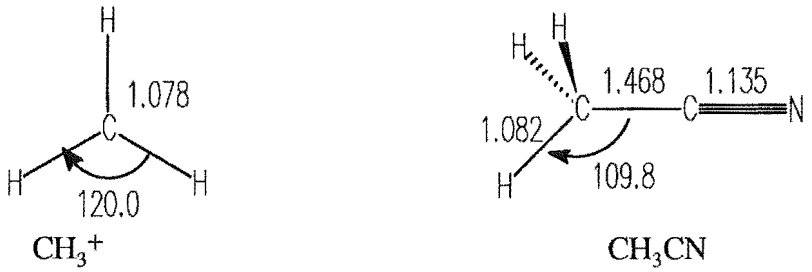

Figure 7-4. Optimised *ab initio* structures for $C_3H_6N^+$ species, reactants, and products [Smith S.C et al (1993)].

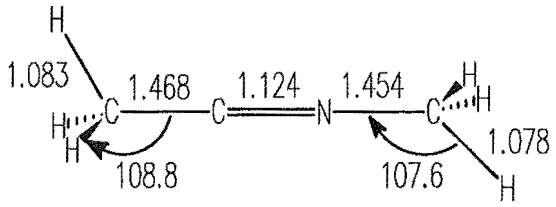

$CH_3CNCH_3^+$

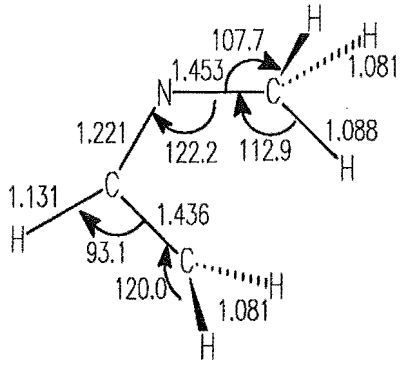

$C_3H_6N^+$ Transition State

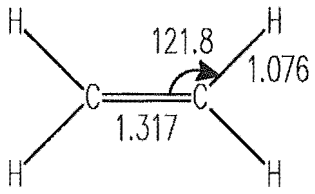

C_2H_4

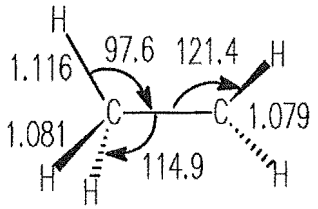

$C_2H_5^+$

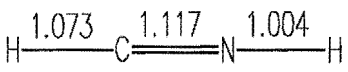

$HCNH^+$

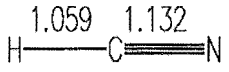

HCN

Figure 7-4. (continued); Optimised *ab initio* structures for $C_3H_6N^+$ species, reactants, and products [Smith S.C et al (1993)].

7.3.3. RRKM Parameters Used

The vibrational frequencies calculated by the ab-initio methods were multiplied by the scale factor 0.89 as recommended by DeFrees and McLean [DeFrees and McLean (1985)]. The rotational modes were expressed in terms of the B value for each mode in cm^{-1}. In order to simplify the calculations the molecules were treated as symmetric tops, with one unique and two degenerate external rotational modes. In order to describe the non symmetric tight transition state as a symmetric top, the arithmetic mean was found for the two closest rotational modes of each species and this was used as the value for the degenerate mode for the assumed symmetric top.

The unique rotation about the "long" axis, which in the loose transition state is the line of centres between the moieties is treated traditionally [Gilbert and Smith (1990)] [Forst (1973)] as an active mode, to and from which energy is rapidly transferred with the other active modes including vibrational and internal rotational modes. The degenerate rotational modes about the two axes orthogonal to the 'long' axis are treated as inactive modes. This is not to say that they play no part in the behaviour of the system, conservation of angular momentum requires that some energy be 'locked ' into these inactive modes, reducing the energy available within the active modes available for crossing the potential (or centrifugal) barrier.

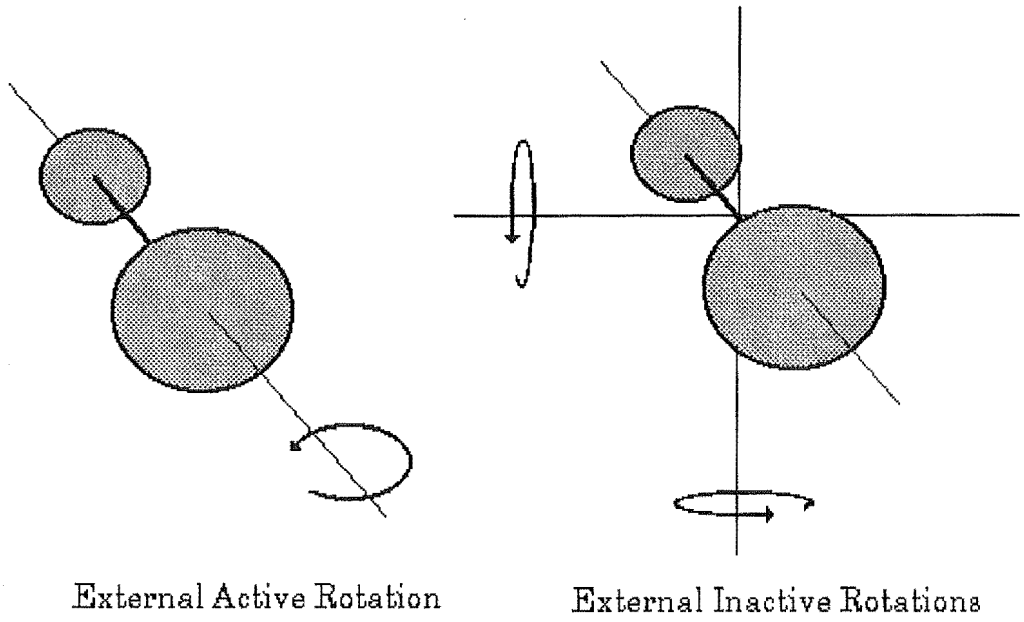

Figure 7-5. The active and inactive external rotations of a symmetric top.

There may be other rotational modes present in a system, for example, internal torsional modes. An example of such an internal torsion is displayed by the species $CH_3CNCH_3^+$ in that the methyl groups may contrarotate about the long axis of the molecule. Also, the loose transition state, the ion dipole complex CH_3^+.....CH_3CN, exhibits a hindered dipole rotation. The rotational constant for the hindered dipole rotation was calculated by the GEOM program. Both the internal torsion and the hindered dipole rotations are treated as active modes.

A complete list of the rotational and vibrational parameters used in this work is given in Table 7-8.

Table 7-8. RRKM parameters used in this work.

$CH_3CNCH_3^+$	Loose Transition State	Tight Transition State
Vibrational Frequencies (cm^{-1}), and Degeneracy		
197 (2)	383 (2)	155 (1)
471 (2)	876 (1)	162 (1)
619 (1)	1079 (2)	341 (1)
957 (1)	1423 (1)	461 (1)
1081 (2)	1457 (2)	688 (1)
1143 (2)	2297 (1)	776 (1)
1413 (1)	2856 (1)	823 (1)
1426 (2)	2925 (2)	1029 (1)
1433 (1)	1350 (1)	1083 (1)
1450 (2)	1372 (2)	1118 (1)
2390 (1)	2873 (1)	1132 (1)
2851 (1)	3060 (2)	1204 (1)
3775 (1)		1417 (1)
2936 (2)		1424 (1)
2985 (2)		1445 (1)
		1471 (1)
		1838 (1)
		2298 (1)
		2841 (1)
		2910 (1)
		2941 (1)
		2965 (1)
		3021 (1)
Inactive External Rotations (B value cm^{-1})		
0.116	Variationally Treated [a]	0.15
Active Rotations (B value, cm^{-1}), Symmetry number, and Dimension		
2.65[b] (3,1)	2.51[b] (3,1)	0.895[b] (1,1)
10.6[c] (3,1)	9.59[c] (2,2)	
	10.05[c] (3,1)	
	0.333[d] (1,2)	

[a] The values ranged from 2.4 to 7.3×10^{-3} cm^{-1}
[b] Active External Rotation
[c] Internal Rotation
[d] Hindered Dipole Rotation

The external inactive rotation of the loose transition state depended on the separation of the two moieties. The transition state separation was found using microcanonical variational treatment, 10 values of the transition state separation together with values for the external rotation were used as input. For each (E,J) state the separation giving minimum flux through the transition state surface was used.

7.3.4. Fitting the Association Fall Off

Having obtained suitably complete *ab initio* data it remained to use the parameters in the context of both RRKM, and Master Equation theory, to gain information about the physical behaviour of the system.

The first step was to use the RRKMIN4 program to calculate unimolecular rates for each channel in the low pressure limit. In order to reproduce the ICR result the model had to fit a branching ratio for the exothermic channel of 0.33. In the ICR experiment the observed bimolecular rate constant for the exothermic channels was 1.8×10^{-9} cm^3 s^{-1} and the collision rate was 5.4×10^{-9} cm^3 s^{-1}.

In order to reproduce the low density branching ratio two parameters could be varied; The barrier height of the tight transition state, $E°$, and the temperature of the system. Using these parameters as variables can be justified in that the *ab initio* energies are not exact and the true temperature of ions in an ICR cell is not accurately known, but suspected to lie above room temperature [Henchman et al (1987)]. The reason being largely due to the use of electron impact ionisation which not only heats the cell but produces ions with a non thermal energy distribution, also electric fields used to contain or drift ions within the cell necessarily add a translational energy component. It is thus not unreasonable to use an elevated thermal temperature for the system.

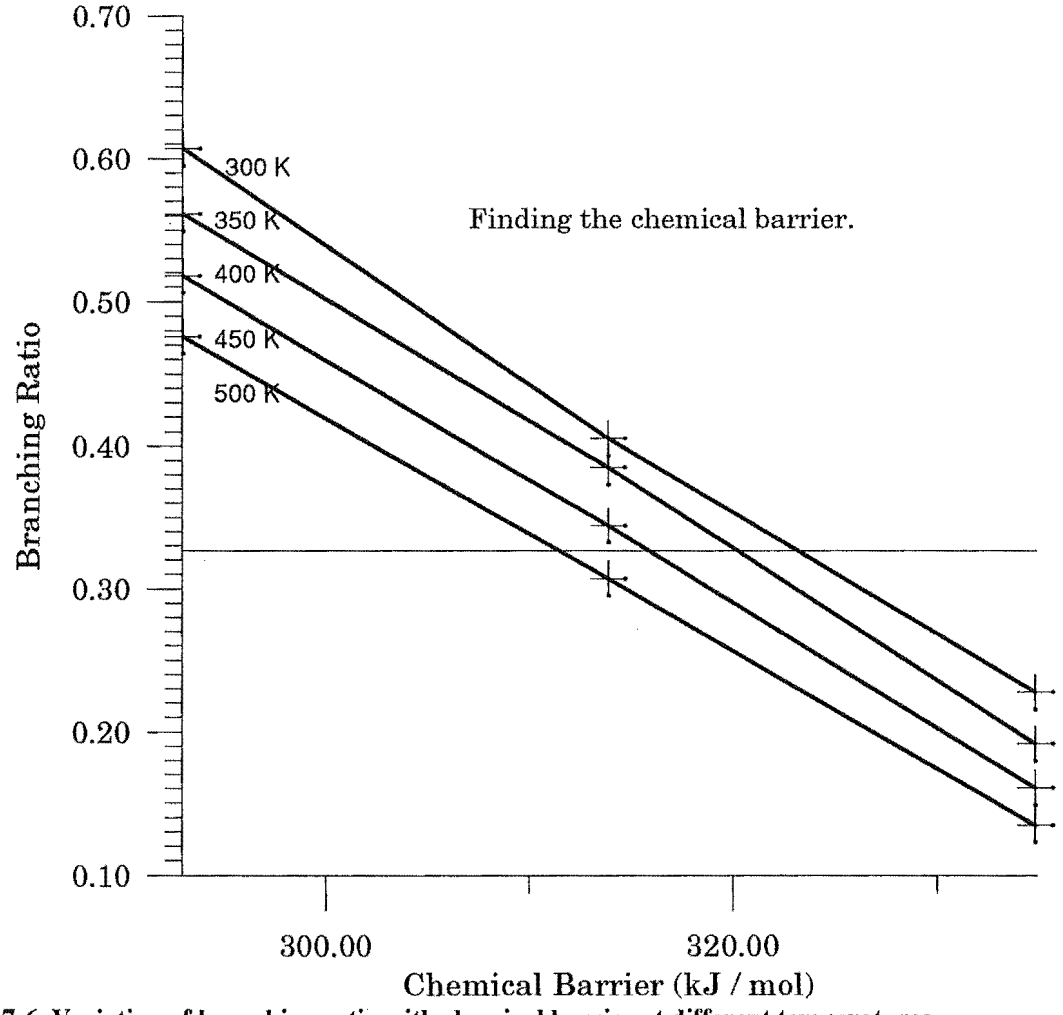

Figure 7-6. Variation of branching ratio with chemical barrier at different temperatures.

The temperature was initially varied from 300 to 500 K in increments of 50K. The barrier height for the exothermic channel $E°$ was varied to fit the branching ratio at each temperature. The branching ratio as a function of chemical barrier height is shown, for different temperatures in Figure 7-6.

Having plotted the branching ratio as a function of $E°$ for different temperatures the exact $E°$ value to use for each temperature was found. It is worthy of note that over the temperature range 300...500K the spread in values of $E°$ was small, 306.8 to 320.2 kJ mol^{-1}. These values can be compared with the *ab initio* result of 327 (see Figure 7-3).

Having obtained a set of values of both T and $E°$ which satisfied the requirements to fit the branching ratio, the MAS77 program was used to solve the master equation for different collisional deactivation parameters. The program used an exponential down treatment of collisional energy transfer, for transfer of both rotational and total energy. The only parameters required were $<\Delta E_{down}>$,the average downward energy transfer per collision, and $<\Delta R_{down}>$, the average downward rotational energy transfer per collision. Two simplifying assumptions were made. Firstly that where the collision partner was the parent neutral, the polyatomic dipole CH_3CN, the rotational energy transfer could be described by the strong collision model. So the rate function for rotational energy transfer depended on the final energy distribution rather than the initial energy distribution. The second assumption that was made was that the $<\Delta E_{down}>$ and $<\Delta R_{down}>$ values for the helium bath gas were the same.

Given each set of T and $E°$ values, the collisional energy transfer parameters were altered until the fall off of the association channel over the ICR pressure range sufficiently closely matched that of the experimental result observed for both CH_3CN and helium bath gases. The association channel rate at higher pressures was not considered as important as that at low pressures. At the high pressure limit, k_f or the capture rate, dominates, and the coupled mode treatment used here is known to overestimate the capture rate. The extent to which this also affects the lower pressure results is discussed below.

7.3.5. Results

The unimolecular lifetime τ defined by $\tau = \frac{1}{\sum_i k_{uni}^i}$ and the low density limit branching ratio for the exothermic channel are given for combinations of T and $E°$ in Table 7-9. Note that at temperatures below 375 K it was found impossible to fit the fall off of the association channel with physically reasonable collisional energy transfer parameters.

Table 7-9. Unimolecular parameters estimated by RRKM treatment.

Temperature [a]	Barrier Height.[b]	Branching Ratio	Lifetime [c]
375	317.2	0.334	77
400	315.1	0.330	56
425	313.0	0.332	41
450	310.9	0.332	30
475	308.8	0.331	22
500	306.8	0.330	17

[a] Units of K, [b] Units of kJ mol^{-1}
[c] Unimolecular lifetime at low density limit units of μs

Having fitted the data at the low pressure limit, the collisional parameters were found by using the MAS77 program to fit the fall off. The results are shown in Table 7-10 below.

Table 7-10. Energy transfer parameters estimated using the master equation program.

Temperature [a]	CH_3CN Bath gas		He Bath gas	
	$\langle\Delta E_{down}\rangle$[b]	$\langle\Delta R_{down}\rangle$[c]	$\langle\Delta E_{down}\rangle$[b]	$\langle\Delta R_{down}\rangle$[b]
375	No Fit		No Fit	
400	150	Strong Collision	125	125
425	390	Strong Collision	200	200
450	950	Strong Collision	300	300
475	2210	Strong Collision	425	425
500	4000	Strong Collision	500	500

[a] Units of K.
[b] Units cm^{-1}.
[c] Every collision results in rapid rotational relaxation.

As can be seen from the above results, over the temperature range covered, the required values of the collisional energy transfer vary significantly. Unfortunately not enough experimental data exists to predict which combination of values is the most physically reasonable. The collisional relaxation experiments discussed above have focussed on aromatic molecules rather than ions, but the results can offer some qualitative guidelines. The $\langle\Delta E_{down}\rangle$ value for collision between excited toluene and Ar has been found to be 260 cm^{-1}, [Hippler et al (1983)]. In the same study the values of the average energy transfer in either direction, (- $\langle\Delta E\rangle$), for helium and Ar are given. The value for helium is roughly 60% of that of Ar. This suggests that reasonable values for $\langle\Delta E_{down}\rangle$ for helium should lie in the region around 100... 200 cm^{-1}. The value of $\langle\Delta E_{down}\rangle$ in this and other studies increases dramatically with the number of atoms in the bath gas, so for a species as large as CH_3CN reasonable values for $\langle\Delta E_{down}\rangle$ could be expected to lie between 400...1000 cm^{-1}.

Using the estimated values of $<\Delta E_{down}>$ for the different temperatures listed above, it seems that the temperature of the ICR experiment lies between 400 and 475 K. The value of 450 K was used to produce a representative fall off curve for each bath gas. The bimolecular association rate was calculated for each of 10 pressures, from the low pressure bimolecular regime through to the saturated, collision dominated limit. In examining these curves it must be remembered that the parameters represent the best estimation of conditions in the ICR experiment, the SIFT high pressure result cannot be reproduced because the temperature is lower, and because the complete coupling of all the vibrational and all but two of the rotational modes overestimates the collision rate.

The association channel fall off achieved using the master equation treatment can be compared with the same fall off calculated using the strong collision approximation for collisional deactivation. A graphic representation of the fall off results is given in Figure 7-7 below. The natural log of the bimolecular rate coefficient for association is plotted as a function of the log of the pressure. The strong collision curve and the curve calculated using a value of 950 cm^{-1} for $<\Delta E_{down}>$ are plotted together.

The experimental termolecular association rate reported by [McEwan et al (1989)] was used to obtain representative experimental points. Table 7-11 lists a series of values of k_2 over the pressure range where termolecular kinetics were observed based on the values of k_3 reported by McEwan et al for both CH_3CN and He bath gases.

Table 7-11. Calculated k_2 values from experimental termolecular rates.

Pressure[a]	CH_3CN Bath gas		He Bath gas	
	k_2[b]	ln k_2	k_2[b]	ln k_2
1×10^{-6}	6.16×10^{-12}	-25.8	3.24×10^{-13}	-28.8
1×10^{-5}	6.16×10^{-11}	-23.5	3.24×10^{-12}	-26.5
5×10^{-5}	3.08×10^{-10}	-21.9	1.62×10^{-11}	-24.9
1×10^{-4}	6.16×10^{-10}	-21.1	3.24×10^{-11}	-24.2

[a] Units Torr
[b] Units $cm^3\ s^{-1}$

Figure 7-7 shows that the effect of the strong collision assumption is to move the fall off curve to lower pressures. The graph also reveals that the high pressure bimolecular rate coefficient exceeds the collision rate calculated by ADO [Su and Chesnavich (1982)]. This is a direct result of the coupled modes assumption.

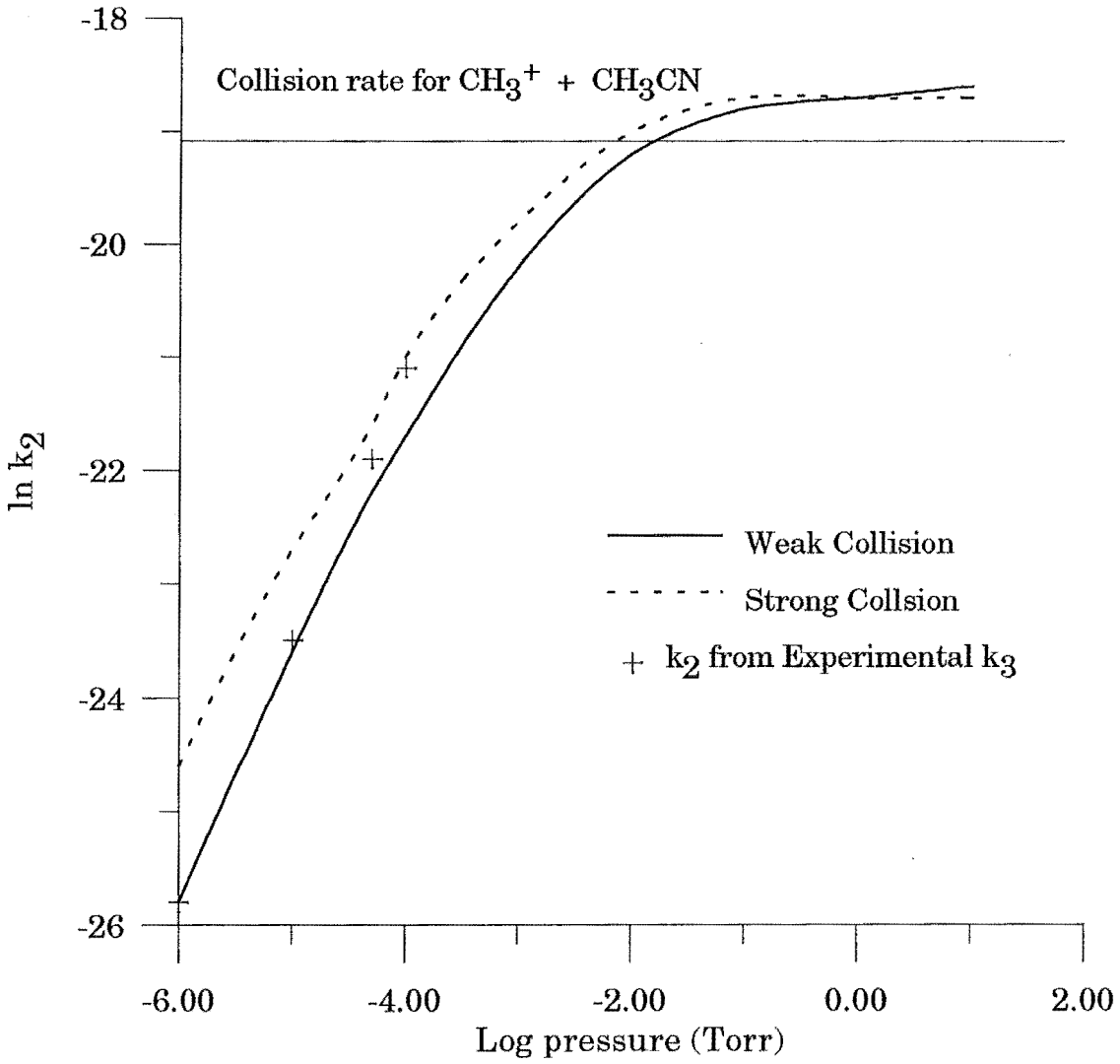

Figure 7-7. Comparison of weak collision, strong collision and experimental fall off curves in CH_3CN at 450K.

The same procedure was used to calculate a complete fall off for helium bath gas. In the case of helium the values for $\langle\Delta E_{down}\rangle$ and $\langle\Delta R_{down}\rangle$ at 450 K were both taken to be 300 cm^{-1} as derived above. The fall off is shown in Figure 7-8 .

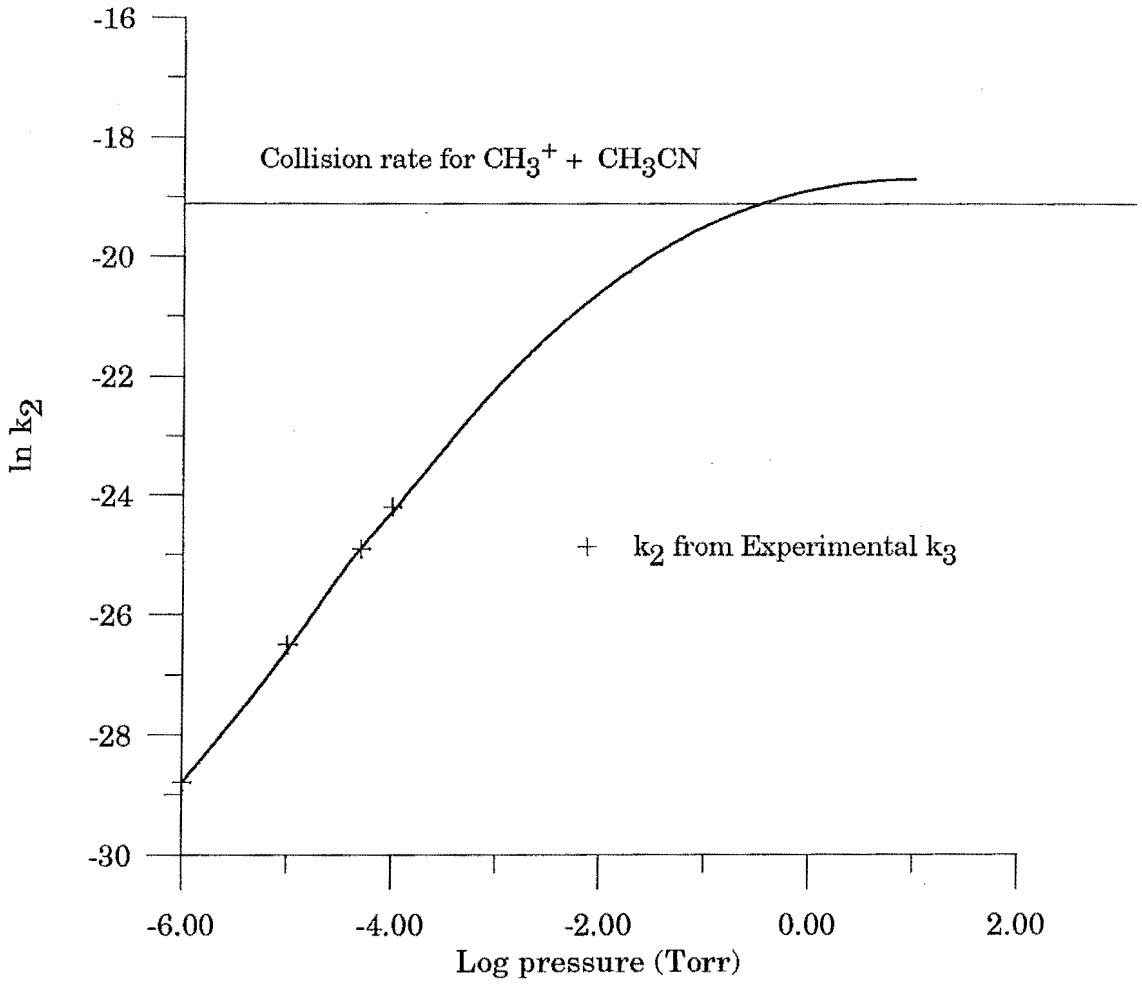

Figure 7-8. Calculated association fall off in helium bath gas at 450 K.

7.3.6. Discussion

The result of the modelling of the $CH_3^+ + CH_3CN$ system described above was a generally good agreement between experimental observation and the predictions of the model. The predictions of the model are to a certain extent empirical in that the temperature and the energy of the tight transition state were varied to fit the branching ratio of the exothermic channels. Bearing this in mind the model still yields important information on the expected lifetime of the complex and the collisional deactivation of the complex in different gases.

The model used in the above work is, however, physically unrealistic in that all the vibrational modes are considered to be active. This assumption is reasonable in the tight transition state where the complex is strongly bound, and there will be significant coupling. The assumption is clearly not correct for the loose transition state, as can be seen by the overestimation of the capture rate.

The loose transition state is best represented as an ion dipole complex at the centrifugal barrier. In this configuration the ion can be thought of as "orbiting" the dipole. Both moieties will retain separate, local vibrational modes. The system will thus

still retain many modes uncoupled to the reaction coordinate. The effect is to overestimate the density of active modes in the transition state between the reactants and the complex, giving an artificially large rate for association. The excessive rate for the channel leading to and from reactants reduces the branching ratio to exothermic products. In order to fit this ratio to the observed value, it was necessary to lower the value of the chemical barrier to the exothermic channel. Altering the barrier to any of the channels has a large effect on the important parameters of the system. Clearly it is desirable to use a model that obviates the need to use an unrealistic energy value.

A modified method for counting the density of states in a loose transition state has been developed by Smith [Smith S.C et al (1993)]. The same parameters as above were used, together with the same method of fitting E° and T to the low density limited branching ratio. Using the modified program Smith found that the appropriate branching ratio could be obtained without using such low values for the chemical barrier to the exothermic channel. The uncoupled modes treatment also gave the correct result at high pressure, where the coupled mode treatment overestimates the capture rate by 170%.

The effect of allowing uncoupled modes can be seen by comparing the unimolecular lifetimes in the low density limit. The lifetime depends strongly on the energetic barrier to exothermic products and the density of states at the transition surface in the channel to reactants. Allowing for uncoupling of modes in effect tightens each exit channel, increasing the complex lifetime. This effect can be seen from Table 7-12.

Table 7-12. Effect of uncoupling the vibrational modes on the unimolecular lifetime.

Temperature[a]	E° [b]	E°(uncoupled)[b]	τ [c]	τ(uncoupled)[c]
400	315	328	56	170
450	311	326	30	107
475	309	324	22	85
500	307	323	17	69

[a] Units of K.
[b] Units of kJ mol^{-1}.
[c] Units of μs.

Another effect of this tightening of the exit channels is to allow more effective collisional stabilisation. Any collisional transfer of energy to the bath gas is more likely to result in stabilisation since the threshold for dissociation is higher. The effect of the coupling of modes upon the estimated $<\Delta E_{down}>$ values is shown in Table 7-13.

Table 7-13. $<\Delta E_{down}>$[a] Values for collisional stabilisation.

Temperature[b]	Coupled Modes		Uncoupled Modes	
	CH_3CN	He	CH_3CN	He
400	150	125	75	No Fit
450	950	300	350	70
475	2210	425	525	100
500	4000	500	1500	250

[a] Units of cm^{-1}
[b] Units of K

The effects of allowing uncoupling of modes is that the effective temperature in the ICR is estimated to be around 475 K, slightly higher than that suggested by the coupled mode result. More significantly, the values required to fit the helium fall off data over the range 400 to 500K are more physically realistic than those required for the coupled mode result.

7.4. Association Reactions in C_2H_2

7.4.1. Introduction

The ion-molecule chemistry of unsaturated hydrocarbons has been a fertile ground for experimentalists. The reactivity of the unsaturated hydrocarbons includes condensation reactions that increase the length of the carbon skeleton of the ions formed. These condensation reactions are of interest for two main reasons. The first is their relevance to the chemistry of combustion processes, for ion-molecule processes may play an important role in the sooting process whereby carbon species, possibly aromatic, may conglomerate to form first large molecules, then small particulate solids. The role of ionic processes in such sooting is not well understood, that is, the relative importance of ionic processes in comparison to radical processes is not well understood [Homann (1984)] [Wersborg et al (1975)].

The second area of interest is in the possible formation in interstellar environments of large unsaturated species, possibly including polyaromatic species [Bohme et al (1991)].

Amongst the species that play significant roles in the ion molecule chemistry of unsaturated hydrocarbons are the species $C_6H_4^+$ and $C_6H_5^+$. These are the predominant C_6 ions and are known to be formed in ion -molecule processes involving both acetylene and benzene. The reactivity and structure of these species have been the subject of

several studies since the early 1970's, and while the systems leading to the production of these ions are quite well understood, the reactivity and structure of these ions and their isomeric forms are not yet well understood.

In an effort to shed some light on the chemistry of these two species a series of experiments were carried out in the SIFT and the ICR. The results, as will be discussed below fell somewhat short of expectations, but the results serve as a guide as to possible avenues for further research which might prove more productive.

7.4.2. Experimental

The first step in the investigation of the system was to use the ICR instrument to measure the rates of the processes involved in the formation of the species $C_6H_5^+$ and $C_6H_4^+$. The reactions have been previously reported in the ICR pressure regime by several authors [Herod and Harrison (1970)] [Maisek and Beauchamp (1974)] [Brill and Eyler (1981)] [Anicich et al (1986)] [Anicich et al (1990)] and in the SIFT and HPMS regimes by other groups [Futrell and Tiernan (1968)] [Knight et al (1987)]. The system therefore provided an excellent opportunity to test the ICR in both drift and trap mode. Although the drift mode was known to produce accurate results, the instrumentation for the trap mode had not been tested, in fact in the course of the experiment the gated integrator was replaced by the PCL718 interface card using a newly written program.

The Reaction of $C_2H_2^+ + C_2H_2$

The only products observed for this reaction were at masses 50^+ and 51^+ as previously reported. The ions at these masses were assumed to be $C_4H_2^+$ and $C_4H_3^+$.

$$C_2H_2^+ + C_2H_2 \rightarrow C_4H_3^+ + H \qquad 0.66 \qquad (7.55a)$$

$$\rightarrow C_4H_2^+ + H_2 \qquad 0.33 \qquad (7.55b)$$

The branching ratio was found to be independent of pressure. The branching ratio of 66:33 compares with the literature value of 68:32 [Anicich (1993)]. The combined rate for these reactions was measured using the drift mode. The pressure range over which measurements were made was from 3.6×10^{-6} Torr to 9.7×10^{-5} Torr. The drift time through the source region was found to be around 0.3 ms and that through the analyser region to be around 1.6 ms. The peak heights for the primary ion and both secondary ions were measured and the program ICRC2 was used to obtain the rate constant by iteration. The collision rates for the ionic species with the C_2H_2 bath gas were calculated by parametrised ADO theory [Su and Chesnavich (1982)] which returns the Langevin collision rate for this system due to the lack of a dipole moment of the neutral species.

$$k_{coll}\ C_2H_2^+\ \ 1.19 \times 10^{-9}\ cm^3\ s^{-1}$$

$$k_{coll}\ C_4H_3^+, C_4H_2^+\ \ 1.03 \times 10^{-9}\ cm^3\ s^{-1}$$

The bimolecular rate coefficient, $k_{2,}$, of reaction (7.55) as a function of pressure. is plotted in Figure 7-9, below.

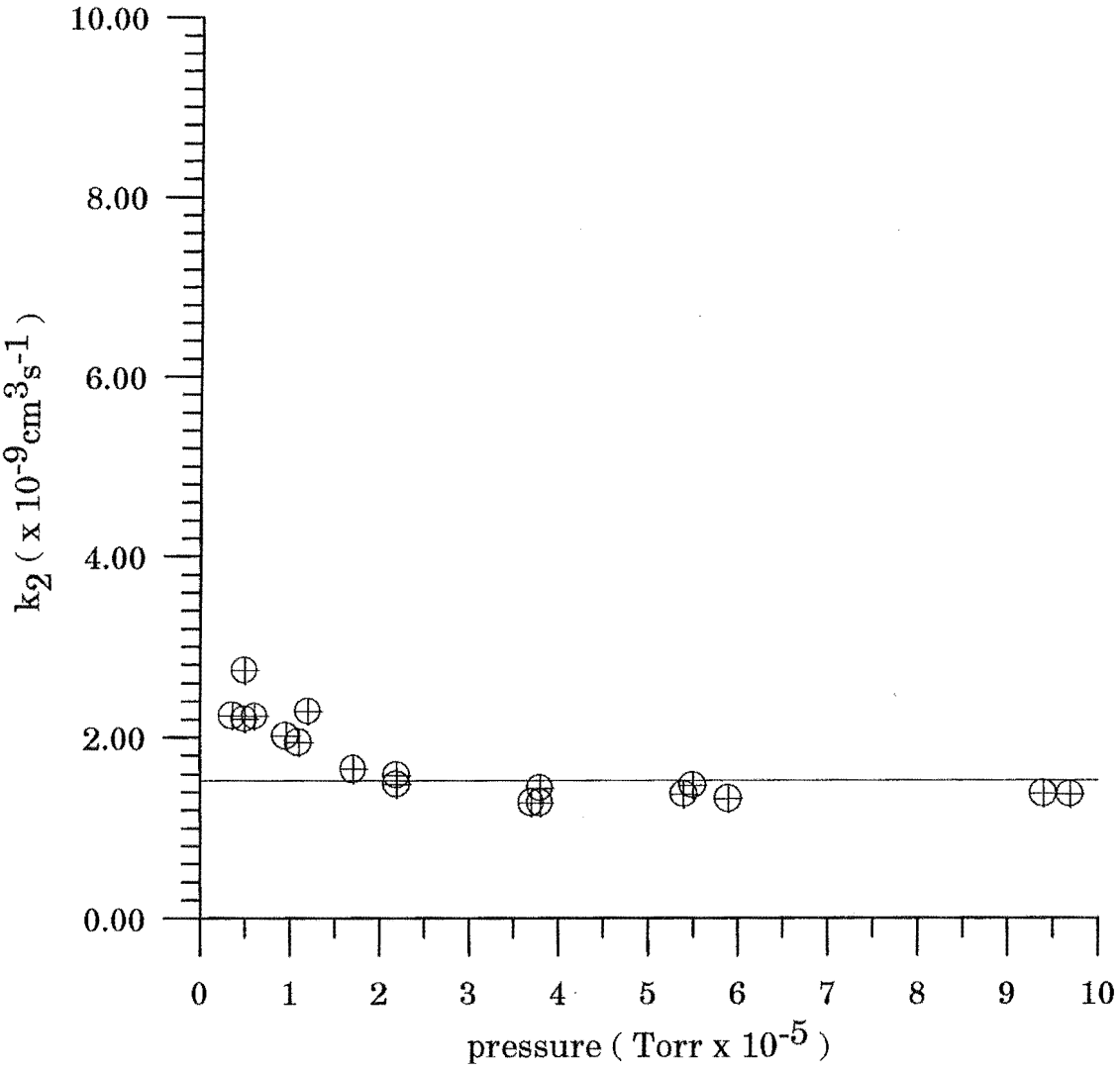

Figure 7-9. k_2, for $C_2H_2^+ + C_2H_2$ measured by ICR in drift mode.

As can be seen the bimolecular rate increased at low pressures. This effect was reproduced in all three experiments and is likely to be the result of the water background signal that was present in the cell. At low pressures this adds a significant perturbation to the measured pressure. Although the rate measurements at low pressure (less than 2×10^{-5} Torr) seem not to be realistic, it is clear that at higher pressures, where the influence of any background partial pressure is insignificant, the bimolecular rate for the combined channels has the value 1.37×10^{-9} cm^3 s^{-1}.

Trap Mode Measurement

In order to examine the bimolecular process at lower pressures than were possible in the drift mode experiment the instrument was used in the trap mode over the pressure range 6.0×10^{-7} to 1.2×10^{-6} Torr.

The trap mode measurement was made by observing the decay of $C_2H_2^+$ in the cell over a 100 ms time base. The signal was processed by the SCOPE program running the PCL718 card as a multichannel analyser and summing the channels under the detect pulse.

The rate as determined by the trap mode measurement was somewhat less than that determined by the drift method at higher pressures. The bimolecular rate k_2 was 1.02×10^{-9} cm^3 s^{-1}. The discrepancy was most likely due to error in calibration of the ionisation gauge, as the absolute measurement of pressure is the most sensitive part of the experiment.

The drift mode rate coefficient of 1.37×10^{-9} cm^3 s^{-1} and the trap mode value of 1.02×10^{-9} cm^3 s^{-1} can be compared with the literature [Anicich (1993)] value of 1.4×10^{-9} cm^3 s^{-1}.

The Reaction of $C_4H_3^+$ with C_2H_2

The reaction of $C_4H_3^+$ with C_2H_2 was studied in the drift mode. The only observed product of the reaction was the adduct ion $C_6H_5^+$,

$$C_4H_3^+ + C_2H_2 \rightarrow C_6H_5^+ . \qquad (7.56)$$

The bimolecular association rate was measured using the parent gas for collisional stabilisation. The pressure range covered was 6×10^{-5} Torr to 4×10^{-4} Torr. At the pressures used it was impossible to simultaneously observe the primary ion $C_2H_2^+$, the secondary ion $C_4H_3^+$, and the tertiary ion $C_6H_5^+$. For this reason the peak heights were analysed using the program ICRSP using 0.933×10^{-9} cm^3 s^{-1} as the rate of formation of the secondary ion.

Several experiments were carried out over the course of three days, and the results were combined, see Figure 7-10. The following experimental parameters were used: the source drift time was 0.2 ms and the analyser drift time 1.9 ms. The collision rates used were calculated by the parametrised ADO method.

k_{coll} $C_4H_3^+$ 1.03×10^{-9} cm^3 s^{-1}

k_{coll} $C_6H_5^+$ 9.75×10^{-10} cm^3 s^{-1}

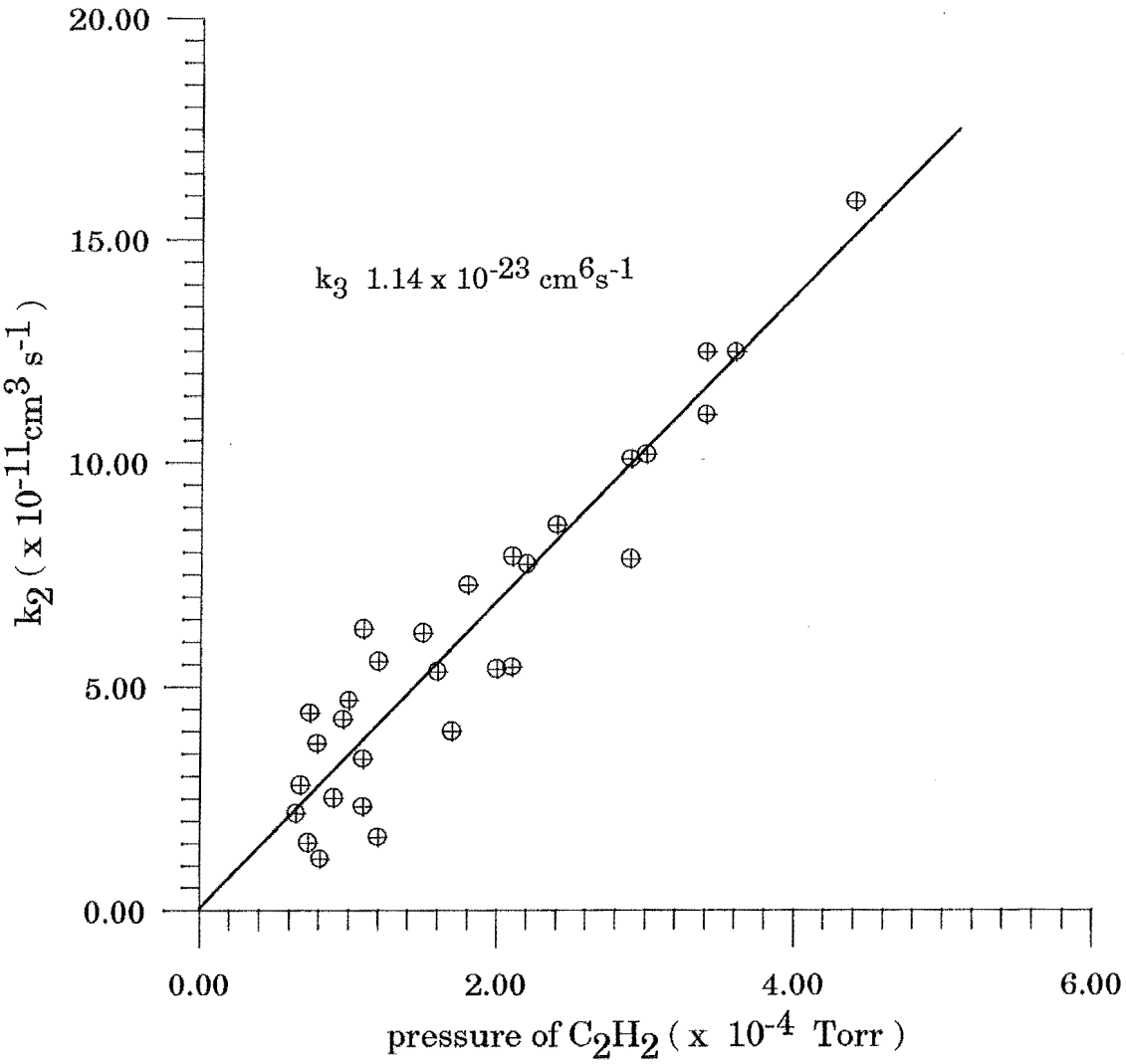

Figure 7-10. Termolecular association of $C_4H_3^+$ in C_2H_2 measured in the ICR in drift mode.

The ternary association rate k_3 in the parent gas was 1.14×10^{-23} cm^6 s^{-1}. The apparent bimolecular rate was not measured at a sufficiently low pressure to confirm or deny the presence of a radiative association process.

Reaction of $C_4H_2^+$ with C_2H_2

The only product of the reaction of $C_4H_2^+$ with the parent neutral was found to be the adduct $C_6H_4^+$,

$$C_4H_2^+ + C_2H_2 \rightarrow C_6H_4^+. \qquad (7.57)$$

The bimolecular association rate was measured in the drift mode for a range of pressures from 6.5×10^{-5} to 18×10^{-5} Torr. The rates were calculated from the observed peak heights of the secondary and tertiary ions using the program ICRSP. The rate of reaction from the primary ion (which could not be observed at the same pressures as the tertiary ion) to the secondary ion was taken to be 4.6×10^{-10} cm^3 s^{-1}. The other experimental parameters were the same as those described above for the reaction of

$C_4H_3^+$. The collision rates of the secondary and tertiary ions were the same as used above. The results of the drift mode experiments are shown in Figure 7-11.

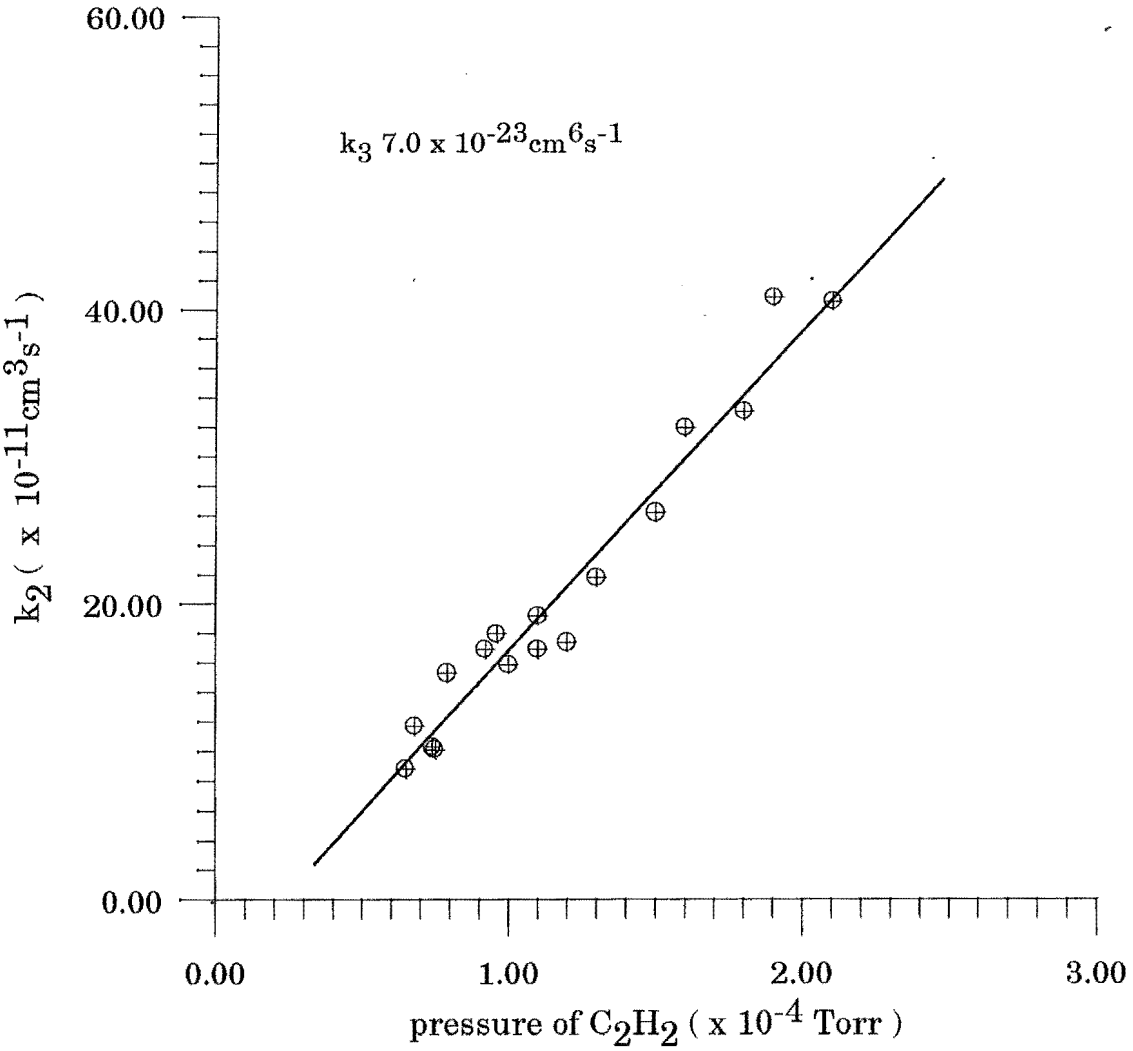

Figure 7-11. Termolecular association of $C_4H_2^+$ in C_2H_2 measured in the ICR in drift mode.

The termolecular association rate was found by plotting the observed bimolecular rate as a function of pressure. The rate k_3 for ternary association in the parent gas was 7.0×10^{-23} cm^6 s^{-1}. The bimolecular rate was not measured at sufficiently low pressure to be able to determine whether or not a radiative process was occurring in concert with the collisional stabilisation. Table 7-14 summarises the reactions observed in acetylene.

Table 7-14. Some reactions of ions in acetylene.

Reactant Ion	Products	Branching Ratio	Rate Coefficient
$C_2H_2^+$	$C_4H_8^+ + H_2$ $C_4H_3^+ + H$	0.33 0.67	$1.2 \pm 0.2 \times 10^{-9}$ cm^3 s^{-1}
$C_4H_2^+$	$C_6H_4^+$	1.0	7.0×10^{-23} cm^6 s^{-1}
$C_4H_3^+$	$C_6H_5^+$	1.0	1.14×10^{-23} cm^6 s^{-1}

7.4.3. Discussion

The results of the measurements of the reaction rate coefficients, made both in the trap mode and in the drift mode, agree well with the reported values measured by Anicich et al [Anicich et al (1986)] [Anicich et al (1990)], and appear to confirm these results. The earlier work by Brill and Eyler [Brill and Eyler (1981)] reported that the association reactions of both $C_4H_2^+$ and $C_4H_3^+$ were saturated at the pressure 1×10^{-5} Torr. Our results confirm the statement made by Anicich et al that the reason for the reported bimolecular behaviour at pressures of 1×10^{-5} Torr and below was that a radiative association process was occurring. The drift mode measurements in this work reveal only the termolecular association process, which shows no sign of saturation at pressures of up to 4×10^{-4} Torr.

While the rate coefficient measurements reveal no new insights into the system, they confirm that the ICR instrument and associated accessories was capable of accurate rate measurement in both drift and trap mode.

7.5. Isomerism of $C_6H_5^+$ and $C_6H_4^+$ Ions

7.5.1. Introduction

The driving idea behind the study of the isomeric forms of $C_6H_5^+$ and $C_6H_4^+$ was the desire to elucidate the chemistry of these species; especially with respect to their role in the interstellar or planetary environment, and also to model the association reactions of the acetylene system using RRKM theory in much the same way as for the $C_3H_6N^+$ system described above. In fact, preliminary calculations were performed in an effort to reproduce the experimentally observed association rate constants of $C_4H_2^+$ with C_2H_2. Unfortunately there was not enough information on the products, since it was not known whether the $C_6H_4^+$ ion was formed as a cyclic or as an acyclic structure or as a mixture of the two. The major stumbling block was the lack of a reasonable idea of the transition states. While calculations were performed on this system by Sudkeaw [Sudkeaw (1991)] they were not able to elucidate the transition state region and so the modelling was shelved. The isomeric distribution of the product ions $C_6H_5^+$ and $C_6H_4^+$ remained an issue, and so experiments on both the SIFT and ICR were carried out in the hope of clearing up some of the inconsistencies and contradictions between previous reports of these systems.

7.5.2. Experimental

The following experiments were carried out using the SIFT. The reagents were for the most part commercially available liquids purified by freeze-pump-thaw cycle, except for the gases acetylene and ethylene, which were obtained from cylinders, and the compound C_4H_2 which had been prepared previously using the preparation of Armitage et al. [Armitage et al (1951)].

The ions were produced by a series of different methods as described in detail below. Once a stable ion signal had been established, the reactant neutral was added and the decay of the ion population measured as a function of neutral flow. As described above the presence of more than one species at the same mass was revealed by a distinct curvature in the semilog plot of the ion decay. The calculation of the initial population and rate of reaction of each isomer was made using the iterative simplex method described in chapter 1. The results therefore for each experimental run consist of a ratio of isomeric populations and the rate of reaction of each isomer with the added neutral.

7.5.3. *Isomers of $C_6H_5^+$*

Several methods were used to prepare the $C_6H_5^+$ ion. The initial aim was to compare the reactivity of $C_6H_5^+$ produced by sequential ion molecule reactions to that produced from electron impact on benzene.

Electron Impact Ionisation of Benzene

In an attempt to produce either or both of the ions $C_6H_5^+$ and $C_6H_4^+$, benzene was used in the ion source and subjected to electron impact. Although the conditions were varied the desired 77^+ and 76^+ signals were always insignificant in comparison to the fragmentation ions at 51^+ and 52^+, that is $C_4H_3^+$ and $C_4H_4^+$. The initial aim of the experiment was to examine the reactivity of the $C_6H_5^+$ and $C_6H_4^+$ ions with C_2H_2. If the fragment ion $C_4H_3^+$ was present in any large amount such a study would be impossible, since the addition of C_2H_2 would produce the reactant ion.

Ionisation of Benzene using Ar^+

An alternative means of ionising C_6H_6 is by ionisation using Ar^+. The ionisation potential of Ar is 15.76 eV. By injecting Ar^+ ions from the ion source and reacting them with benzene added from the first neutral inlet a signal of $C_6H_5^+$ was obtained. Concomitant with this signal were several fragment ions including $C_3H_3^+$, $C_4H_4^+$ and also the parent ion $C_6H_6^+$. The parent ion signal was by far the largest. The ionisation of benzene by Ar^+ was rejected as a convenient means of producing $C_6H_5^+$.

Ionisation of Bromobenzene using Ar^+

The ionisation of bromobenzene using Ar^+injected from the ion source provided a good source of $C_6H_5^+$,

$$Ar^+ + C_6H_5Br \rightarrow C_6H_5^+ + Br + Ar \quad \Delta H^\circ \ -471 \text{ kJ mol}^{-1} . \qquad (7.58)$$

A range of other fragment ions were produced, but none were present in large enough concentrations to interfere significantly with the experiment. However an ion was observed at 154^+, which was believed to correspond to reaction between $C_6H_5^+$ and the neutral C_6H_5Br.

$$C_6H_5^+ + C_6H_5Br \rightarrow C_6H_5.C_6H_5^+ + Br \qquad (7.59)$$

The significance of this reaction is that it could deplete the population of reactive $C_6H_5^+$ relative to the population of the unreactive isomer at large flows of C_6H_5Br.

Ionisation of Bromobenzene using Kr^+

The ionisation potential of Kr is somewhat lower than that of Ar, at 13.99 eV compared to that of Ar of 15.76 eV. Ionisation of a neutral species by Kr^+ is likely to lead to a less energetic state than that produced by Ar^+ ionisation. When neutral bromobenzene was reacted with Kr^+ from the ion source the ions formed included $C_6H_4^+$ and $C_6H_5^+$, but again there was a large signal at 154^+ due presumably to the reaction described above.

Ionisation of Bromobenzene using Ne^+

In order to produce the $C_6H_5^+$ ion from bromobenzene with differing amounts of energy it was thought that Ar^+, Kr^+, and Ne^+ could all be used to ionise the bromobenzene neutral. The different ionisation potentials of the atomic ions would produce $C_6H_5^+$ in different distributions of internal energy and possibly in different isomeric distributions. While ionisation by both Ar^+ and by Kr^+ produced workable signals of $C_6H_5^+$ ionisation by the energetic Ne^+ ion (ionisation potential of Ne 21.56 eV) produced mainly fragmentation into smaller units such as C_4 species and the $C_6H_5^+$ signal was too small for rate measurement.

Electron Impact Ionisation of Bromobenzene

The ionisation of bromobenzene in the ion source was performed in order to compare the results from this source with those from ionisation by Ar^+, Kr^+, and Ne^+. The injection of 77^+ from the ion source was accompanied by fragmentation to give 51^+ and a small amount of 74^+. The 51^+ signal, due to $C_4H_3^+$ was minimised by careful tuning, but was still a sizeable fraction of the total ion signal. The presence of 50^+, $C_4H_2^+$ was also observed. The reaction of $C_6H_5^+$ produced in this way was studied using C_6H_6 as a reagent gas, using C_2H_2 and C_2H_4 as reagents was not suitable owing to the reactions of the $C_4H_3^+$ species with the added neutrals to produce $C_6H_5^+$. The reaction of $C_4H_3^+$ with C_2H_2 is described above, the reaction with C_2H_4 was observed in the SIFT but the overall rate was not measured. The products of the reaction were 77^+, with small signals due to 79^+ and apparently some 78^+.

$$C_4H_3^+ + C_2H_4 \rightarrow C_6H_5^+ + H_2 \quad (7.60a)$$
$$\rightarrow C_6H_6^+ + H \quad (7.60b)$$
$$\rightarrow C_6H_7^+ . \quad (7.60c)$$

The literature value for reaction between $C_4H_3^+$ and C_2H_4 is 2.6×10^{-10} cm^3 s^{-1} measured by Herod and Harrison [Herod and Harrison (1970)].

$C_6H_5^+$ from Electron Impact using a Mixture of C_2H_2 and C_4H_2

Initial attempts to produce the ions $C_6H_5^+$ and $C_6H_4^+$ from electron impact on acetylene in the ion source were unsuccessful. It was found however that, by using a mixture of acetylene and diacetylene (C_4H_2) in a ratio of 1:10, at a high pressure in the ion source, both $C_6H_5^+$ and $C_6H_4^+$ could be obtained by producing $C_4H_3^+$ and $C_4H_2^+$ in the ion source and adding acetylene at the first neutral inlet. By ensuring that sufficient

acetylene was added to remove almost all the $C_4H_n^+$ a reasonably clean reactant ion signal was produced. The drawback of this method was of course that an excess flow of C_2H_2 would to a certain extent deplete the population of the reactive isomer before the ion swarm reached the second neutral inlet where the rate of reactant ion loss was measured as a function of neutral flow.

Results

The results of the measurements are tabulated below in Table 7-15. The results reveal that for all of the methods used to generate $C_6H_5^+$ at least two isomers, of greatly different reactivity were formed. The results suggest that the most reactive isomer reacted at close to the collision rate with all of the neutral reagents that were used. The less reactive isomer seemed to react with a rate coefficient at least two orders of magnitude lower than that for the more reactive isomer. The difference in reactivity can be clearly seen in Figure 7-12.

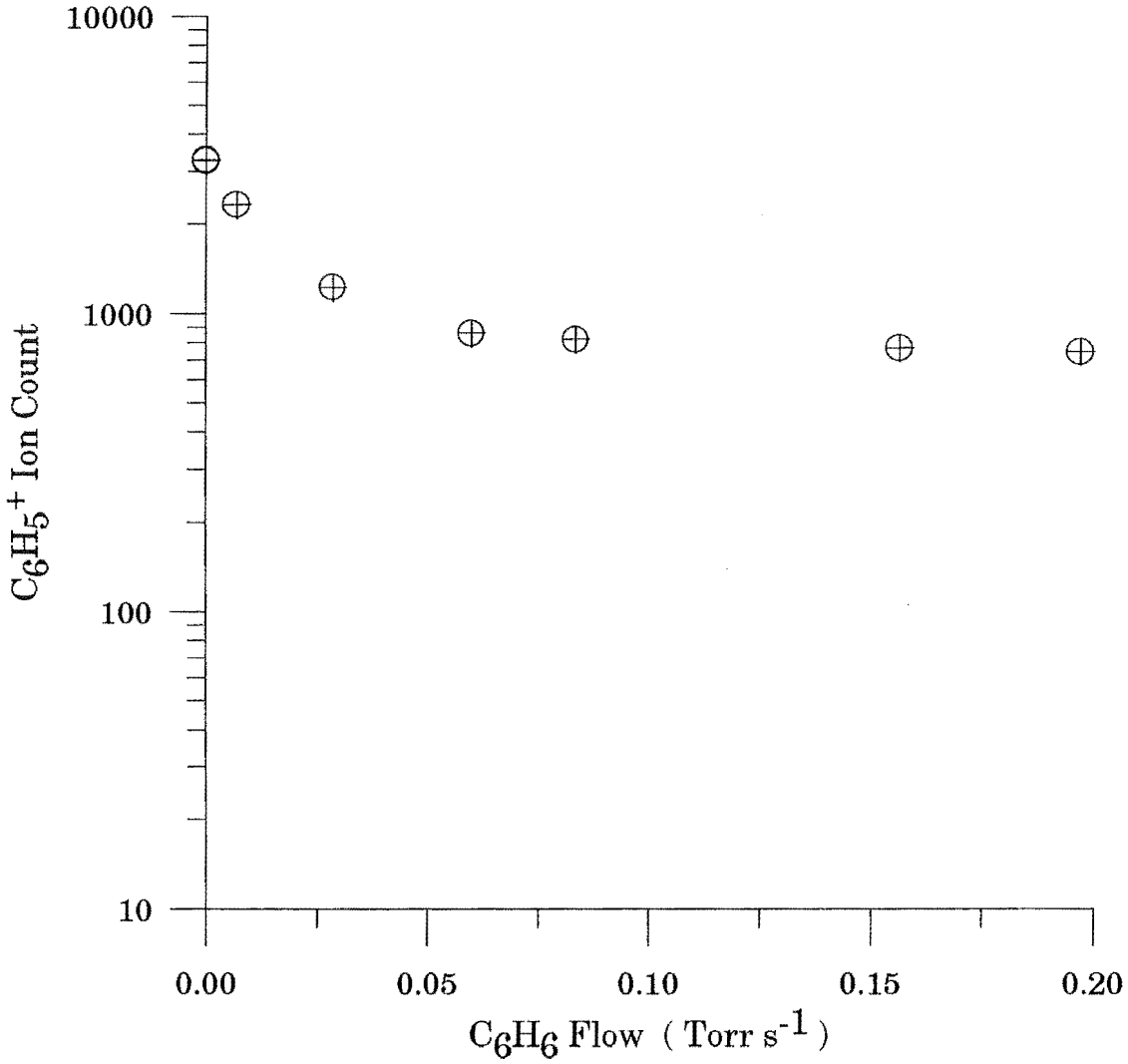

Figure 7-12. Double exponential decay of $C_6H_5^+$ formed by Ar^+ + C_6H_5Br, upon reaction with C_6H_6 showing curvature due to the different reactivities of the two isomers.

The determination of the product of each reaction was not easy, in all cases there were several impurity ions present in the flow tube. The product in the reactions with C_2H_2

and with C_6H_6 seemed to be the cluster ion of $C_6H_5^+$ with the respective neutral. The product of the reaction with C_4H_2 was not determined.

Although the results are consistent in that the presence of both isomers is shown in all cases, the ratio of isomeric populations is variable. The only rule that can be discerned is that the more reactive isomer predominates. The results are tabulated in Table 7-15.

Table 7-15. Isomeric distributions of $C_6H_5^+$ from different precursors.

Ion Source gas	Ionisation method	Neutral	k_2 [a]	k_2' [a]	k_{coll} [a]	Ratio[b]
C_6H_5Br	Ar^+	C_2H_2	1.1	.001	1.0	0.54
	Kr^+	C_2H_2	0.8	.001	1.0	7.4
	Ar^+	C_2H_4	0.7	.001	1.1	1.4
	Kr^+	C_2H_4	0.8	.001	1.1	32
	Ar^+	C_6H_6	1.4	.001	1.2	16.2
	Kr^+	C_6H_6	1.4	.001	1.2	5.8
C_6H_6	e impact	C_6H_6	1.1	.01	1.2	2.7
C_2H_2	e impact	C_6H_6	2.1	.001	1.2	3.5

[a] Rates in units of $cm^3\ s^{-1}$
[b] Ratio of initial populations of Reactive to Unreactive Isomers

Discussion

The existence of more than one isomer of $C_6H_5^+$ has been reported by a number of groups, [Speranza et al (1977)] [Brill and Eyler (1981)] [Eyler and Campana (1983/84)] [Knight et al (1987)][Giles et al (1989)] [Ausloos et al (1989)]. In general the results indicate that one isomer is reactive, forming adducts with a number of species, including H_2, C_4H_2, C_2H_2 and C_6H_6. There is also at least one unreactive isomer, which exhibits a rate coefficient for association at least an order of magnitude smaller than the more reactive isomer.

The possible structures and energies of the isomers have been estimated by a MNDO/3 study by Tasaka et al [Tasaka et al (1981)] with a further study of the phenylium ion performed by Bernadi et al [Bernadi et al (1988)]. The results of Tasaka et al suggest that the lowest energy isomer has a cyclic or phenylium structure, and that the next most stable structures are two acyclic species with calculated heats of formation about 60 kJ mol^{-1} greater than that of the phenylium ion. The authors report that the activation barrier to interconversion of the isomers is 250 kJ mol^{-1} for conversion from the cyclic to the acyclic isomer, ie the ring opening process, and is 190 kJ mol^{-1} for the formation of the cyclic structure from the acyclic species. In order to be able to assign a

structure to each of the observed isomers, attempts have been made to produce a particular isomer by using different precursors and ionisation techniques.

The techniques used by different groups included sequential ion-molecule reactions of acetylene, electron impact on benzene vapour and dehalogenation of halobenzenes.

The sequential ion-molecule reactions of acetylene give rise to the $C_6H_5^+$ ion through the step

$$C_4H_3^+ + C_2H_2 \rightarrow C_6H_5^+, \qquad (7.56)$$

which is significantly exothermic. Using the values tabulated for heats of formation by Lias et al the process is more than 300 kJ mol^{-1} exothermic, producing $C_6H_5^+$ with sufficient internal energy to isomerise. The results of this work agree with those of Brill and Eyler, Eyler and Campana, Giles et al and Ausloos et al, in that the $C_6H_5^+$ ions produced from acetylenic association reactions exist as a mixture of isomers. This conclusion runs contrary to the results of Knight et al. The method used by Knight et al was similar to that used in this work, and it is possible that an excess of C_2H_2 added at the first neutral inlet could have removed the reactive isomer component before the neutral reagent was added.

The electron impact ionisation of benzene was found in this work, and that of Giles et al and Knight et al to result in a mixture of isomers.

The dehalogenation of halobenzenes has been carried out by Eyler and Campana and by Ausloos et al. The former work concluded that the ion formed was the lowest energy isomer, the phenylium ion and that it was unreactive with acetylene, the latter work reached the opposing conclusion, that the phenylium ion was the reactive isomer. The use of Ar^+ and Kr^+ to produce $C_6H_5^+$ from C_6H_5Br is reported by Ausloos et al to yield significantly different distributions of the isomers, the lower energy process, ionisation by Kr^+ yielding a higher proportion of reactive isomer, supporting the authors suggestion that the phenylium ion is the more reactive. The results of the experiments described in this work show no such correlation.

Conclusion

The ion $C_6H_5^+$ can exist as either of two (or possibly more) isomeric structures. One structure is reactive and readily forms an adduct with unsaturated hydrocarbons at close to the collision rate. The other isomer is relatively unreactive.

A mixture of isomers was formed when $C_6H_5^+$ was formed by all the methods employed in this work. In all but one case the reactive isomer predominated. Without more detailed analysis it can be said that the reactive ion is likely therefore to be the lower energy isomer, which is believed to be the cyclic or phenylium form.

7.5.4. *Isomers of $C_6H_4^+$*

The same methods that were used in attempts to produce $C_6H_5^+$ were also tried to produce $C_6H_4^+$. While some $C_6H_4^+$ was observed from the various ionisation techniques used on the aromatic species the signal was too small to use for a rate measurement. This prevented comparison with the results of Knight et al for $C_6H_4^+$ produced from electron impact on C_6H_6. It is interesting to note that Knight et al were able to generate a suitable (although quite small) signal from benzene whereas this was not possible in this work. Although the same SIFT instrument was used in both experiments the ion sources used were completely different. The only method that was found to yield a suitable signal of $C_6H_4^+$ was that of sequential ion-molecule reactions. Using C_4H_2 in the ion source, the ion $C_4H_2^+$ was injected into the flow tube whereupon it was reacted at the first neutral inlet with C_2H_2.

In order to avoid the possible confusion that might result from using a variety of reactant neutrals, only benzene was used as the neutral to be added from the second neutral port. A typical SIFT result, showing clearly the different rates of reaction with benzene is shown in Figure 7-13.

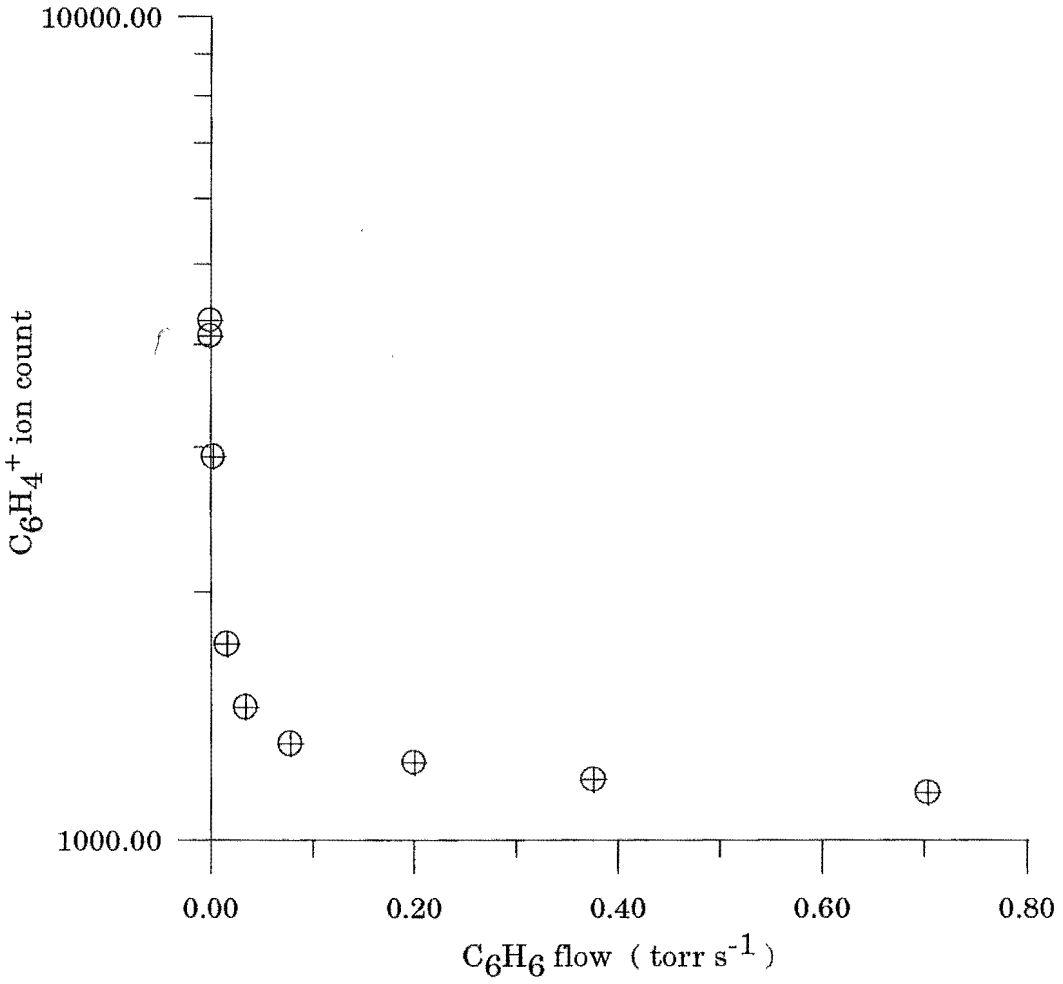

Figure 7-13. Double exponential decay of $C_6H_4^+$ upon addition of C_6H_6.

The results showed a disturbing variation in the calculated ratio of the reactive species to the unreactive species. The method of preparation and the reactant neutral were constant, so any variation in the result cast doubts upon the experimental method. The problem was thought to arise due to depletion of the reactive population by reaction with C_2H_2 neutral, present in excess at the first neutral inlet. In order to overcome the problem the procedure FLOWREADER, was adapted to measure the C_2H_2 flow at the first neutral inlet. This flow was measured before and after each experimental rate measurement, and the isomeric ratio was found as a function C_2H_2 flow. By extrapolating back to zero flow it was intended to measure the true isomeric ratio at the time of formation.

Results

The initial experiments yielded isomer ratios of between 3.0 to 1.1. The ratios measured as a function of C_2H_2 flow are graphed below, in Figure 7-14. The product of the reaction was difficult to determine since several ionic species were present in the flow tube. The products observed were m/z 102, 128 and 154. The first product ion, at m/z 102 was attributed to association of $C_6H_4^+$ with C_2H_2 at the first neutral inlet. The second product, at m/z 128 was thought to be the adduct of $C_4H_2^+$, which was the injected ion, with C_6H_6.The major product of $C_6H_4^+$ with C_6H_6 was thus reasoned to be the adduct at m/z 154.

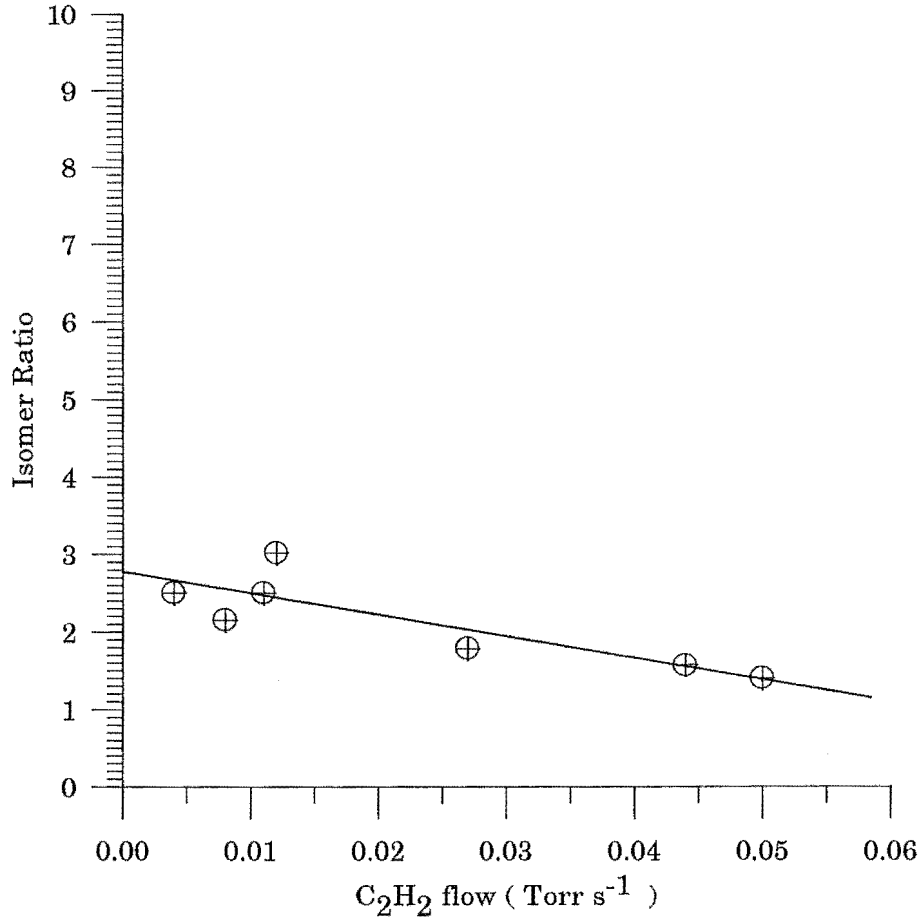

Figure 7-14. Ratio of the reactive to unreactive isomers of $C_6H_4^+$ plotted as a function of the flow of C_2H_2.

Discussion

The existence of more than one isomer of $C_6H_4^+$ has been reported previously [Ausloos (1981)] [Knight et al (1987)] [Van der Hart et al (1989)]. The work by Van der Hart et all which used photo dissociation of cyanobenzene to confirm the existence of an acyclic isomer includes a MNDO study of the energies and geometries of several $C_6H_4^+$ isomers. The authors suggest that the acyclic structures, and 6 possible structures are reported are up to 150 kJ mol^{-1} more stable than the three cyclic or benzyne isomers studied. The greater stability of the acyclic isomers is supported by a study by Sudkeaw [Sudkeaw (1991)] using both AM1 and Hartree Fock methods.

Brill and Eyler [Brill and Eyler (1981)] report the $C_6H_4^+$ ion being formed from sequential ion-molecule reactions of acetylene, and report that it underwent addition with C_2H_2. Although the authors report in the same paper that $C_6H_5^+$ formed from sequential reactions in acetylene exists as a mixture of isomers they do not report observing a mixture of isomeric forms of $C_6H_4^+$.

Knight et al report that the isomer of $C_6H_4^+$ formed from the reaction of $C_4H_2^+$ with C_2H_2 reacts with acetylene at a significantly lower rate than $C_6H_4^+$ formed by electron impact on benzene.

The results in the present work indicate that $C_6H_4^+$ is formed from the sequential ion-molecule reactions of acetylene as a mixture of two isomers. Furthermore, the reaction rate of the more reactive isomer with benzene is close to the collision rate. From the SIFT measurement it seems that the more reactive isomer predominates.

Again the SIFT measurement seems to contradict the result of Knight et al, again a possible reason may be that Knight et al used an excess of C_2H_2 at the first neutral inlet. It is also possible that the reactivity of the isomers to C_2H_2 as used as a reactant by Knight et al may be different to that to C_6H_6 which was used as a reactant in the present study to prevent interference from the $C_4H_2^+$ which was also in the flow tube.

7.6. Conclusion

7.6.1. Association of acrylonitrile

The reaction of acrylonitrile with CH_2CHCN^+ was studied in the SIFT and an overall bimolecular rate coefficient of 1.5×10^{-9} cm^3 s^{-1} was obtained. The dimerisation reaction observed by Petrie et al [Petrie et al (1991),(1992)] confirmed, but a small channel leading to proton transfer was also observed.

The proton transfer channel dominated in the ICR pressure regime and the rate was measured using both trap and drift mode techniques over a pressure range of $1.2 \times$

10^{-6} to 2×10^{-5} Torr. The bimolecular rate coefficient for the proton transfer reaction was 2.5×10^{-9} cm^3 s^{-1}.

The protonated acrylonitrile reacted rapidly with neutral acrylonitrile to form a proton bound dimer. The ternary association rate coefficient for the proton bound dimer was measured in the trap mode and was found to be 1.23×10^{-23} cm^6 s^{-1}. The rate of proton bound dimer formation was also measured in the SIFT and a value of 1.3×10^{-9} cm^3 s^{-1} was obtained.

7.6.1. RRKM modelling of the reaction $CH_3^+ + CH_3CN$

The reaction of the methyl ion with acetonitrile was modelled using a microcanonical transition state RRKM treatment. The structures and energies used were derived entirely from ab-initio calculations.

The model yielded estimates of the collisional energy transfer parameters in both acetonitrile and helium bath gases. For acetonitrile bath gas the $<\Delta E_{down}>$ value was estimated as 950 cm^{-1}, and for helium the $<\Delta E_{down}>$ and $<\Delta R_{down}>$ values were both estimated at 300 cm^{-1}. The unimolecular lifetime of the collision complex $CH_3CNCH_3^+$ at 450K was estimated at 30 μs.

The treatment used made the unrealistic assumption that all vibrational modes were coupled to the reaction coordinate. The results of the model were compared to the uncoupled treatment used by Smith et al [Smith et al (1993)], and were found to overestimate the $< \Delta E_{down} >$ values, and underestimate the lifetime.

7.6.2. Isomers of $C_6H_4^+$ and $C_6H_5^+$

The sequential ion-molecule reactions of acetylene were studied in the ICR and yielded results in agreement with the results of Anicich et al [Anicich et a (1986) (1990)].

The ion $C_6H_5^+$, prepared either from sequential ion-molecule reactions of acetylene, or from electron impact on benzene, or from chemiionisation of bromobenzene was found to exist as a mixture of isomers. One isomer was reactive, associating with unsaturated hydrocarbons at close to the collision rate. The other isomer was somewhat unreactive.

The ion $C_6H_4^+$ was formed by sequential ion-molecule reactions of acetylene. It was found to exist as a mixture of two isomers, one reactive and one unreactive. The reactive isomer made up 75% of the ion population .

CHAPTER EIGHT

A SUMMARY

8.1. Conclusions

The reactions of t-C_4H_9Cl with a number of protonated bases have been studied in both the SIFT and the ICR. The reactions exhibit a channel that gives the products t-$C_4H_9^+$, B, and HCl, where B is the base used. This channel is apparently fast, proceeding at up to half of the collision rate even though it may be significantly endothermic, by up to 40 kJ mol^{-1}. The channel is even observed with a branching ratio of 50% when it is nominally 50 kJ mol^{-1} endothermic. The entropy change associated with the reaction has been estimated to produce a $T\Delta S$ factor of around 33 kJ mol^{-1} at 300K. This cannot be used to definitively rule out the proposed mechanism because of the uncertainties involved in the estimation.

The most plausible explanations for the observations include; a major error in the tabulated thermochemical information, and the possibility that the products are formed as a weakly bound complex that dissociates upon focussing into the ion detection region.

The isomers of $C_3H_6N^+$ were studied in a proton affinity bracketing study using the SIFT. The product of the reaction of methyl cation with acetonitrile was not protonated ethyl cyanide, as had previously been suggested. The most likely structure for the product ion in this case being $CH_3CNCH_3^+$.

The product of the reaction between protonated hydrogen cyanide and ethylene was also found not to posses the ethyl cyanide structure. The product was confirmed as possessing the ethyl isocyanide structure.

Neither of the above reactions were considered likely to lead to an interstellar synthesis of ethyl cyanide upon dissociative recombination of the product ion.

The reactions of the methoxy methyl cation, $CH_3OCH_2^+$,with selected oxygen and nitrogen bases were studied in the SIFT. The ion may play a significant role in the chemistry of oxygen rich interstellar clouds. The reactivity of the ion is characterised by three processes; CH^+ transfer, methyl cation transfer, and association. The exothermic proton transfer channel is not observed because of an activation barrier.

The product distribution depends on the lifetime of the collision complex, and whether the base possesses a labile hydrogen. In the absence of a labile hydrogen., the S_N2 process of methyl cation transfer can proceed, but only if the lifetime of the collision

complex is sufficiently long. Where the base posses a labile hydrogen CH^+ transfer from the cation is the dominant process.

The reaction between CH_2CHCN^+ and neutral acrylonitrile exhibits two major channels, collisionally stabilised association, and proton transfer. At the low pressures of the ICR instrument (0.12 to 2.0 $\times$ 10^{-5} Torr) only the proton transfer channel was observed. The rate coefficient for proton transfer was 2.5 $\times$ 10^{-9} cm^3 s^{-1}. At 0.3 Torr, in the SIFT both proton transfer and association channels were observed. The overall bimolecular rate coefficient for the reaction measured in the SIFT was 1.5 $\times$ 10^{-9} cm^3 s^{-1}.

Protonated acrylonitrile, CH_2CHCNH^+, reacted rapidly with the neutral species to form the proton bound dimer, $CH_2CHCNH.\ CH_2CHCN^+$. This reaction was observed in both the SIFT and the ICR. The ternary association rate coefficient for collisional association in CH_2CHCN bath gas was found to be 1.23 $\times$ 10^{-23} cm^6 s^{-1}. The bimolecular rate of the same reaction at 0.3 Torr, was 1.3 $\times$ 10^{-9} cm^3s^{-1}.

The ion molecule system $CH_3^+ + CH_3CN$ was modelled using an RRKM treatment. *Ab initio* values were used for the energies and structures of the reactants, products, and transition state species. The model was fitted to the branching ratio of the exothermic channels (8.1a), and (8.1b) at the low pressure limit.

$$CH_3^+ + CH_3CN \rightarrow H_2CN^+ + C_2H_4 \quad (8.1a)$$

$$\rightarrow C_2H_5^+ + HCN \quad (8.1b)$$

$$\rightarrow CH_3CN.\ CH_3^{+\cdot} \quad (8.1c)$$

The model showed that the collisional deactivation process in the parent gas, CH_2CHCN could not be treated as a strong collision process. The value of $\langle\Delta E_{down}\rangle$ was estimated at around 950 cm^{-1}. The value of $\langle\Delta E_{down}\rangle$ and $\langle\Delta R_{down}\rangle$ in helium was estimated at 300 cm^{-1}. The model did however overestimate the temperature in the ICR cell, as being significantly above room temperature, around 450 K. The lifetime of the collision complex $CH_3CNCH_3^+$ at this temperature was estimated to be 30 μs.

The species $C_6H_5^+$ and $C_6H_4^+$ from a variety of sources were both observed to possess isomers of different reactivity. Whether prepared by electron impact, or chemical ionisation, of benzene or bromobenzene; or by sequential ion-molecule reactions in acetylene, the ion $C_6H_5^+$ existed as a mixture of two isomeric forms . One isomer reacted at almost the collision rate with the unsaturated hydrocarbons acetylene, ethylene, and benzene.

The ion $C_6H_4^+$ formed from sequential ion-molecule reactions in acetylene was also found to exist as two isomers. The more reactive isomer made up 75% of the ion population.

8.2. Suggestions for further work

The reactions of t-C_4H_9Cl with selected protonated bases raised several questions, not all of which have been conclusively answered in this work. The foremost question is whether the products of the reaction are the ions that are observed in the SIFT detection region. It is possible that the products are formed as weakly bound clusters that dissociate on sampling in the detection region.

Although there is no direct evidence that this is the case, it is one possible explanation for the relatively efficient formation of t-$C_4H_9^+$, despite the apparently large endothermicity of the overall reaction. A useful experiment would be to repeat many of the SIFT experiments using an ICR. If the products are formed as complexes this should be easier to observe in the ICR instrument. The drawbacks of using the ICR are, the difficulty of preventing side reactions from the parent gas, and the difficulty in determining the true temperature of the ions. The temperature of the ions is of crucial importance in this system.

The general question of whether or not endothermic processes can be fast could well be fruitful ground for a statistical model such as RRKM theory. The selection of a suitable model system, however, requires careful consideration. Physically realistic structures for transition states should be chosen.

The use of statistical modelling on the reactions of t-butyl chloride would be somewhat more difficult. The species involved are large, and the mechanism obscure. In order to model the system accurately an ab-initio study would have to be performed, which would not be a trivial task.

The reaction of $C_2H_5^+$ with HCN is known not to produce the adduct, $C_3H_6N^+$. The reactions of the methyl cation with acetonitrile, and protonated hydrogen cyanide with ethylene, have been shown to be unlikely to lead to the formation of C_2H_5CN upon dissociative recombination. This leaves the question of, where does the C_2H_5CN that is observed in interstellar clouds come from? Two avenues could be explored. The first is to look for an ion-molecule reaction that produces an ion with the $C_2H_5CNH^+$ structure. The second avenue would be to examine the products of electron-ion recombination of the known isomers of $C_3H_6N^+$. Current theory predicts that only the $C_2H_5CNH^+$ ion should give efficient formation of ethyl cyanide, but this theory is somewhat speculative and requires experimental verification.

The reaction of $CH_3OCH_2^+$ with ethanol gave different products when studied in the ICR than were observed in the SIFT. In the context of the proposed reaction mechanism, this difference in reactivity can be explained as due to the difference in collision complex lifetime at the different pressures. In order to confirm the proposed

mechanism, the reaction could be studied over as wide a pressure range as possible. The CH^+ transfer channel can be expected to increase in importance as the lifetime of the collision complex increases.

The association reactions of the acrylonitrile system, studied in the ICR and the SIFT also exhibit a strong pressure dependence. The reaction of CH_2CHCN^+ with acrylonitrile is dominated by the proton transfer process at low pressure. At SIFT pressures association dominates. Given appropriate ab-initio values, this system would make an excellent candidate for the same RRKM treatment applied to the reaction of CH_3^+ with acetonitrile. The uncoupled mode treatment used by Smith [Smith et al (1993)] will be required because of the significant dipole moment of acrylonitrile (3.87 Debye).

The information obtained from such a study would include lifetimes of the collision complex, and collisional energy transfer parameters. The collisional energy transfer parameters in particular would be very informative. As discussed above, very little is known about the collisional deactivation of such ionic species.

The study of the isomerism of $C_6H_5^+$ and $C_6H_4^+$ ions described in this work leaves considerable scope for further work. A major problem in the study of $C_6H_5^+$ was the inability to produce a signal corresponding to a single isomer. The report of Ausloos et al [Ausloos et al (1989)] suggests that ion assisted dehalogenation of halobenzenes may provide such a signal. An injection of H_3^+ or HCO^+ from the ion source reacting with bromobenzene at the first neutral inlet may provide only the lower energy isomer. The reactivity of this isomer could be compared with that of $C_6H_5^+$ prepared using the means discussed in this work. One aspect that was found to be important in a study of this nature is the influence of neutral flow on the isomeric distribution. For any future studies, where the target ion is produced by an ion-molecule reaction in the flow tube, the flow rate of the neutral should be measured. This allows an estimation of the isomeric distribution at zero flow. This was carried out for $C_6H_4^+$ in this work, but not for $C_6H_5^+$.

The ICR was used to study the decay of both ions at long (1000 ms) delay times. This work was inconclusive. Both $C_6H_5^+$ and $C_6H_4^+$ showed evidence of two isomeric populations, one reacting rapidly, the other relatively unreactive. The $C_6H_5^+$ species was formed from ion-molecule reactions of acetylene and also from electron impact on bromobenzene. The $C_6H_4^+$ species was formed from sequential ion-molecule reactions of acetylene. The results confirm the SIFT experiments, but the decay curves show a large statistical spread of values, due to variation in the filament emission. This variation is normally not significant in a trap mode experiment over 100 or 200 ms, but over a timebase of 1000 ms it becomes significant.

If the problem of variation in filament emission can be solved, or a way around it can be developed, the ICR could be used in conjunction with the SIFT to study this system.

In general, the research possibilities of using both the SIFT and the ICR in conjunction are great. The study of fast three body association rate coefficients, for systems of astrochemical interest, over the complete pressure fall off is particularly promising. If this can be done in conjunction with a suitable modelling study, as shown in the work done on $CH_3^+ + CH_3CN$, the information yielded about collisional processes and about complex lifetimes will be significant. This is immediately relevant to the important area of association in interstellar clouds and in planetary atmospheres.

The use of double resonance ejection in the ICR cell to directly measure the lifetime of collision complex species has been reported by Anicich. This technique, used in conjunction with SIFT and ICR rate measurements, opens up a wealth of possibilities to obtain quantitative information.

A profitable area for further research would be the long delayed installation of a set of drift rings into the SIFT. As described earlier, some of the preliminary work has been completed. The drift assembly and electronics are awaiting installation. The drift tube, when operational, will greatly expand the capabilities of the instrument.

Two areas that have been mentioned above could be further studied using a flow tube. The isomerism of species such as $C_6H_4^+$ and $C_6H_5^+$ could well be studied as a function of ion energy. If a single isomer can be formed at a given energy, then increasing the energy until a mixture of isomers is observed, will give information about the height of the barrier to isomerisation of that isomer. If a mixture of isomers is observed, then as the energy of the ion is increased, the isomeric distribution should reach a limiting value determined by the density of states of each isomer at that energy. This could well be used to derive structural information.

A further method for examining isomerism using a drift flow tube could be mobility measurement. Depending on the experimental set up used, it may be possible to determine differences in ion mobility due to structure. This experiment would require both an effective "shutter" system, and a fast ion counting system, in order to measure an arrival time distribution. For systems such as $C_6H_4^+$ and $C_6H_5^+$, where there are believed to be both cyclic and acyclic isomers, the mobility's could well be an efficient means of assigning structure to an isomer.

The other area where variation of ion energy could be a useful technique is in the study of ion-molecule thermochemistry, for example in the reactions of t-C_4H_9Cl. The use of SIFDT experiments to determine free energy and entropy changes in a reaction has been reported by Javahery et al [Javahery et al (1991)]. If accurate thermochemical quantities could be derived for some of the important species that are involved in the

reactions of t-C_4H_9Cl with protonated bases such as ethanol or acetonitrile, much of the speculation concerning the system could be cleared up.

REFERENCES

Adams N.G. (1992)
"Spectroscopic Determination of the Products of Electron-Ion Recombination"
Adv. Gas. Phase. Ion Chem. **1**,(p.271) Adams N.G., Babcock L.M. (eds)
JAI Press, Greenwich Conneticut.

Adams N.G., and Smith D. (1976a)
Int. J. Mass Spectrom. Ion Processes. ***21***, 349.

Adams N.G., and Smith D. (1976b)
J. Phys. B, ***9***, 1439.

Adams N.G., and Smith D. (1988)
in *"Techniques for the Study of Ion-Molecule Reactions"*, Farrar J.M., and Saunders W.H. (eds), Techniques of Chemistry, ***20***, Wiley Interscience, New York.

Adams N.G., Bohme D.K., Dunkin D.B., and Ferguson E.E. (1970)
J. Chem. Phys ***52***, 3133.

Adams N.G., Church M.J., and Smith D. (1975)
J. Phys. D, ***8***, 1409.

Allemann M., Kellerhals H., and Wanczek K.P. (1983)
Int. J. Mass Spectrom. Ion Physics. ***46***, 139.

Anicich V.G. (1993)
"Evaluated Bimolecular Ion-Molecule Gas Phase Kinetics of Positive Ions for Use in Modelling the Chemistry of Planetary Atmospheres, Cometary Comae, and Interstellar Clouds."
J. Phys. Chem. Ref. Data ***22***, 1469.

Anicich V.G., and Bowers M.T. (1974)
J. Am. Chem. Soc. ***96***, 1279.

Anicich V.G., Huntress W.T., and McEwan M.J. (1986)
J. Phys.Chem. ***90***, 2446.

Anicich V.G., Sen A.D., Huntress W.T., and McEwan M.J. (1990)
J.Chem. Phys. ***93***, 7163.

Anicich V.G., Sen A.D., Huntress W.T., and McEwan M.J. (1991)
J.Chem. Phys. ***94***, 4189.

Anicich V.G., Sen A.D., McEwan M.J., and Smith S.C. (1994)
J.Chem. Phys. ***100***, 5696.

Armitage J.B., Jones E.R.H., and Whiting M.C. (1951)
J. Chem. Soc. ***154***, 44.

Ausloos P. (1981)
J. Am. Chem. Soc. ***103***, 3931.

Ausloos P., Lias S.G., Buckley T.J., and Rogers E.E. (1989)
Int. J. Mass Spectrom. Ion Processes, ***92***, 65.

Bardsley J.N. (1968)
J. Phys. B, ***1,*** 365.

Bass L.M., Kemper P.R., Anicich V.G., and Bowers M.T. (1981)
J. Am. Chem. Soc. ***103***, 5283.

Bates D.R. (1950)
Phys. Rev. ***78***, 492.

Bates D.R. (1989)
Ap. J. ***344***, 351.

Bates D.R., and Herbst E. (1988)
"Radiative Association"
in *"Rate Coefficients in Astrochemistry"* Millar T.J., and Williams D.A. (Eds)
Kluwer Academic Publishers, Dordrecht.

Beauchamp J.L. (1967)
J.Chem. Phys. ***46***, 1231.

Beauchamp J.L., and Armstrong J.T. (1969)
Rev. Sci. Instrum. ***40***, 123.

Beauchamp J.L., Anders L.R., and Baldschwieler J.D. (1967)
J. Am. Chem. Soc. ***89***, 4569.

Benson S.W. (1976)
"Thermochemical Kinetics, 2nd Ed."
Wiley-Interscience, New York.

Bernadi F., Grandinetti F., Guarino A., and Robb M.A. (1988)
Chem. Phys. Lett. ***153***, 309.

Bierbaum V.M., Ellison G.B., Futrell J.H., and Leone S.R. (1977)
J.Chem. Phys. ***67***, 2375.

Blake G.A., Sutton E.C., Masson C.R., and Phillips T.G. (1987)
Ap. J. ***315***, 521.

Bohme D.K., Hemsworth R.S., Rundle H.W., and Schiff H.I. (1973)
J.Chem. Phys. ***58***, 3504.

Bohme D.K., Wlodek S., Zimmerman J.A, and Eyler J.R. (1991)
Int. J. Mass Spectrom. Ion Processes, ***109***, 31.

Bolden R.C., Hemsworth R.S., Shaw M.J., and Twiddy N.D. (1970)
J. Phys. B, ***3***, 45.

Bouchoux G., Flament J.P.,Hopilliard Y., Tortajada J., Flamang R., and Maquestiau A. (1989)
J. Am. Chem. Soc. ***111***, 5560.

Bouchoux G., Nguyen M.T., and Longevialle P. (1992)
J. Am. Chem. Soc. ***114***, 10000

Bowers M.T., and Su T. (1975)
"Theory of Ion Polar Molecule Collisions"
in *"Interactions between Ions and Molecules"* Ausloos P. (Ed)
NATO ASI Series, ***B6***, Plenum, New York.

Bowers M.T., Elleman D.D., and King J.J. (1969)
J.Chem. Phys. ***50***, 4787.

Bowers M.T., Aue D.H., Webb H.M., and McIver R.T. (1971)
J. Am. Chem. Soc. ***93***, 4314.

Bowers M.T., Su T., and Anicich V.G. (1972)
J.Chem. Phys. ***58***, 5175.

Brill F.W., and Eyler J.R. (1981)
J. Phys .Chem. ***85***, 1091.

Bruce J.E., and Eyler J.R. (1992)
J. Am. Soc. Mass. Spectrom. ***3***, 727.

Capone L.A., Prasad S.S., Huntress W.T., Whitten P.C., Dubach J., and Santhanam K. (1981)
Nature ***293***, 45.

Casanova J., Schuster R.E, and Werner N.D (1963)
J. Chem. Soc. 4280.

Cates R.D. and Bowers M.T. (1980)
J. Am. Chem. Soc. ***102***, 3994.

Celli F., Weddle G., and Ridge D.P. (1980)
J.Chem. Phys. ***73***, 801.

Chesnavich W.J., Su T., and Bowers M.T. (1980)
J.Chem. Phys. ***72***, 2641.

Clow R.P., and Futrell J.H. (1971)
Int. J. Mass Spectrom. Ion Physics, ***22***, 527.

Comisarow M.B. (1971)
J.Chem. Phys. ***55***, 205.

Comisarow M.B. (1978)
in *"Ion Cyclotron Resonance Spectrometry"* Hartmann H., and Wanczek K.P. (eds), Lecture Notes in Chemistry, ***7***, Springer Verlag, Berlin.

Comisarow M.B. (1982)
in *"Ion Cyclotron Resonance Spectrometry 2"* Hartmann H., and Wanczek K.P. (eds), Lecture Notes in Chemistry, ***31***, Springer Verlag, Berlin.

Comisarow M.B., and Marshall A.G. (1974)
Chem. Phys. Lett. ***25***, 282.

Comisarow M.B., and Marshall A.G. (1975)
J.Chem. Phys. ***62***, 293.

Comisarow M.B., and Marshall A.G. (1976)
J.Chem. Phys. ***64***, 110.

Damm M., Deckert F., Hippler H., and Troe J. (1991)
J. Phys .Chem. ***95***, 2005.

Deakyne C.A., and Meot-Ner (Mautner) M. (1990)
J. Phys .Chem. ***94***, 232.

Deakyne C.A., Meot-ner (Mautner) M., Buckley T.J., and Metz R. (1987)
J.Chem. Phys. ***86***, 2334.

DeFrees D.J., and McLean A.D. (1985)
J.Chem. Phys. ***82***, 333.

Del Bene J.E., and Frisch M.J. (1989)
Int. J. Quantum Chem., Quantum Chem. Symp. ***23***, 371.

Dove J.E., and Raynor S. (1979)
J. Phys .Chem. ***85***,127.

Dunbar R.C. (1990)
Int. J. Mass Spectrom. Ion Processes, ***100***, 423.

Dunkin D.B., Fehsenfeld F.C., Schmeltekopf A.L., and Ferguson E.E. (1968)
J.Chem. Phys. ***49***, 1365.

Eyler J.R., and Campana J.E. (1983/84)
Int. J. Mass Spectrom. Ion Processes, ***55***, 171.

Eyring H. (1935)
J.Chem. Phys. ***3***, 107.

Eyring H., Hirschfelder J.O., and Taylor H.S. (1936)
J.Chem. Phys. **4,** 479.

Ferguson E.E., Fehsenfeld F.C., Dunkin D.B., Schmeltekopf A.L., and Schiff H.I. (1964)
Planet. Space Sci. **12**, 1169.

Fisher E., and Armentrout P.B. (1990)
Int. J. Mass Spectrom. Ion Processes, **101**, R1.

Fisher J.J., and McMahon T.B. (1990)
Int. J. Mass Spectrom. Ion Processes, **100**, 701.

Forst W. (1973)
"Theory of Unimolecular Reactions"
Academic Press, New York

Francl T.J., Sherman M.G., Hunter R.L., Locke M.J., Bowers W.D., and McIver R.T. (1983)
Int. J. Mass Spectrom. Ion Processes, **54,** 189.

Franklin J.L., Wada Y., Natalis P.,and Hierl P.M. (1966)
J. Phys .Chem. **70**, 2353.

Freeman C.G., Harland P.W., and McEwan M.J. (1978)
Aust. J. Chem. **31**, 2157.

Futrell J.H., and Tiernan T.O (1968)
J. Phys .Chem. **72**, 158.

Galloway E.T., and Herbst E. (1991)
Ap. J. **376**, 351.

Gardner F.F., and Winnewisser G. (1975)
Ap. J. Lett. **195,** L127.

Gilbert R.G., and McEwan M.J. (1985)
Aust. J. Chem. **38**, 231.

Gilbert R.G., and Smith S.C. (1990)
"Theory of Unimolecular and Recombination Reactions"
Blackwell, Oxford.

Giles K., Adams N.G., and Smith D. (1989)
Int. J. Mass Spectrom. Ion Processes, **89**, 303.

Gioumousis G., and Stevenson D.P. (1955)
J.Chem. Phys. **29**, 294.

Glosik J., Rakshit A.B., Twiddy N.D., Adams N.G., and Smith D. (1978)
J. Phys. B, **11,** 3365.

Graul S.T., and Squires R.R. (1988)
"Advances in Flow Reactor Techniques for the Study of Gas Phase Ion Chemistry"
Mass. Spec. Rev. ***7***, 263.

Gross M.L., and Wilkins C.L. (1982)
in *"Ion Cyclotron Resonance Spectrometry 2"* Hartmann H., and Wanczek K.P. (eds),
Lecture Notes in Chemistry, ***31***, Springer Verlag, Berlin.

Gupta S.K., Jones E.G., Harrison A.G., and Myher J.J. (1967)
Can. J. Chem. ***45***, 3107.

Haney M.A., and Franklin J.L. (1969)
J. Phys .Chem. ***73***, 4328.

Harrison A.G., and Shannen T.W. (1965)
J.Chem. Phys. ***43***, 4206.

Henchman M. (1987)
"Entropy-Driven Reactions Summary of the Panel Discussion"
in *"Structure/Reactivity and Thermochemistry of Ions"* (p.381)
Ausloos P., and Lias S.G. (eds), NATO ASI Series , ***C 193***, D. Reidel, Dordrecht.

Henchman M., Smith D., and Adams N.G. (1987)
"On the Need to Determine Effective Temperatures in Measuring the Rates of Ion Molecule Reactions"
in *"Structure/Reactivity and Thermochemistry of Ions"* (p.376)
Ausloos P., and Lias S.G. (eds), NATO ASI Series, ***C193***, D. Reidel, Dordrecht.

Herbst E. (1978)
Ap. J. ***222***, 508.

Herbst E. (1985)
Ap. J. ***291***, 226.

Herbst E. (1987)
Ap. J. ***313***, 867.

Herbst E., and Leung C.M. (1990)
Astron. Astrophys. ***233***, 117.

Herbst E., Smith D., Adams N.G., and Macintosh B.J. (1989)
J. Chem. Soc., Faraday Trans. 2, ***85***, 1613.

Herod A.A., and Harrison A.G. (1970)
Int. J. Mass Spectrom. Ion Physics, ***4***, 415.

Hipple J.A., Sommer H., and Thomas H.A. (1949)
Phys. Rev. ***76***, 1877.

Hippler H., Troe J., and Wendelken H.J. (1983)
J.Chem. Phys. ***78***, 6709.

Hippler H., Strang H.W., and Troe J. (1986)
J. Phys .Chem. ***90***, 6167.

Homann K,H., (1984)
20th Symposium (Int.) on Combustion, (p.857)
The Combustion Institute, Pittsburgh, Penn.

Howorka F., Fehsenfeld F.C., and Albritton D.L. (1979)
J. Phys. B, ***12***, 4189.

Howorka F., Dotan I., Fehsenfeld F.C., and Albritton D.L. (1980)
J.Chem. Phys. ***73***, 758.

Hunter R.L., Sherman M.G., and McIver R.T. (1983)
Int. J. Mass Spectrom. Ion Physics, ***50***, 259.

Huntress W.T., and Pinizzotto R.F. (1973)
J.Chem. Phys. ***59***, 4742.

Huntress W.T., McEwan M.J., Karpas Z, and Anicich V.G. (1980)
Ap. J. Supp. Series ***44***, 481.

Ikezoe Y., Matsuoka S., Takebe M., and Viggiano A. (1987)
"Gas Phase Ion-Molecule Reaction Rate Constants Through 1986"
Ion Reaction Research Group of The Mass Spectroscopy Society of Japan, Tokyo.

Javahery G., Tichy M., and Twiddy N.D. (1991)
"The Application of a Selected Ion Flow Tube to Determine Proton-Affinity Differences"
in "*Fundamentals of Gas Phase Ion Chemistry*" Jennings K.R (ed)
NATO ASI Series, ***C347***, Kluwer Academic Publishers, Dordrecht.

Johnson D.R., Lovas F.J., Gottlieb C.A., Gottlieb E.W., Litvok M.M., Giuelin M., and Thaddeus P. (1977)
Ap. J. ***218***, 370.

Karpas Z., and Meot-Ner (Mautner) M. (1989)
J. Phys .Chem. ***93***, 1859.

Kebarle P. (1988)
in *"Techniques for the Study of Ion-Molecule Reactions"*
Farrar J.M., and Saunders W.H. (eds)
Techniques of Chemistry, ***20***, Wiley-Interscience,New York.

Keister J.W., Riley J.S., and Baer T. (1993)
J. Am. Chem. Soc. ***115***, 12613.

Kemper P.R., and Bowers M.T. (1982)
Rev. Sci. Instrum. ***53***, 989.

Kemper P.R., and Bowers M.T. (1988)
in "*Techniques for the Study of Ion Molecule Reactions*"
Farrar J.M., and Saunders W.H. (eds)
Techniques of Chemistry, ***20***, Wiley-Interscience, New York

Kemper P.R., Bass L.M., and Bowers M.T. (1985)
J. Phys .Chem. ***89,*** 1105.

Kim J.K., Anicich V.G., and Huntress W.T.
Unpublished Results, Reported by Anicich (1993).

Kinter M.T., and Bursey M.M. (1986)
J. Am. Chem. Soc. ***108***, 1797.

Kleingeld J.C., and Nibbering N.M.M. (1982)
Org. Mass Spectrom. ***17***, 136.

Knight J.S. (1986)
"Selected Ion Flow Tube Studies of some Gaseous Ion-Molecule Reactions"
PhD Thesis, University of Canterbury, New Zealand.

Knight J.S., Freeman C.G., and McEwan M.J. (1986)
J. Am. Chem. Soc. ***108***, 1404.

Knight J.S., Freeman C.G., McEwan M.J., Anicich V.G., and Huntress W.T. (1987) *J. Phys .Chem.* ***91***, 3898.

Kofel P., and McMahon T.B. (1988)
J. Phys .Chem. ***92***, 6174.

Lee J.P., and Comisarow M.B. (1985)
Appl. Specrosc. ***41***, 93.

Lias S.G. (1987)
in "*Structure/Reactivity and Thermochemistry of Ions*", Ausloos P., and Lias S.G. (eds)
NATO ASI Series, ***C 193***, D. Reidel, Dordrecht.

Lias S.G., Bartmess J.E., Liebman J.F., Holmes J.L., Levin R.D., and Mallard W.G. (1988)
J. Phys. Chem. Ref. Data. ***17***, (Supplement 1).

McEwan M.J. (1980)
IAU Symp, **87**, 299.

McEwan M.J. (1992)
"Flow Tube Studies of Small Isomeric Ions"
Adv. Gas. Phase. Ion Chem. ***1***, (p.1) Adams N.G.,and Babcock L.M. (eds)
JAI Press, Greenwich Connecticut.

McEwan M.J. (1993)
Private communication from author.

McEwan M.J., Anicich V.G., Huntress W.T., Kemper P.R., and Bowers M.T. (1980)
Chem. Phys. Lett. ***75***, 278.

McEwan M.J., Denison A.B., Anicich V.G. and Huntress W.T (1987)
Int. J. Mass Spectrom. Ion Processes, ***81,*** 247.

McEwan M.J., Denison A.B., Huntress W.T., Anicich V.G., Snodgrass J., and Bowers M.T. (1989)
J. Phys .Chem. ***93***, 4064.

McIver R.T. (1970)
Rev. Sci. Instrum. ***41***, 555.

McIver R.T., and Dunbar R.C. (1971)
Int. J. Mass Spectrom. Ion Physics, ***7***, 471.

McIver R.T., Hunter R.L., Ledford E.B., Locke M.J., and Francl T.J. (1981)
Int. J. Mass Spectrom. Ion Physics, ***39***, 65.

Mackay G.I., Betowski D., Payzant J.D., Schiff H.I., and Bohme D.K. (1976)
J. Phys .Chem. ***80***, 2919.

Mackay G.I., Hopkinson A.C., and Bohme D.K. (1978)
J. Am. Chem. Soc. ***100***, 7460.

Mackay G.I., Vlachos G., Bohme D., and Schiff H.I., (1980)
Int. J. Mass Spectrom. Ion Physics, ***36***, 259.

McMahon T.B., and Beauchamp J.L. (1971)
Rev. Sci. Instrum. ***42***, 1632.

McMahon T.B., and Beauchamp J.L .(1972)
Rev. Sci. Instrum. ***43***, 509.

MacNeil K.A.G., and Futrell J.H. (1972)
J. Phys .Chem. ***76***, 409.

Maisek P.G., and Beauchamp J.L. (1974)
Int. J. Mass Spectrom. Ion Physics, ***15***, 49.

Marshall A.G. (1985)
Acc. Chem. Res. ***18***, 316.

Marx R., Mauclaire G., and Derai R. (1983)
Int. J. Mass Spectrom. Ion Physics, ***47***, 155.

Matsumotu A., Okada S., Taniguchi S., and Hayakawa T. (1975)
Bull. Chem. Soc. Japan. ***48***, 3387.

Matthews H.E., and Sears T.J. (1983)
Ap. J. ***272***, 149.

Meot-Ner (Mautner)M. (1987)
"Entropy Driven Ion-Molecule Reactions"
in *"Structure/Reactivity and Thermochemistry of Ions"*, Ausloos P., and Lias S.G. (eds)
NATO ASI Series, ***C 193***, D. Reidel, Dordrecht.

Meot-Ner (Mautner) M. (1991)
J. Phys .Chem. ***95***, 6581.

Meot-Ner (Mautner) M., and Karpas Z. (1986)
J. Phys .Chem. ***90***, 2206.

Meot-Ner (Mautner) M., and Sieck L.W. (1991a)
J. Am. Chem. Soc. ***113***, 4449.

Meot-Ner (Mautner) M., and Sieck. L.W (1991b)
Int. J. Mass Spectrom. Ion Processes. ***109***, 187.

Meot-Ner (Mautner) M., and Smith S.C. (1991)
J. Am. Chem. Soc. ***113***, 862.

Meot-Ner (Mautner) M., McEwan M.J., and Wilson P.F. (1993)
To be Submitted.

Miasek P.G., and Harrison A.G. (1975)
J. Am. Chem. Soc. ***97***, 714.

Millar T.J., Herbst E., and Charnley S.B. (1991)
Ap. J. ***369***, 147.

Mitchell J.B.A. (1990)
Phys.Rep. ***186***, 215.

Moran T.F., and Hamill W.H. (1963)
J.Chem. Phys. ***39***, 1413.

Moreu C, and Bongrand J.C (1920)
Ann. Chemie. ***14***, 47.

Morton T.H. (1988)
in "*Techniques for the Study of Ion Molecule Reactions*"
Farrar J.M., and Saunders W.H. (eds)
Techniques of Chemistry, ***20***, Wiley-Interscience, New York.

Nielson P.V., Bowers M.T., Chau M., Davidson W.R., and Aue D.H. (1978)
J. Am. Chem. Soc. ***100***, 3649.

Okada S., Abe Y., Taniguchi S., and Yamabe S. (1987)
*J. Am. Chem. Soc.****109***, 295.

Orlando R., Ridge D.P., and Manson B. (1990)
J. Am. Soc. Mass. Spectrom. ***1***, 144.

Pau J.K., Jhong K.K., and Caserio M. (1987)
J. Am. Chem. Soc. ***100***, 3838.

Petrie S. (1991)
"A Selected Ion Flow Tube Study of Some Gas-Phase Ion-Molecule Reactions of Potential Relevance to the Chemistry of Dense Interstellar Clouds."
PhD Thesis, University of Canterbury, New Zealand.

Petrie S., Freeman C.G., McEwan M.J., and Meot-ner (Mautner) M. (1989)
Int. J. Mass Spectrom. Ion Processes, ***90***, 241.

Petrie S., Freeman C.G., Meot-Ner M., McEwan M.J., and Fergusson E.E. (1990)
J. Am. Chem. Soc. ***112***, 7121.

Petrie S., Chirnside T.J., Freeman C.G., and McEwan M.J (1991)
Int. J. Mass Spectrom. Ion Processes, ***107***, 319.

Petrie S., Freeman C.G., and McEwan M.J. (1992)
Mon. Not. R. astr. Soc. ***257***, 438.

Pritchard H.O. (1984)
"The Quantum Theory of Unimolecular Reactions"
Cambridge University Press, Cambridge.

Rahbee A. (1985)
J.Chem. Phys. ***117***, 352.

Rahbee A (1986)
Int. J. Mass Spectrom. Ion Processes, ***72***, 3.

Robinson F.N.H. (1959)
J. Sci. Instr. ***36***, 481.

Robinson P.J. and Holbrook K.A. (1972)
"Unimolecular Reactions"
Wiley Interscience, London.

Roche A.E., Sutton M.M., Bohme D.K., and Schiff H.I. (1971)
J.Chem. Phys. ***55***, 5480.

Ryan K.R., and Harland P.W. (1974)
Int. J. Mass Spectrom. Ion Physics, ***15***, 197.

Sen A.D., Huntress W.T., Anicich V.G., McEwan M.J., and Denison A.B. (1991)
J.Chem. Phys. ***94***, 5462.

Sen Sharma D.K., and Kebarle P. (1982)
J. Am. Chem. Soc. ***104,*** 19.

Sharp T.E., Eyler J.R., and Li E. (1972)
Int. J. Mass Spectrom. Ion Physics, ***9***, 421.

Sieck L.W., and Meot-Ner (Mautner) M. (1982)
J. Phys .Chem. ***86***, 3647.

Smith B.J., and Radom L. (1993)
J. Am. Chem. Soc. ***115***, 4885.

Smith D. (1988)
"Formation and Destruction of Molecular Ions in Interstellar Clouds"
Phil. Trans. R. Soc. London A, ***324***, 257.

Smith D (1992)
Chem. Rev. ***92***, 1473.

Smith D., and Adams N.G. (1979)
"Recent Advances in Flow Tubes : Measurement of Ion-molecule Rate Coefficients and Product Ratios"
in "*Gas Phase Ion Chemistry Volume 1*" Bowers M.T. (ed)
Academic Press, New York.

Smith D., and Adams N.G. (1988)
"The Selected Ion Flow Tube (SIFT) : Studies of Ion-Neutral Reactions"
Adv. At. Mol. Phys ***24***, 1.

Smith D., and Adams N.G. (1989)
J.Chem. Soc., Faraday Trans. 2, ***85***, 1613.

Smith D.L., and Futrell J.H (1972/73)
Int. J. Mass Spectrom. Ion Physics, ***10***, 405.

Smith R.D., and Futrell J.H. (1978)
J.Org. Mass. Spectrom. ***13***, 688.

Smith S.C., Wilson P.F., Sudkeaw P., Macalgan R.G.A.R., McEwan M.J., Anicich V.G., and Huntress W.T. (1993)
J.Chem. Phys. ***98***, 1944.

Solomon P.M., Jefferts K.B., Peuzius A.A., and Wilson R.W. (1971)
Ap. J. Lett. ***199***, L81.

Sommer H., Thomas H.A, and Hipple J.A. (1951)
Phys Rev. ***82***, 697.

Speranza M., Sefcik M.D., Henis J.M.S., and Gaspar P.P. (1977)
J. Am. Chem. Soc. ***99***, 5583.

Su T., and Bowers M.T. (1973)
J.Chem. Phys. ***58***, 3027.

Su T., and Chesnavich W.J. (1982)
J.Chem. Phys. **76**, 5183.

Sudkeaw P. (1991)
"*Theoretical Chemistry*"
PhD Thesis, University of Canterbury, New Zealand.

Szulejko J.E., and McMahon T.B. (1993)
J. Am. Chem. Soc. ***115***, 7839.

Tasaka M., Ogata M., and Ichikawa H. (1981)
J. Am. Chem. Soc. ***103***, 1885.

Toselli B.M., Brenner J.D., Yerram M.L., Chin W.E., King K.D., and Barker J.R. (1991)
J.Chem. Phys. ***95***, 176.

Treager J.C. (1986)
Int. J. Mass Spectrom. Ion Processes, ***66***, 271.

Troe J. (1977)
J.Chem. Phys. ***66***, 4745.

Troe J. (1979)
J. Phys .Chem. ***83***, 115.

Van der Hart W.J., and Van Sprang H.A. (1977)
J. Am. Chem. Soc. ***99***, 32.

Van der Hart W.J., Oosterveld E., Molenaar-Langeveld T.A., and Nibbering N.M.M. (1989)
Org. Mass. Spectrom. ***24***, 59.

Vogt J., and Beauchamp J.L. (1975)
J. Am. Chem. Soc. ***97***, 6682.

Wang M., and Marshall A.G. (1988)
Anal.Chem. ***60***, 341.

Wersberg B.L., Yeung A.C., and Howard J.B. (1975)
15th Symposium (Int.) on Combustion, (p.1439)
The Combustion Institute, Pittsburgh, Penn.

Weston E.R., and Flynn G.W. (1992)
Ann. Rev. Phys. Chem. ***43***, 559.

Wincel H., Fokkers R.H., and Nibbering N.M.M. (1980)
Int. J. Mass Spectrom. Ion Physics, ***73***, 2310.

Wobschall D et al (1963)
Phys. Rev. ***131***, 1565.

Wobschall D. (1965)
Rev. Sci. Instrum. ***36***, 466.

Wronka J., and Ridge D.P. (1982)
Rev. Sci. Instrum. ***53***, 491.

Wronka J Phd Thesis

Yerram M.L., Brenner J.D., King K.D., and Barker J.R. (1990)
J. Phys .Chem. ***94***, 6341.

APPENDIX : COMPUTER PROGRAMS

Some changes to the formatting have been made to condense the code and to make it easier to follow .

SUBROUTINE FLOWREADER

```
SUB flowreader (cbase%, flo!)
'
'This routine is supposed to set up the pcl718 counter 1 and 2 to operate
'as a pacer trigger for a/d sampling. The sampling rate can be changed by
'simple editing of the dat%() variables for function 17.The value set at
'the moment is 10hz. The number of points taken is set in dat%(0) for
'function 4.
'
DIM dat%(4), ary1%(600), ary2%(600)
dat%(0) = cbase%
dat%(1) = 2         'selects interrupt level
dat%(2) = 3         'selects DMA irq3 apparently
er% = 0
fun% = 0
CALL pcl718(fun%, SEG dat%(0), SEG ary1%(0), SEG ary2%(0), er%)
IF er% <> 0 THEN PRINT "Initialisation of pcl card has failed !": STOP
'Note that at present only channel 0 is used
dat%(0) = 0: dat%(1) = 0
fun% = 1
CALL pcl718(fun%, SEG dat%(0), SEG ary1%(0), SEG ary2%(0), er%)
IF er% <> 0 THEN PRINT "A/D multiplexer setting Functon 1 has failed !": STOP
"
'Set pacer trigger rate at 10Hz (1MHZ divided by 100000 (dat%(0)*dat%(1))
dat%(0) = 100
dat%(1) = 1000
fun% = 17
CALL pcl718(fun%, SEG dat%(0), SEG ary1%(0), SEG ary2%(0), er%)
IF er% <> 0 THEN PRINT "Pacer trigger setting function 17 has failed !": STOP
'
'At present the number of conversions is 100 which gives 10s at 10HZ
dat%(0) = 100
dat%(1) = 1
fun% = 4
CALL pcl718(fun%, SEG dat%(0), SEG ary1%(0), SEG ary2%(0), er%)
IF er% <> 0 THEN PRINT "A/D conversion routine function4 has failed !": STOP
'
n% = 99
sum! = 0: sumx! = 0: sumy! = 0: sumx2! = 0: sumxy! = 0: sumy2! = 0
'
FOR i = 0 TO n%
    x! = i / 10      'time=number divided by pacer rate (10hz)
    y! = ary1%(i) / 4095  'converts into volts

    sum! = sum! + 1
    sumx! = sumx! + x!
    sumy! = sumy! + y!
    sumx2! = sumx2! + x! * x!
    sumxy! = sumxy! + x! * y!
```

```
    sumy2! = sumy2! + y! * y!
NEXT i

delta! = sum! * sumx2! - sumx! * sumx!
a! = (sumx2! * sumy! - sumx! * sumxy!) / delta!
b! = (sumxy! * sum! - sumx! * sumy!) / delta!
c! = n% - 2

r! = (sum! * sumxy! - sumx! * sumy!) / SQR(ABS(delta! * (sum! * sumy2! - sumy! * sumy!)))

flo! = b!'The flow is the slope in volts per second
END SUB
```

SUBROUTINE ONESHOT

```
SUB oneshot (cbase%)
'
'This segment sets up the counter 0 on the pcl card as a programmable
'oneshot. The base address of the card is cbase% this must be correct.
'The time base data sent to the counter is adjustable , any number of
'counts up to  65535 can be used. The clock input from the dedicated
'hardware is also switchable between 1khz and 100hz
 '
'cbase% = &H300      'base adress
GOTO 2323
ncounts! = 1000     '1000 counts at 100hz gives 10s
'
'The following segment converts ncounts into a high and a low bite to be
'sent to base + 12 for the counter.
'
k3! = (ncounts! / 4096): k3% = INT(k3!)
det! = ncounts! - (k3% * 4096)
k2! = (det! / 256): k2% = INT(k2!)
det! = det! - (k2% * 256)
k1! = (det! / 16): k1% = INT(k1!)
det! = det! - (k1% * 16)
k0! = det!: k0% = INT(k0!)
lowbite% = k0% + (k1% * &H10)
highbite% = k2% + (k3% * &H10)
'
'
OUT cbase% + 3, &H0  'disables the counter
OUT cbase% + 15, &H32  'sets counter 0 in monostable mode see p50 of manual
OUT cbase% + 3, &H10  'sends D4 positive to reset system (hopefully)
OUT cbase% + 12, lowbite%
OUT cbase% + 12, highbite%

END SUB
```

SUBROUTINE READCOUNT

```
SUB readcount (cbase%, count&)
'This segment of code is supposed to wait untill the status nibble on the
' dedicated hardware shows the terminal count signal. The code will then
'read the 6 bcd digits from the multiplexer using the two select channels
'd0 and d1 at address  base +3 .

'                        input byte (base + 3)

'       select0 (D0)     select1   (D1)     High Nibble      Low Nibble
'       ------------     -----------       -----------      ----------
'       0                anything          not used         status
'       1                0                 DIGIT 4          DIGIT 0
'       1                1                 DIGIT 5          DIGIT 1
'       0                0                 DIGIT 2          status
'       0                1                 DIGIT 3          status

' status nibble
' D0  status (0=still counting   1=finished counting)
' D1  8254 clock output
' D2  ?
' D3  not used

DIM digit%(6), bcd%(6)
repeet:
' Select the status nibble
OUT cbase% + 3, &H4
' NB Check that cbase% is a shared or global variable
'Now read the status nibble
x% = INP(cbase% + 3) AND &H1
IF x% = 1 THEN GOTO repeet

'If the program has got this far the count should be complete
'now the code will ask for and read the bcd digits in sequence.
OUT cbase% + 3, &H0   'This disables the clock (D2) and gets bcd digit 2
digit%(3) = INP(cbase% + 3)
OUT cbase% + 3, &H1
digit%(4) = INP(cbase% + 3)
OUT cbase% + 3, &H3
digit%(2) = INP(cbase% + 3)
OUT cbase% + 3, &H2
digit%(1) = INP(cbase% + 3)
'
'This segment of code is designed to deconvolute the bcd numbers that
'contain the ion count and then convert them to decimal
bcd%(0) = digit%(1) AND &HF
bcd%(1) = digit%(2) AND &HF
bcd%(5) = digit%(2) AND &HF0: bcd%(5) = bcd%(5) / &HF
bcd%(3) = digit%(4) AND &HF0: bcd%(3) = bcd%(3) / &HF
bcd%(2) = digit%(3) AND &HF0: bcd%(2) = bcd%(2) / &HF
bcd%(4) = digit%(1) AND &HF0: bcd%(4) = bcd%(4) / &HF
count& = bcd%(0) + 10 * bcd%(1) + 100 * bcd%(2) + 1000 * bcd%(3)
count& = count& + bcd%(4) * 10 ^ 4 + bcd%(5) * 10 ^ 5
END SUB
```

EXTRACT FROM SIFT2D

This extract from the controlling routine shows how the subroutines are called in the course of the SIFT measurement. The code below is trigerred by the operator pressing a button on the keyboard.

```
 flowsum = 0
    FOR t = 1 TO SCAN%    ' Scan thru different masses for a given flow
        'CALL control(mass(t) / 200 * 4095)
        IF fl% = 1 THEN GOTO again1

        oneshot cbase%                                  SETS UP PCL CARD
        LOCATE 14, 60: COLOR 15
        PRINT "Rhubarb..."
        BEEP: BEEP

        OUT cbase% + 3, &H4      'enables counter 0     TRIGGERS THE DIGITAL
                                                        RATEMETER
        flowreader cbase%, flow                         AND STARTS THE FLOW
                                                        MEASUREMENT

        readcount cbase%, kount&                        READS THE ION COUNT
WHEN
                                                        FLOWREADER FINISHES

        flow = flow * factor!
        flowsum = flowsum! + flow
        results(fl%, t) = count&
        GOSUB displaycount                              SCALES AND DISPLAYS THE
ION
                                                        COUNTS AND NEUTRAL
FLOWS
```

PROGRAM RATECONA

```
DECLARE SUB Voodoochild (curveno%, numb%, ecks!(), why&(), baseline&, basesig&)
DECLARE SUB Experimentaldetails (Timebase!, nt%, ns%)
DECLARE SUB Switchsettings ()
DECLARE SUB connections ()
DECLARE SUB sample (nt%, ns%, v&(), vsig&())
DECLARE SUB switch (mode$)
DECLARE SUB curves ()
DECLARE SUB delay (num%)
DECLARE SUB initializer ()
'program to replace ratecon.for by VGA.
    CLS
    initializer
u0:
    CLS
    LOCATE 7, 20: PRINT "            MAIN MENU"
    LOCATE 10, 23: PRINT "  SELECT OPTION AND ENTER NUMBER"
    LOCATE 12, 23: PRINT "    [1] SELECT SWITCH SETTINGS"
    LOCATE 14, 23: PRINT "    [2] MEASURE A RATE CONSTANT"
    LOCATE 16, 23: PRINT "    [3] I/O CONNECTION DETAILS "
    LOCATE 18, 23: PRINT "    [4] QUIT"
    LOCATE 20, 23: INPUT "    Enter No  "; q%
    SELECT CASE q%
        CASE IS = 1
            Switchsettings
        CASE IS = 2
            curves
        CASE IS = 3
            connections
        CASE IS = 4
            GOTO lastbit
        CASE ELSE
            GOTO u0
    END SELECT
    GOTO u0
lastbit:
    s$ = "all voltages zero"
    switch s$
'-------------------------------------------------------------------------------
    END
```

SUB initializer

```
'This subroutine initialises the PCL718 card and must be run before any
' other call is made to a PCL718 function
'-------------------------------------------------------------------------------
   DIM dat%(4), ary1%(1), ary2%(1)
   port& = &H300
   dat%(0) = port&
   dat%(1) = 3: dat%(2) = 3
   er% = 0: fun% = 0
   CALL pcl718(fun%, SEG dat%(0), SEG ary1%(0), SEG ary2%(0), er%)
   IF er% <> 0 THEN STOP
'-------------------------------------------------------------------------------
END SUB
```

SUB connections

```
'This subroutine contains instructions on how to set up the distribution
' box to run the ICR from the PCL718 card.
    CLS
    PRINT "A.  DIGITAL OUTPUT BOX.  (BNC's labelled 0-5)"
    PRINT "   ----------------------------------------"
    PRINT "   BNC 0 goes to socket labelled 'manual' to rear of gated int' unit."
    PRINT "   BNC 1 goes to socket labelled 'remote' to rear of gated int' unit."
    PRINT "   BNC 2 goes to socket labelled '+ve ' on same panel."
    PRINT "   BNC 3 goes to socket labelled '-ve ' on same panel."
    PRINT : PRINT
    PRINT "B.  ANALOG INPUT/OUTPUT BOX (BNC's in 0-3, out 1,2)"
    PRINT "   ----------------------------------------------"
    PRINT "   BNC OUT 1 goes to socket 'delay time in' rear of gated int' unit."
    PRINT "   BNC IN 0 goes to detect pulse from front panel."
    PRINT "   BNC IN 2 goes to output from the gated integrator."
    PRINT : PRINT "   Press any key to continue  "
    DO: LOOP WHILE INKEY$ = ""
    END SUB
```

SUB delay (num%)

```
'This routine causes the PCL718 card to send an analog voltage 0-5V to the
' ICR delay time line controlling the delay time.

    DIM dat%(4), ary1%(3), ary2%(3)
    dat%(0) = 0
    dat%(1) = num%
    fun% = 15

    CALL pcl718(fun%, SEG dat%(0), SEG ary1%(0), SEG ary2%(0), er%)
        IF er% <> 0 THEN PRINT "ERROR IN FUNCTION 15 er% ="; er%
'END SUB
```

SUB curves

```
    DIM xb&(100), xbsig&(100), x1&(100), x1sig&(100), t!(100)
    Experimentaldetails Timebase!, nt%, ns%
    FOR i = 1 TO nt%
    t!(i) = i * (Timebase! / nt%)
    NEXT i
c11:
    FOR curveno% = 1 TO 2
        CLS
        LOCATE 5, 22: PRINT "Measurement of Experimental Curve "; curveno%
        LOCATE 6, 22: PRINT "------------------------------- "
        LOCATE 8, 22: PRINT "    Are you ready to start ?"
        LOCATE 10, 22: PRINT "       [1] = start "
        LOCATE 11, 22: PRINT "       [2] = restart "
        LOCATE 12, 22: PRINT "       [3] = quit "
c1:
        LOCATE 14, 22: INPUT "      Enter No "; q&
        SELECT CASE q&
            CASE IS = 1
                'do nothing
            CASE IS = 2
                GOTO c11
            CASE IS = 3
                GOTO c99
            CASE ELSE
```

```
                GOTO c1
            END SELECT
            CLS : PRINT " Measuring baseline now, Plate Polarity Negative"
'set switches to remote and negative ions
            s$ = "remote negative"
            switch s$
'call subroutine sample
            sample nt%, ns%, xb&(), xbsig&()
'calculate baseline value and variation
            sx& = 0
            sxsq& = 0
            FOR i = 1 TO nt%
                sxsq& = sxsq& + (xb&(i) * xb&(i))
                sx& = sx& + xb&(i)
            NEXT i
            sigma! = sxsq& - (sx& * sx& / nt%)
            sigma! = SQR(sigma! / (nt% - 1))
            bas& = INT(sx& / nt%)
            basesig& = INT(sigma!)
            CLS : PRINT "Baseline = "; : PRINT USING "######"; bas&
            PRINT "Sigma    = "; : PRINT USING "######"; basesig&
            PRINT "Press any key to measure curve with plates positive."
            DO: LOOP WHILE INKEY$ = ""
'measure curve using positive voltages on the trapping plates
           CLS :  PRINT "Measuring curve1 now ; Plate Polarity Positive "
c2:
'set switches to remote and positive ions
            s$ = "remote positive"
            switch s$
'call subroutine sample
            sample nt%, ns%, x1&(), x1sig&()
'display values of signal and error for each point
           IF nt% > 20 THEN scroll% = 1
            j% = 0
clab1:
            CLS
            PRINT "Time (s) "; TAB(21); "Voltage"; TAB(32); "Error"
            PRINT "---------"; TAB(21); "-------"; TAB(32); "-----"
            FOR i% = 1 TO 20
                j% = j% + 1
                IF j% > nt% THEN
                    scroll% = 0
                    EXIT FOR
                END IF
               PRINT t!(j%); TAB(21); x1&(j%); TAB(32); x1sig&(j%)
            NEXT
            SELECT CASE scroll%
                CASE IS = 1
                   PRINT : PRINT "Press any key for next 20 points"
                    DO: LOOP WHILE INKEY$ = ""
                    GOTO clab1
                CASE ELSE
                     'carry on
            END SELECT
            INPUT "Repeat this run ?  [Y] or [N]  :"; q$
            IF UCASE$(q$) = "Y" THEN GOTO c2

'Save the curve to a data file, using subroutine  Voodoochild to
'write sequential data file containing cureve data
```

```
        Voodoochild curveno%, nt%, t!(), x1&(), bas&, basesig&
        NEXT
c99:
        END SUB

SUB Experimentaldetails (Timebase!, nt%, ns%)
'This subroutine recieves data from the keyboard and sends it to the
'subroutine CURVES
d1:
    CLS
    PRINT "  Rate Constant Determination, experimental data input"
    PRINT "  ------------------------------------------------------"
    PRINT
    PRINT "  Enter the full scale time base in ms "
d3:
    PRINT : INPUT "  50  100  200  500  1000 or 2000    "; Timebase!
    SELECT CASE Timebase!
        CASE 50, 100, 200, 500, 1000, 2000
            'do nothing
        CASE ELSE
            GOTO d3
    END SELECT
    Timebase! = Timebase! / 1000
    PRINT : PRINT "  How many data points are required "
d4:
    PRINT : INPUT "  (Maximum 100)   "; nt%
        IF nt% > 100 OR nt% < 1 THEN GOTO d4
    PRINT : PRINT "  How many samples per point needed"
d5:
    PRINT : INPUT "  (Maximum 500)   "; ns%
        IF ns% > 500 OR ns% < 1 THEN GOTO d5
    CLS
    PRINT "  Timebase  "; Timebase!; " s"
    PRINT "  No Points "; nt%
    PRINT "  Samples   "; ns%
d6:
    PRINT : INPUT "  Do you want to change anything Y/N "; q$
    SELECT CASE UCASE$(q$)
        CASE IS = "Y"
            GOTO d1
        CASE IS = "N"
            'do nothing
        CASE ELSE
            PRINT "Please enter Y(es) or N(o) only "
            GOTO d6
    END SELECT
END SUB


SUB sample (nt%, ns%, v&(), vsig&())
   DIM samp&(1000), dat%(4), ary1%(3), ary2%(3)

'Send the appropriate voltage to the delay time unit,
'assume d/a has maximum=5V corresponding to 4095
    num1% = INT(4095 / nt%)
    FOR i = 1 TO nt%
        num% = num1% * i
        nn% = 0
'output the delay voltage by calling subroutine delay
        delay num%
```

```
'go through a/d reading procedure,
      FOR ii = 1 TO ns%
'test for first detect pulse after sending the new delay time
'This function sets the a/d to measure channel 1 then 2 each time called
      dat%(0) = 0: dat%(1) = 1: fun% = 1
      CALL pcl718(fun%, SEG dat%(0), SEG ary1%(0), SEG ary2%(0), er%)
           IF er% <> 0 THEN PRINT "ERROR IN FUNCTION 1 er% ="; er%
'Function3 measures the analog voltage on a channel.
      fun% = 3
      flag& = 0
s1:
      CALL pcl718(fun%, SEG dat%(0), SEG ary1%(0), SEG ary2%(0), er%)
        IF er% <> 0 THEN PRINT "ERROR IN FUNCTION 3 er% = "; er%
      SELECT CASE dat%(0)
           CASE IS > 300
'first or second detect pulse depending on state of flag
                CALL pcl718(fun%, SEG dat%(0), SEG ary1%(0), SEG ary2%(0), er%)
                IF flag& = 1 THEN GOTO s2
                flag& = 1
                GOTO s1
           CASE ELSE
                CALL pcl718(fun%, SEG dat%(0), SEG ary1%(0), SEG ary2%(0), er%)
                GOTO s1
      END SELECT
'now we can measure the signal
s2:
      CALL pcl718(fun%, SEG dat%(0), SEG ary1%(0), SEG ary2%(0), er%)
           chan0& = dat%(0)
      CALL pcl718(fun%, SEG dat%(0), SEG ary1%(0), SEG ary2%(0), er%)
           IF chan0& > 300 THEN GOTO s2
           samp&(ii) = dat%(0)
      NEXT ii
      sxsq& = 0
      sx& = 0
      FOR j = 1 TO ns%
        sxsq& = sxsq& + (samp&(j) * samp&(j))
        sx& = sx& + samp&(j)
      NEXT j
      sigma& = sxsq - INT(sx * sx& / ns%)
      sigma& = INT(SQR(sigma& / (ns% - 1)))
      v&(i) = INT(sx& / ns%)
      vsig&(i) = sigma&
    NEXT i
END SUB
```

SUB switch (mode$)

```
'subroutine to operate D/O to remote switches
'at present this routine contains driver to initialise pcl718
'Channel 0= remote          Channel 1= manual
'Channel 2= positive        Channel 3= negative
'-------------------------------------------------------------------------

      DIM dat%(4), ary1%(1), ary2%(1)
      IF mode$ = "remote positive" THEN num% = 5
      IF mode$ = "remote negative" THEN num% = 9
      IF mode$ = "manual positive" THEN num% = 6
      IF mode$ = "manual negative" THEN num% = 10
      IF mode$ = "all voltages zero" THEN num% = 0
      fun% = 21: dat%(1) = INT(num% / 256): dat%(0) = num% - (dat%(1) * 256)
```

```
    CALL pcl718(fun%, SEG dat%(0), SEG ary1%(0), SEG ary2%(0), er%)

    IF er% <> 0 THEN STOP
'-------------------------------------------------------------------------------
END SUB
```

SUB Switchsettings

```
u1:
  CLS
  PRINT " Enter the appropriate setting No "
  PRINT "    [1] remote positive"
  PRINT "    [2] remote negative"
  PRINT "    [3] manual positive"
  PRINT "    [4] manual negative"
  INPUT "     "; z%
  SELECT CASE z%
  CASE IS = 1
    s$ = "remote positive"
  CASE IS = 2
    s$ = "remote negative"
  CASE IS = 3
    s$ = "manual positive"
  CASE IS = 4
    s$ = "manual negative"
  CASE ELSE
    GOTO u1
  END SELECT
  switch s$

END SUB
```

SUB Voodoochild (curveno%, numb%, ecks!(), why&(), baseline&, basesig&)

```
'THIS SUBROUTINE IS DEDICATED TO THE MEMORY OF JAMES MARSHALL AKA
JIMI HENDRIX
'this is why the title and labels may seem a little esoteric

electricladyland:
    CLS
    INPUT "Enter a TITLE for this curve    "; title$
    INPUT "Enter the gas pressure in Torr  "; p1!
    INPUT "Enter the I.G calibration factor "; cal1!
    PRINT "Enter any comments you may have on the line below "
    INPUT ": "; comments$

    CLS
    PRINT DATE$
    PRINT TIME$
    PRINT title$
    PRINT "Curve No "; curveno%
    PRINT comments$
    PRINT "Pressure is "; : PRINT USING "#.##^^^^"; p1!
    PRINT "Calibration factor is "; : PRINT USING "###.##"; cal1!
    INPUT "Do you want to change anything ? [Y] / [N] :"; q$
    IF UCASE$(q$) = "Y" THEN GOTO electricladyland
```

```
ThirdStonefromtheSun:

    CLS
    INPUT "Enter a filename for this curve "; filename$
    filename$ = MID$(filename$, 1, 8)
    filename$ = filename$ + ".dat"
    path$ = "c:\icr\"
    path$ = path$ + filename$
    PRINT "File will be written to path  "; path$
    INPUT "Change this ? [y] or [n] "; q$
    IF UCASE$(q$) = "Y" THEN GOTO ThirdStonefromtheSun
    OPEN path$ FOR OUTPUT AS #1
    WRITE #1, DATE$
    WRITE #1, TIME$
    WRITE #1, title$
    WRITE #1, curveno%
    WRITE #1, comments$
    WRITE #1, pressure!
    WRITE #1, calibration!
    WRITE #1, baseline&
    WRITE #1, basesig&
    WRITE #1, numb%
    FOR eye = 1 TO numb%
        WRITE #1, ecks!(eye)
        WRITE #1, why&(eye)
    NEXT
    CLOSE #1
    END SUB
```

PROGRAM RATECONX

```
DECLARE SUB curvecomparitor (OhNo%, press1!, press2!, npts1%, npts2%, cal1!, cal2!,
t1!(), t2!())
DECLARE SUB resultprinter (np%, title1$, comments1$, press1!, cal1!, bas1&, basesig1&,
title2$, comments2$, press2!, cal2!, bas2&, basesig2&, t!(), y1&(), y2&(), r!(), rsig!(), intexp!,
sigintexp!, slope!, sigslope!, r!, deltaP!, rate!, errate!)
DECLARE SUB filereader (curveno%, day$, hour$, title$, no%, comments$, pressure!,
calibration!, baseline&, basesig&, npts%, t!(), y&())
DECLARE SUB rationalizer (np%, press1!, press2!, cal1!, cal2!, bas1&, bas2&, basesig1&,
basesig2&, t!(), y1&(), y2&(), r!(), rsig!(), deltaP!)
DECLARE SUB linefitter (x!(), y!(), npts%, a!, SIGMAA!, B!, SIGMAB!, r!)
DECLARE SUB pointdeleter (np%, t!(), r!(), rsig!(), y1&(), y2&())
DECLARE SUB LINFIT (x!(), y!(), SIGMAY!(), npts%, MODE%, a!, SIGMAA!, B!,
SIGMAB!, r!)
        DIM t1!(100), t2!(100), y1&(100), y2&(100), r!(100), rsig!(100), lnr!(100),
lnrsig!(100)
        DIM t!(100), x!(100), y!(100)
main0001:
        n% = 1
        filereader n%, day1$, hour1$, title1$, no1%, comment1$, press1!, cal1!, bas1&,
basesig1&, np1%, t1!(), y1&()
main0011:
        n% = 2
        filereader n%, day2$, hour2$, title2$, no2%, comment2$, press2!, cal2!, bas2&,
basesig2&, np2%, t2!(), y2&()
        curvecomparitor er%, press1!, press2!, np1%, np2%, cal1!, cal2!, t1!(), t2!()
        IF er% = 1 THEN
                CLS
main0002:
                INPUT " Enter [Q] to quit or [R] to read some more files :"; q$
                SELECT CASE UCASE$(q$)
                        CASE "Q"
                                GOTO main1111
                        CASE "R"
                                GOTO main0001
                        CASE ELSE
                                GOTO main0002
                END SELECT

        END IF
        np% = np1%
        FOR i = 1 TO np%
                t!(i) = t1!(i)
        NEXT
        rationalizer np%, press1!, press2!, cal1!, cal2!, bas1&, bas2&, basesig1&, basesig2&,
        t!(), y1&(), y2&(), r!(), rsig!(), deltaP!
main0003:
        FOR i = 1 TO np%
                lnr!(i) = LOG(r!(i))
                lnrsig!(i) = rsig!(i) / r!(i)
        NEXT
        MODE% = 0
        LINFIT t!(), lnr!(), lnrsig!(), np%, MODE%, intercept!, sigintercept!, slope!, sigslope!,
r!
        IF intercept! > 88 THEN intercept! = 88
        IF intercept! < -88 THEN intercept! = -88
```

```
        intexp! = EXP(intercept!)
        sigintexp! = sigintercept! * intexp!
        rate! = -1 * slope! / (deltaP! * 3.24E+16)
        errate! = sigslope! / (deltaP! * 3.24E+16)
        CLS
        PRINT "Calculation of rate constant completed "
        PRINT "The INTERCEPT was determined to be "; : PRINT USING "##.##"; intexp!
        PRINT "The INTERCEPT Error was          "; : PRINT USING "##.##"; sigintexp!
        PRINT "The SLOPE     was determined to be "; : PRINT USING "+###.###"; slope!
        PRINT "The SLOPE Error was              "; : PRINT USING "#.###"; sigslope!
        PRINT "The Linear Correlation Coefficient "; : PRINT USING "+.###"; r!
        PRINT : PRINT "Using a calibration factor of "; : PRINT USING "##.##"; cal1!
        PRINT "At a pressure difference of "; deltaP!; " torr"
        PRINT
        PRINT "The RATE CONSTANT was determined to be "; : PRINT USING "
        #.###^^^^"; rate
        PRINT "The RATE CONSTANT Error was          "; : PRINT USING "#.###^^^^";
errate!
        PRINT "The units of the rate constant are cm^3/molecule/s"
        PRINT : PRINT "press any key to plot the curve ... ": DO: LOOP WHILE INKEY$ =
""

        plotcurve np%, t!(), lnr!(), lnrsig!(), intexp!, slope!
main0004:

        CLS
        PRINT "Select the appropriate option from the list below "
        PRINT "-------------------------------------------------"
        PRINT : PRINT " [1] Delete data point(s) and re-fit the curve "
        PRINT : PRINT " [2] Print out the results to the line printer "
        PRINT : PRINT " [3] not available"
        PRINT : PRINT " [4] Start over with some new curves "
        PRINT : PRINT " [5] quit "
        PRINT : INPUT "  "; q%
        SELECT CASE q%
                CASE 1
                        pointdeleter np%, t!(), r!(), rsig!(), y1&(), y2&()
                        GOTO main0003
                CASE 2
                        resultprinter p%,title1$,comments1$,press1!,cal1!,bas1&,basesig1&,
title2$, comments2$, press2!, cal2!, bas2&, basesig2&, t!(), y1&(), y2&(), r!(), rsig!(),
intexp!,sigintexp!, slope!, sigslope!, r!, deltaP!, rate!,errate!
                        GOTO main0004
                CASE 3
                        'glroutine
                        GOTO main0004
                CASE 4
                        GOTO main0001
                CASE 5
                        END
                CASE ELSE
                        GOTO main0004
        END SELECT
main1111:

handler:
        IF ERR = 53 THEN
                PRINT : PRINT "This file does not exist press a key to try again "
                DO: LOOP WHILE INKEY$ = ""
                IF n% = 1 THEN GOTO main0001
```

```
            IF n% = 2 THEN GOTO main0011
        END IF
END
```

SUB curvecomparitor (OhNo%, press1!, press2!, npts1%, npts2%, cal1!, cal2!, t1!(), t2!())

```
'This subroutine compares the two curves read from file to determine wether they
'will be suitable for calculation of a rate constant, or if they will need
'further editing first.
        OhNo% = 0: oops = 0
        PRINT "Comparing the two curves for Compatibility"
        IF press1! > press2! THEN
            OhNo% = 1
            PRINT "ERROR , pressure1 is larger than pressure2 . "
        END IF
        IF npts1% <> npts2% THEN
            OhNo% = 1
            PRINT "ERROR , Curves contain different no's of points . "
            GOTO cc1
        END IF
        FOR i = 1 TO npts1%
            IF t1!(i) <> t2!(i) THEN oops = 1
        NEXT
        IF oops = 1 THEN
            OhNo% = 1
            PRINT "ERROR , Time arrays are not compatible with each other ."
        END IF
cc1:
        IF cal1! <> cal2! THEN
            OhNo% = 1
            PRINT "ERROR , Calibration factors disagree ."
        END IF
'-------------------------------------------------------------------------
END SUB
```

SUB filereader (curveno%, day$, hour$, title$, no%, comments$, pressure!, calibration!, baseline&, basesig&, npts%, t!(), y&())

```
'Subroutine to read curves from sequential data files
'-------------------------------------------------------------------------
        CLS
        PRINT "Input of Data from Sequential Data files "
        PRINT "---------------------------------------- "
        PRINT
        PRINT "Enter the filename for curve "; curveno%
        INPUT "    "; filename$
        IF LEN(filename$) > 11 THEN
            filename$ = MID$(filename$, 1, 8)
            filename$ = filename$ + ".dat"
        END IF
        path$ = "c:\icr\" + filename$
fr1:
        PRINT : PRINT "File to be read has path  "; path$
        INPUT "Change this ? [y] or [n] "; q$
        IF UCASE$(q$) = "Y" THEN
            PRINT : PRINT "You must input the complete path, including drive etc "
            INPUT "Enter New Path "; path$
            GOTO fr1
        END IF
        ON ERROR GOTO handler
```

```
        OPEN path$ FOR INPUT AS #1
        INPUT #1, day$
        INPUT #1, hour$
        INPUT #1, title$
        INPUT #1, no%
        INPUT #1, comments$
        INPUT #1, timebase!
        INPUT #1, samples%
        INPUT #1, pressure!
        INPUT #1, calibration!
        INPUT #1, baseline&
        INPUT #1, basesig&
        INPUT #1, npts%
        FOR i = 1 TO npts%
                INPUT #1, t!(i)
                INPUT #1, y&(i)
        NEXT
        CLOSE #1
        CLS
        PRINT "Data for Curve "; curveno%
        PRINT day$
        PRINT hour$
        PRINT title$
        IF no% <> curveno% THEN
                PRINT "* * * CURVE NUMBER OF THIS FILE = "; no%; " * * * *"
                PRINT "Press any key to start again... "
                DO: LOOP WHILE INKEY$ = ""
                GOTO fr1
        END IF
        PRINT comments$
        PRINT "Timebase "; timebase!; "   Samples/Point "; samples%
        PRINT "Pressure was "; pressure!; " Torr"
        PRINT "I.G cal factor "; calibration!
        PRINT "Baseline was "; baseline&
        PRINT "Baseline error "; basesig&
        PRINT : PRINT "Press any key to display data points ": DO: LOOP WHILE INKEY$ =
        ""
        IF npts% > 20 THEN scroll% = 1
        j% = 0
fr2:
        CLS
        PRINT " Time (s) "; TAB(20); "  Curve "
        PRINT "-----------"; TAB(20); "--------"
        FOR i = 1 TO 20
                j% = j% + 1
                IF j% > npts% THEN
                        scroll% = 0
                        EXIT FOR
                END IF
                PRINT t!(j%); TAB(20); y&(j%)
        NEXT
        IF scroll% = 1 THEN
                PRINT "Press any key for the next 20 points "
                DO: LOOP WHILE INKEY$ = ""
                GOTO fr2
        END IF
        PRINT : INPUT "Enter [R] to restart if this data is unsuitable "; q$
        IF UCASE$(q$) = "R" THEN GOTO fr1
'-------------------------------------------------------------------------
END SUB
```

```
SUB LINFIT (x!(), y!(), SIGMAY!(), npts%, MODE%, a!, SIGMAA!, B!, SIGMAB!, r!)
'*************************************************************************
'This sub is taken from RATECON.FOR wtiten by Dr V.G. Anicich
'    SUBROUTINE LINFIT
'
' PURPOSE
'      MAKE A LEAST-SQUARES FIT TO DATA WITH A STRAIGHT LINE
' Y = A + B * X
'
' USAGE
'      CALL LINFIT (X, Y, SIGMAY, NPTS, MODE, A, SIGMAA, B, SIGMAB, R)
'
'    DESCRIPTION OF PARAMETERS
'      X     - ARRAY OF DATA POINTS FOR INDEPENDENT VARIABLE
'      Y     - ARRAY OF DATA POINTS FOR DEPENDENT VARIABLE
'      SIGMAY - ARRAY OF STANDARD DEVIATIONS FOR Y DATA POINTS
'      NPTS   - NUMBER OF PAIRS OF DATA POINTS
'      MODE   - DETERMINES METHOD OF WEIGHTING LEAST-SQUARES FIT
'             +1 (INSTRUMENTAL) WEIGHT(I) = 1./SIGMAY(I)**2
'              0 (NO WEIGHTING) WEIGHT(I) = 1.
'             -1 (STATISTICAL)  WEIGHT(I) = 1./Y(I)
'      A     - Y INTERCEPT OF FITTED STRAIGHT LINE
'      SIGMAA - STANDARD DEVIATION OF A
'      B     - SLOPE OF FITTED STRAIGHT LINE
'      SIGMAB - STANDARD DEVIATION OF B
'      R     - LINEAR CORRELATION COEFFICIENT
'    SUBROUTINES AND FUNCTION SUBPROGRAMS REQUIRED
' NONE
'*************************************************************************
'      ACCUMULATE WEIGHTED SUMS
     SUM! = 0!
     SUMX! = 0!
     SUMY! = 0!
     SUMX2! = 0!
     SUMXY! = 0!
     SUMY2! = 0!
     FOR i = 1 TO npts%
          X1! = x!(i)
          y1! = y!(i)
     IF MODE% = -1 THEN
          IF y1! < 0 THEN WEIGHT% = 1! / (-1 * y1)
          IF y1! > 0 THEN WEIGHT% = 1! / (y1)
          IF y1! = 0 THEN WEIGHT% = 1!
          GOTO 41
     END IF
     IF MODE% = 0 THEN
          WEIGHT% = 1!
          GOTO 41
     END IF
     IF MODE% = 1 THEN WEIGHT% = 1! / SIGMAY(i) ^ 2
41 :  SUM! = SUM! + WEIGHT%
     SUMX! = SUMX! + WEIGHT% * X1!
     SUMY! = SUMY! + WEIGHT% * y1!
     SUMX2! = SUMX2! + WEIGHT% * X1! * X1!
     SUMXY! = SUMXY! + WEIGHT% * X1! * y1!
     SUMY2! = SUMY2! + WEIGHT% * y1! * y1!
     NEXT i
       CALCULATE COEFFICIENTS
```

```
        AND STANDARD DEVIATIONS
    delta! = SUM! * SUMX2! - SUMX! * SUMX!
    a! = (SUMX2! * SUMY! - SUMX! * SUMXY!) / delta!
    B! = (SUMXY! * SUM! - SUMX! * SUMY!) / delta!
    IF MODE% = -1 OR MODE% = 1 THEN
        VARNCE = 1!
        GOTO 67
    END IF

        C! = npts% - 2
        VARNCE! = (SUMY2! + a! * a! * SUM! + B! * B! * SUMX2! - 2! * (a! * SUMY! +
        B! * SUMXY! - a! * B! * SUMX!)) / C!
67 :  SIGMAA! = SQR(ABS(VARNCE! * SUMX2! / delta!))
        SIGMAB! = SQR(ABS(VARNCE! * SUM! / delta!))
        r! = (SUM! * SUMXY! - SUMX! * SUMY!) / SQR(ABS(delta! * (SUM! * SUMY2! -
        SUMY! * SUMY!)))
END SUB


SUB plotcurve (npts%, x!(), y!(), sigy!(), intercept!, slope!)
'-------------------------------------------------------------------------------
        SCREEN 9, 0
        WINDOW (0, 0)-(640, 350)
        LINE (40, 20)-(600, 330), 15, B
'draw crosshatches on x and y axes
        FOR i = 1 TO 9
                LINE (40 + 56 * i, 20)-(40 + 56 * i, 30), 15
                LINE (40 + 56 * i, 320)-(40 + 56 * i, 330), 15
                LINE (590, 20 + 31 * i)-(600, 20 + 31 * i), 15
                LINE (40, 20 + 31 * i)-(50, 20 + 31 * i), 15
        NEXT
        lineend! = intercept! * EXP(slope! * x!(npts%))
        IF slope! < 0 THEN
                maxy! = LOG(intercept!)
                miny! = LOG(lineend!)
        ELSE
                maxy! = LOG(lineend!)
                miny! = LOG(intercept!)
        END IF
        FOR i = 1 TO npts%
                IF y!(i) > maxy! THEN maxy! = y!(i)
                IF y!(i) < miny! THEN miny! = y!(i)
        NEXT
        maxy! = 1.1 * maxy!
        miny! = 1.1 * miny!
        fullscale! = (maxy! - miny!)
        fulltime! = x!(npts%)
'draw the experimental points
        FOR i = 1 TO npts%
                x! = (x!(i) / fulltime! * 560) + 40
                y! = ((y!(i) + ABS(miny!)) / fullscale! * 310) + 20
                LINE (x! - 5, y!)-(x! + 5, y!), 12
                LINE (x!, y! - 5)-(x!, y! + 5), 12
'Note that at present error bars are not generated,ysig!(i) contains
' the appropriate data.
        NEXT
'draw the fitted line
        LINE (40, ((LOG(intercept!) + ABS(miny!)) / fullscale! * 310) + 20)-(600,
        ((LOG(lineend!) + ABS(miny!)) / fullscale! * 310) + 20)
```

```
        LOCATE 25, 1: PRINT "Press any key to return to menu ": DO: LOOP WHILE
        INKEY$ = ""
        'CALL plotter(ftitle$, "c:\printgl\", npts%, miny!, maxy!, fulltime!, fullscale!,
        intercept!, lineend!, x!(), y!())
SCREEN 0
CLS
'--------------------------------------------------------------------------
END SUB
```

SUB pointdeleter (np%, t!(), r!(), rsig!(), y1&(), y2&())

```
'subroutine to allow bad data to be removed from the arrays r!() and rsig!()
' The routine does not affect the raw data which is of course on disc.
'--------------------------------------------------------------------------
pd01:
        IF np% > 20 THEN scroll% = 1
        j% = 0
pd02:
        CLS
        PRINT "Point No"; TAB(15); "Time (s)"; TAB(25); "Ratio "; TAB(35); "Error "
        PRINT "--------"; TAB(15); "---------"; TAB(25); "------"; TAB(35); "-------"
        FOR i = 1 TO 20
                j% = j% + 1
                IF j% > np% THEN
                        scroll% = 0
                        EXIT FOR
                END IF
                PRINT j%; TAB(15); t!(j%); TAB(25); r!(j%); TAB(35); rsig!(j%)
        NEXT
        IF scroll% = 1 THEN
                PRINT "Press any key for next 20 points "
                DO: LOOP WHILE INKEY$ = ""
                GOTO pd02
        END IF
        PRINT : INPUT "Enter Point No for point to delete (0 to quit) "; d%
        IF d% = 0 THEN GOTO label03
        np% = np% - 1
        IF d% = np% + 1 THEN GOTO pd01
        FOR i = d% TO np%
                t!(i) = t!(i + 1)
                r!(i) = r!(i + 1)
                rsig!(i) = rsig!(i + 1)
                y1&(i) = y1&(i)
                y2&(i) = y2&(i)
        NEXT
        GOTO pd01
label03:
'--------------------------------------------------------------------------
END SUB
```

SUB rationalizer (np%, press1!, press2!, cal1!, cal2!, bas1&, bas2&, basesig1&, basesig2&, t!(), y1&(), y2&(), r!(), rsig!(), deltaP!)

```
'This subroutine takes the arrays of signal for each of the two runs, and
'derives the array of the ratio of these two values, this array is r!()
'--------------------------------------------------------------------------
        deltaP! = (press2! * cal2!) - (press1! * cal1!)
        FOR i = 1 TO np%
                r!(i) = (y2&(i) - bas2&) / (y1&(i) - bas1&)
                IF r!(i) < .0001 THEN r!(i) = .0001
                y1mb! = y1&(i) - bas1&
```

```
                rsig!(i) = basesig1& * (1 + r!(i)) / y1mb!
        NEXT
'now display the arrays on the screen
        IF np% > 20 THEN scroll% = 1
        j% = 0
r1:
        CLS
        PRINT " Time (s) "; TAB(20); "Curve 1 "; TAB(30); "Curve 2 "; TAB(40); "Ratio ";
TAB(50); "Error "
        PRINT "----------"; TAB(20); "--------"; TAB(30); "--------"; TAB(40); "------";
TAB(50); "------"
        FOR i = 1 TO 20
                j% = j% + 1
                IF j% > np% THEN
                        scroll% = 0
                        EXIT FOR
                END IF
        PRINT t!(j%); TAB(20); y1&(j%); TAB(30); y2&(j%); TAB(40); : PRINT USING
        "##.###"; r!(j%); TAB(50); : PRINT USING "#.###"; rsig!(j%)
        NEXT
        IF scroll% = 1 THEN
                PRINT "Press any key for the next 20 points "
                DO: LOOP WHILE INKEY$ = ""
                GOTO r1
        END IF
        PRINT "Press any key to continue ": DO: LOOP WHILE INKEY$ = ""
'---------------------------------------------------------------------------
END SUB
```

SUB resultprinter (np%, title1$, comments1$, press1!, cal1!, bas1&, basesig1&, title2$, comments2$, press2!, cal2!, bas2&, basesig2&, t!(), y1&(), y2&(), r!(), rsig!(), intexp!, sigintexp!, slope!, sigslope!, r!, deltaP!, rate!, errate!)

```
        CLS
        INPUT "Enter a short title for the output "; t$
        PRINT : PRINT "Ensure that the printer is on line and paper is OK "
        PRINT : PRINT "Press any key to continue ": DO: LOOP WHILE INKEY$ = ""
        LPRINT t$
        LPRINT
        LPRINT "Curve 1 : "; title1$
        LPRINT comments1$
        LPRINT "Pressure "; press1!; "  Cal factor "; cal1!
        LPRINT "Baseline "; bas1&; " Error "; basesig1&
        LPRINT
        LPRINT "Curve 2 : "; title2$
        LPRINT comments2$
        LPRINT "Pressure "; press2!; "  Cal factor "; cal2!
        LPRINT "Baseline "; bas2&; " Error "; basesig2&
        LPRINT
        LPRINT " Time (s) "; TAB(20); "Curve 1 "; TAB(30); "Curve 2 "; TAB(40); "Ratio ";
        TAB(50); "Error "
        LPRINT "----------"; TAB(20); "--------"; TAB(30); "--------"; TAB(40); "------";
        TAB(50); "------"
        FOR i% = 1 TO np%
            LPRINT t!(i%); TAB(20); y1&(i%); TAB(30); y2&(i%); TAB(40); : LPRINT
        USING "##.###"; r!(i%); TAB(50); : LPRINT USING "#.###"; rsig!(1)
        NEXT
        PRINT : PRINT
        PRINT "The INTERCEPT was determined to be "; : LPRINT USING "##.##"; intexp!
        LPRINT "The INTERCEPT Error was          "; : LPRINT USING "##.##"; sigintexp!
```

```
        LPRINT "The SLOPE     was determined to be "; : LPRINT USING "+###.###"; slope!
        LPRINT "The SLOPE Error was                 "; : LPRINT USING "#.###"; sigslope!
        LPRINT "The Linear Correlation Coefficient "; : LPRINT USING "+.###"; r!
        LPRINT : LPRINT "Using a calibration factor of "; : LPRINT USING "##.##"; cal1!
        LPRINT "At a pressure difference of "; deltaP!; " torr"
        LPRINT
        LPRINT "The RATE CONSTANT was determined to be "; : LPRINT USING
        "#.###^^^^"; rate
        LPRINT "The RATE CONSTANT Error was           "; : LPRINT USING "#.###^^^^";
        errate!
END SUB
```

PROGRAM SCOPE

```
DECLARE SUB remotecontrol (setting$)
DECLARE SUB printdata (points%, tcurve!(), curve!())
DECLARE SUB dumper ()
DECLARE SUB graphdials (scalefactor%, tbase%, iterations%, twindow%)
DECLARE SUB graphswitches ()
DECLARE SUB graph (curve!(), tcurve!(), tbase!, points%)
DECLARE SUB delay (d1%)
DECLARE SUB initialiser ()
DECLARE SUB integrator (twindow%, points%, volts!(), time!(), iterations%, number%,
offset!, integral!, tbase!, curve!(), tcurve!())
DECLARE SUB xxx (volts!(), time!(), iterations%, number%, offset!, integral!)
DECLARE SUB keysoff ()
DECLARE SUB drawswitches ()
DECLARE SUB drawdials (voltsperdiv!, tbase%, tdelay%, twindow%, points%, iterations%,
offset!)
DECLARE SUB drawscreen (volts!(), time!(), twindow!, fullscale!, points%, mode$, curve!(),
tcurve!(), tbase!)
'-------------------------------------------
    CLS
'-------------------------------------------
'dim arrays etc
'-------------------------------------------
    DIM time!(300), volts!(300), curve!(300), tcurve!(300)
'-------------------------------------------
'initialise  pcl718 card
'-------------------------------------------
    initialiser
'-------------------------------------------
'set initial values to reasonable ones
'-------------------------------------------
    tbase% = 100: tbase! = tbase% / 1000
    points% = 10
    tdelay% = 10: tdelay! = tdelay% / 1000
    twindow% = 2: twindow! = twindow% / 1000
    iterations% = 1
    offset! = 0!
    voltsperdiv! = 1.5: fullscale! = voltsperdiv! * 10
    mode$ = "storage"
    polarity$ = "remote positive"
    FOR i = 1 TO 300
        volts!(i) = 1
        time!(i) = i / 50000
    NEXT
'-------------------------------------------
'set "hot keys" up
'-------------------------------------------
    ON KEY(1) GOSUB changetime    'note key(1) also used by sub graph
    ON KEY(2) GOSUB changedelaytime
    ON KEY(3) GOSUB changewindow
    ON KEY(4) GOSUB changeiterations
    ON KEY(5) GOSUB changepoints
    ON KEY(6) GOSUB changevoltsperdiv
    ON KEY(7) GOSUB changeoffset
    ON KEY(8) GOSUB firescope
    ON KEY(9) GOSUB togglepolarity
    ON KEY(10) GOSUB measurecurve
```

```
        ON KEY(30) GOSUB graphmode
        ON KEY(31) GOSUB quit

        SCREEN 9
        drawswitches
'-----------------------------------------
'this is the point the above subs will return to
'-----------------------------------------
line01:
'-----------------------------------------
'draw the scope screen and plot the points
'-----------------------------------------
        drawscreen volts!(), time!(), twindow!, fullscale!, points%, mode$, curve!(), tcurve!(),
tbase!
'-----------------------------------------
'turn "hot keys" on
'-----------------------------------------
        KEY(1) ON
        KEY(2) ON
        KEY(3) ON
        KEY(4) ON
        KEY(5) ON
        KEY(6) ON
        KEY(7) ON
        KEY(8) ON
        KEY(9) ON
        KEY(10) ON
        KEY(30) ON
        KEY(31) ON
        drawdials voltsperdiv!, tbase%, tdelay%, twindow%, points%, iterations%, offset!

        DO: LOOP
'-----------------------------------------
changetime:
'-----------------------------------------
'This changes the default timebase in ms
'-----------------------------------------
        keysoff
        IF mode$ = "graph" THEN

                LOCATE 2, 72: PRINT "    "
                LOCATE 2, 72
                INPUT scalefactor%
                IF scalefactor% < 1 OR scalefactor% > 100 THEN GOTO changetime
                LOCATE 2, 72: PRINT "    "
                RETURN graph01
        ELSE
        LOCATE 3, 60: PRINT "          "
        LOCATE 3, 60
        INPUT tbase%
        SELECT CASE tbase%
                CASE 50, 100, 200, 500, 1000
                'these are acceptable values
                CASE ELSE
                GOTO changetime
        END SELECT
        LOCATE 3, 60: PRINT "          "
        tbase! = tbase% / 1000
        RETURN line01
        END IF
```

```
'-----------------------------------------
changepoints:
'-----------------------------------------
'This changes the number of points to measure
'-----------------------------------------
      keysoff
            IF mode$ = "graph" THEN
                  printdata points%, tcurve!(), curve!()
                  RETURN graph01
            ELSE
                  LOCATE 6, 60: PRINT "           "
                  LOCATE 6, 60
                  INPUT points%
                  IF points% < 1 OR points% > 300 THEN GOTO changepoints
                  LOCATE 6, 60: PRINT "           "
                  RETURN line01
            END IF
'-----'-----------------------------------------
changedelaytime:
'-----------------------------------------
       keysoff
            IF mode$ = "graph" THEN
            LOCATE 3, 7
            PRINT "                                 "
            LOCATE 3, 7: INPUT ; title$
            LOCATE 3, 7
            PRINT "                                 "
            RETURN graph01
      ELSE
            LOCATE 4, 60: PRINT "           "
            LOCATE 4, 60
            INPUT tdelay%
            IF tdelay% < 0 OR tdelay% > tbase% THEN GOTO changedelaytime
            LOCATE 4, 60: PRINT "           "
            tdelay! = tdelay% / 1000
            RETURN line01
       END IF
'-----------------------------------------
changeoffset:
'-----------------------------------------
      keysoff
      LOCATE 8, 60: PRINT "           "
      LOCATE 8, 60
      INPUT offset!
      IF offset! < -10 OR offset! > 10 THEN GOTO changeoffset
      LOCATE 8, 60: PRINT "           "
      RETURN line01
'-----------------------------------------
togglepolarity:
'-----------------------------------------
      keysoff
      IF polarity$ = "remote positive" THEN
            polarity$ = "remote negative"
            GOTO togglepolarity01
      END IF
      IF polarity$ = "remote negative" THEN
            polarity$ = "remote positive"
            GOTO togglepolarity01
      END IF
togglepolarity01:
```

```
        remotecontrol polarity$
        RETURN line01
'-------------------------------------------
changewindow:
'-------------------------------------------
        keysoff
        IF mode$ = "graph" THEN
                dumper
                RETURN graph01
        ELSE
                LOCATE 5, 60: PRINT "           "
                LOCATE 5, 60
                INPUT twindow%
                IF twindow% < 0 OR twindow% > 600 THEN GOTO changewindow
                LOCATE 5, 60: PRINT "           "
                twindow! = twindow% / 1000
                RETURN line01
        END IF
'-------------------------------------------
firescope:
'-------------------------------------------
        keysoff
        mode$ = "storage"
        dvalue% = INT((tdelay% / tbase%) * 4095)
        delay dvalue%
        number% = INT(twindow% * 50)
        xxx volts!(), time!(), iterations%, number%, offset!, integral!
        RETURN line01
'-------------------------------------------
changeiterations:
'-------------------------------------------
        keysoff
        IF mode$ = "graph" THEN
                mode$ = "storage"
                LINE (0, 0)-(640, 350), 0, BF
                drawswitches
                RETURN line01
        ELSE
                LOCATE 7, 60: PRINT "           "
                LOCATE 7, 60
                INPUT iterations%
                IF iterations% < 1 OR iterations% > 10 THEN GOTO changeiterations
                LOCATE 7, 60: PRINT "           "
                RETURN line01
        END IF
'-------------------------------------------
measurecurve:
'-------------------------------------------
        keysoff
        mode$ = "integrator"
        GOSUB integrator
        RETURN line01
'-------------------------------------------
savedata:
'       keysoff
'       filewriter points%, time!(), vionsignal!()

        RETURN line01
'-------------------------------------------
changevoltsperdiv:
```

```
'-----------------------------------------------
    keysoff
    IF mode$ = "graph" THEN
        LINE (50, 270)-(450, 330), 0, BF
        LINE (50, 270)-(450, 330), 7, B
        LOCATE 21, 8
        PRINT "Data will be saved to dir c:\grapher "
        LOCATE 22, 8
        PRINT "Press Any Key To Continue....."
        COLOR 2, 0
        DO: LOOP WHILE INKEY$ = ""
savedata01:
        LINE (50, 270)-(450, 330), 0, BF
        LINE (50, 270)-(450, 330), 7, B
        LOCATE 21, 8
        PRINT "Enter a Filename (max 8 letters) "
        LOCATE 22, 8: INPUT ; f$
        filename$ = LEFT$(f$, 8) + ".dat"
        direct$ = "c:\grapher\"
        path$ = direct$ + filename$
savedata02:
        LINE (50, 270)-(450, 330), 0, BF
        LINE (50, 270)-(450, 330), 7, B
        LOCATE 21, 8
        PRINT "Path to send data on is "; path$

        LOCATE 23, 8
        INPUT "Change Anything ? <y> or <n> "; q$
        SELECT CASE UCASE$(q$)
            CASE IS = "Y"
                LINE (50, 270)-(450, 330), 0, BF
                LINE (50, 270)-(450, 330), 7, B
                LOCATE 21, 8
                PRINT "Enter a new path BE CAREFUL to be accurate"
                LOCATE 22, 8
                INPUT path$
                GOTO savedata02
            CASE IS = "N"
                'do nothing
            CASE ELSE
                GOTO savedata02
        END SELECT
        largest! = .01
        FOR i = 1 TO points%
            IF curve!(i) > largest! THEN largest! = curve!(i)
        NEXT
        OPEN path$ FOR OUTPUT AS #1
            FOR i = 1 TO points%
                normalised! = curve!(i) / largest!
                PRINT #1, tcurve!(i), normalised!
            NEXT
         WRITE #1,
         CLOSE #1
        LINE (50, 270)-(450, 330), 0, BF
        LINE (50, 270)-(450, 330), 7, B
        RETURN graph01
    ELSE
        LOCATE 2, 60: PRINT "           "
        LOCATE 2, 60
        INPUT voltsperdiv!
```

```
        IF voltsperdiv! < 0 OR voltsperdiv! > 1 THEN GOTO changevoltsperdiv
        LOCATE 2, 60: PRINT "            "
        fullscale! = voltsperdiv! * 10
        RETURN line01
    END IF
'-------------------------------------------
graphmode:
'-------------------------------------------
    keysoff
    IF mode$ <> "integrator" THEN RETURN line01
    mode$ = "graph"
    scalefactor% = 50
    title$ = "Untitled"
graph01:
'-------------------------------------------
'set up appropriate hot keys
'-------------------------------------------
    KEY(1) ON  'used to change scale factor
    KEY(2) ON  'used to supply a title
    KEY(3) ON  'prints the screen
    KEY(4) ON  'used to quit the mode
    KEY(5) ON  'prints the data
    KEY(6) ON
    COLOR 7, 0
'-------------------------------------------
'clear the screen
'-------------------------------------------
    LINE (0, 0)-(640, 350), 0, BF
     graphswitches
     graphdials scalefactor%, tbase%, iterations%, twindow%
'-------------------------------------------
'draw the scope screen
'-------------------------------------------
    LINE (50, 50)-(450, 250), 0, BF
    LINE (50, 50)-(450, 250), 7, B
'-------------------------------------------
'Add the graticules
'-------------------------------------------
    FOR x = 70 TO 230 STEP 20
        LINE (50, x)-(450, x), 7, , &HCCCC
    NEXT
    FOR x = 90 TO 450 STEP 40
        LINE (x, 50)-(x, 250), 7, , &HCCCC
    NEXT
'-------------------------------------------
'better put in the time scale
'-------------------------------------------
    'FOR i = 1 TO 20
    'LOCATE i, 1
    'PRINT i

    'NEXT
    'FOR i = 1 TO 70 STEP 5
    'LOCATE 1, i
    'PRINT i
    'NEXT
    LOCATE 19, 7: PRINT "0 ms"
    LOCATE 19, 50: PRINT INT(tbase! * 1000); " ms"
    LOCATE 3, 7: PRINT title$
```

```
        COLOR 10, 0
'-------------------------------------------
'Plot the points on the screen
''-------------------------------------------
'The scope is working as a gated integrator. The display should be
'integral vs delay time. The maximum time is tbase% . The integral values
'held in array curve!() must be sorted then scaled.
'-------------------------------------------
        biggest! = curve!(1)
        FOR i = 1 TO points%
            IF curve!(i) > biggest! THEN biggest! = curve!(i)
        NEXT i
        IF biggest! < .001 THEN biggest = .001
'-------------------------------------------
'scale using scale factor
'-------------------------------------------
        size! = scalefactor% / 100 * 200
        FOR i = 1 TO points%
            y% = INT(200 - (curve!(i) / biggest! * size!) + 50)
            x% = INT(tcurve!(i) / tbase! * 400) + 50
            IF y% < 50 THEN y% = 50
            IF y% > 250 THEN y% = 250
            IF x% < 50 THEN x% = 50
            IF x% > 450 THEN x% = 450
            LINE (x% - 2, y% - 2)-(x% + 2, y% + 2), 10, B'CIRCLE (x%, Y%), 3, 10
        NEXT i
       DO: LOOP

        STOP
'---------------------------------------
quit:
        keysoff
        LOCATE 10, 10: INPUT "Quit <Y> or <N> "; q$
        SELECT CASE UCASE$(q$)
        CASE "Y"
        GOTO endbit
        CASE "N"
        'do nothing
        CASE ELSE
        LOCATE 10, 10: PRINT "                    "
        GOTO quit
        END SELECT
        RETURN line01
'---------------------------------------
integrator:
'---------------------------------------

        DIM background!(300)
'-------------------------------------------
'set plates to -ve for background
'-------------------------------------------
        setting$ = "remote negative"
        remotecontrol setting$
'-------------------------------------------
'measure background curve
'-------------------------------------------
        FOR i = 1 TO points%
        dvalue% = INT(i / points% * 4095)
        delay dvalue%
        number% = INT(twindow% * 50)
```

```
        xxx volts!(), time!(), iterations%, number%, offset!, integral!
        background!(i) = integral!
        NEXT i
'-------------------------------------------------
'set plates to +ve
'-------------------------------------------------
        setting$ = "remote positive"
        remotecontrol setting$
'-------------------------------------------------
'measure curve
'-------------------------------------------------
        FOR i = 1 TO points%
        dvalue% = INT(i / points% * 4095)
        delay dvalue%
        number% = INT(twindow% * 50)
        xxx volts!(), time!(), iterations%, number%, offset!, integral!
        curve!(i) = integral! - background!(i)
        tcurve!(i) = tbase! / points% * i
        NEXT i
        RETURN
'-----------------------------------------
endbit:
        END
```

SUB delay (d1%)

```
        DIM dat%(4), ary1%(3), ary2%(3)
        dat%(0) = 0: dat%(1) = d1%: fun% = 15
        CALL pcl718(fun%, SEG dat%(0), SEG ary1%(0), SEG ary2%(0), er%)
END SUB
```

SUB drawdials (voltsperdiv!, tbase%, tdelay%, twindow%, points%, iterations%, offset!)

```
'-------------------------------------------------------------------------
'sub to draw the dials that display the various vital quantities
'-------------------------------------------------------------------------
        LINE (370, 0)-(600, 120), 0, BF
        LINE (370, 0)-(600, 120), 2, B
        COLOR 2, 0
        LOCATE 2, 50: PRINT "Volts/Div "
        LOCATE 3, 50: PRINT "Timebase  "
        LOCATE 4, 50: PRINT "Delaytime "
        LOCATE 5, 50: PRINT "Window    "
        LOCATE 6, 50: PRINT "Points    "
        LOCATE 7, 50: PRINT "Iterations"
        LOCATE 8, 50: PRINT "Offset V  "
        COLOR 12, 0
        LOCATE 2, 60: PRINT USING "#.###"; voltsperdiv!
        LOCATE 3, 60: PRINT USING "#####"; tbase%
        LOCATE 4, 60: PRINT USING "#####"; tdelay%
        LOCATE 5, 60: PRINT USING "#####"; twindow%
        LOCATE 6, 60: PRINT USING "#####"; points%
        LOCATE 7, 60: PRINT USING "#####"; iterations%
        LOCATE 8, 60: PRINT USING "+#.##"; offset!
        COLOR 2, 0
END SUB
```

```
SUB drawscreen (volts!(), time!(), twindow!, fullscale!, points%, mode$, curve!(), tcurve!(),
tbase!)
'time!() = Array of time values
'volts!() = Array of voltage values
'twindow! = Maximum time value, in storage scope mode
'points%  = Number of points , used when mode= integrator
'fullscale! this is the fullscale voltage
'curve!() = Array of integral values
'tcurve!()  Array of values (s) of delay times
'tbase!   = Maximum delay time (s) used  in integrator mode
'-------------------------------------------------
'draw the scope screen
     LINE (50, 50)-(350, 250), 0, BF
     LINE (50, 50)-(350, 250), 7, B
'-------------------------------------------------
'Add the graticules
     FOR x = 70 TO 230 STEP 20
          LINE (50, x)-(350, x), 7, , &HCCCC
     NEXT
     FOR x = 100 TO 300 STEP 50
          LINE (x, 50)-(x, 250), 7, , &HCCCC
     NEXT
     COLOR 10, 0
'-------------------------------------------------
'Plot the points on the screen
     SELECT CASE mode$
     CASE IS = "integrator"
'The scope is working as a gated integrator. The display should be
'integral vs delay time. The maximum time is tbase% . The integral values
'held in array curve!() must be sorted then scaled.
     biggest! = curve!(1)
     FOR i = 1 TO points%
          IF curve!(i) > biggest! THEN biggest! = curve!(i)
     NEXT i
     IF biggest! < .001 THEN biggest = .001
     FOR i = 1 TO points%
          y% = INT(200 - (curve!(i) / biggest! * 180) + 50)
          x% = INT(tcurve!(i) / tbase! * 300) + 50
          IF y% < 50 OR y% > 250 THEN y% = 250
          IF x% < 50 OR x% > 350 THEN x% = 350
          CIRCLE (x%, y%), 3, 10
     NEXT i
     CASE ELSE
'-------------------------------------------------
'storage scope emulation, so max no points to plot = twindow!*50,000
          n% = INT(twindow! * 50000)
          FOR i = 1 TO n%
               x% = i + 50
               y% = INT(200 - ((volts!(i) / fullscale!) * 200) + 50)
               IF y% < 50 OR y% > 250 THEN y% = 250
               IF x% < 50 OR x% > 350 THEN x% = 350
               PSET (x%, y%)
          NEXT i
     END SELECT
'-------------------------------------------------
'Turn the color back to normal
     COLOR 2, 0

END SUB
```

SUB drawswitches

```
'sub to draw the switches on the right hand side of the screen including
'the mode currently selected
'-------------------------------------------------------------------------------
      LINE (370, 130)-(600, 320), 0, BF
      LINE (370, 130)-(600, 320), 2, B
      COLOR 2, 0
      LOCATE 11, 50: PRINT "<F1> Change Timebase  "
      LOCATE 12, 50: PRINT "<F2> Change Delaytime "
      LOCATE 13, 50: PRINT "<F3> Set Window       "
      LOCATE 14, 50: PRINT "<F4> Change Iterations"
      LOCATE 15, 50: PRINT "<F5> Set No Points    "
      LOCATE 16, 50: PRINT "<F6> Change Volts/Div "
      LOCATE 17, 50: PRINT "<F7> Change Offset    "
      LOCATE 18, 50: PRINT "<F8> Fire Scope       "
      LOCATE 19, 50: PRINT "<F9> Toggle Polarity  "
      LOCATE 20, 50: PRINT "<F10> Measure Curve   "
      LOCATE 21, 50: PRINT "<F11> Not active      "
      LOCATE 22, 50: PRINT "<F12> Quit            "
      END SUB
```

SUB dumper

```
REM subroutine to dump graphics screen to printer
gdump:
REM
REM open file to talk to the printer
OPEN "LPT1" FOR OUTPUT AS #1
REM make sure basic doesn't add any cr/lf's
WIDTH #1, 255
REM advance paper
PRINT #1, CHR$(10); CHR$(13); CHR$(10); CHR$(13);
REM select 7/72 line spacing
REM print #1,chr$(27)"1";
REM allow for largest screen ( VGA )
 FOR y% = 0 TO 480 STEP 4
 REM select quad density mode on printer
 PRINT #1, CHR$(27); "Z"; CHR$(128); CHR$(7);
FOR x% = 0 TO 639
    byt% = 0
    IF POINT(x%, y%) > 0 THEN byt% = byt% + 192
    IF POINT(x%, y% + 1) > 0 THEN byt% = byt% + 48
    IF POINT(x%, y% + 2) > 0 THEN byt% = byt% + 12
    IF POINT(x%, y% + 3) > 0 THEN byt% = byt% + 3
    PRINT #1, CHR$(byt%); CHR$(byt%); CHR$(byt%);
 NEXT x%
REM feed the paper 21/216" and return carriage
PRINT #1, CHR$(27); "J"; CHR$(24); CHR$(13);
NEXT y%
REM ADVANCE PAPER AT END OF DUMP
'PRINT #1, CHR$(13); CHR$(10); CHR$(13); CHR$(10)
REM close printer channel
CLOSE 1
END SUB
```

```
SUB graphdials (scalefactor%, tbase%, iterations%, twindow%)
'--------------------------------------------------------------------------
'sub to draw the dials that display the various vital quantities
'--------------------------------------------------------------------------
    LINE (460, 0)-(620, 120), 0, BF
    LINE (460, 0)-(620, 120), 2, B
    COLOR 2, 0
    LOCATE 2, 60: PRINT "ScaleFactor "
    LOCATE 3, 60: PRINT "Timebase    "
    LOCATE 4, 60: PRINT "Iterations  "
    LOCATE 5, 60: PRINT "Window (ms) "
    COLOR 12, 0
    LOCATE 2, 72: PRINT USING "####"; scalefactor%
    LOCATE 3, 72: PRINT USING "####"; tbase%
    LOCATE 4, 72: PRINT USING "####"; iterations%
    LOCATE 5, 72: PRINT USING "####"; twindow%
    COLOR 2, 0
END SUB
```

```
SUB graphswitches
'sub to draw the switches on the right hand side of the screen including
'the mode currently selected
    LINE (460, 130)-(620, 320), 0, BF
    LINE (460, 130)-(620, 320), 2, B
    COLOR 2, 0
    LOCATE 11, 60: PRINT "<F1> Change Scale "
    LOCATE 12, 60: PRINT "<F2> Change Title "
    LOCATE 13, 60: PRINT "<F3> Print Screen "
    LOCATE 14, 60: PRINT "<F4> Quit Mode    "
    LOCATE 15, 60: PRINT "<F5> Print Data   "
    LOCATE 16, 60: PRINT "<F6> Save Data    "
    LOCATE 17, 60: PRINT "<F7> Not active   "
    LOCATE 18, 60: PRINT "<F8> Not active   "
    LOCATE 19, 60: PRINT "<F9> Not active   "
    LOCATE 20, 60: PRINT "<F10> Not active  "
    LOCATE 21, 60: PRINT "<F11> Not active  "
    LOCATE 22, 60: PRINT "<F12> Not active  "
END SUB
```

```
SUB initialiser
    DIM dat%(4), ary1%(3), ary2%(3)
    PORT% = &H300          'SET I/O PORT ADDRESS
    dat%(0) = PORT%        'GET I/O PORT ADDRESS
    dat%(1) = 3            'SELECT INTERRUPT LEVEL 3
    dat%(2) = 1            'SELECTE D.M.A. IRQ3
    er% = 0                'ERROR RETURN CODE
    fun% = 0               'FUNCTION 0
    CALL pcl718(fun%, SEG dat%(0), SEG ary1%(0), SEG ary2%(0), er%)
    IF er% <> 0 THEN PRINT "DRIVER INITIALIZATION FAILED!": STOP
END SUB
```

```
SUB keysoff
    KEY(1) OFF
    KEY(2) OFF
    KEY(3) OFF
    KEY(4) OFF
    KEY(5) OFF
```

```
        KEY(6) OFF
        KEY(7) OFF
        KEY(8) OFF
        KEY(9) OFF
        KEY(10) OFF
        KEY(30) OFF
        KEY(31) OFF
END SUB

SUB printdata (points%, tcurve!(), curve!())
"sub to print out array of integral values with time values and
'any comments desired
        LINE (50, 270)-(450, 330), 0, BF
        LINE (50, 270)-(450, 330), 7, B
        LOCATE 21, 8
        PRINT "Please ensure that the printer is ON LINE "
        LOCATE 22, 8
        PRINT "Press Any Key To Continue....."
        COLOR 2, 0
        DO: LOOP WHILE INKEY$ = ""
printdata01:
        LINE (50, 270)-(450, 330), 0, BF
        LINE (50, 270)-(450, 330), 7, B
        LOCATE 21, 8
        PRINT "Enter a (short) Title for the print out .."
        LOCATE 22, 8: INPUT ; t$
        LINE (50, 270)-(450, 330), 0, BF
        LINE (50, 270)-(450, 330), 7, B
        LOCATE 21, 8
        PRINT "Enter any comments on next line (ie Pressure) "
        LOCATE 22, 8
        INPUT ; c$
printdata02:
        LINE (50, 270)-(450, 330), 0, BF
        LINE (50, 270)-(450, 330), 7, B
        LOCATE 21, 8: PRINT t$
        LOCATE 22, 8: PRINT c$
        LOCATE 23, 8
        INPUT "Change Anything ? <y> or <n> "; q$
        SELECT CASE UCASE$(q$)
        CASE IS = "Y"
                GOTO printdata01
        CASE IS = "N"
                'do nothing
        CASE ELSE
                GOTO printdata02
        END SELECT
'print out the information in an economical fashion
        LPRINT
        LPRINT
"*****************************************************************************
"
        LPRINT
        LPRINT DATE$
        LPRINT TIME$
        LPRINT t$
        LPRINT c$
        LPRINT
        LPRINT ; TAB(1); "TIME"; TAB(10); "INTEGRAL"; TAB(40); "TIME"; TAB(50);
"INTEGRAL"
```

```
    j = 1
    FOR i = 1 TO INT(points% / 2) + 1
    LPRINT USING "+##.#####"; TAB(1); tcurve!(j); TAB(10); curve!(j); TAB(40); tcurve!(j
+ 1); TAB(50); curve!(j + 1)
    j = j + 2
    NEXT i
END SUB

SUB remotecontrol (setting$)
'--------------------------------------------------------------------------
'subroutine to remotely control the plate polarity
'--------------------------------------------------------------------------
    DIM dat%(4), ary1%(1), ary2%(1)
    IF setting$ = "remote positive" THEN num% = 5
    IF setting$ = "remote negative" THEN num% = 9
    IF setting$ = "manual positive" THEN num% = 6
    IF setting$ = "manual negative" THEN num% = 10
    IF setting$ = "manual" THEN num% = 0
    fun% = 21: dat%(1) = INT(num% / 256): dat%(0) = num% - (dat%(1) * 256)
    CALL pcl718(fun%, SEG dat%(0), SEG ary1%(0), SEG ary2%(0), er%)
    END SUB

SUB xxx (volts!(), time!(), iterations%, number%, offset!, integral!)
'--------------------------------------------------------------------------
'Note that the next line carries the atod range. This must correspond to the
'setting of switch 5 on the pcl718 card
    atod! = 10
    z = iterations%
    DIM dat%(4), ary1%(600), ary2%(600), dummy%(10, 600)
    PORT% = &H300          'SET I/O PORT ADDRESS
    dat%(0) = PORT%        'GET I/O PORT ADDRESS
    dat%(1) = 3            'SELECT INTERRUPT LEVEL 3
    dat%(2) = 1            'SELECTE D.M.A. IRQ3
    er% = 0                'ERROR RETURN CODE
    fun% = 0               'FUNCTION 0
    CALL pcl718(fun%, SEG dat%(0), SEG ary1%(0), SEG ary2%(0), er%)
    IF er% <> 0 THEN PRINT "DRIVER INITIALIZATION FAILED!": STOP
FOR i = 1 TO z
'--------------------------------------------------------------------
'Set up the multiplexer to the appropriate values
    dat%(0) = 1       'SET START CHANNEL NUMBER
    dat%(1) = 1       'SET STOP  CHANNEL NUMBER
    fun% = 1          'FUNCTION 1
    CALL pcl718(fun%, SEG dat%(0), SEG ary1%(0), SEG ary2%(0), er%)
    IF er% <> 0 THEN PRINT "SET SCAN CHANNEL FAILED! RE-ENTER": STOP
'--------------------------------------------------------------------
'Set the pacer trigger to 50khz (1mhz/20)
    dat%(0) = 2        'COUNTER 2 DIVISOR
    dat%(1) = 10       'COUNTER 1 DIVISOR
    fun% = 17          'FUNCTION 17
    CALL pcl718(fun%, SEG dat%(0), SEG ary1%(0), SEG ary2%(0), er%)
    IF er% <> 0 THEN PRINT "SET PACER TRIGGER FAILED!": STOP
'--------------------------------------------------------------------
'Do the number% of atod measurements and save using dma transfer
    dat%(0) = number%     'NUMBER OF CONVERSIONS
    dat%(1) = &H7000      'MEMORY SEGMENT TO HOLD A/D DATA
    dat%(2) = 1           'PACER TRIGGER
    dat%(3) = 0           'NON-RECYCLE SCANNING
    fun% = 6              'FUNCTION 6
    CALL pcl718(fun%, SEG dat%(0), SEG ary1%(0), SEG ary2%(0), er%)
```

```
    IF er% <> 0 THEN PRINT "PERFORM FUNCTION 6 FAILED!": STOP
    n = dat%(0)
'-------------------------------------------------------------------
'Move data from memory to array ary1%(), ary2%() contains the channel no
    dat%(0) = number%        'NUMBER OF DATA TO BE MOVED
    dat%(1) = &H7000         'SOURCE MEMORY SEGMENT
    dat%(2) = 0              'STARTING DATA NUMBER
    fun% = 9                 'FUNCTION 9
    CALL pcl718(fun%, SEG dat%(0), SEG ary1%(0), SEG ary2%(0), er%)
    IF er% <> 0 THEN PRINT "PERFORM FUNCTION 9 FAILED!": STOP
'-------------------------------------------------------------------
'Move this lot of data to the multi dimensional holding array
    FOR j = 0 TO number% - 1
    dummy%(i, j) = ary1%(j)
    NEXT j
'-------------------------------------------------------------------
'Turn off the interrupt activity
    fun% = 7
    CALL pcl718(fun%, SEG dat%(0), SEG ary1%(0), SEG ary2%(0), er%)
NEXT i
'-------------------------------------------------------------------
'Find the average value of each channel and calculate the integral of
'the Voltage signal
    integral! = 0
    FOR j = 0 TO number% - 1
        sum& = 0
        FOR i = 1 TO z
            sum& = sum& + dummy%(i, j)
        NEXT i
        volts!(j + 1) = ((sum& / 4096) / z) * atod! + offset!
        time!(j + 1) = (j + 1) / 50000
        integral! = integral! + volts!(j + 1)
    NEXT j
'-------------------------------------------------------------------
'PRINT volts!(11) / atod! * z * 4096
LOCATE 1, 20: PRINT "Integral= "; integral!
END SUB
```